Altered function of CCK-Positive Interneurons in mice over-expressing the Schizophrenia risk gene Neuregulin 1

Dimitrios Kotzadimitriou
Keble College
University of Oxford

Thesis submitted for the Degree of
Doctor of Philosophy
Michaelmas 2016

To my parents Stavroula and Thomas,
for being there no matter what

Abstract

The Neuregulin 1 (NRG1)-ErbB4 signalling pathway is implicated in critical processes for the development and function of neuronal circuits. Post mortem studies have reported that elevated expression of NRG1 type 1 isoform is associated with schizophrenia. Importantly previous behavioural studies in mice that overexpress the NRG1 type 1 isoform ($NRG1^{tg\text{-}type\text{-}I}$) have suggested a schizophrenia endophenotype including impairment in the hippocampus-dependent spatial working memory, prepulse inhibition (PPI) of the startle reflex and alterations in the gamma band rhythmogenesis This study aims to reveal the cellular targets of the NRG1-ErbB4 signalling pathway and putative alterations in the function of the hippocampal network in $NRG1^{tg\text{-}type\text{-}I}$ mice.

Immunocytochemical analysis showed that the NRG1 receptor ErbB4 is predominantly localized in interneurons comprising parvalbumin positive (PV) and cholecystokinin (CCK) expressing cells. Comparison of the density of ErbB4-positive cells between the hippocampus of wild type (WT) and $NRG1^{tg\text{-}type\text{-}I}$ mice suggested that NRG1 over-expression resulted in decreased number of ErbB4 immunopositive hippocampal interneurons. This is consistent with the proposed role of the NRG1-ErbB4 signalling in the migration of GABAergic cells during neurodevelopment and with the NRG1-mediated internalisation of the ErbB4 receptors. CCK-positive cells are a major target of NRG1-ErbB4 signalling, and therefore the NMDA receptor and AMPA receptor components of glutamatergic transmission were analysed in this population of cells by performing whole cell recordings of evoked and miniature excitatory post synaptic currents. Glutamatergic neurotransmission in CCK-positive cells was found to be compromised in the hippocampus of $NRG1^{tg\text{-}type\text{-}I}$ mice. This change was attributed to hypofunction of NMDA receptors but not AMPA receptors post-synaptically. Next, the inhibitory output of CCK-positive cells to pyramidal cells was examined. Analysis of the optogenetically elicited inhibitory post synaptic currents (IPSCs) did not reveal any changes in the properties of the GABAergic synapse formed by these cells due to NRG1 over-expression Finally, the effects of this NMDA receptor hypofunction in the recurrent inhibition were analysed by performing whole cell recordings during the gamma relevant optogenetic entrainment of the hippocampal network. It was found that the disynaptic inhibition, a key synaptic interaction for the generation of gamma oscillations, depends on the NMDA receptors and was altered in the hippocampus of $NRG1^{tg\text{-}type\text{-}I}$ mice.

Together these data point out a key modulatory role of the NRG1-ErbB4 signalling in the neurodevelopment of cortical microcircuits and a link between ErbB4 and NMDA receptor function with a possible association to schizophrenia pathogenesis.

Declaration

The work presented in this thesis was carried out in the Department of Pharmacology and the MRC Anatomical Neuropharmacology unit, University of Oxford. The research presented in this thesis is my own work unless otherwise stated.

Ms Kathryn Newton provided assistance with the immunocytochemical reactions and confocal microscopy through the experimental procedures presented in this thesis.

Dr Karri Lamsa performed the analysis of the experiments presented in the chapter 6 of this thesis. However all the recordings were performed by myself.

The immunocytochemical reaction in Figure 5-1 C1-3 was performed by Dr Diogo Rombo.

The in situ hybridization images shown in Figure 1-3 and Figure 7-1 were adapted from Deakin et al., 2012

No part of this thesis has been submitted for any other examination.

Approximate word count 50,000

Acknowledgments

My time in Oxford was one of the most important and formative experiences in my life. I would like to express my gratitude to all the people that followed me through this quest, and helped me develop as a researcher. Without them the completion of this project would not be possible.

First and foremost, I would like to deeply thank my supervisor, Research professor Karri Lamsa for giving me the opportunity to work in his lab and for his guidance and constant support during the course of my DPhil. While, studying under his supervision, I developed my scientific thinking and learned the working methods of testing a research hypothesis. His enthusiasm and motivation especially in challenging periods is an inspiration for my future.

I would like also to deeply thank my co-supervisors Dr Liliana Minichiello and Professor Marco Capogna for their support, advice and guidance especially during the last critical period of my studies.

I am also particularly thankful to Professor Peter Somogyi, for giving me a unique chance to work in his lab the year before embarking for this DPhil and for giving his time to better my work. His remarks made me to foster a critical reasoning about scientific results and methods.

Special thanks to Wiebke Nissen, Diogo Rombo and Tim Viney for originally introducing me to *in vitro* and *in vivo* electrophysiology, stereotaxic surgery and immunocytochemistry as well as for their help, scientific advice, and stimulating conversations throughout the period of this project.

Many thanks to; Kathryn Newton for her assistance with the immunocytochemistry and microscopy, Pavel Perestenko for his excellent advice and patience with biochemistry, Barbara Zonta for her advice about western blotting, Ben Micklem for his advice with microscopy and IT support, Liz Norman and Jane Janson for their help and advice concerning the welfare of experimental animals.

Great thanks to Petrina, Suckvir, Lorenz, Armando, for their companionship, advice and the discussions we had in the lab. Petrina, you were always an example of patience and determination. Thank you for encouraging me!

A big Köszönöm szépen! to Victor, Adam, Robert, Melinda, Eszter, Janos and Szabina for welcoming me in Szeged, for all their immense help with me adapting to a new lab, setting up equipment and for our stimulating discussions and companionship. You made my stay in Szeged a wonderful experience. I am glad that I had the chance to meet you all.

I feel deeply privileged that during this adventure I had the opportunity to have as fellow travellers and friends; Adamantios, Alexei, Ayesha, Eleutheria, Ioanna, Marco and Vasilleios, with whom together figured out about science and how to live it. You know more than anyone that it was a long journey and you were always having my back.

Finally, I would like to sincerely thank, the MRC, Keble College and Keble Association for supporting me throughout my research.

Table of Contents

Abbreviations/Acronyms

AAC	axo-axonic cell
AAV	adeno-associated virus
Alv	alveus
AMPAR	a-amino-3-hydroxy-5-methyl-4-isoxazolepropionic acid receptor
ANOVA	analysis of Variances
APS	ammonium persulphate
ATD	amino-terminal domain
BACE	β-site of amyloid precursor protein cleaving enzyme
BisC	bistratified cell
BSc	basket cell
CAMKII	Ca^{2+}/calmodulin-dependent protein kinase
CB	calbindin
CB1R	cannabinoid receptor type 1
CCK	cholecystokinin
CGP55845	2S)-3-[[(1S)-1-(3,4-Dichlorophenyl)ethyl]amino-2-hydroxypropyl](phenylmethyl) phosphinic acid hydrochloride
ChR2	channelrhodopsin 2
CIQ	(3-chlorophenyl) (6,7-dimethoxy-1-((4-methoxyphenoxy)methyl)-3,4-dihydroisoquinolin-2(1 H)-yl)methanone
CNS	central nervous system
CNV	copy number variant
CR	calretinin
CRD	cysteine-rich domain
CTD	carboxyl-terminal domain CTD
DG	dentate gyrus
DIC-IR	differential interference contrast-infrared system
DL-AP5	DL-2-amino-5-phosphonopentanoic acid
DSI	Depolarisation induced suppression of inhibition
DSM	Diagnostic and Statistical Manual of Mental Disorders
EC	entorhinal cortex
EDTA	Ethylenediaminetetraacetic acid
EEG	electroencephalography

EGF	epidermal growth factor
eIPSC	evoked inhibitory post-synaptic current
EPSC	excitatory post-synaptic current
ErbB4	v-erb-a erythroblastic leukemia viral oncogene homolog 4 (avian)
E_{NMDAR}	NMDA receptor reversal potential
E_{EPSCs}	EPSCs reversal potential
eYFP	enhanced yellow fluorescent protein
GABA	γ – aminobutyric acid
GAD-67	67 kDa isoform of glutamate decarboxylase
GADPH	Glyceraldehyde 3-phosphate dehydrogenase
GAT-1	GABA transporter 1
GWAS	genome-wide association study
HAP	haplotype
HPC	hippocampus proper
HS	hippocampo -septal cell
ICD	International Classification of Diseases
ICDs	intracellular sites
Ig	immunoglobulin
iGluR	ionotropic Glutamate receptor
ING	Interneuron Network Gamma
IPSC	inhibitory post-synaptic current
IPSPs	inhibitory post-synaptic potentials
ISI	Interneunon - specific interneurons
KN-62	4-[(2S)-2-[(5-isoquinolinylsulfonyl) methylamino]-3-oxo-3-(4-phenyl-1-piperazinyl) propyl] phenyl isoquinoline sulfonic acid ester
LBD	ligand- binding domain
LFP	local field potential
LM-PP	lacunosum moleculare perforant pathway associated cell
LTP	Long-Term Potentiation
MCPG	RS)-α-Methyl-4-carboxyphenylglycine disodium salt
MEG	magnetoencephalography
mEPSC	miniature excitatory post-synaptic current
mGluRs	metabotropic receptors

mIPSCs	miniarure Inhibitory Post-synaptic Currents
MOS	minimal optical stimulation
mRNA	Messenger RNA
NBQX	2,3-Dioxo-6-nitro-1,2,3,4-tetrahydrobenzo[f]quinoxaline-7-sulfonamide disodium
NCG	neurogliaform cell
NMDAR	N-methyl-D-aspartate receptor
nNOS	neuronal nitric oxide synthase
NPY	neuropeptide Y
NRG1	Neuregulin-1
O-LM	oriens-lacunosum-moleculare cell
PaS	Parasubiculum
PB	phosphate buffer
PFA	paraformaldehyde
PING	Pyramidal Interneuron Network Gamma
PiTX	(Picrotoxin) 1 to 1mixture of picrotoxinin and picrotin
PPI	prepulse inhibition
PPR	paired pulse ratio
PSD	Post-synaptic density
PrS	presubiculim
PV	parvalbumin
QX-314	Lidocaine N-ethyl bromide
Ra	access resistance
REM	Rapid Eye Movement
s.l	stratum lucidum
s.l-m	stratum lacunosum-moleculare
s.o	stratum oriens
s.p	stratum pyramidale
s.r	stratum radiatum
SC	Schaffer Collateral
SDS	sodium dodecyl sulfate
SEM	standard error mean
sEPSC	spontaneous EPSC
SNPs	single nucleotide polymorphism
SOM	somatostatin
Sub	subiculum

SWRs	Sharp Wave Ripples
TACE	tumor necrosis factor- α converting enzyme TACE
TBS	Tris-buffered saline
TEMED	(N,N,N,N-Tetramethylethane-1,2-diamine)
THC	(2)-trans-Δ^9-tetrahydrocannabinol
TMc	C-terminal transmembrane domain
TMD	transmembrane domain
TMn	N-terminal transmembrane domain
TTX	Tetrodotoxin
Tx	Triton x 100
Vh	holding potential
VIP	vasoactive intestinal peptide
WHO	Word Health Organization
WT	wild type
2-AG	2-arachinodyl glycerol

1 General introduction

The brain is the biological correlate of consciousness, reasoning and decision making. A crucial question is which neuronal circuits contribute to these processes. To answer this question, neuroscience research follows two different approaches. A top-down approach investigates the emergence of these complex processes searching for the correlative activity of neuronal networks in specific brain areas by probing whether the activity of individual neurons and their synaptic interactions correlates with specific behaviours. This can also be applied to a disease phenotype modelled in experimental animals.

On the contrary, a bottom-up approach is often used to modify or specifically alter the small-scale factors in the brain, like the function of specific neuron types and their synaptic connections, to understand whether and how these alterations may change the animal's behavioural phenotype. Often, the most fruitful strategies include features from both approaches. For instance, it is important to know whether the observed neurobiological alterations in a disease animal model are indeed responsible for the disease phenotype by testing whether a specific modulation in healthy animals results in a similar phenotype. This typically involves targeting and modifying specific genes and gene products of interest.

One signalling pathway increasingly investigated during past years due to its involvement in a plethora of neurodevelopmental processes related to synaptic organization of neuronal networks and its potential involvement in various neuropsychiatric disorders such as schizophrenia, is the neuregulin 1 (NRG1)- v-erb-a erythroblastic leukemia viral oncogene homolog 4 (avian) (ErbB4) signalling pathway.

In this thesis, I used a top-down approach to examine the effects of the NRG1-ErbB4 signalling pathway dysregulation on synaptic physiology in the hippocampus. Specifically I used a genetically modified mouse line showing enhanced NRG1 type I expression. Using a combination of electrophysiological, immunocytochemical and optogenetics methods, I study how the hippocampal circuitry is altered in this mouse line, which has been reported to exhibit alterations in the co-ordinated rhythmic hippocampal network activity and the hippocampus-dependent working memory, both of which are commonly associated features of cognitive symptoms in schizophrenia.

In this introductory chapter, I review the current research outcomes on the NRG1-ErbB4 signalling pathway as a modulator of neuronal circuits and its relation to schizophrenia. In particular, I review its role in the maturation of the hippocampal networks responsible for co-ordinated rhythmic activities and the hippocampal working memory function.

1.1 The NRG1 protein

Neuregulin 1 (NRG1) is a member of the neuregulin family of epidermal growth factor (EGF) like-proteins currently comprising six different proteins (NRG1-6) (Mei and Nave, 2014). The NRG1 is the first described and the most intensively studied member of this protein family, originally characterised as a factor responsible for regulating synapse formation and the expression of acetylcholine receptors (Corfas et al., 1993, Falls et al., 1993). Similar to the other NRGs, alternative promoters and different splice variants give rise to distinct amino terminal sequences that define the "type" of NRG1. Currently six types of NRG1 (type I-VI) are known (with more than 30 isoforms) in humans. Among these, types I-III are highly conserved in rodents (Steinthorsdottir et al., 2004) and their specific expression has been found to be regulated by neuronal activity in the CNS (Ozaki et al., 2004, Liu et al., 2011).

Initially transcribed as membrane-anchored precursor peptides (often defined with the "pro-"prefix) NRG1s traverse the cell membrane via a C-terminal transmembrane domain (TMc). The EGF domain has three different variants known as α, β or γ, and it is located at the beginning of the extracellular protein domain and connected to the N-terminal region either via an immunoglobulin (Ig) domain (in types I,II,IV, V) or directly -in types III, VI). In addition, it is connected to the TMc domain via a linker region, which is also connected to the cytoplasmic tail (variants a, b and c) (Figure 1-1). Interestingly, the type III NRGs contain a cysteine-rich domain (CRD) and an extra N-terminal transmembrane domain (TMn), resulting in a double passage of the peptide through the membrane (Mei and Xiong, 2008)

1.1.1 NRG1 signal transduction

It has been demonstrated that immature membrane-anchored pro-NRG1 proteins are subject to proteolytic cleavage and that this takes place proximally to the C-terminal part of the EGF protein domain either by the tumor necrosis factor- α converting enzyme (TACE) (Loeb et al., 1998), or the β-site of amyloid precursor protein cleaving enzyme (BACE) (Hu et al., 2006), or the memapsin beta (Yokozeki et al., 2007). This process results to the release and diffusion of the "mature" NRG1 protein containing the EGF and Ig domains. However, in this process the NRG1 type III is an exception, due its double transmembrane passage, the proteolytic cleavage does not release any N-terminal protein domains leaving the EGF domain juxtapositioned to the plasma membrane. NRG1 signalling is thought to be mediated mainly via this EGF domain, which predominantly activates the ErbB group of epidermal growth factor receptors comprising 4 members known as ErbB1-4. The ErbB1-4 receptors possess tyrosine kinase activity, and their activation initiates a pleiotropic cascade of downstream signalling pathways in the CNS that is involved in various developmental processes such as neuronal differentiation and migration (Flames et al., 2004, Liu et al., 2005,) axon myelination (Brinkmann et al., 2008), synapse

maturation and the control of neurotransmitter systems (Ozaki et al., 1997, Liu et al., 2001, Gu et al., 2005, Li et al., 2007, Woo et al., 2007, Ting et al., 2011, Yin et al., 2013, Agarwal et al., 2014, Vullhorst et al., 2015). The signal transduction is achieved by the formation of ErbB receptor dimers upon the interaction with the NRG1- EGF ligand. Hitherto, it has been found that NRG1 can bind and stabilise the formation of structural ErbB2-ErbB3, ErbB2-ErbB4 and ErbB3-ErbB4 heterodimers or ErbB4-ErbB4 homodimers. The dimerization is followed by receptor auto-phosphorylation at the receptors' intracellular sites (ICDs), leading to the recruitment of several of kinases. The docking of specific adaptor proteins eventually activates downstream signalling pathways in the target cells including cellular cascades for protein synthesis, gene transcription and protein phosphorylation. These reactions have been comprehensively described and discussed in recent reviews (Mei and Xiong, 2008, Mei and Nave, 2014).

Of all the members of this epidermal growth factor family, the ErbB4 is the only one that can autonomously be activated by the NRG1 peptides. In contrast to ErbB2 which is supposed to act as a co-receptor of other ErbBs and ErbB3 whose dimers kinase activity has been suggested to be defective (Guy et al., 1994, Tzahar et al., 1996). Thus, it follows that the main mediator of NRG1s signalling is the ErbB4 receptor. Depending on the type of NRG1 (types I,II,IV,V,VI), proteolytic cleavage can release the bioactive soluble N-terminal residues into the extracellular milieu activating ErbBs receptors in a juxtacrine way. Alternatively in the case of NRG1 type III, the cleaved N-terminal residues remain attached to the plasma membrane mediating a paracrine mode of activation.

However, apart from this "forward" fashion of signalling (NRG1→ErbBs), a signal transduction with an opposite "backward" direction (ErbBs→NRG1) type of signal transduction has also been proposed. This is supposed to be mediated both by the membrane-anchored NRG1

type III and possibly by immature NRG1s (pro-NRG1) acting as receptors for the extracellular domain of ErbB4. Activation of the NRG1 molecule by the ErbB4 can lead to proteolytic cleavage by γ-secretases of the intracellular domain (ICD) of the NRG1 protein and its translocation to the nucleus. So far, this mode of signalling has been implicated in regulation of gene expression and trafficking of certain neurotransmitter receptors (Bao et al., 2003, Bao et al., 2004, Hancock et al., 2008, Zhong et al., 2008).

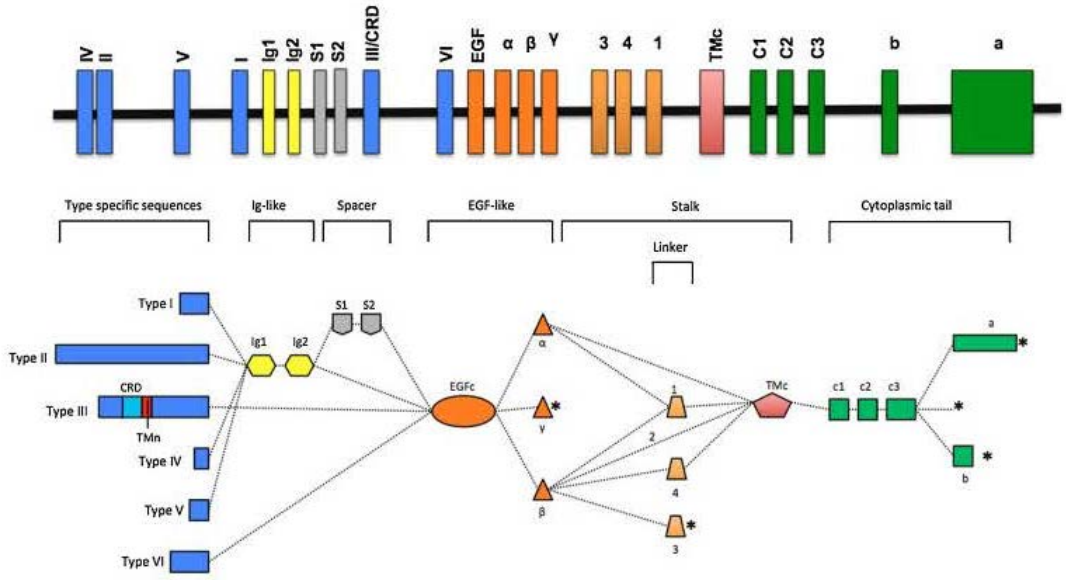

Figure 1-1 Distinct NRG1 isoforms resulting from alternative splicing and different promoter activity. Six characterised NRG1 isoforms (types I-VI) with the correspondent exons (upper schematic) are illustrated in blue. EGFc, the core epidermal growth factor domain shown in orange. Types I, II, IV and V contain the Ig, Immunoglobulin like domain (yellow). Type III contains the CRD, cysteine- rich domain, and TMn, N-terminal transmembrane domain. * indicates stop codon. Adapted from (Mostaid et al., 2016).

1.1.2 NRG1 as a regulator of neurotransmission

One of the roles of NRG1 characterised in detail is the regulation of neuronal development and synaptic function in the CNS. Expression of NRG1 has been reported to be prominent in neocortex, hippocampus, cerebellum and brain stem of mammals. In these structures NRG1 is expressed by pyramidal cells, but also interneurons and glial cells (Chen et al., 1994, Corfas et al., 1995, Kerber et al., 2003, Law et al., 2004). Current consensus is that the

main NRG1 receptor, ErbB4, is exclusively expressed in interneurons and not in pyramidal cells. Evidence for this comes from immunocytochemical studies showing that ErbB4 is not expressed in glutamatergic pyramidal nerve cells, but is present in specific GABAergic interneuron populations expressing either cholecystokinin (CCK), parvalbumin (PV), calretinin (CR), calbindin (CB), neuronal nitric oxide synthase (nNOS), neuropeptide Y (NPY) or somatostatin SOM (but see Neddens and Buonanno,2010) in both the primate and rodent brain (Yau et al., 2003, Fazzari et al., 2010, Neddens and Buonanno, 2010, Katona et al., 2014) raising the likelihood that specific GABAergic interneuron types are prime targets of the NRG1 signalling.

Given that both the ligand and the receptor are expressed in distinct components of neuronal networks, several studies have tried to delineate their roles in development and modulation of neurotransmitter systems. Next, I will provide a review of the studies that investigated the effects on the excitatory and the inhibitory neurotransmission, as well as in neuronal migration and synapse formation.

1.1.2.1 Effects of NRG1 on excitatory glutamatergic transmission

The main neurotransmitter that mediates synaptic excitation in the brain is the amino acid glutamate. Upon its release pre-synaptically, glutamate activates a number of ionotropic (iGluRs) and metabotropic receptors (mGluRs) on the post-synaptic cell. A variety of experimental approaches - such as transgenic mice lines, acute application of exogenous NRG1 peptides or direct brain injection of these peptides have been employed in the past in order to investigate the function of NRG1 in glutamatergic transmission. Most of the studies have focused on the transmission mediated through iGluRs in particular the a-amino-3-hydroxy-5-methyl-4-isoxazolepropionic acid receptor (AMPAR) and N-methyl-D-aspartate receptor (NMDAR). Possible effects on ionotropic kainate receptors have not been specifically studied.

The two types of receptors are tetrameric complexes comprising four protein subunits. The ionotropic glutamate subunits show similar structural and domain organization at the plasma membrane containing four domains; First, the extracellular amino-terminal domain (ATD) implicated in the regulation of trafficking and assembly of functional receptor complexes as well as in the opening probability of the receptor channel (Kuusinen et al., 1999, Leuschner and Hoch, 1999, Ayalon and Stern-Bach, 2001, Meddows et al., 2001, Ayalon et al., 2005, Yuan et al., 2009). Second, the extracellular ligand-binding domain (LBD) responsible for binding the neurotransmitter glutamate, but in addition asparate, glycine and D-serine specifically for NMDARs (Armstrong and Gouaux, 2000, Lampinen et al., 2002, Armstrong et al., 2003, Furukawa and Gouaux, 2003). Third, a transmembrane domain (TMD) with its four transmembrane loops (M1-4), forms the ion pore of the fully assembled receptor channel (Wo and Oswald, 1995). Fourth, an intracellular carboxyl-terminal domain (CTD) contains post-translational phosphorylation sites. Distinct phosphorylation states on the C-terminal domain regulates the receptor trafficking and localization in the plasma membrane. In addition, it plays important role in the receptor endocytosis and also determine various biophysical properties (such as ionic pore ion selectivity and conductance) of the receptor channel (Roche et al., 1996, Tingley et al., 1997, Scott et al., 2001, Scott et al., 2003, Chung et al., 2004, Oh and Derkach, 2005, Sanchez-Perez and Felipo, 2005, Boehm et al., 2006, Lin and Huganir, 2007, Lin et al., 2009).

The AMPA receptor subunits (GluA1-GluA4) can be assembled into functional receptor channel complex as homo-(identical subunits) or hetero (different) – meric combinations. On the other hand, functional NMDA receptor complexes are only formed by two GluN1 combined with two GluN2 or one GluN2 and one GluN3 subunits (Traynelis et al., 2010).

Following a seminal discovery by Stefansson et al. (2002) demonstrating that single nucleotide polymorphisms (SNPs) in regulatory loci of the NRG1 gene are associated with schizophrenia (Stefansson et al., 2002) (reviewed further in section 1.2.2), various studies on either gain- or loss-of-function of NRG1 signalling were carried out to shed light on possible effects of NRG1 on excitatory transmission. However, these studies have generated contrasting results from various brain regions and distinct cell types and have used different experimental paradigms including several genetic mouse models. In addition, some of the studies employed exogenous application of various forms of NRG1 peptides. Thus, it is possible that inconsistent results emerge, at least partially, from altered NRG1 transmission during gestation and development, leading to chronic rearrangements not occurring following acute application. Nonetheless, these inconsistencies could also highlight the pleiotropoic effects of NRG1 in excitatory neurotransmission.

Studies that have focused on AMPAR receptor-mediated post-synaptic responses have produced highly variable results. Facilitation of the NRG1-ErbB4 signalling pathway either via genomic or acute elevation of NRG1 (using exogenously applied NRG1) have reported receptor hypofunction in Cornus Ammonis (CA1) pyramidal cells (Agarwal et al., 2014) (for further review of hippocampal anatomy see section 1.3.1) , no alterations in CA1 and layer V pyramidal cells, (Chen et al., 2010, Abe et al., 2011, Ting et al., 2011, Yin et al., 2013) as well as increased receptor function in GABAergic interneurons (Abe et al., 2011, Ting et al., 2011). However, AMPAR hypofunction in CA1 pyramidal cells has also been reported due to downregulation of the NRG1-ErbB4 pathway (Agarwal et al., 2014).

Similarly, investigations of the effects of NRG1 dysregulation on NMDARs have produced inconsistent results. It has been shown that activation of the NRG1-ErbB4 signalling either via acute application, or using genomic interventions, can alter NMDAR function either

lowering the expression level and trafficking of specific NMDAR subunits (Gu et al., 2005, Hahn et al., 2006, Abe et al., 2011, Luo et al., 2014) but see (Ozaki et al., 1997, Kato et al., 2010, Long et al., 2012), or by decreasing NMDAR-mediated currents in cortical pyramidal cells (Gu et al., 2005), but see (Chen et al., 2010) and finally by changing the phosphorylation status of NMDAR subunits (Hahn et al., 2006). On the other hand, downregulation of NRG1 has also been found to interfere with the receptor's functional properties such as by preventing phosphorylation status of specific NMDAR subunits (Bjarnadottir et al., 2007) and also by altering the receptor-ligand binding properties in diverse ways (Stefansson et al., 2002, Newell et al., 2013) but see (Dean et al., 2008, Long et al., 2012). In addition, recent evidence suggests that NRG1 can also affect the presynaptic release of glutamate in the CA1 area and the layer 5 pyramidal cells (Yin et al., 2013, Papaleo et al., 2016).

Notably, in another study by Vullhorst and colleagues (Vullhorst et al., 2015), it was shown that application of the NRG2, that similarly to NRG1 signals via ErbB4 receptors, causes specific hypofunction of NMDAR-mediated currents exclusively in ErbB4-positive and not in ErbB4-negative neurons. Furthermore, this NMDAR hypofunction was found to dependent on the association of GluN2B with the ErbB4 receptor, and resulted from the internalization of the NMDAR receptor complex.

Table 1-1 summarises the recent results on the effects of NRG1 on the excitatory glutamatergic neurotransmission and indicates the specific experimental approach employed in the studies, as well as, it lists the brain region and cell types studied.

In summary, the above studies suggest that alterations in the NRG1-ErbB4 signalling pathway affect several aspects of glutamatergic transmission. Both hyper- and hypo- activity of the NRG1-ErbB4 signalling change the excitatory neurotransmission, often leading qualitatively to similar changes and both over-expressing and hypomorphic NRG1 transgenic mice display

schizophrenia relevant endophenotypes (reviewed further in section 1.2.3). This led to the hypothesis that alterations in NRG1 expression levels may follow an inverted "U" mode of action, such that either too much or too little NRG1 signalling causes pathological changes (Agarwal et al., 2014). However, despite the previous research efforts there is not a common consensus about the effects of NRG1 on the glutamatergic transmission. This, can be explained by the distinct experimental designs, but can also reflect the pleotropic modulatory roles of the NRG1-ErbB4 signalling in specific brain areas and in different cell types. This highlights the necessity to study the NRG1-ErbB4 signalling in specific brain regions and in well-identified neuronal cell types.

Even though ErbB4, the main receptor of NRG1, is currently considered to be exclusively expressed in specific classes of interneurons (Vullhorst et al., 2009, Neddens and Buonanno, 2010), our knowledge of how the excitatory transmission is affected in these GABAergic cells is very limited. However, the fact that several studies have identified alterations onto glutamatergic synapses formed at pyramidal cells, can also suggests that ErbB4 maybe not the sole mediator of NRG1.

Table 1-1 Effects of NRG1 on excitatory glutamatergic transmission in the neocortex and hippocampus

Key Reference	***Experimental paradigm***	***Brain region-cell type***	***Results on AMPAR-mediated transmission***	***Results on NMDAR -mediated transmission***
Agarwal et al., 2014	Genomic, NRG1 (all isoforms) homozygous null mutants	Hippocampus- CA1 pyramidal cells	*(rec at Vh= -70mV)* 1.sEPSCs amplitude decreased, frequency unchanged 2. mEPSCs amplitude and frequency decreased	n/a
Agarwal et al., 2014	Genomic, CRD-NRG1 (type III) over-expression	Hippocampus-CA1 pyramidal cells	*(rec at Vh= -70mV)* 1.sEPSCs amplitude and frequency unchanged	n/a
Yin et al., 2013	Genomic, NRG1 type I; over-expression	Hippocampus- CA1 pyramidal cells	*(rec at Vh= -70mV)* 1.mEPSCs amplitude unchanged; frequency decreased 2.NMDAR/AMPAR ratio of evoked EPSCs unchanged	NMDAR/AMPAR ratio of evoked EPSCs unchanged
Ting et al., 2011	Acute application of NRG1 (EGF domain of the β -type NRG1)	Neuron culture of dissociated neurons 1.Unidentified GABAergic interneurons 2. Pyramidal cells	*(rec at Vh= -65mV)* 1. mEPSCs in unidentified GABAergic interneurons; amplitude and frequency increased 2. mEPSCs in Pyramidal cells; amplitude and frequency unchanged	n/a
Abe et al., 2011	Peripheral administration (subcutaneous injection) of common core EGF domain of NRG1 β1 (eNRG1)	Frontal cortex, primary motor area 1.PV positive-Interneurons 2. Layer V pyramidal cells	*(rec at Vh= -69 mV)* 1. mEPSCs in PV interneurons; amplitude increased; frequency unchanged. Increased levels of GluA1 in cytoplasmic tissue fractions. No differences in membrane tissue fractions 2. mEPSC in layer V pyramidal cells; amplitude and frequency unchanged	GluN2A levels decreased; GluN1A and GluN2B levels unchanged in cytoplasmic fractions. No differences in membrane tissue fractions
Abe et al., 2011	Acute application of common core EGF domain of NRG1 β1 (eNRG1)	Frontal cortex primary motor area-PV positive-interneurons	*(rec at Vh= -69mV)* mEPSCs in PV interneurons; amplitude and frequency unchanged	n/a
Kato et al., 2010	Genomic NRG1 type 1 over-expression	Prefrontal cortex, hippocampus, striatum	n/a	GluN2A/B and GluN1 levels unchanged

Gu et al., 2005	Acute application of core EGF domain of NRG1 β1	Prefrontal cortex; neuron cultures and acute slices- Pyramidal cells	n/a	NMDAR evoked EPSCs amplitude decreased. GluN1 increased internalization via a clathrin/dynamin dependent pathway
Ozaki et al., 1997	Acute application of N-terminal domain of the neuregulin-β1 isoform	Cerebellum neuron cultures	n/a	GluN2C increased expression dependent on NMDAR synaptic activity
Hahn et al., 2006	Acute application of mixture of neuregulin 1β and 1α	Human prefrontal cortex post-mortem tissue and ; lysate	n/a	GluN2A decreased phosphorylation in SZ brains. GluN1 decreased recruitment via phosphotidyl inositol phospholipase C-g1 (PIPLC-g1)
Papaleo et al., 2016	Genomic human NRG1 type IV isoform over-expression	Medial prefrontal cortex 1. Layer V Pyramidal cells 2. GABAergic interneurons	*(rec at Vh= -70 mV)* 1.mEPSCs Layer V pyramidal cells ; frequency decreased, amplitude unchanged sEPSCs frequency increased 2. sEPSCs Layer V interneurons (LTS,RS and FS) frequency and amplitude unchanged but a trend for increased amplitude in FS	n/a
Stefansson et al., 2002	Genomic NRG1 type I knockout; downregulation	Forebrain	n/a	NMDAR ligand binding reduction
Newell et al., 2013	Genomic,NRG1 transmembrane domain knockout; Downregulation	Cingulate, sensory and motor cortices	n/a	NMDAR ligand binding increase
Dean et al., 2008	Genomic, NRG1 transmembrane domain knockout Downregulation	Cortex layer (I-III),striatum	n/a	NMDAR ligand binding unchanged

Luo et al., 2014	Genomic, N-terminal fragment of human NRG1 β1a over-expression	Hippocampus	n/a	GluN1 and Glun2A/2B levels reduced
Bjarnadottir et al., 2007	Genomic, NRG1 transmembrane domain knockout Downregulation	Hippocampus	n/a	GluN2B hypophosphorylated
Long et al., 2015	Genomic, NRG1 type III transmembrane domain knockout; Downregulation	Prelimbic cortex	n/a	GluN1, GluN2A/2B/2C, NR3 mRNA levels unchanged. GluN2B hypophosphorylated
Long et al., 2012	Genomic, NRG1 type III transmembrane domain knockout;Downregulation	Cingulate cortex, caudate putamen, hippocampus, dorsolateral septum, retrosplenial granular cortex	n/a	NMDAR binding unchanged
Chen et al., 2010	Acute application of core EGF domain of NRG1 β1	Hippocampus-CA1 pyramidal cells	mEPSCs frequency and amplitude unchanged	mEPSCs frequency and amplitude unchanged

Rec; recording, Vh; holding potential in whole cell patch clamp recordings, mEPSCs; miniature Excitatory Post-synaptic Currents, sEPSCs; spontaneous excitatory post-synaptic currents

1.1.2.2 Effects of NRG1 on GABAergic inhibitory neurotransmission

In the CNS fast synaptic inhibition is provided by GABAergic interneurons, releasing γ – aminobutyric acid (GABA). Even though they numerically account only for 20% (Markram et al., 2004) of the total neuronal population, their extensive local projection (one interneuron can target up to 1200 pyramidal cells) makes them powerful modulators of cortical circuits. Fast synaptic inhibition is accomplished by activation of post-synaptic $GABA_A$ receptors ($GABA_AR$), and the evoked inhibitory post-synaptic potentials (IPSPs) are often hyperpolarising by transiently shifting the post-synaptic membrane potential in a negative direction and away from the action potential firing threshold. $GABA_ARs$ are composed of five pore forming subunits, with multiple subtypes giving rise to 19 different isoforms: α1-6, β1-3, γ1-3, δ, ε, π, ρ 1-3 and θ. A functional receptor channel is composed of two α, two β, and one of either γ, δ , ε, π or Θ subunit isoforms (Schofield et al., 1987). The biophysical properties of the receptor depend on the subunit assembly (Sigel et al., 1990, Minier and Sigel, 2004). All subunit isoforms share a common structural organization, consisting of an extracellular N' terminal domain linked with 4 other domains (M1-4), which traverse the plasma membrane so that the C' terminus becomes extracellular. The M2 domain is responsible for shaping the ion pore of the $GABA_A$ receptor channel (Sigel and Steinmann, 2012).

Similar to the studies on the effects of NRG1 on excitatory transmission, investigations of its effects on GABAergic inhibition have also produced inconsistent results. For example, it has been reported that acute application of the NRG1 domain on acute brain slices increased the depolarization induced release of GABA in various brain regions including the prefrontal cortex and the amygdala, but has no effect on spontaneous GABA release, suggesting that NRG1 could interfere with presynaptic terminals (Woo et al., 2007, Chen et al., 2010, Wen et al., 2010, Abe et al., 2011, Bi et al., 2015). However, studies using cell cultures have shown that application of

NRG1 can alter the expression of $GABA_A$Rs in many ways and the effect varies in regards to the brain region and cell types examined. It was reported that treatment of cultured cerebellar granule cells with NRG1 promotes the expression of β1 $GABA_A$R subunit suggesting facilitation of GABAergic transmission (Rieff et al., 1999). On the contrary, acute application of NRG1 in the hippocampal neuron cultures was reported to decrease expression of the α $GABA_A$R subunit also leading to supressed post-synaptic GABAergic currents (Okada and Corfas, 2004). In addition, another study showed that genomic over-expression of the soluble Ig-NRG1 compromises miniature Inhibitory Post-synaptic Currents (mIPSCs) by reducing these quantal currents amplitude in the CA1 area pyramidal cells (Yin et al., 2013). However, on the contrary the over-expression of non- soluble CRD-NRG1 was found to increase the frequency of mIPSCs in the CA1 pyramidal cells, whereas down-regulation of the NRG1 (all isoforms) was reported to selectively increase the amplitude of mIPSCs in CA1 pyramidal cells without an effect on their spontaneous release frequency (Agarwal et al., 2014) suggesting pre- and post-synaptic synaptic changes respectively. However, expression of the human NRG1 type IV isoform was found not to affect the GABAergic synapse either pre- or post- synaptically in, onto layer 5 pyramidal cells (Papaleo et al., 2016).

Of note, modifications in the functionality of the ErbB4 receptor have also been reported to interfere with the GABAergic transmission. For instance, the frequency of mIPSCs in the CA1 pyramidal cells in ErbB4 null mutants was found to be decreased, whereas the IPSCs paired-pulse ratio generated by action potential-evoked GABA release remained unchanged. This suggests that activity of the ErbB4 receptor is fundamental for the maintenance and formation of the GABAegic synapse too (Fazzari et al., 2010).

Overall, these studies show that GABAergic synapses are under the control of NRG1-ErbB4 signalling in various ways, and that this may depend on the brain region and cell type as well as on the type of NRG1 variant (reviewed further in result chapter 5)

Table 1-2 summarises the results on the effects of NRG1 on the GABAergic inhibitory neurotransmission, and shows the experimental method employed as well as the brain region and the specific cell type studied.

Table 1-2 Effects of NRG1 on inhibitory transmission

Key Reference	*Experimental paradigm*	*Brain region-cell type*	*Effect on $GABA_AR$-mediated transmission*
Woo et al., 2007	Acute application of core EGF domain of NRG1 β1	Prefrontal cortex- pyramidal cells	eIPSCs amplitude increased mIPSCs unchanged
Chen et al., 2010	Acute application of core EGF domain of NRG1 β1	Hippocampus- CA1 pyramidal cells	eIPSCs amplitude increased mIPSCs frequency increased
Abe et al., 2011	Peripheral administration (subcutaneous injection) of common core EGF domain of the NRG1 β1 (eNRG1)	Frontal cortex and primary motor area	Polysynaptic eIPSCs amplitude increased, monosynaptic eIPSCs unchanged, mIPSCs unchanged
Rieff et al., 1999	Acute application of NRG1 Ig domain	Dissociated cerebellar granule cells cells	GABA-activatedcurrent amplitude increased, β1 subunit increased expression
Okada and Corfas, 2004	Acute application, NRG1 Ig domain	Hippocampal organotypic cell cultures - CA1 pyramidal cells	mIPSCs amplitude decreased $GABA_A$receptors α1 and β1 subunit expression decreased
Yin et al., 2013	Genomic NRG1 type I over-expression	Hippocampus- CA1 pyramidal cells	mIPSCs amplitude decreased but frequency not changed, α1 subunit decreased expression (forebrain lysates)
Agarwal et al., 2014	Genomic NRG1 (all isoforms) homozygous null mutants	Hippocampus- CA1 pyramidal cells	mIPSCs amplitude increased, frequency decreased
Agarwal et al., 2014	Genomic CRD-NRG1 (type III) over-expression	Hippocampus- CA1 pyramidal cells	mIPSCs amplitude unchanged but frequency increased
Papaleo et al., 2016	Genomic human NRG1 type IV isoform over-expression	Medial prefrontal cortex - layer 5 pyramidal cells	mIPSCs amplitude and frequency unchanged

eIPSCs; evoked Inhibitory Post-synaptic Currents, mIPSCs; miniature Inhibitory Postynaptic Currents

1.1.3 NRG1 as a regulator of organization and development of neuronal networks

One well known function of the NRG1-ErbB4 signalling is its involvement in the development of cortical circuits. Expression of ErbB4 mRNA in the rodent cortex starts at embryonic day 18 (E18) and reaches its peak levels at time of birth (postnatal day 0, i.e. by P0). Then, the expression gradually decreases by up to 40% of its peak levels and remains relatively constant during the adulthood (Yau et al., 2003). This suggests that ErBb4 has particularly active role during embryonic neurodevelopment.

1.1.3.1 Role of NRG1 signalling in the structural development of neuronal networks

Even though exact mechanisms of how the NRG1-ErbB4 signalling participates in the development and assembly of cortical circuits are not yet understood, it has been proposed that the signalling serves to guide ErbB4-expressing interneurons through migratory streams from ganglionic eminences of the developing cortex acting either as a chemoattractant (Flames et al., 2004), or a chemorepellant (Li et al., 2012). Indeed, disturbance in the NRG1-ErbB4 signalling pathway results in alterations in the number of GABAergic cells in the cortex. It was shown that the ErbB4 null mutant mice display reduced numbers of several interneurons populations in the hippocampus as adults (Neddens and Buonanno, 2010). Similarly, NRG1 conditional knock-out mutant mice exhibit decreased number of interneurons too, specifically in mid- and caudal cortical regions (Flames et al., 2004). Moreover, it has been demonstrated that NRG1 over-expression but not down-regulation, results in a reduced number of interneurons in the cortex including PV+ GABAergic cells (Agarwal et al., 2014).

Apart from the role of NRG1 signalling in controlling the migration of the GABAergic cells, results from various studies indicate that NRG1-ErbB4 signalling pathway can interfere with the synaptic connectivity of interneurons and pyramidal cells NRG1 most likely via activation of the ErbB4 receptors (Fazzari et al., 2010). Thus far it has been proposed that loss

of both Ig- and CRD NRG1 signalling hamper the growth of thalamocortical axons to their cortical targets in the brain (Lopez-Bendito et al., 2006). Furthermore, in a seminal study by Krivosheya and colleagues (2008), it was demonstrated that both the increased and the reduced levels of the ErbB4 receptor, as well as an acute application of NRG1 in the hippocampal cell cultures, have a direct impact on neurite growth and inhibit the maturation of both the excitatory and the inhibitory synapses onto ErbB4 expressing interneurons (Krivosheya et al., 2008).

1.1.3.2 Role of NRG1 signalling in neurophysiological features of neuronal circuits

As described above, NRG1 signalling interferes with several aspects of the organization of brain circuits such as neurotransmission mechanisms, neuronal migration and synapse maturation. Based on these findings and the possible association of this pathway with neuropsychiatric disorders such as schizophrenia, some studies have investigated a role of the NRG1 in regulation of functional aspects of the neuronal circuits focusing on synaptic plasticity and generation of co-ordinated rhythmic network activities. Hitherto, most of these studies investigating the effects of NRG1 signalling on synaptic plasticity have concentrated on the Schaffer Collateral- CA1 pathway. There is a common agreement that facilitation of the NRG1-ErbB4 signalling leads to suppression and depotentiation of long- term potentiation (LTP) in this pathway. The effects are mediated via the ErbB4 receptor in experimental models using the acute NRG1 application and in mice displaying NRG1 over-expression (Huang et al., 2000, Kwon et al., 2005, Bjarnadottir et al., 2007, Kwon et al., 2008, Pitcher et al., 2008, Agarwal et al., 2014). Notably, in the study conducted by Agarwal and colleagues it was reported that both CRD-NRG1 over-expressing mice and hypomorphic NRG1-Ig animals display similar decrease in the induction and the maintenance of Schaffer Collateral (SC) LTP in the CA1 area. These findings again show that both the gain and the loss of NRG1 signalling have detrimental effects on synaptic function. However, in another study where the levels of NRG1-Ig were genomically

elevated, it was reported that LTP was unaffected (Deakin et al., 2012). Thus, there are again some discrepancies between the studies.

It is important to consider that the effects of alterations of the NRG1 signalling could be probably subject to distinct experimental conditions, such as genomic or acute interventions, the signalling loss or gain of function, the specific NRG1 isoform used in the studies, the brain region and cell types. Yet, even though the precise effects of the NRG1 signalling in the brain are not fully understood, the existing studies suggest that bidirectional modifications of this pathway can strongly interfere with maturation of neuronal networks. This indicates an inverted "U" mode-of-action so that both hyper- and hypoactivity of the NRG1 signalling lead to abnormal cortical wiring.

In the following sections I will discuss recent evidence for an association of the NRG1 with schizophrenia pathogenesis.

1.2 NRG1 and its relevance to schizophrenia

Schizophrenia is a complex neuropsychiatric disorder affecting 0.7% of the world population (McGrath et al., 2008). It is characterised by cognitive, emotional and perception disturbances. Traditionally, its clinical diagnosis is based on three broad categories classified as positive, negative and cognitive symptoms. The positive symptoms are associated with the psychotic features including delusions and hallucinations. The negative symptoms include flat emotions, reduction in motivation and impaired speech. The cognitive symptomatology is associated with social withdrawal and cognitive impairment such as learning and memory deficits.

Like most psychiatric disorders, schizophrenia diagnosis relies on symptoms and not on biological markers. It is currently based on criteria listed by the World Health Organization

(WHO) International Classification of Diseases (ICD) or the American Psychiatric Association's Diagnostic and Statistical Manual of Mental Disorders (DSM). Even though these guidelines provide tools for a valid clinical diagnosis, the clinical symptomatology and treatment outcomes vary significantly among patients. This has led to the assumption that schizophrenia as a clinical phenotype embodies a number of different underlying pathogenic mechanisms giving rise to a similar clinical manifestation. In accordance with this, to date no single causal genetic mutations associated with schizophrenia have been identified. Given that heritability estimates of the disorder range between 65 and 80% (Sullivan et al., 2003, Lichtenstein et al., 2009), research efforts have instead mostly been focused on the identification of genetic variations that constitute at risk genetic loci, such as single nucleotide polymorphisms (SNPs) and copy number variants (CNVs). More than 100 such "genetic risk factors" have already been connected to schizophrenia pathogenesis. Therefore, it is likely that this mental disorder may depend on combinatorial effects of several genetic loci in a patients' genome, which even if they differ in their biological effects, can increase the likelihood for the disease development in a synergistic way.

1.2.1 Neurobiology of schizophrenia

Nowadays, it is widely accepted that schizophrenia is a neurodevelopmental disorder (Rapoport et al., 2012) and that the illness manifestation is an outcome of altered brain development processes resulting in alterations in the function of brain neuronal networks. Even though exact understanding of the pathology is still lacking, recent advances in biobehavorial research methods have led to several neuroanatomical and physiological discoveries correlating with the disorder's clinical manifestations especially in brain areas associated with information encoding and processing such as the prefrontal cortex and hippocampus.

The dopaminergic system is one of the first circuits in the brain that was suspected to be involved in schizophrenia (Carlsson, 1977). It has been hypothesised that hypofunction of the

mesocortical dopaminergic system could underlie the emergence of the negative and the cognitive symptomatology, whereas hyperfunction of the mesolimbic dopaminergic pathway is probably responsible for processes leading to psychosis and other positive symptoms (Weinberger, 1987, Davis et al., 1991). These implications of the dopamine system, especially regarding the psychosis, are further supported by the antipsychotic effects mediated by antagonism of dopamine receptors (Delay et al., 1952). However, it is possible that disturbances of the dopaminergic signalling are secondary to the glutamatergic and the GABAergic systems dysfunction, eventually leading to subcortical dysregulation of dopaminergic neurons and dopamine release (Howes and Kapur, 2009). Indeed, both these neurotransmission systems and their interactions have been implicated in the disease pathology, giving rise to the glutamatergic and the GABAergic hypotheses of the schizophrenia respectively.

The glutamatergic hypothesis of schizophrenia originates from the observation that use or abuse of NMDAR antagonists such as ketamine and phencyclidine can trigger psychotic episodes in humans, similar to those observed in diagnosed patients (Javitt and Zukin, 1991, Krystal et al., 1994). Currently, disturbances of the NMDAR neurotransmission, particularly in GABAergic interneurons, are supposed to substantially contribute to the pathogenic mechanism of the disease (Lisman et al., 2008). Studies using transgenic mouse lines with selective ablation of NMDARs in GABAergic neurons expressing PV have been demonstrated to generate behavioural phenotypes similar to schizophrenia (Belforte et al., 2010, Korotkova et al., 2010). However, the idea that the NMDAR hypofunction solely in PV+ cells generates the disease phenotypes of schizophrenia has recently been challenged. Instead, it has been proposed that NMDAR hypofunction in PV+ cells render brain networks more prone to exhibit the schizophrenia-associated behavioural and electrophysiological alterations, and the actual phenotypes only occur when NMDAR hypofunction co-exists in other neuron types (Bygrave et

al., 2016). This implies that the disease pathogenesis could emerge from deficits in neurotransmission in several neuron types.

Furthermore, apart from the changes influencing the activation of GABAergic cells, increasing evidence also implies deficits in the GABAergic signalling *(The GABAergic hypothesis)*, for a comprehensive review see (Lewis, 2014, Gonzalez-Burgos et al., 2015). In support of this hypothesis, *post mortem* analyses of brains from schizophrenic patients have been shown to exhibit reduced levels of the 67 kDa isoform of glutamate decarboxylase (GAD-67), the primary enzyme mediating GABA-synthesis and the GABA transporter 1 (GAT-1) which is responsible for GABA reuptake from the synaptic cleft upon its release (Volk et al., 2000, Volk et al., 2001). In addition, the expression levels of certain interneuron-specific neuronal markers such as the calcium binding protein PV, are reduced in schizophrenic subjects (Hashimoto et al., 2003). These changes imply altered inhibitory output from these cells in the patients. Hence, it follows that the excitation/inhibition balance is disrupted in cortical circuits compromising normal brain operations by possibly altering the temporal precision of action potential firing in neuronal circuits.

The coordinated firing activity of neurons manifests as brain oscillations commonly observed as periodic fluctuations of the local field potential (LFP). The neuronal processes underlying the LFP oscillations are considered to perform information encoding and processing including, data transfer, packing and unpacking for higher-order brain functions such as sensory perception and cognition (Lisman and Buzsaki, 2008). It is expected that pathological changes affecting the mechanisms of network firing and synchronization, observed as altered oscillations, could be connected to the impaired cognition in the schizophrenia. The association between schizophrenia and the brain oscillations has been investigated mainly in connection with gamma (i.e. 30-80 Hz) and theta (i.e. 5-12 Hz) frequency rhythms.

Indeed, both electroencephalography (EEG) and magnetoencephalography (MEG) recordings have shown that the power and synchrony of gamma band oscillations are reduced in schizophrenia patients compared to healthy control individuals (Kwon et al., 1999, Haig et al., 2000, Spencer et al., 2003, Sun et al., 2013). Furthermore, the overall synchrony of the theta frequency oscillations across cortical regions and its power have also been found to be impaired in schizophrenia patients in particular during working memory behavioural tasks (Schmiedt et al., 2005, Berger et al., 2016)

Although complex neurobiological alterations are associated with the disease and potentially contribute to the disease pathogenesis, it is still challenging to explain the pathophysiology of schizophrenia in order to improve treatments. One interesting hypothesis that can recapitulate some of the above findings and could therefore represent a general pathophysiological process underlying the disease, is that a consortium of risk factors leads to alterations in NMDAR neurotransmission in interneurons and the temporal coordination of their GABA release. This, in turn could lead to aberrant spike timing of the cortical neurons, the aberrant neuronal synchronization and finally the altered oscillations in the cortical circuits. In turn this could also lead to neuron's disinhibition which may result to the dopamine dysregulation in the subcortical areas (Lisman et al., 2008).

1.2.2 NRG1 signalling is a susceptibility disease pathway to schizophrenia

The *NRG1* gene was first implicated in schizophrenia following a linkage disequilibrium study in Icelandic patients with a specific haplotype (HAP_{ICE}) significantly associated with the disease (Stefansson et al., 2002). This study identified an increased burden of single nucleotide polymorphisms in the 5' regulatory gene region raising the likelihood that altered levels of the NRG1 protein, rather than the protein structural functionality, could confer an increased risk for the disease pathogenesis. Nevertheless, in the recent genome-wide association study (GWAS)

for schizophrenia by the (Schizophrenia Working Group of the Psychiatric Genomics, 2014), NRG1 SNPs did not meet genome-wide significance ($P= 5 \times 10^{-8}$). Even though, this study is supposed to be the most comprehensive genetic analysis performed in order to understand schizophrenia, it has divided opinions of how to interpret GWAS in the field of complex neuropsychiatric disorders. A number of experts in the field have argued that this type of study provides a clear standard and can reveal real associations between the risk genetic loci and the false positives. Thus, the absence of NRG1 variant signal in this investigation may challenge its relevance to the disease. Yet, care must be taken when interpreting genome-wide studies, since the use of a single statistical threshold to declare significance can often miss the detection of rare genetic variants or loci with high nucleotide variations. Indeed a genetic study in an Australian cohort of schizophrenic patients performed by Weickert and colleagues (2012), demonstrated that the 5' upstream regions of the NRG1 gene had an unusual high nucleotide diversity when compared to other human genetic loci (75 in total), and importantly this diversity was significantly higher in patients with schizophrenia. This finding led to the hypothesis that the NRG1 gene intronic and regulatory regions are genetically highly unstable and prone to the genetic changes that, if accumulated to an individual's proband, can still contribute to the disease pathogenesis (Weickert et al., 2012). Thus, considering this, from a statistical and biological standpoint, it is possible that the high allelic heterogeneity of the genetic locus reflects an unstable genomic region susceptible to a genetic change with deleterious effects on the regulation of gene expression and at the same time can explain the loss of the statistical significance in the GWAS studies (Mostaid et al., 2016).

Furthermore, it should be noted that genetic association and expression studies have also identified the NRG1 receptor ErbB4 as a candidate gene for the disease pathogenesis (Silberberg et al., 2006, Law et al., 2007, Walsh et al., 2008). Even though, it is not clear how genetic

variation of the NRG1 pathway confers the susceptibility for the disease, several studies have proposed that NRG1 hypersignalling is likely to be responsible. This hypothesis is corroborated by the finding that NRG1 type 1 mRNA levels were increased in the prefrontal cortex and the hippocampus in *post mortem* studies of the brains of individuals with schizophrenia (Hashimoto et al., 2004, Law et al., 2006). It has also been found that this increase is regulated by SNPs located in the 5' regulatory gene region. Importantly, the NRG1 mRNA elevation is accompanied by increased NRG1 protein levels as well (Chong et al., 2008, Weickert et al., 2012). However, some studies have not been able to replicate the above findings and instead have reported unchanged or even reduced levels of NRG1 in schizophrenic patients. (Hahn et al., 2006, Boer et al., 2009, Parlapani et al., 2010).

Recently, it has been demonstrated how bidirectional changes in the NRG1 signalling can affect brain physiology. Indeed, studies in both over-expressing and hypomorphic NRG1 animals have consistently reported deficits in behavioural responses associated with the disorder. These include changes in the Prepulse Inhibition (PPI) of the startle reflex- an assessment of sensorimotor gating linked to schizophrenia- (Braff et al., 1978, Swerdlow et al., 2008) and impaired performance in working memory-related tasks (Stefansson et al., 2002, Chen et al., 2008, Deakin et al., 2009, Deakin et al., 2012, Yin et al., 2013, Agarwal et al., 2014, Luo et al., 2014). Different interpretations of the pathophysiology of mouse behavioural phenotypes have been put forward. On balance, the findings reviewed in this section demonstrate prominent effects of the NRG1 signalling upon cortical circuits involved in higher brain functions, such as prefrontal cortex and hippocampus.

In summary, although there is no a clear consensus regarding the association between NRG1 and schizophrenia, the involvement of NRG1 in the development of excitatory and inhibitory neurotransmission suggests that disruption of its signalling could lead to complex

neuropathological conditions. Thus the investigation of NRG1 signalling not only provides useful information on the development of neural circuits, but may also facilitate the understanding of diseases in which these circuits become awry during development.

In this thesis, the effects of NRG1 over-expression are studied in the hippocampal circuitry, which is responsible for mediating higher brain functions. In the following paragraphs, I provide an overview of cytoarchitecture of the hippocampal formation, its cellular physiology and its oscillatory activity.

1.3 The hippocampal formation

The hippocampal formation is a brain structure located in the temporal lobe. It is subdivided in different interconnected regions that together constitute a functional unit. The main regions are: dentate gyrus (DG) and the "hippocampus proper" (HPC) which is further subdivided to *Cornu Ammonis* (CA) 1-3 areas, subiculum (Sub), presubiculum (PrS), parasubiculum (PaS) and entorhinal cortex (EC) (Amaral and Witter, 1989). In this thesis the term hippocampus refers to the DG and the "hippocampus proper" together.

1.3.1 Cytoarchitecture of hippocampal formation and functional connectivity

In a simplistic schematic, the excitatory glutamatergic principal cells of the regions and areas are connected via unidirectional pathways. The main glutamatergic cells of the DG (granule cells) receive prominent excitatory synaptic inputs from the layer II of the EC *(perforant pathway)* (Steward, 1976). In turn their axons project to the hippocampal proper CA3 area and constitute the hippocampal mossy fibres (Claiborne et al., 1986). In succession, the CA3 pyramidal cells form collateral projections *(Schaffer collaterals)* (Ishizuka et al., 1990) to the CA1 area. Further to this trisynaptic pathway (EC→ DG→CA3→ CA1), the CA1 pyramidal cells project to various brain regions and predominantly to subicular principal cells, that in turn send their axons back to the infragranular layers of the EC, closing this EC-hippocampal

synaptic loop (Swanson et al., 1978). In addition, further excitatory connections have been described in the EC-hippocampal circuitry including direct projection of the EC layer III to the CA1 area *(temporoamonic pathway)* (Amaral, 1993). Furthermore, other main connections include a) the associational interconnection of the CA3 pyramidal cells (Schaffer, 1892), b) the disynaptic excitatory loop between granule and mossy cells in the DG (Jackson and Scharfman, 1996), and c) the commisular projections of the mossy and the CA3 pyramidal cells to the same areas of the contralateral hippocampus (Amaral and Witter, 1989). All these hippocampal regions have laminar organization of neurons .Specifically, the CA1-3 regions are divided into the following laminae (listed from superficial to deeper layers): a) *Alveus* (Alv), which is a region consisting mainly of white matter and axon collaterals of the principal neurons, b) *Stratum oriens* (s.o) where mainly axon collaterals and basal dendrites of the pyramidal cells are located, c) *Stratum pyramidale* (s.p) in which pyramidal cell and some interneuron cell bodies are densely packed, d) *Stratum radiatum* (s.r) with distinct radial appearance emerging mainly from pyramidal cells apical dendrites e) *Stratum lacunosum-moleculare* (s.l-m), which also contains the distal apical dendrites of pyramidal cells and axonal projections of the temporoamonic pathway. In addition, the, *stratum lucidum* (s.l) is located between s.p and s.r of the CA3 area, delineating the termination of the mossy fibers (Amaral and Witter, 1989).

Importantly, firing activity of the principal cells is under the control of a wide variety of GABAergic interneurons found virtually in all hippocampal strata. Many distinct types of GABAergic interneurons exist in the hippocampus, and they synaptically target specific subcellular domains of the pyramidal cells. The GABAergic cells exhibit cell type-specific firing activity during hippocampal network activities. Thus, distinct pyramidal cell subcellular compartments receive GABAergic input from specific interneuron types at specific time points during network activities providing spatiotemporal GABAergic inhibitory control of these cells

(Klausberger and Somogyi, 2008). This spatiotemporal control is critical for the physiological neuronal activity flow through the hippocampal pathways and the different hippocampal regions. It regulates the spatial arrangement and the temporal dynamics of the discharging glutamatergic principal cells during various network oscillations, which support distinct brain states and are therefore critical in the hippocampal processes of encoding, transmitting and storing neuronal information. These oscillations are thought to represent the synchronous activity of the neurons and are associated with higher brain functions such as working memory function (Lisman and Buzsaki, 2008, Buzsaki, 2015). The hippocampal circuits are complex and contain a great diversity of specialised interneuron types. Most of the detailed knowledge of the hippocampal interneuron types comes from studies in the CA1 area. The cell type classification is based on anatomical, neurochemical and physiological features of these cells. So far, more than 20 different types of GABAergic interneurons have been described in the CA1 area (Klausberger and Somogyi, 2008). Many of the types described in CA1 are also found in the CA3 region whereas some are region-specific.

1.3.1.1 Structural classification of hippocampal interneurons

Axon and dendritic arborisation of GABAergic interneurons provides important information of how the synaptic inputs and their inhibitory outputs are organised in the hippocampus. According to the axonal arborisation, two broad categories of interneurons can be characterized: 1) *Perisomatic targeting* and 2) *Dendrite targeting interneurons*. The first category includes interneurons that synaptically innervate predominantly or exclusively the somatic region of principal cells, the very proximal dendrites or the axon initial segment. Given that the perisomatic region is the subcellular domain for synaptic inputs integration from all different cell domains, this population of afferent inhibitory interneurons strongly regulates the output of their target post-synaptic pyramidal cells and controls the occurrence and the timing

of the pyramidal cells action potentials. Interestingly, a specific cell type of this category, which exclusively targets only the axon initial segment of pyramidal cells, the *axo-axonic cell* (AACs) (Somogyi et al., 1983), can have depolarizing effects in certain conditions (Szabadics et al., 2006, Woodruff et al., 2010). Therefore, it has been suggested that AACs could occasionally have an excitatory rather than inhibitory post-synaptic effects on their target pyramidal cells, challenging the concept that GABAergic interneurons are always inhibitory.

The other major cell type of this category is the *basket cell* (BSc). Basket cells form synapses mainly in the soma and proximal dendrites of the pyramidal neurons. They are further neurochemically subdivided to PV-positive BSc and CCK-positive BSc cells (Freund and Buzsaki, 1996) which also differ significantly in their functional properties such as action potential kinetics, firing frequency and control of GABA release from their synapses (see section 1.3.1.3) . All the aforementioned cell types are found both in the CA1 and the CA3 areas.

Cells belonging to the dendrite targeting category provide inhibition to the dendritic tree, which is also the location where most of the excitatory synaptic connections are located. Hence, activity of these afferent interneurons mainly influence the excitatory inputs efficiency to the pyramidal cells. Common interneuron types in this category are: The *oriens-lacunosum-moleculare cell* (O-LM) with axon arborisation mainly in *lacunosum moleculare*. These interneurons receive excitation from the pyramidal cells axon collaterals in the s.o and they target these cell dendrites in s.l-m (Lacaille et al., 1987). Dendrite-targeting cells that send their axons to both s.o and s.r include the *bistratified cell* (BisC) (Buhl et al., 1994) and in the CA1 area the *ivy cell* (Fuentealba et al., 2008, Armstrong et al., 2012, Somogyi et al., 2012) In the same category, cells with their axon mainly in s.l-m, (although it can also spread into s.r) include the *lacunosum moleculare perforant pathway associated cell* (LM-PP) (Hajos and Mody, 1997) (Vida et al., 1998) and neurogliaform cell (NGC) (Cajal, 1922, Armstrong et al., 2012) .

Besides, these two major categories of GABAergic cells, there are two further distinct classes of interneurons that have specific neuronal targets. The first is a group of GABAergic cells that exclusively innervate other interneurons: the *Interneunon - specific interneuron*s (ISI) (Acsady et al., 1996, Gulyas et al., 1996) and they are further subdivided to three types (ISI I-III), according to their neurochemical profile. Their distinct anatomical morphology and innervation pattern indicates that these cells participate in other interneurons activity synchronization, and in parallel provide disinhibition to pyramidal cells. The second group includes GABAergic interneurons that in addition to their local inhibitory circuitry in the hippocampus, project their axons outside the hippocampus. Hence these GABAergic cells are referred to as *"projection GABAergic cells"* or *"long range interneurons"*. For example, one cell type in this group is the *hippocampo -septal cell* (HS). Somata of these cells are located in the s.r. of the CA1 and CA3 areas or in s.l. and s.r. of the CA3 area of the hippocampus. Their axon makes local ramification in the hippocampus in various laminar layers and projects though the septo-hippocampal axis to both pyramidal cells (mainly in subiculum) to and other GABAergic interneurons (mainly in medial septum) (Gulyas et al., 2003). Hence, the HS cells provide coincident inhibition in its target neurons all along the septo-hippocampal axis and thus they are supposed to play crucial role in the generation of theta band activity. Finally, it is important to note that GABAergic synaptic connections exist between many hippocampal interneuron types, although their exact innervation densities and patterns are not well known. It has been estimated that at least 10% of GABAergic axon terminals form synapses onto other local hippocampal interneurons (Sik et al., 1995, Cobb et al., 1997, Kohus et al., 2016). Importantly, it is expected that the interneuron-interneuron connections between the common GABAergic cells contribute to hippocampal network activity synchronization and thus oscillations, but as stated above these connections are still poorly understood.

Given that most of GABAergic interneurons receive excitatory inputs from the local pyramidal cells and from glutamatergic neurons in different hippocampal areas as well from various extrahippocampal areas, while in turn provide local inhibition, to their cellular targets, it is assumed that they provide inhibition both in a “feedforward” and “feedback fashion. However, some specialised interneurons operate exclusively in one way. A classic example of a GABAergic interneuron operating predominantly in feedback inhibition is the O-LM cells that as mentioned receive excitation from the pyramidal cells axon collaterals in the s.o and provide GABAergic output to these cell dendrites in s.l-m. On the contrary, NGC cells are considered predominantly feedforward interneurons, since they probably receive most of their input from EC and correspondingly inhibit neurons in very local fashion. Similarly I-SI cells, provide their inhibition in a feedforward fashion, since they receive excitation from local CA pyramids, but possibly project exclusively to other interneurons.

1.3.1.2 Neurochemical classification of hippocampal interneurons

Many hippocampal GABAergic interneuron types with specialised anatomical features also exhibit specific combination of neurochemical markers. Common markers analysed in interneurons include calcium binding proteins such as parvalbumin (PV), calretinin (CR) and calbindin (CB),neuropeptides including the neuropeptide Y (NPY) or vasoactive intestinal peptide (VIP) and peptide hormones like somatostatin (SST) and cholecystokinin (CCK) (Somogyi and Klausberger, 2005). Hence, the specific neurochemical profile of an interneuron is commonly used along to its structure to identify cell type. A good example is BCs cells. Even though the two BC types show largely similar axon arborisation in the hippocampal layers, they differ in their neurochemical profile by either expressing PV or CCK, the latter co-expressing with cannabinoid receptor type 1 (CB_1R) (Marsicano et al., 1999, Katona et al., 2009, Glickfeld and Scanziani, 2006). In addition, various hippocampal GABAergic cell types show

characteristic combination of specific neuronal markers according to their anatomical structure. For instance, PV is also expressed in AACs, O-LM and BisC, but SST is expressed only in the latter two, and NPY is only found in BisCs (Somogyi and Klausberger, 2005). Thus, specific combination of the neurochemical markers can be reliably used in the classification of the GABAergic cells.

1.3.1.3 Functional classification of hippocampal interneurons

In order to better understand the role of distinct GABAergic cell types in the activity of neuronal networks, analysis of their physiological properties is also needed. Certain neurophysiological features characterise specific interneuron subpopulations. These include intrinsic neuronal properties such as the action potential kinetics and firing pattern. In this regard the two type of BCs serve again as a good example: It has been shown that PV+ BCs display faster membrane time constants than CCK+ BCs, making them fast integrators of the excitatory synaptic inputs that they receive. One the other hand, slower constants of the CCK+ BCs enables them to integrate synaptic inputs over larger time windows (Glickfeld and Scanziani, 2006). Furthermore, the PV + cells, when depolarized display high frequency "fast" non-accommodating action potentials firing (Kawaguchi et al., 1987, Szabo et al., 2010). In contrast, in the CCK+ BCs the action potential firing pattern is clearly slower and shows firing frequency accommodation termed as "regular" (Pawelzik et al., 2002, Szabo et al., 2010). Moreover, the GABAergic output from the two BC types differs. The PV + BCs cells provide temporally accurate and stable inhibition with high probability of post-synaptic IPSCs and often shows depressing IPSCs during repetitive activity (Hefft and Jonas, 2005, Glickfeld and Scanziani, 2006). On the contrary, the CCK+ BCs generate "fluctuating" IPSC amplitudes in post-synaptic pyramidal cell meaning that the evoked IPSCs strength substantially varies between different events. In addition, the evoked post-synaptic IPSCs exhibit less time precise temporal accuracy

and to generate asynchronous neurotransmitter release (Hefft and Jonas, 2005, Glickfeld and Scanziani, 2006, Daw et al., 2009, Ali and Todorova, 2010). It has also been reported that the two types of BCs differ in their post-synaptic $GABA_A$Rs subunit composition in pyramidal cells. The PV BCs are forming synapses with alpha1 subunit-containing receptors (Klausberger et al., 2002), whereas receptor channels in CCK+ BC synapses on pyramidal cells have alpha2 subunits (Nyiri et al., 2001). The different composition of $GABA_A$Rs has been associated with the receptors' distinct biophysical properties. The $GABA_A$Rs containing the alpha1 subunit show lower affinity to GABA, slower IPSC rise time and faster IPSC decay time than the alpha2 containing receptor channels (Lavoie et al., 1997). Importantly the two different BCs types also differ in the timing of their firing during specific hippocampal oscillations such as gamma-, theta- and sharp wave ripple (SWR) activity episodes, and therefore probably have distinct roles in shaping the firing activity of pyramidal cells in these rhythmic activity patterns (Klausberger et al., 2005, Lasztoczi et al., 2011).

Although specific functional features of most hippocampal interneurons are far less known, several characteristics like the short membrane time constants, the fast spiking feature and non-acccomodating action potentials, as well as the IPSC features are consistently seen in PV expressing neurons and therefore serve as additional identification features for this interneuron subpopulation (Buhl et al., 1996, Pawelzik et al., 2002, Hu et al., 2014). In addition, the longer membrane time constant, the regular and accommodating action potential firing pattern and asynchronous mode of GABAergic release, commonly characterise GABAergic interneurons with CCK expression (Pawelzik et al., 2002, Daw et al., 2009, Ali and Todorova, 2010, Calvigioni et al., 2016, Kohus et al., 2016).

In summary, the classification of different interneuron types can rely on the anatomical, neurochemical and functional criteria and usually follows a combination of them.

1.3.1.4 Hippocampal theta rhythm and sharp wave ripples

Brain "rhythms" are oscillations observed in the LFP when neuronal networks generate co-ordinated synchronous activity of neurons. Hippocampal oscillatory activity comprises various distinct patterns, known as theta (4-12 Hz), gamma (25-30 Hz *low range* and 80-120 Hz *high range*) and Sharp Wave Ripples (SWRs) (110-200 Hz) (Buzsaki et al., 1983, Bragin et al., 1995). These distinct activity forms are taking place during specific brain states and are generated by the interplay of the excitatory glutamatergic principal cells and the GABAergic interneurons.

Theta oscillations are mainly observed during exploratory behaviours and rapid eye movement sleep (REM) (Colgin, 2013). Although exact mechanisms for its rhythmogenesis are not fully understood, it is known that this type of synchronous activity heavily depends on the medial septum GABAergic input, which presumably acts as a theta frequency pacemaker in the hippocampal networks (Freund and Antal, 1988, Varga et al., 2008) and defines the timing of firing in some hippocampal interneurons (Lapray et al., 2012, Katona et al., 2014).

Importantly, it has been reported that during exploratory behaviour of an animal, its spatial location trajectory is represented by the successive sequential firing of CA1 pyramidal cells. These pyramidal cells are known as "place cells", since they are specifically activated at a particular locus in the tract called a "place field". Spiking of combination of place cells occurs at a particular phase of a LFP theta oscillation cycle when the animals moves in the tract, and spiking for each place cell occurs progressively earlier as the animal comes closer to its specific place field. This phenomenon, termed as phase precession and is thought to be the culprit of the neural representation of navigation maps in the brain (O'Keefe and Recce, 1993). Notably, similar sequential pattern of place cell firing is repeated during REM-phase sleep, and it has been proposed that during this theta rhythm activity, consolidation of memory engrams is taking

place (Louie and Wilson, 2001, Manns et al., 2007). When the animal changes to inactive behaviours, such as waking immobility, and when the Rapid Eye Movement (REM)-sleep shifts to slow-wave non-REM sleep, SWRs activity patterns start taking place. The SWR activity is generated by the hippocampal circuitry by the co-ordinated discharge of the local GABAergic interneurons independent of glutamatergic extrahippocampal inputs (Kubota et al., 2003).

Interestingly, it has been shown that during, SWRs most of the hippocampal pyramidal cells are silenced due to the strong GABAergic input they receive from the active perisomatic -targeting inhibitory interneurons (English et al., 2014). However, despite the "general inhibition of pyramidal cells during SWRs episodes, it has been shown that few pyramidal cells are active and their firing follows the sequential firing of the place cells during previous sessions of active exploration (Wilson and McNaughton, 1994, Kudrimoti et al., 1999, Lee and Wilson, 2002, Karlsson and Frank, 2009). One likely explanation for this replay of place cell firing during SWRs, is that during the earlier behaviours, selected synapses of pyramidal cells mainly comprising "place cells" are becoming sufficiently potentiated during theta periods and as a result they surmount this inhibitory tone during SWRs and fire action potentials. Thus, the physiological roles of the SWR replay have been hypothesised to be the spatial memory consolidation, the retrieval of earlier memory representations but also the future planning of yet unexplored spatial trajectories (Siapas and Wilson, 1998, Girardeau et al., 2009, Nakashiba et al., 2009, Dupret et al., 2010).

1.3.1.5 Hippocampal gamma oscillations

Gamma oscillations occur in multiple cortical areas including the hippocampus and are often nested in the theta activity (Bragin et al., 1995). In the hippocampus, there are two major types of gamma activity; the slow range (25-30Hz) and fast (80-120 Hz) originating from distinct inputs. It has been suggested that the slow gamma predominantly emerges intrinsically in the

CA1 area, whereas the fast gamma generation requires excitatory input from the entorhinal cortex (Colgin et al., 2009). However, in both situations current views argue that their generation depends on the interplay between the local excitatory and the inhibitory neurons (Buzsaki and Wang, 2012) and up to date, various interneuron types expressing either PV or CCK have been shown to associate their firing to gamma oscillations LFP (Tukker et al., 2007).

Two hypotheses on the mechanism of patterned hippocampal gamma oscillations have been proposed. The first theory suggests that the gamma oscillations mainly arise when reciprocally silenced interneurons synchronise their firing through tonic or sustained excitation provided by the activity of cholinergic or glutamatergic metabotropic receptors *(Interneuron Network Gamma, ING model)* (Whittington et al., 2000). The second theory proposes that the sustained excitation of pyramidal cells and their mutual disynaptic inhibition through interneurons mediate the emergence of gamma cycles *(Pyramidal Interneuron Network Gamma, PING model)* (Oren et al., 2006, Oren et al., 2010).

Despite the fact that the mechanisms underlying gamma oscillations are not fully understood and the possibility that both models can be valid in different brain circuits, current experimental evidence supports that at least in hippocampus, the gamma rhythms emerge from a PING like mechanism (further reviewed in chapter 6). It has also been proposed that the two types of gamma oscillations (i.e fast and slow) may be involved in distinct situations and different brain functions. Fast gamma, driven by the entrorhinal input, can be associated with encoding recent spatial information concerning current location of an animal (Brun et al., 2002, Fyhn et al., 2004), whereas the intrinsic slow gamma rhythms could mainly have a role in memory retrieval processes (Brun et al., 2002, Steffenach et al., 2002). Indeed it has been recently shown that place cells firing at a given place field is preferentially shaped by theta-nested fast gamma oscillations (Bieri et al., 2014, Lasztoczi and Klausberger, 2016). On the

other hand, it has been shown that the firing of place cells is influenced by slow gamma before the animal's entrance to the centre of their preferred place field (Bieri et al., 2014). Together, these findings suggest that the two types of gamma might indeed serve different processes involved in spatial memory and differentially coordinate the spatial coding modes of the place cells. Namely, fast gamma supports encoding of the current spatial information, whereas slow gamma could enable retrieval and prediction of the spatial information of upcoming locations (Bieri et al., 2014, Colgin, 2016)

Deficits in the spatio-temporal structure of hippocampal gamma oscillations may account for the schizophrenia related cognitive deficits. Given that emergence of the gamma oscillations is the outcome of the interplay between interneurons and pyramidal cells (PC→ IN→ PC), elucidation of possible neurobiological alterations compromising the functional precision of their interaction could be particularly informative for the understanding of the aberrant oscillations and the impaired working memory performance, associated with schizophrenia symptomatology. Therefore, in this thesis I will explore possible neurobiological alterations associated with NRG1 dysregulation with a focus on the synaptic interaction between hippocampal pyramidal cells and specific GABAergic interneurons.

1.4 Context and objectives of this thesis

1.4.1 Context of thesis

Earlier research has provided evidence that dysregulation of NRG1 signalling, and in particular increased NRG1 type I levels in the brain, are associated with schizophrenia (see section 1.2.2). To study the neurobiological impact of the NRG1 level up-regulation, specific approaches including different transgenic mice lines have been employed. Here, the effects of NRG1 dysregulation are studied in a mouse strain that overexpresses specifically the type 1 of NRG1. In this transgenic mouse strain the neuronal NRG1 type I β1α isoform is selectively

expressed in various areas of the brain under the neuronal Thy 1.2 promoter, ($NRG1^{tg\text{-}type\text{-}I}$ mice) (Michailov et al., 2004) with the transgene construct expression beginning at postnatal day 6-10 (P6-10) (Caroni, 1997). *In situ* hybridization analysis has shown that the NRG1 type 1 mRNA over-expression is observed in most of cortical areas including the hippocampus and certain midbrain nuclei with no clear over-expression in the striatum or the cerebellum. The levels of the NRG1 type 1 mRNA were estimated to be 8-10 fold higher in the $NRG1^{tg\text{-}type\text{-}I}$ mice than in wild type littermates (WT)(Deakin et al., 2009).

The previously-published behavioural phenotypes include: a) Increased pre-pulse inhibition (PPI) of the startle reflex, b) Locomotor hyperactivity observed in aged animals (12 months old) and c) Age-emergent impairment in the hippocampus-dependent spatial working memory tests (10 months old) (Deakin et al., 2009, Deakin et al., 2012). From a neurobiological perspective, it has also been reported that acute hippocampal slices from the $NRG1^{tg\text{-}type\text{-}I}$ mice exhibit reduced carbachol induced gamma oscillatory frequency (Deakin et al., 2012) but no changes in the magnitude of LTP in the CA3 to CA1 glutamatergic pathway. Of great importance were the research findings that glutamatergic transmission is impaired at the level of NMDA receptors in PV+ basket cells, but not in the pyramidal cells of the CA3 area (Nissen, 2012). This finding is in line with my hypothesis here that NRG1 type I exerts its effects mainly through ErbB4 receptors that are selectively expressed in specific types of interneurons.

As it has been discussed in section 1.2.1, the most prominent hypothesis for schizophrenia pathogenesis include perturbation of the *GABAergic, glutamatergic and dopaminergic* neurotransmission. Given the multifactorial nature of the disease, it is unlikely that a single risk gene could account for the whole spectrum of neurobiological changes and the following symptoms seen in the full disease phenotype. From that perspective, transgenic mouse lines carrying genomic alterations associated with schizophrenia, such the one used in the current

study, can only reveal specific neurophysiological effects of a single risk factor. Previous studies, consistent with the *glutamatergic hypothesis* for schizophrenia, have observed hypofunction of NMDAR receptors in hippocampal PV basket positive interneurons in NRG1$^{tg\text{-}type\text{-}I}$ mice. On the contrary, it was demonstrated that GABA mediated synaptic inhibition remained unaffected, suggesting that alterations of the hippocampal circuitry could be a product of impaired excitation of at least this interneuron sub-group. Given that the coordinated hippocampal activity is thought to dependent on the recruitment of GABAergic interneurons (see 1.3.1.5), the presence of interneuron specific alterations due to NRG1 signalling dysregulation, could result in altered circuitry rhythmogenesis. A hypothesis that was confirmed by the reported alterations of pharmacologically induced gamma activity in slices from NRG1$^{tg\text{-}type\text{-}I}$ mice. Since cognitive processes, such as working memory, are supported by gamma band oscillations (see 1.2.1), it would be predicted that such activity disturbances could lead to cognitive deficits, a core clinical manifestation of schizophrenia. Indeed, a series of behavioural tests have established that these mice exhibit age emergent working memory impairment. In Summary, these findings demonstrate that the NRG1$^{tg\text{-}type\text{-}I}$ mice, display synaptic alterations originating from impairment of glutamatergic neurotransmission, with consequences in cortical circuitry operations and cognitive functions, which are closely associated with our current understanding for schizophrenia symptomatology and pathogenesis (Figure 1-2).

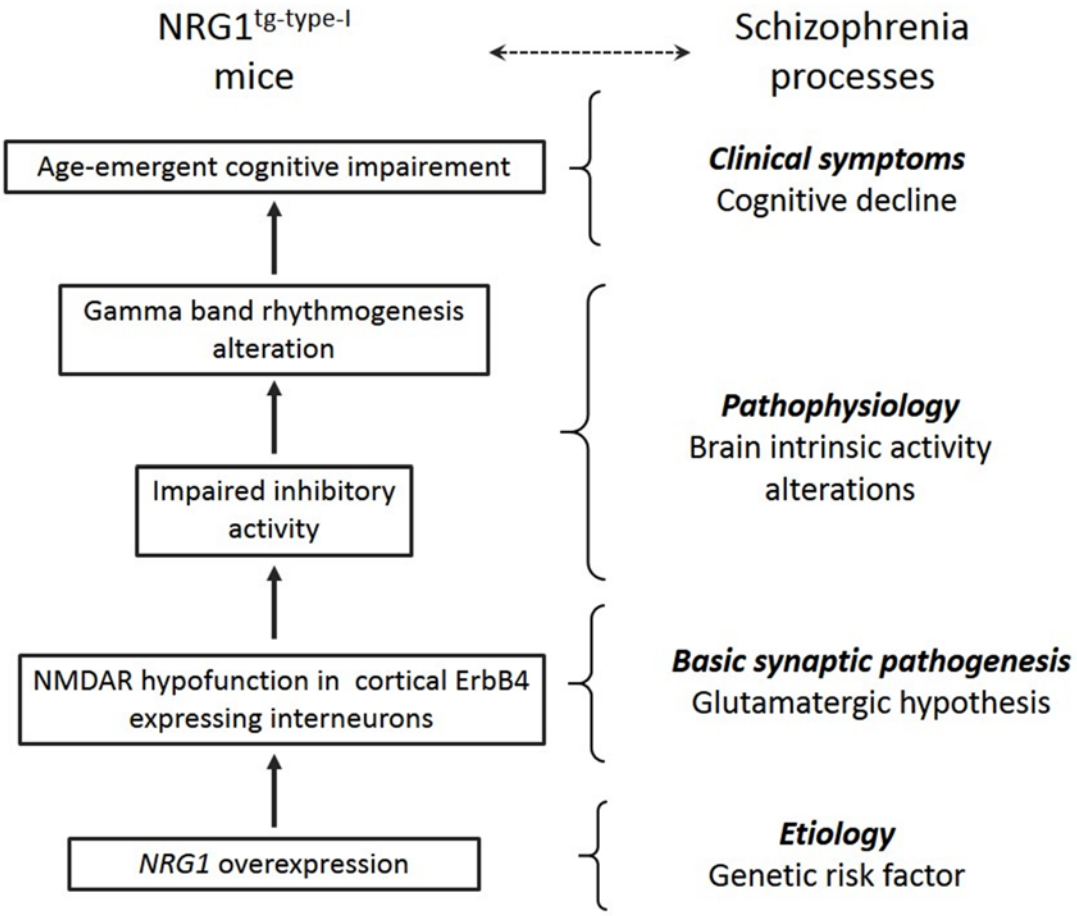

Figure 1-2. A schematic representation illustrating a potential link between basic synaptic NMDA receptor hypofunction in cortical inhibitory neurons, brains intrinsic activity as well as cognitive symptoms, caused by *NRG1* overexpression, highlighting a potential relevance to key features of schizophrenia. According to the current hypothesis genetic overexpression of NRG1 produce a decrease of NMDAR function in interneurons expressing the ErBb4 receptor (such as PV positive cells). This reduction in glutamatergic neurotransmission induces changes in GABA inhibitory activity and results in gamma oscillation disturbance giving rise to impairments in working memory.

The earlier findings of a schizophrenia-like endophenotype, altered gamma rhythmogenesis as well synaptic dysfunction in PV+ basket cells due to NRG1 over-expression inspired the further examination of the effects of the NRG1 type I over-expression on the cellular and synaptic function, with a particular focus on its effects on CCK+ interneurons. In the framework of NRG1 signalling and schizophrenia pathogenesis, these neurons are of particular interest. Firstly, they express the main NRG1 receptor, ErbB4, a fact that renders them a prime cellular target of this signalling pathway and secondly they constitute a major component of the endocannabinoid neuromodulation system via the CB1Rs, which are particularly enriched in their axons. The importance of the latter, comes from the suspected perturbation of the endocannabinoid system in schizophrenia and the use of cannabis as a contributing factor for eliciting psychotic symptoms in individuals, for recent reviews see; Manseau et al., 2015, Volk et al., 2016 but see Ksir et al., 2016. In the brain, CB1Rs are activated by endogenous cannabinoids, such as arachinodyl ethanolamide (anandamine) and 2-arachinodyl glycerol (2-AG) released from post synaptic pyramidal cells, as well as by the major psychoactive component of cannabis, the (2)-trans-Δ^9-tetrahydrocannabinol (THC) (Matsuda et al., 1990, Devane et al., 1992, Mechoulam et al., 1995, Sugiura et al., 1995) leading to the suppression of the output of these cells (Pitler and Alger, 1992, 1994, Wilson and Nicoll, 2001). Given that, CCK+ cells regulate the activity of their post-synaptic pyramidal cells as well as of PV+ interneurons, the non-physiologically regulated activation of CB1R due to exogenous THC can compromise the normal recruitment of GABAergic inhibition and alter rhythmogenesis (Skosnik et al., 2016). Therefore, focusing on the CCK+ expressing neuronal population, could reveal the cellular specific alterations mediated by a schizophrenia risk gene and whether it constitutes a convergence point in terms of dysfunctional inhibition, emerging from two separate risk factors.

1.4.2 Aims of thesis

The aims of this thesis are to identify whether the NRG1 type I over-expression is associated with neurobiological changes of ErbB4-expressing interneurons in hippocampus as well as to uncover any potential changes in both excitatory inputs and inhibitory outputs in a major population of ErbB4 expressing hippocampal interneurons that express CCK. Finally, it attempts to explain how changes in the synaptic neurotransmission in these neurons could affect their interaction with pyramidal cells and the generation of hippocampal gamma oscillations. Below, specific aims of the thesis chapters are listed together with the relevant experimental details.

Chapter 3 aims to establish the expression profile of the ErbB4 receptor in hippocampal interneurons in WT and in the mice over-expressing the NRG1 type I. In addition, it examines whether the NRG1 over-expression is associated with alterations in the density of ErbB4 immunopositive hippocampal neurons. For this, immunocytochemical analysis of the ErbB4 expression for interneurons expressing either PV or CCK in the $NRG1^{tg\text{-}type\text{-}I}$ and the WT animals was performed.

Chapter 4 aims to reveal whether the NRG1 over-expression effects the excitatory input onto CCK+ interneurons. Both stimulus-evoked and the spontaneous quantal release of glutamate neurotransmission are compared between $NRG1^{tg\text{-}type\text{-}I}$ and WT mice.

Chapter 5 examines whether the increased levels of NRG1 type I alters the function of the GABAergic synapses from CCK+ cells. Selective optical stimulation of opsin-expressing CCK+ cell axons was used to examime the synaptic input onto pyramidal cells in NRG1 transgenic mice and WT littermates.

Chapter 6 investigates whether the feedback inhibition loop, a key mechanism for generation of hippocampal gamma oscillations, is altered in the NRG1 over-expressing mice.

This is achieved by the selective photostimulation of glutamatergic fibres at low gamma frequency while recording post-synaptic EPSCs and disynaptic IPSCs in pyramidal cells.

In the final chapter, *Chapter 7*, the overall research outcomes of this thesis are discussed and interpreted in the light of a schizophrenia like endophenotype.

The overall aims in the context of the hypothesis for schizophrenia pathogenesis are outlined in the Figure 1-3 below.

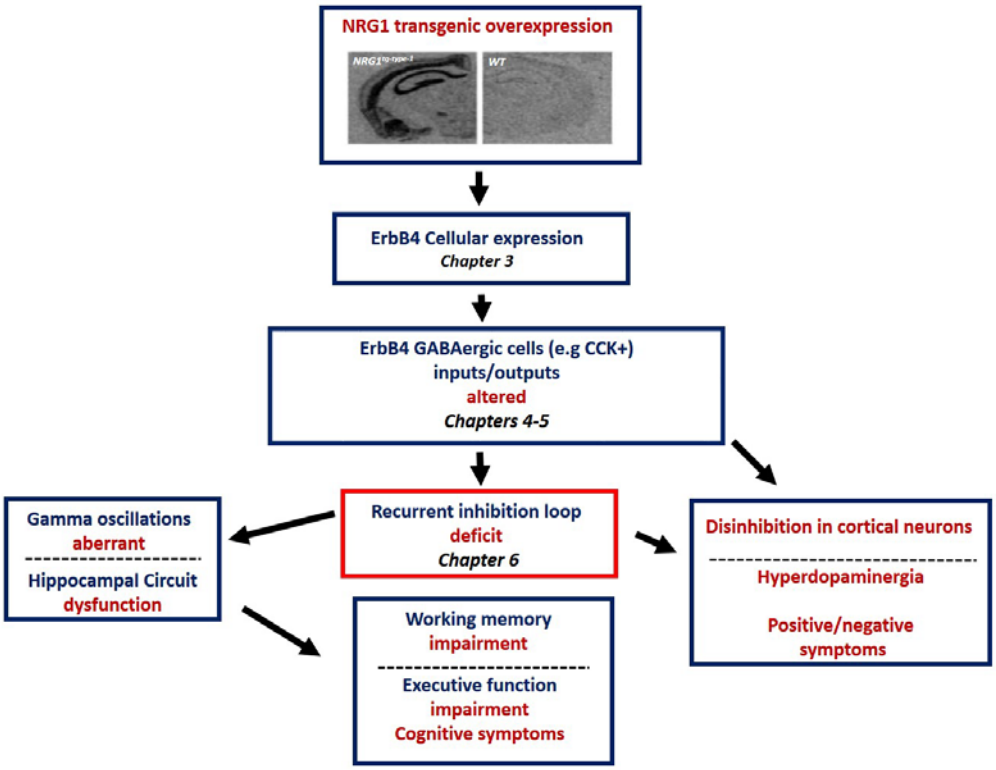

Figure 1-3. A simplified schematic showing the main aims of this thesis in the context of a hypothesised interaction between the NRG1 and neuronal networks, possibly generating a schizophrenia pathogenic mechanism. Mimicking the increased NRG1 levels in schizophrenia patients, the NRG1 over-expression occurs in various brain regions including the hippocampus. Upper panel: In situ hybridization for NRG1 type 1 mRNA in the NRG1$^{tg\text{-}type\text{-}1}$ (left) and the WT mice brain (right) (Deakin et al., 2009). Immunocytochemical analysis reveals cellular targets of NRG1 showing ErbB4 receptor-expressing cells (chapter 3). NRG1 is involved in the regulation of neurotransmitter systems, hence dysregulation of the NRG1 signalling could directly affect the excitatory input and inhibitory output of ErBb4+ interneurons such as CCK+ GABAergic cells (chapter 4-5). Synaptic interplay between the INs and pyramidal cell generates hippocampal gamma rhythms via the recurrent inhibitory loop. It's expected that alterations in this synaptic circuit can produce deficits (chapter 6) in gamma oscillations and in higher hippocampus-dependent brain functions (e.g working memory, executive function), both of which are features included in cognitive symptomatology of schizophrenia. The altered function of the interneurons could also contribute to subcortical disinhibition and hypodopaminergia underlying the schizophrenia negative and the positive symptoms. Blue: Multilevel-neurophysiological interactions that participate in the neural network operations and the cognitive processes, Red: Possible, pathogenetic cascade resulting in a range of schizophrenia-associated features.

2 Methods and materials

2.1 Experimental animals and ethics

In this study, multiple mouse lines have been used according to the desired experimental design. The experimental procedures were performed in compliance with the UK Home Office (scientific procedures) Act (1986) and the guidelines of the University of Oxford with personal licence stipulations. The experimental animals were kept in same gender cages at groups of 2-6 or in isolation. The animals had *ad libidum* access to food and water and were on a 12 hour dark-light cycle at 22 ± 1°C.

2.1.1 Transgenic neuregulin 1 type I over-expressing mice (NRG1$^{tg\text{-}type\text{-}I}$)

Mice over-expressing neuregulin 1 type β1a isoform (NRG1$^{tg\text{-}type\text{-}I}$ mice) were initially generated as described previously (Michailov et al., 2004). The construct containing multiple copies of *NRG1 type 1* DNA to be expressed under the Thy 1.2 promoter was injected in fertilized oocytes. Heterozygous male mice for the transgene from the original founder line transgene were donated by Prof. Klaus Nave (Max-Planck-Institute for Molecular Medicine, Göttingen, Germany).We then backrossed them with WT C57BL/6J female mice (Harlan, UK) in the Oxford. Only, heterozygous transgenic mice were used for breeding because the homozygous NRG1$^{tg\text{-}type\text{-}I}$ genotype is lethal. The heterozygous mice were further crossed with different -Cre mouse lines as described in section 2.1.2. Experiments were performed in 2-6 month-old heterozygous mice carrying the construct for the *NRG1 type 1* and in wild type littermates. Mice of both sexes were used in the experiments. The NRG1 mutant mice exhibit 8-10 times increase in the levels of the NRG1 type I mRNA while the construct expression under the Thy 2.1 promoter starts during first postnatal week (Deakin et al., 2009). Heterozygous NRG1$^{tg\text{-}type\text{-}I}$ mice develop a movement related tremor ‘shaking’, caused by peripheral over myelination. Typically this becomes visible after 2 weeks of age. Previous genotyping for the detection of the over-

expression of the NRG1 type I transgene in heterozygous mice in the lab have showed a 100% correlation between the observed phenotype ('shaking' or not) and the revealed genotype ($NRG1^{tg\text{-}type\text{-}I}$ or WT). Therefore in this study the animals were exclusively phenotyped.

2.1.2 Cre-mouse lines

During this study the following mouse strains were crossbred with $NRG1^{tg\text{-}type\text{-}I}$ mice for experimental procedures.

- PV-Cre $^{+/+}$ mice (The Jackson Laboratory, B6;129P2-Pvalbtm1[cre]Arbr/J; stock number: 008069) or PV-Cre $^{+/+}$ crossbred with $Ai9^{+/+}$ mice (The Jackson Laboratory, B6.Cg-Gt[ROSA]26Sortm9[CAG-tdTomato]Hze/J; stock number: 007909), PV-Cre $^{+/-}$; $Ai9^{+/+}$ mice to turn out tdTomato expression in PV+ cells, and were subsequently crossed with heterozygous $NRG1^{tg\text{-}type\text{-}I}$ males. Littermates of this breeding as well as from the crossing of $NRG1^{tg\text{-}type\text{-}I}$ heterozygous males with WT C57BL/6J female mice were used for whole cell patch clamp recordings of a) stimulus-evoked mediated EPSCs and glutamatergic quantal currents, from distinct neurons in hippocampal slices (chapter 4), b) Immunocytochemical and western blot analysis of ErbB4 receptor expression (chapter 3).
- Heterozygous CCK-Cre mice (BAC-CCK-$Cre^{+/-}$) females (Geibel et al., 2014) generously donated by Dr Liliana Minichielo and were crossed with heterozygous $NRG1^{tg\text{-}type\text{-}I}$ males. Offsprings of this breeding were used for light evoked IPSCs (chapter 5).
- CaMKII-$Cre^{+/+}$ mice (The Jackson laboratory, B6.Cg-Tg [Camk2a-cre]T29-1Stl/J; stock number: 005359,) were crossbred with male $NRG1^{tg\text{-}type\text{-}I+/-}$ mice. Littermates were used for whole cell recordings of light-evoked EPSCs/disynaptic IPSCs (chapter 6).

2.2 Hippocampal slice preparation

Mice were anaesthetized with intraperitoneal injection of pentobarbitone sodium (20% w/v, dosage 0.2 mg/g; Pharmasol, Andover UK). Anaesthetised mice were decapitated when their breathing rate was depressed approximately to 1 breath per second and the pedal reflex responses had ceased. The brain was rapidly removed and immersed in ice cold (0-4°C) cutting solution (Table 2.1) bubbled with 95 % O_2 and 5% CO_2 gas mixture. The cerebellum and olfactory bulb were excised and discarded. To obtain transverse slices from the ventral hippocampus, the dorsal site of the neocortex was gently flattened to generate a flat surface. The brain was then glued to a microtome plate from the dorsal site using cyanoacrylate adhesive. Brain slices were cut from the brain block at a caudal-ventral axis direction to produce transverse slices of ventral and mid-ventral hippocampus. To obtain slices from the dorsal hippocampus the two brain hemispheres were separated instead and the two hippocampi were glued at the level of prefrontal cortex therefore coronal slices were obtained.

In both approaches, slices from left and right hemispheres were used. Thickness of the slices was set to 250 μm using a HM650V vibrating microtome (Carl Zeiss AG, Oberkochen, Germany). The slices were immersed in cutting solution at 32°C with constant bubbling of 95% O_2 and CO_2 gas mixture for about 20 minutes to allow their metabolic recovery. Next, slices were transferred and kept at least for 1 hour before recordings in an interface storage chamber that contained oxygenated (as above with 95% O_2 and CO_2 gas mixture) Earle's balanced salt solution (EBSS) (Invitrogen, Paisley, UK) supplemented with 3 mM $MgCl_2$, 1 mM $CaCl_2$ and 27 mM glucose (Table 2-1), at room temperature (20-24 °C).

Table 2-1 Solutions for preparation, storage and recording of hippocampal slices

	Compound	Concentration
Cutting and recovery solution	Sucrose	75 mM
	NaCl	87 mM
	KCl	2.5 mM
	$MgCl_2$	7 mM
	$CaCl_2$	0.5 mM
	$NaHCO_3$	25 mM
	NaH_2PO_4	1.0 mM
	Glucose	25 mM
	pH	7.2
	Osmolality	295-300 mOsm/L
Storage interface chamber solution	EBSS *containing*	
	NaCl	117.2 mM
	KCl	5.33 mM
	NaH_2PO_4	1.01 mM
	$NaHCO_3$	26.19 mM
	D- Glucose	5.56 mM
	Supplemented with	
	$MgCl_2$	3 mM
	$CaCl_2$	1 mM
	Glucose	27 mM
	pH	7.2
	Osmolality	290-295 mOsm/L
Recording solution (aCSF)	NaCl	119 mM
	KCl	2.5 mM
	$MgSO_4$	1.3 mM
	$CaCl_2$	2.5 mM
	NaH_2PO_4	1.25 mM
	$NaHCO_3$	25 mM
	Glucose	11 mM
	pH	7.2
	Osmolality	290-295 mOsm/L

All solutions were equilibrated with 95% O_2 and 5% CO_2 with continuous gassing. For experiments the slices were stored in aCSF at room temperature (22-24°C).

2.3 Pharmacological compounds used in the study

The drugs used in this study were applied via a superfusion system in the recording chamber. All pharmacological compounds were first prepared as stock solutions, stored in a freezer (-20°C), and finally diluted to the recording solution on the day of the experiment. Details of the drugs including their dilution ratios from stock solutions are listed below in Table 2-2.

Table 2-2 Pharmacological compounds used in this study

Drug	nomenclature	supplier	Target biological activity	Stock solution	Final concentration
DL-AP5	DL-2-amino-5-phosphonopentanoic acid	Ascent Scientific, UK	NMDAR antagonist	100 mM in 100 mM NaOH (in ddH_2O)	100 μM
CGP55845	(2S)-3-[[(1S)-1-(3,4-Dichlorophenyl)ethyl] amino-2-hydroxypropyl] (phenylmethyl) phosphinic acid hydrochloride	Tocris Bioscience, Bristol, UK	GABA-B receptor antagonist	1 mM in DMSO	1 μM
KN-62	4-[(2S)-2-[(5-isoquinolinylsulfonyl) methylamino]-3-oxo-3-(4-phenyl-1-piperazinyl) propyl] phenyl isoquinoline sulfonic acid ester	Tocris Bioscience, Bristol, UK	Cell-permeable inhibitor of CaM kinase II	3 mM in DMSO	3 μM
MCPG	(RS)-α-Methyl-4-carboxyphenylglycine disodium salt	Tocris Bioscience, Bristol, UK	Group I mGlu Receptor antagonist	100 mM in NaOH	200 μM
NBQX	2,3-Dioxo-6-nitro-1,2,3,4-tetrahydrobenzo[f] quinoxaline-7-sulfonamide disodium salt	Abcam Biochemicals, Cambridge, UK or Sigma Aldrich, UK	AMPA/ kainate Receptor antagonist	25 mM in ddH_2O	25 μM
Picrotoxin (PiTX)	1:1 mixture of picrotoxinin and picrotin	Tocris Bioscience, Bristol, UK	GABA-A receptor antagonist	50 mM in ethanol	100 μM
Tetrodotoxin (TTX)	Octahydro-12-(hydroxymethyl)-2-imino-5,9:7,10adimethano-10aH-[1,3]dioxocino[6,5-d]pyrimidine-4,7,10,11,12-pentol + citrate buffer	Abcam Biochemicals, Cambridge, UK	Na+ voltage-dependent channel selective inhibitor	1 mM in ddH_2O	1 μM

DMSO: Dimethyl sulfoxide; ddH_2O: double distilled water

2.4 Electrophysiological recordings

Whole-cell recordings in hippocampal slices were performed in a submerged recording chamber (Luigs & Neumann, Ratingen, Germany and mounted at the stage of a BX51WI (Olympus, Southend, UK) upright microscope equipped with a 20× immersion objective with 2× and 4× zooms reaching up to a 80× magnification. Hippocampal areas and cells were visualized with a differential interference contrast-infrared system (DIC-IR) (Luigs & Neumann, Ratingen, Germany and a CCD video camera (Till Photonics, Gräfelfing, Germany). Brain slices were continuously superfused with oxygenated (95% O_2 with CO_2 mixture) aCSF (Table 2-1) using a closed pump- driven circuit (Watson- Marlow, Falmouth, UK) at a rate of (4-8 ml/min) at 28-30 °C. Slices were held firm in the chamber using a horseshoe-shaped platinum harp slice grid. Recording electrodes were pulled from borosilicate glass capillaries (GC150F-10, Harvard Apparatus, Edenbridge, UK), with a P-97 horizontal microelectrode puller (model, Sutter Instrument Co., Novato, CA, USA).

Whole-cell clamp recordings were established following formation of gigaseal (>1 GΩ) between the pipette tip and cell membrane. Recordings were started 5 minutes after breaking into to whole-cell from the gigaseal. Electrophysiological signals were recorded with a Multiclamp 700B amplifier (Molecular Devices, Sunnyvale, CA, USA) and low-pass filtered at 4 kHz with built-in Bessel-filter. The electrical inputs were digitized at 10 or 20 kHz with a Digidata 1400 interface and acquired with a Clampex software version 10.2 (Molecular devices, Sunnyvale, CA, USA). The intracellular solution (for details see Table 2-3) was supplemented with 0.3% neurobiotin (Vector Laboratories, Burlingame, CA, USA) to allow *post-hoc* cell visualizations and structure analysis. Following the whole-cell recordings, the recording electrode was gently retracted from the patched cell, and the slice was placed in an interface

storage chamber or in some cases kept in the recording chamber for at least 30 min (but less than 1 h) in order to enable the adequate diffusion of neurobiotin inside the cell.

Finally, slices containing the recorded neurobiotin-filled cells were immersed in fixative solution containing 4% paraformaldehyde, 15% picric acid and 15 % glutaraldehyde (unless stated otherwise). Access resistance (Ra) during whole-cell recordings was constantly monitored throughout the experiments with 10 or 7 mV/5ms seal test pulses in the voltage-clamp mode (Ogden 1994), and not compensated. Of note the Ra values reported in the result chapters are probably overestimated, because of step current distortion during signal acquisition filtering. For whole-cell recordings experiments, two different pipette filling solutions were used. Details of the solutions are given in the Table 2-3 below. Caesium-based filling solutions were used for electrically evoked and miniature EPSC recordings (chapter 4) as well for the light-evoked EPSCs and disynaptic IPSCs (chapter 6), in order to block K^+ conductance and reduce membrane leak currents. In the recordings of light-evoked IPSCs (chapter 5), K^+ -based solution was used to ensure physiological intracellular ionic conditions.

Table 2-3 Intracellular solutions

Intracellular solution type	Composition		Experimental paradigm
Cs-Methanesulphonate -based	Cs-Methanesulphonate	145 mM	-Electrical stimulation-evoked EPSCs (chapter 4) -Miniature EPSCs (mEPSCs) (chapter 4) -Light stimulation-evoked EPSCs and disynaptic IPSCs (chapter 6)
	HEPES	20 mM	
	CsOH	10 mM	
	NaCl	8 mM	
	Mg-ATP	2 mM	
	Na-GTP	0.3 mM	
	QX-314 bromide	5 mM	
	Neurobiotin	0.3 % (w/v)	
	pH	7.2	
	Osmolality	295-300 mOsm/L	
K-gluconate -based)	K-gluconate	145 mM	-Light stimulation-evoked minimal optical IPSCs (chapter 5)
	NaCl	8 mM	
	HEPES	25 mM	
	Mg-ATP	2 mM	
	Na-GTP	0.2 mM	
	KOH-EGTA	0.2 mM	
	QX-314 bromide	5 mM	
	Neurobiotin	0.3 % (w/v)	
	pH	7.2	
	Osmolality	295-300 mOsm/L	

2.4.1 Electrical stimulation-evoked excitatory post-synaptic currents

Excitatory post-synaptic currents (EPSCs) were elicited by focal stimulation with a concentric tungsten bipolar stimulus electrode. Stimuli (50-100 μs) were applied through a current stimulus isolator (50-300 μA) delivered every 15s and triggered by the Clampex software (Molecular devices, Sunnyvale, CA, USA). The stimulation electrode was placed in the CA3 area *stratum oriens* (s.o) aiming to activate associative and commissural fibres (see experiments studying the ratio of the NMDA- and AMPA receptor-mediated EPSCs in chapter 4) Details on the intracellular solution used in the recordings are listed shown in Table 2-3. Whole-cell patches were performed from visually identified somata. Pharmacologically isolated AMPAR-mediated

EPSCs (in continuous presence of GABA-A and -B receptor blockers PiTX-100 µM and CGP55845 1-µM) were recorded in voltage-clamp mode at -60 mV. Following the blockade of AMPA/kainate receptors with NBQX (25 µM), the NMDAR EPSCs were measured at various membrane potentials from -20 till +50 mV, and I-V relation for the NMDAR component currents was made in this range using a linear fitting of the regression curve with the NMDAR EPSC amplitudes. Values for the NMDAR-mediated current component was taken from the regression curve at +40 mV above the NMDAR EPSC reversal potential (E_{NMDAR}). This allowed comparison of NMDAR-component amplitudes similarly at +40 mv from E_{NMDAR} in individual neurons. AMPA EPSC amplitude estimate was determined as an average of AMPA- EPSCs peak amplitudes at -60 mV. Monosynaptic component of AMPAR EPSCs was visually verified. Recordings of both the AMPAR and NMDAR-mediated currents were post-hoc low passed filtered at 1kHz.

2.4.2 Miniature excitatory post-synaptic currents

Spontaneous miniature EPSCs (mEPSCs) were recorded from cells in ventral CA3 s.r or at its border with s.l or s.l-m . Whole-cell voltage clamp recordings were performed in the continuous presence of PiTX (100 µM) and CGP55845 (1 µM) to block GABAergic transmission, and TTX (1 µM) the action potential blocker, allowing only recordings of spontaneous glutamatergic release mediated events. Cells were first clamped at -65mV and miniature Excitatory Post-Synaptic currents (mEPSC) were recorded for at least 2 minutes. At this holding potential all events were presumed to be AMPA receptor-mediated. Following blockage of AMPA and kainate receptors by wash-in of NBQX (25 µM), the cells were clamped at +40mV to record NMDA receptor-mediated mEPSCs for at least 2 minutes. Finally, to confirm the NMDA receptor origin of the currents at +40 mV, the antagonist DL-AP5 (100 µM) was bath applied. Recordings were *post-hoc* band pass filtered (4Hz- 5kHz). Detection criteria

for AMPAR-mediated mEPSCs were: minimum amplitude; 5 pA in a 0.5-100 ms time window, with noise rejection of 0.5 ms. For the NMDAR mEPSCs the criteria were: minimum amplitude; 7 pA in a 0.8-200 ms time window, with noise rejection of 0.8 ms.

2.4.3 Light stimulation-evoked inhibitory post-synaptic currents

Optogenetically elicited inhibitory post-synaptic currents (IPSCs) recordings (chapter 5) were carried out in coronal slices from NRG1 over-expressing mice and their WT littermates. For these experiments mice were from the breeding line of BAC-CCK-Cre$^{+/-}$ crossed with NRG1$^{tg\text{-}type\text{-}I}$ mice and were injected with an adeno-associated virus serotype 2 or 5 (AAV2/5)-ChR2-eYFP to express channelrhodopsin (ChR2) and enhanced yellow fluorescent protein (eYFP) in a Cre dependent manner in CCK+ expressing neurons (for details in *in vivo* injections see section 2.5). Slice preparation, storage and recordings were performed under minimal ambient light conditions to avoid random ChR2 photo activation. Hippocampal slices from mice were screened for ChR2-eYFP neuronal expression under an epifluorescence microscope (Leica DM5000B, Wetzlar, Germany) equipped with a CCD camera (ORCA-ER, Hamamatsu Photonics K.K., Iwata, Japan) and appropriate eYFP filter sets (excitation: 450-490nm; emission: 515-565 nm; beam splitter: 510 nm; Leica, Wetzlar, Germany). Slices that displayed clear expression of eYFP in the CA3 area, were selected and stored in the interface chamber for experiments. Putative pyramidal cell somata inside the s.p of the ventral hippocampal CA3 were whole-cell clamped at 0 mV to ensure a strong driving force for Cl^- and Inhibitory Post Synaptic Currents (IPSCs) were isolated with NBQX (25 μM) and DL-AP5 (100 μM). Excitation of ChR2 (excitation 450 ± 25 nm) -expressing presynaptic fibres was achieved by blue laser light (473 nm) using a standard 'Endow GFP/EGFP band-pass filter set' (#41017, excitation: HQ470/40x; beam splitter: Q495LP; emission: HQ525/50m; Chroma, Bellows Falls, VT, USA). A blue light spot of 20-80 μm diameter (achieved by a 113 or 400 μm fibre light guide for laser–microscope

coupling; Rapp OptoElectronic, Hamburg, Germany) was systematically moved along the s.p. or at its borders to a site where ChR2 photostimulation reliably elicited IPSCs post-synaptically. Next, the intensity (nominal laser maximal output power 100 mW) of the laser was adjusted accordingly either to a value that was just above the threshold to elicit ideally the activation of a single or few CCK+ cell axons i.e (Minimal optical stimulation-MOS) approach, or to constantly and reproducibly elicit IPSCs in the post-synaptic cell. The IPSCs were measured by delivering two 50 ms intermittent light pulses (paired pulses) every 15s. Recordings were *post hoc* low passed (1 kHz) filtered and the light evoked IPSCs were visually verified from the background noise.

2.4.4 Light stimulation-evoked EPSCs and disynaptic IPSCs

The experiments on the light elicited EPSCs and disynaptic IPSCs (chapter 7) were performed from hippocampal slices from littermates of the breeding line CaMKII-Cre$^{+/-}$ crossed with NRG1$^{tg\text{-}type\text{-}I}$ (see section 2.1.2) which were first transfected with (AAV2/5)-ChR2-eYFP to express channelrhodopsin and eYFP in a Cre dependent manner in pyramidal cells (for details in *in vivo* injections see section 2.5). Slice preparation, selection of slices for experiments, and their storage was carried as explained previously in section 2.4.3, with the exception that the slices were stored and recorded in the presence of CAMKII inhibitor (KN-62, 3 μM) and the blocker of group I metabotrobic glutamate receptors (MCPG, 200 μM) to inhibit long term plasticity effects by repetitive glutamatergic fibre stimulation (Lamsa et al., 2007). An 80 μm diameter blue laser spot achieved by a 400 μm cross sectional fibre light guide (technical specifications as in 2.4.2) was positioned inside s.p or at its borders with s.r or s.o. The CA3 area was surgically separated from the CA1 region making a cut between the areas with a razor blade to supress generation of polysynaptic activity in the CA3 area by antidromic stimulation, and its propagation to the CA1 area. Pyramidal cell somata in the dorsal hippocampal s.p of CA1 area

were whole-cell patch clamped. During the whole cell recording, five successive 473 nm laser light-pulses at 20 Hz (of 3 ms long, 50 ms interval) were delivered. Light-stimulation evoked disynaptic IPSCs were recorded at measured reversal potential for EPSCs (E_{EPSCs}) The evoked EPSCs were recorded at -70 mV. Post-synaptic cell voltage-clamp potential was alternated and the stimuli (a barrage of 5 pulses at 20 Hz) for the IPSCs and the EPSCs were applied in an interleaved manner clamping the post-synaptic cell either at E_{EPSCs} or at -70 mV. Stable baseline of the EPSCs and IPSCs were obtained for at least 5 minutes. The IPSC and the EPSC total charges were measured in 500 ms time window from train stimulation -induced post-synaptic current onset. Finally to explore the contribution of NMDARs in the disynaptic inhibition, the NMDA blocker DL-AP5 (100 µM) was applied via superfusion.

2.5 *In vivo* injection of Adeno-associated viral constructs

2.5.1 Adeno-associated viral constructs

In order to generate precisely timed action potential firing of specific molecularly defined neuron subpopulations in this study, the viral targeting of opsins into Cre-recombinase expressing mice was employed. In brief, this methodological tool relies on the insertion of double-floxed inverse opsin vector into an adeno-associated virus. Upon injection of the viral particles in to the brain, only cells that express the Cre-recombinase will recognise the LoxP sites flanking the opsin and the fluorophore genes. Thus, activation of the Cre-LoxP system leads to expression of the light activating opsins and eYFP fluorophore in specific defined cell types (see 2.1.2). According to the experimental paradigm two Cre-mice lines have been employed (see 2.4.3, 2.4.4). In this study the adeno- associated virus serotype 2 or 5 construct carrying fusion genes for ChR2 and eYFP (AAV2/5: ChR2-eYFP) (vector sequence: pAAV-EF1a-sCreDIO hChR2(H134R)-EYFP-WPRE, Vector Core Services, Gene Therapy Centre Virus, University of North Carolina, USA) was used. The vector contained the double-floxed open

reading frame (DIO) for the ChR2-eYFP fusion protein, whose expression was driven under the EF-1a (elongation factor-1a) promoter and increased by WPRE: (woodchuck hepatitis B post-transcriptional regulatory element). The viral particle suspension (titre ± 4 x 10^{12}/mL) was stereotaxically injected into either dorsal or ventral hippocampus in Cre-recombinase expressing mice crossed with NRG1$^{tg\text{-}type\text{-}I}$ (see section 2.1.2).

2.5.2 Stereotaxic injections of AAV-constructs in the hippocampus

The AAV2/5:ChR2-eYFP particle suspension was stereotactically injected into the ventral CA3 area of heterozygous BAC-CCK-Cre$^{+/-}$/ NRG1$^{tg\text{-}type\text{-}I}$ and WT littermates at the following stereotaxic coordinates: 2.70 mm caudal, 2.75 mm lateral from bregma and at 3.60 mm, 3.40 mm and 2.60 mm depth from the brain surface. Stereotaxic injections into the dorsal hippocampus CA1 area of heterozygous CAMKIIa/ NRG1$^{tg\text{-}type\text{-}I}$ and WT littermates, were performed with the following coordinates: 1.70 mm caudal, 1.40 lateral from bregma and at 1.60 mm, 1.40mm and 1.20 mm depth from the brain surface. All injections were performed in 1.5-2 month old mice as follows: Animals were first anaesthetised with 4% isoflurane applied at a rate of 1-1.5 ml/min and placed to the surgical stereotaxic frame (Model 1900; Kopf Instruments, California, USA). The head was secured with non-invasive ear bars, and ocular lubricant (Allergan, Marlow, UK) was applied. The scalp was shaved with electric clippers, and the operative field was disinfected with iodine solution, whereupon 5% lidocaine ointment was locally applied on the area. Animal's breathing was monitored by eye as an indicator of depth of anaesthesia. When the breathing rate was stable and slowed down to 0.5 - 1 breaths per second, perioperative analgesia was administered with buprenorphine (0.1mg/Kg; Vetergesic, Alstoe Animal Health, York, UK). Under a surgical stereoscope (Wild Heerbrugg M655, Gais, Switzerland) the cranium was exposed by a sagittal, 5-7 mm incision tailing the middle line expanding from bregma to lambda. Using the stereotaxic arm, the injection coordinates were

determined and a craniotomy was performed with a microtorque drill. Then, a 33-gauge needle attached to a Hamilton Microlitre Syringe (UK) was placed to the appropriate stereotaxic coordinates as detailed earlier in this paragraph. A total volume of 800 nL of virus suspension was injected in the hippocampus of each hemispheres with a rate of 80 nL/min and using an automatic motorised pump driven syringe (Ultra Microsyringe pump/ Micro4 controller; World Precision instruments, Sarasota, FL, USA). Injections at the specific depths were performed by firstly injecting at the deepest site 300 nL of the virus suspension. After 2 minutes wait, in order to enable diffusion of the viral suspension in the injected locus, the needle was retracted by 0.2mm reaching the next injection site where 300 nL of the virus suspension were injected again. Following 2 further minutes wait, the needle was lifted again by 0.2mm for the third and final injection site of 200 nL of the virus suspension. Finally, the needle was retracted by 0.2mm after 2 minutes wait, and then fully retracted from the brain. This virus particle suspension injection method ensured good transfection across the dorso-ventral axis of the hippocampus. Next, the scalp incision was closed up with absorbable sutures and tissue adhesive glue. At the end bupivacaine hydrochloride 0.25% was applied on the wound and the animal was released from the stereotaxic frame. To restore the fluids and electrolytes balance post-surgically 200 μl glucose saline (NaCl 0.9% w/v -glucose 5% w/v) were administered by subcutaneous injection. The animal was then transported to a heated cage for recovery and post-operative monitoring. To allow sufficient ChR2-eYFP expression, hippocampal slices were prepared from the injected mice 11-21 days after surgery.

2.6 Anatomical processing of hippocampal tissue and immuno-cytochemistry

2.6.1 Acute hippocampal slices fixation and re-sectioning

Following the whole cell recordings, the recording electrode containing 0.3% neurobiotin in the intracellular solution was gently retracted from the patched cell soma. Next, the slice was gently removed from the recording chamber with a pipette and dropped fixed in 1-3 ml volume of fixative solution containing 4% paraformaldehyde (PFA), 0.15% picric acid and occasionally 0.05% glutaraldehyde in 0.1M phosphate buffer (PB), (pH= 7.4). When glutaraldehyde was used, final fixative solution was prepared daily by applying it to the mixture of the PFA and picric acid in PB.

Following overnight fixation at 4°C, slices were thoroughly washed (3-5 times,10 minutes) with PB 0.1 M, then and stored at 4°C in PB 0.1M supplemented with 0.05% sodium azide as a fungicide at 4°C. For re-sectioning of the fixed hippocampal slices, slices were firstly embedded in 20% gelatine and fixed again in the fixative solution as described earlier in this paragraph (4% paraformaldehyde, 0.15% picric acid). The gelatine block was glued on a microtome plate with a cyanoacrylate adhesive and slices were re-sectioned at 60 μm thick slices using Leica VT1000S vibrating microtome (Leica Biosystems ,Germany).

2.6.2 Whole brain perfusion-fixation and sectioning

For the immunocytochemical analysis reported in Chapter 3, the brain sections were obtained from perfusion-fixed brains. In this procedure, mice were first anaesthetised with 4% isoflurane at a rate of 1-1.5 ml/min and then further anaesthetised with intraperitoneal injection of pentobarbitone sodium (20% w/v, dosage 0.2 mg/g; Pharmasol, Andover UK). The mice were transcardialy perfused with 50 mL of 0.1 M phosphate buffer saline (PBS), followed by 100 mL of fixative (4% PFA, 15% picric acid; pH= 7.4). Then, the skull was opened and the brain was

removed and post-fixed for at least 24 hours in the fixative detailed above at 4°C. For sectioning of the fixed brain, the brain blocks were glued on a microtome plate with a cyanoacrylate adhesive. Finally, 60 μm thickness sections were cut in ice cold 0.1M PB. Sections were stored at 4°C in 0.1M PB with 0.05% sodium azide.

2.6.3 Visualisation of recorded cells with streptavidin and tissue immuno-cytochemistry

2.6.3.1 Visualisation of whole-cell clamp -recorded cells

In order to visualise the recorded cells, the re-sectioned slices were washed with 50mM Tris-buffered saline (pH= 7.4) with 0.3% Triton X-100 (TBS-Tx) (3-5, 10 minutes) to permeabilise cell membranes. All 60 μm thick sections obtained from an individual slice were incubated overnight with streptavidin conjugated to either AlexaFluor 488 or Cy3 fluorophore (details listed in Table 2-4). Following the incubation, the sections were washed (3-5 times, 10 min) with TBS-Tx, then mounted with vectashield mounting medium on microscope glass slides, and covered with glass cover slips. Their fluorescence was examined with an epifluorescence microscope (Leica DM5000B, Wetzlar, Germany) equipped with a CCD camera (ORCA-ER, Hamamatsu Photonics K.K., Iwata, Japan) and the appropriate filter sets (L5 or Y3).

2.6.3.2 Immunohistochemical reactions in recorded and visualised neurons

Sections that were further selected for immunohistotochemical reactions were unmounted and washed with TBS-Tx (3-5 times, 10 min), blocked with 20% normal horse serum (NHS, Vector laboratories) in TBS-Tx for 1 hour at room temperature (22-24 ^{o}C), and then incubated with the relevant primary antibodies (Table 2-4) for 2 nights at 4°C in TBS-Tx with 1% NHS. After several washes (3-5 times, 10 min) with TBS-Tx, sections were incubated overnight with the appropriate fluorochrome conjugated secondary antibodies in TBS-Tx with 1% NHS (Table 2-4).

Finally, sections were washed with TBS-Tx (3-5 times, 10min) and mounted with vectashield. Evaluation of the immunocytochemical reactions was first performed with the epifluorescence microscope and immunopositivity of individual neurons was ultimately confirmed under laser scanning confocal microscope (Zeiss LSM 710, Carl Zeiss, Jena, Germany) with Zen2008 software. Micrographs were adjusted for brightness and contrast only. Immunoreactivity for a particular neuromarker was assessed after comparing the fluorescence signal in relevant parts of the streptavidin visualised cell with similar cell compartments of unfilled cells of the area. Immunopositivity for CB_1R was confirmed when at least two separate segments of the cell's recovered axon displayed the characteristic antibody (guinea pig-CB_1R;Table 2-4) staining in axon boutons. Immunopositivity for pro-CCK was confirmed by the distinctive semilunar "peri–Golgi" antibody (rabbit-pro CCK, Table 2-4) pattern of staining.

2.6.3.3 Quantification of PV and ErbB4 positive neurons in hippocampus

Perfused brain blocks from the $NRG1^{tg\text{-}type\text{-}I}$ mice and their wild type littermates (see 2.6.2) were cut into 60 μm thick transverse sections. Sections containing the hippocampal formation were washed (3-5 times, 10 min) with TBS-Tx and blocked with 20% normal horse serum (NHS) in TBS-Tx for 1 hour at room temperature (22-24 ^{o}C). This was followed by a two night incubation with the primary antibodies: rabbit anti-ErbB4 and guinea pig anti-PV (Table 2-4) in TBS-Tx with 1%NHS at 4°C. After washes (3-5 times, 10) with TBS-Tx, sections were incubated overnight with Alexa 488-conjugated and Alexa 647-conjugated secondary antibodies, respectively (for details see Table 2-4) in TBS-Tx with 1% NHS. Sections containing mid-ventral hippocampus from both hemispheres, were scanned using an epifluorescence microscope (AxioImager M2; Zeiss) using Stereoinvestigator software (MBF Bioscience, UK). Optical sections of 1 μm were acquired using a 20× objective at a final depth of 20 μm from the section surface, whilst the first 1μm from the section surface was defined as a guard zone and

not scanned. Brightness and contrast acquiring settings were adjusted for each section, in order to achieve good visualization of all positive cells for a specific neuromarker across all sections areas. Cell counting for cells positive for a specific neuromarker was performed off-line using the stereoinvestigator software. Distinct hippocampal regions were visually delineated and analysed as individual anatomically defined subregions as follows: CA1-2 alv/s.o/s.p, CA1-2 s.r/s.l-m, CA3 alv/s.o/s.p and CA3 s.l/s.r/s.l-m. Cells were counted when the cell somata or nuclei came into focus with the optical dissector.

Table 2-4 Antibodies and streptavidin conjugates used for immunohistochemistry

Primary antibodies

Antigen	Species	type	supplier	Product code	Dilution*
CB_1R	Guinea-pig	Polyclonal	Frontier Science	Cb1-GP-Af530-1	1:1000
Pro-CCK	Rabbit	Polyclonal	Gift from prof. Masayoshi Watanabe	n/a	1:500
PV	Guinea-pig	Polyclonal	Synaptic systems	195004	1:2000
ErbB4	Rabbit	Polyclonal anti-antiserum 5941	Gift from prof. Andres Buonanno	n/a	1:500

Secondary antibodies

Conjugate	Species		supplier	Product code	Dilution
CY5	Donkey anti Guinea pig		Jackson immunoresearch	706-175-148 (discontinued)	1:250
CY3	Donkey anti Guinea pig		Jackson immunoresearch	706-165-148	1:400
Alexa 647	Donkey anti Guinea pig		Invitrogen	706-605-148	1:250
Alexa 488	Donkey anti Rabbit		Invitrogen	A21206	1:500
Dylight 649	Donkey anti Rabbit		Jackson immunoresearch	711-495-152 (discontinued)	1:250

Streptavidin conjugates

Conjugate	Species		Supplier	Product code	Dilution
Alexa 488			Invitrogen	s-32354	1:2000
CY3			Thermofisher	s-A1010	1:2000

*Dilutions in TBS-Tx containing 1% NHS

2.7 Immunoblot assay

2.7.1 Hippocampal lysates preparation

To obtain hippocampal tissue samples from both the $NRG1^{tg\text{-}type\text{-}I}$ mice and their control littermates, animals were anaesthetised with isoflurane as described earlier in this chapter and decapitated with a guillotine when the pedal reflex was withdrawn. The skull was surgically opened using a scalpel, and the brain was quickly removed and the two hippocampi were excised free on an ice-cold metal plate. Hippocampi from left and right hemisphere were collected and then immediately placed into an eppendorf tube, immersed to liquid nitrogen and stored at -80 °C. Hippocampal lysates from the isolated hippocampi were prepared in ice-cold lysis buffer, (Table 2-5) with a plastic douncer (40 strokes) and by ~30 passages through a 27½ gauge syringe followed by 5 minute sonication (30 s ON/OFF). The composition of the lysis buffer ensured the cell lysis as well as the solubilisation of the cell membranes, while protecting the protein content from proteolysis and changes of phosphorylation state. Next, the samples were incubated for 75 minutes rotating at 4 °C. Afterwards, the homogenates were centrifuged at 4000 G for 10 minutes at 4 °C and the supernatant was collected.

Table 2-5 Composition of the lysis buffer

Compound	Stocks concentration (in ddH_2O)	Lysis buffer concentration
Tris (pH= 7.5)	1M	20 mM
NaCl	0.5M	50 mM
EDTA	0.5M	1 mM
SDS	20%	0.1%
Triton X-100	10%	1%
Protease inhibitors cocktail (Roche); product code: 11873580001	1 PI tablet / 1 ml ddH_2O	2%
Phosphatase inhibitors cocktail 2 (Sigma); product code: P 5726	-	1%
Phosphatase inhibitors cocktail 3 (Sigma); product code: P 0044	-	1%

2.7.2 Bradford protein assay

Each hippocampal lysate sample was quantified for its protein content by performing the Bradford assay. Using a 96 well plate, 5µl of (1:20 diluted in ddH_2O) the lysate sample as well as bovine serum albumin (BSA) protein samples were diluted in ddH_2O at known concentrations and added in duplicates in the plate. Then, 250 µl of Bradford Reagent (Bio-Rad; USA, catalog # 500-0006) was added to each well. The samples were placed in an orbital shaker. Absorbance shift of the coomassie dye towards blue, resulting from the protein binding, was measured on a plate reader (Thermo Scientific multiscan ex, USA) at 620 nm. A standard curve of the BSA samples was plotted and samples lysate total protein concentrations were determined against the standard curve.

2.7.3 Pouring SDS-Page gels

The SDS-Page gels in this study were custom made. For this, a Bio-Rad mini gel apparatus was used, consisting of two glass plates separated by spacers and mounted onto a pouring stand. The resolver gels used in this study contained 6% or 10% of acrylamide and their composition is listed in Table 2-6. Polymerization of acrylamide was achieved by addition of TEMED (*N*,*N*,*N*,*N*-Tetramethylethane-1,2-diamine) and APS (Ammonium persulphate) (Table 2-6). The resolver gel was poured in between the glass plates up to the level where the comb would lie. A layer of iso-butanol was used to cover the acrylamide, and the gel was left to set for about 45 minutes at room temperature (22-24 ^{o}C). Next, the layer of iso-butanol was removed and the upper edge of the revolver gel was washed several times with ddH_2O. Next the stacker gel mix (Table 2-6) was added up to the top of the plates and the comb was inserted to form the sample wells. After approximately 30 minutes the acrylamide gels were ready to use.

Table 2-6 Composition of resolving and stacking gels for Tris-glycine SDS polyacrylamide gel electrophoresis

resolver gel 6%	resolver gel 10%	stacking gel 4%
5.3 ml ddH_2O	4.0 ml ddH_2O	3.4 ml ddH_2O
2.0 ml 30% acrylamide mix	3.3 ml 30% acrylamide mix	0.83 ml 30% acrylamide mix
2.5 ml 1.5 Tris (pH 8.8)	2.5 ml 1.5 Tris (pH 8.8)	0.63 ml 1.5 Tris (pH 6.8)
0.05 ml (Sodium lauryl sulphate) 20% SDS	0.05 ml (Sodium lauryl sulphate) 20% SDS	0.025 ml (Sodium lauryl sulphate) 20% SDS
0.1 ml 10% (Ammonium persulphate) APS	0.1 ml 10% (Ammonium persulphate) APS	0.05 ml 10% (Ammonium persulphate) APS
0.008 ml N, N, N', N' - tetramethylethylenediamine (TEMED)	0.008 ml N, N, N', N' - tetramethylethylenediamine (TEMED)	0.005 ml N, N, N', N' - tetramethylethylenediamine (TEMED)

2.7.4 SDS PAGE electrophoresis

Hippocampal lysates were diluted in 2- or 5 times to a sample buffer containing 100Mm (or 2× increased) DTT, 10% glycerol, 2% SDS, 2mM Tris HCl and 0.1 % (w/v) bromophenol blue crystals and incubated at 95°C for 5 minutes to denature proteins. Samples containing 60 μg or 120 μg of total protein as well as the molecular weight markers (catalog # 161-0373, Bio-RAD,USA) were loaded and run on SDS-PAGE gels (Table 2-6) using the following running buffer: 125 mM Tris Base, 1M glycine, 0.01% SDS. Electrophoresis started at 0.02pA for 15 minutes, until all samples passed through the stacking gel and afterwards at 0.03pA for ~45 minutes until proteins were well separated as assessed by the molecular weight markers running simultaneously with the samples. Following electrophoresis, the acrylamide gel was removed from the plates and equilibrated for ~ 15 minutes in cold transfer buffer containing: 25 mM Tris, 192 mM glycine, 20% methanol, 0.01% SDS. Proteins transfer was on a nitrocellulose membrane. Firstly, the polyacrylamide gel was transferred to a cassette lying on four 3MM filter papers and a fibre pad, then the nitrocellulose membrane was placed on top of the gel and 4 more 3MM filter papers were placed on top together with a fibre pad. The assembled cassette was

fixed in a tank filled with cold stirring transfer buffer and the whole apparatus was immersed in ice. The gel was left to transfer for 75 minutes at 100 V.

2.7.5 Immunoblotting

Once the protein transfer was completed, the nitrocellulose membrane was removed from the tank and washed for approximately ~5 minutes with PBSxTx and washed for at least 5 minutes. Next the membrane was blocked for nonspecific binding with the Odyssey proprietary blocking buffer (product code: P/N 927-40000, LI-COR Biosciences, USA) for 1 hour shaking at room temperature. After blocking the membrane was cut between ~ 250 and 110 kDa and below ~37 kDa for ErbB4 immunoblotting and the housekeeping protein Glyceraldehyde 3-phosphate dehydrogenase (GADPH) respectively (see Table 2-7 for details on primary antibodies used). Membranes were incubated with primary antibodies overnight at 4 °C in Odyssey blocking buffer supplemented with 0.01% tween -20. Then, washes with PBS x Tx (5 times, 5 min) membranes were incubated with the appropriate fluorescent secondary antibody (Table 2-7) for 1 hour at room temperature. Finally, after (5 times, 5 min) washes with PBS x Tx, the membranes were ready to be scanned with an infrared scanner (Odyssey Clx scanner, LI-COR Biosciences, USA). The digital scans were analysed on the Image Studio Lite software (LiCor, USA).

Table 2-7 Antibodies used for immunoblotting

Primary antibodies	specification	Dilution*
Rabbit anti ErbB4 (5941)	Gift from prof. Andres Buonanno (Neddens and Buonanno, 2010)	1:900
Rabbit anti GADPH	Sigma Aldrich (G9545)	1:10000
Secondary antibody		
IRDye® 800CW Goat anti-Rabbit	LI-COR Biosciences (P/N 925-32211)	1:5000

*Diluted in Odyssey® blocking buffer supplemented with 0.01% Tween-20

2.8 Statistical analysis

Normal distribution of data sets was assessed by Shapiro-Wilk test. When data showed normal distribution, values were expressed as the mean ± standard error mean (SEM) of number (n) of recorded cells (electrophysiological recordings), or n of slices (quantification of PV and ErbB4-positive neurons) or n of hippocampal lysate samples. Statistical significance was assessed by two – tailed Student's t-test or two-way analysis of variances (ANOVA), when comparing the data from the two genotypes. When data sets did not display normal distribution, the statistical significance was assessed using the non-parametric Mann-Whitney U-test and values are expressed as median and quartiles. A P value < 0.05 was considered to account for significant difference when comparing two groups. No statistical methods were used in this study to predetermine sample sizes. Nevertheless, the reported sample sizes conformed to those commonly used in analogous studies. Analyses were performed with GraphPad Software (La Jolla, CA, USA) or SigmaPlot software (Systat Software Inc., London, UK).

3 Localization of NRG1-ErbB4 cellular targets in the hippocampus of WT and NRG1 over-expressing mice

3.1 Introduction - Cellular and subcellular localization of the ErbB4 receptor

Given the implications of the NRG1-ErbB4 signalling pathway in pathogenesis of schizophrenia, some immunocytochemical studies have aimed to identify the cellular and subcellular loci of this signalling pathway in order to reveal specific anatomical targets for the associated pathological processes. However, these earlier reports have produced conflicting results on whether the ErbB4 receptor is expressed both in pyramidal and GABAergic cells (Mechawar et al., 2007, Thompson et al., 2007), or if its expression is limited to GABAergic inhibitory interneurons (Gerecke et al., 2001, Vullhorst et al., 2009, Fazzari et al., 2010).The debate on ErbB4 expression cellular locus has finally been resolved now, as a result of rigorous studies from Prof. Andras Buonannos's research group demonstrating that some antibodies for ErbB4 used in earlier studies show non-specific cross-reactivity with brain proteins. Subsequently, the group generated a number of antisera with higher epitope-specificity. These antibodies were used for systematic immunocytochemical analyses of the ErbB4 expression in brain slices demonstrating specific expression in GABAergic interneurons and not in pyramidal cells. Hence, it has become commonly accepted that the early studies with the less specific anti-ErbB4 antibodies have resulted in erroneous results of the ErbB4 expression in pyramidal neurons (Vullhorst et al., 2009). Detailed immunocytochemical analyses by the Buonanno's research group of the ErbB4 localization in interneurons revealed that the receptor is not equally present in all inhibitory interneuron subpopulations, but is mainly localized in GABAergic cells that are immunopositive for PV, CCK or nNOS. Therefore, interneurons expressing these neuromarkers proteins are considered the prime targets of the NRG1 signalling (Neddens and

Buonanno, 2010). Interestingly, recent studies in the macaque and human brain show that similar to the rodent brain, the ErbB4 receptor expression in primates is widespread both in cortical and subcortical areas (Neddens and Buonanno, 2011, Neddens et al., 2011). This observation indicates that the NRG1-ErbB4 signalling has large scale effects in the brain development and function. However, in order to investigate the importance of the signalling pathway in the brain, it is required to identify the subcellular loci of its effectors: in other words the subcellular localization of the ErbB4 receptor. Both *in situ* hybridization experiments and the immunocytochemical analyses suggest that the ErbB4 localization is predominantly or even exclusively restricted to the post-synaptic somatodendritic cell domains of the GABAergic cells (Neddens and Buonanno, 2011, Neddens et al., 2011). Previous studies reporting a pre-synaptic expression of the ErbB4 receptor are therefore dubious, since these studies are also entirely based on the commercially available antibodies against the ErbB4 receptor (Woo et al., 2007, Fazzari et al., 2010) that have been recently reported to show non-specific binding.

Given that dysregulation of the NRG1-ErbB4 signalling pathway has been associated with circuit alterations in several brain regions, and that the ErbB4 is selectively expressed in the GABAergic inhibitory neurons, my experiments in this chapter aim to do following: a) To further verify the identity of NRG1 signalling target neurons in the hippocampus by performing immunocytochemical analysis of the PV or CCK expressing interneurons using the non-commercial antibody against the ErbB4 receptor donated by Prof. Buonanno (serotype 5941), and b) to compare the density (cell count / mm^3) in the hippocampus of the GABAergic cells immunopositive either for PV or ErbB4, and for both in the NRG1 over-expressing ($NRG1^{tg\text{-}type\text{-}I}$) mice and wild type (WT) littermates. This is an important analysis in order to establish whether the NRG1 over-expression has effects on the ErbB4+ cell density in the mammalian hippocampus.

3.2 ErbB4 expression in hippocampal interneurons expressing either PV or CCK

3.2.1 Results

ErbB4 expression was studied in interneurons expressing either PV or CCK in the mouse hippocampus. To investigate the co-localization of the ErbB4 receptor with PV+ interneurons, slices from 3 WT and 3 $NRG1^{tg\text{-}type\text{-}I}$ adult mice were tested using double immunostaining for PV and ErbB4. Whereas, in order to assess the receptor's expression in the CCK+ cells, the immunohistological studies were performed in mice (n= 2) that displayed genetic fluorophore marker expression in CCK+ cells. For this purpose, hippocampal slices were prepared from BAC-CCK-$Cre^{+/-}$ mice crossbred with Ai9 $^{+/+}$ mice. This breeding produced animals showing tdTomato expression in CCK+ cells. In brief, the following primary antibodies were used in the study: the rabbit anti-ErbB4 (Custom made A. Buannanno lab) and guinea pig anti-PV (synaptic systems) subsequently probed with anti-rabbit- Alexa 488-conjugated and anti-guinea pig Alexa 647-conjugated secondary antibodies, both raised in donkey. Specific details of the immunocytochemical protocols in different mice strains are found in Chapter 2 (see sections 2.1.2, 2.6.3.2, 2.6.3.3).

In all sections (n = 9 sections from 3 WT mice; n = 12 sections from 3 $NRG1^{tg\text{-}type\text{-}I}$ mice) processed for the double immunofluorescence for ErbB4 and PV, substantial co-expression for these neuromarkers was observed in interneurons located in the s.p, s,r and s.o of the CA1-3 hippocampal areas. There were no observed differences in the co-expression for the two neuromarkers between the WT and the $NRG1^{tg\text{-}type\text{-}I}$ mice hippocampi. On average ~80 % of all PV immunopositive interneuron somata across all the hippocampal areas were found to be ErbB4 immunopositive (Figure 3-1) (for co-expression estimate analysis, see below section 3.3).

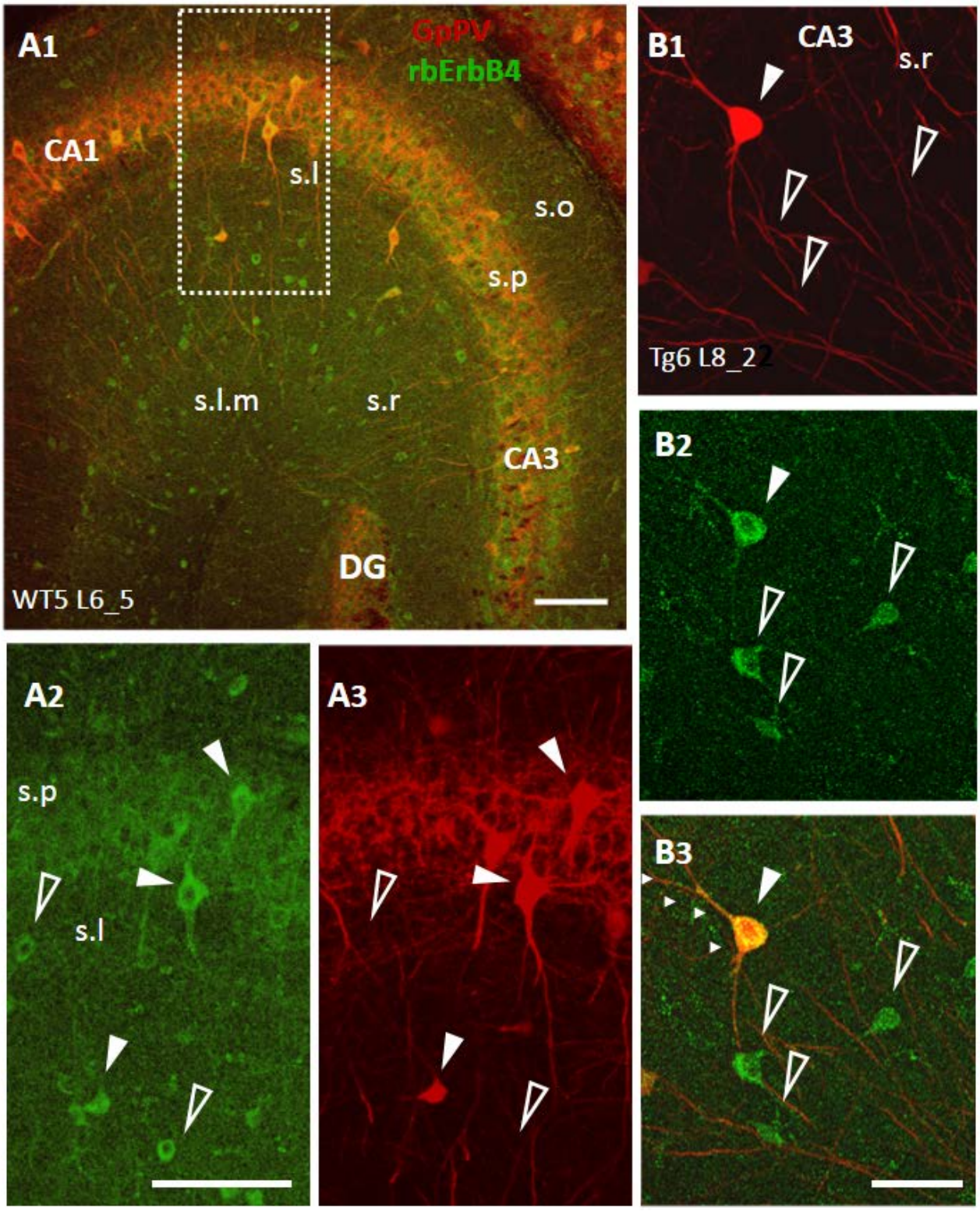
A1
GpPV
rbErbB4
CA1
s.l
s.o
s.p
s.l.m
s.r
CA3
DG
WT5 L6_5
B1
CA3
s.r
Tg6 L8_2
B2
A2
s.p
s.l
A3
B3

Figure 3-1 ErbB4 is strongly expressed in PV-positive interneurons. (A1) Confocal stack images of double immunostaining for PV and ErbB4 from a hippocampal section of WT mice (WT5 L6-5). The PV and the ErbB4-positive cells are prominently found in s.p and s.o in the CA1-CA3 areas. In addition, large number of PV-negative cells express the ErbB4 receptor (green) mainly in s.r, s.l and s.l-m (PV, red,). (A2-3) Distinct ErbB4 (A2) and PV (A3) immunoreactions, (magnified A1 dash box area) showing co-expression (filled arrowheads) or only ErbB4 immunopositivity (open arrowheads). Scale bars 100 µm. (B1-3) Stack images for PV and ErbB4 immunoreactions from a NRG1$^{tg\text{-}type\text{-}I}$ mouse hippocampus (Tg6 L8_2). (B1) PV. (B2) ErbB4. (B3) overlap. The filled chevron shows a PV-positive cell co-expressing the ErbB4, the open chevrons indicate PV-negative cell somata, which are ErbB4-positive. The small filled chevron highlights ErbB4-positive signal in dendrites. Scale bar 50 µm.

I next investigated the expression of the ErbB4 in CCK+ interneurons. I opted to use slices from BAC-CCK-Cre$^{+/-}$; Ai9$^{+/+}$ mice that display td Tomato signal in CCK+ cells, because the best antibodies available against CCK and ErbB4 were both raised in the same host species. In addition, the expected localization of positive reactions for the detection of these proteins is similar focusing on the somatic cell domain: A fact that could render the co-localization for the two markers problematic. The results showed that similar to the PV-positive cells, the CCK-expressing neurons consistently express the ErbB4 receptor.

However, there are some aspects that need to be taken in to consideration concerning these results. First, it is possible that neurons that displayed Td Tomato signal in the mice may not all represent cells exhibiting positive immunoreaction for the CCK protein, which is the main criterion that would traditionally classify them as CCK+ cells. This possibility rises from the subtle, but constant activation of the CCK transcript promoter in several interneuronal lineages during early brain development. In adult mice, positive immunoreactivity for the CCK protein is not observed in these cells. In particular, this disconnection between the detection of CCK protein and the transcript has been reported in interneurons deriving during early development from the Medial Gaglionic Eminence (MGE) (Tricoire et al., 2011). It follows that in the BAC-CCK-Cre$^{+/-}$ mice x Ai9$^{+/+}$ mice, the constituent CCK gene promoter activation could trigger the expression of Cre recombinase and the consequent Td tomato “false” positive signal in some cells. Although it is difficult to estimate exact proportion of such cells among all Td-expressing

neurons in these mice, it is noteworthy that, the immunostaining results for PV revealed their minimal overlap with the Ai9-probed CCK cells in this transgenic line both in the prefrontal cortex (Geibel et al., 2014) and in the hippocampus and (lab observation). Given that in the hippocampus most of the MGE derived interneurons are PV immunoreactive, the latter observations largely excludes the possibility of large number of "false" tagging of the non-CCK positive cells with td Tomato in these mice and further supports the ErbB4 expression in CCK-positive neurons.

Second, given that a number of pyramidal cells in hippocampus also express CCK (Morino et al., 1994) it is possible that in this line the Td Tomato fluorescence can also be present in pyramidal cells. This was indeed confirmed in the CA1 region of these mice (Geibel et al., 2014). Even though, this likelihood is indeed confirmed mainly in the CA1 region of these mice (Geibel et al., 2014), all the observed CCK/ErbB4 positive interneurons displayed characteristic interneuronal morphology. In contrast, ErbB4 receptor staining decorating the soma and dendrites of cells displaying characteristic somatic or dendritic pyramidal morphology was never observed, (Figure 3-1, Figure 3-2). This finding is in line with the earlier reports for confined expression of the ErbB4 receptor in GABAergic cells (Vullhorst et al., 2009).

A third point of consideration is whether, the ErbB4 receptor is also expressed in CCK+ interneurons in NRG1 over-expressing mice. This analysis, has not performed yet mainly due to experimental impediments, concerning the establishment of a BAC-CCK-Cre $^{+/+}$ founder mice line and the subsequent backcrossing with Ai9$^{+/+}$ and NRG1$^{tg\text{-}type\text{-}I}$ mice. Thus, even though expression of ErbB4 in CCK-positive interneurons is suspected in NRG1$^{tg\text{-}type\text{-}I}$ as well, mainly due to the observation of expression of the ErbB4 in PV-negative cells in those mice (Figure 3-1), this assumption needs to be further explored.

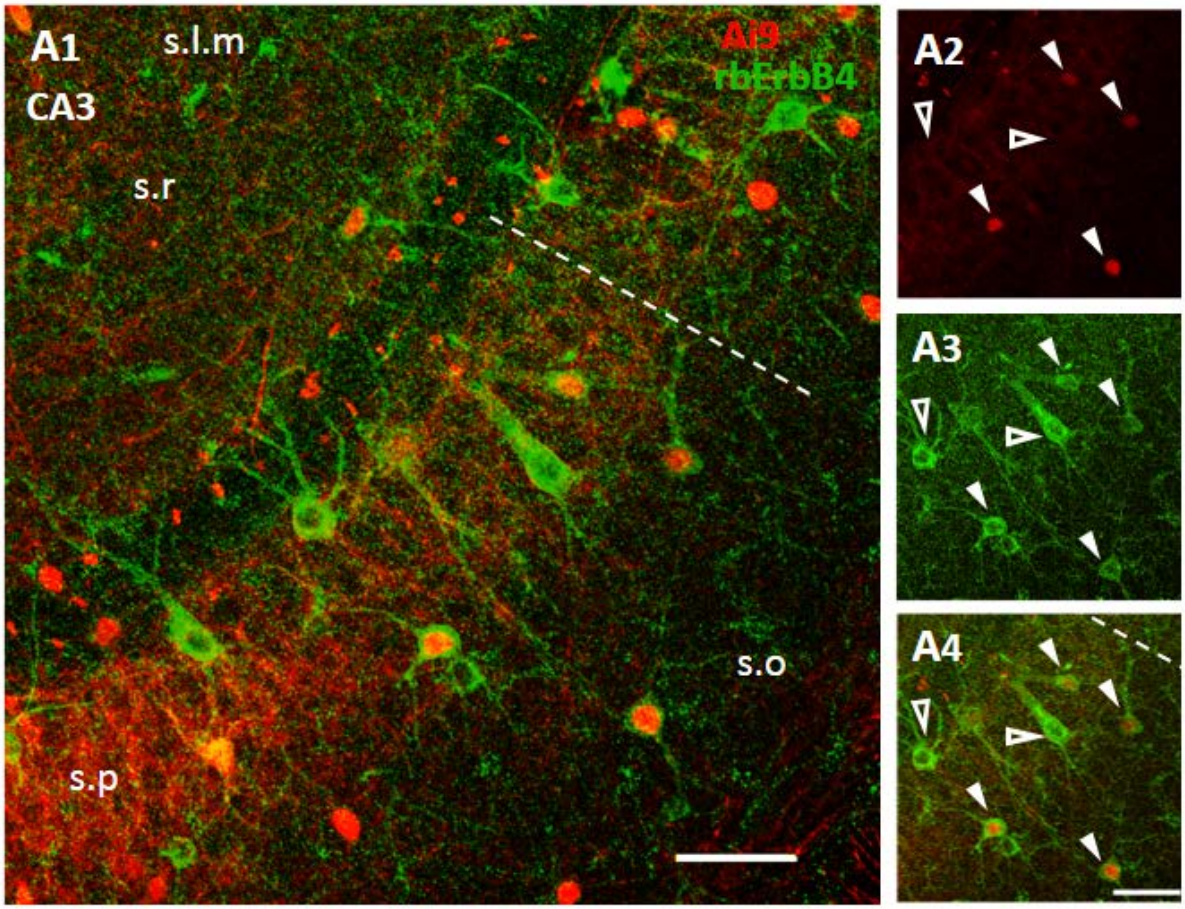

Figure 3-2 ErbB4 is consistently expressed in CCK-positive cells. (A1) Collapsed confocal stack image of immunostaining for ErbB4 receptor in a hippocampal slice from a BAC-CCK-Cre $^{+/-}$ x Ai9$^{+/+}$ mouse (red, Td – tomato signal; green, ErbB4 immunoreaction). Note positive ErbB4 immunoreaction in numerous Td-tomato expressing cells in all regions of the CA3. (A2-4) Single channel fluorescence stack images in the dashed line – indicated area. (A2) Td-tomato fluorescence signal in CCK-expressing cells. (A3) ErbB4 immunopositive somata. (A4) Overlap of the Td-tomato signal with the ErbB4 receptor immunofluorescence. Filled arrowheads show cells with the CCK and the ErbB4 signals. Open arrowheads point at ErbB4-positive cells with no Td-tomato signal. Scale bars 50 μm.

3.3 Comparative analysis of the ErbB4 expression in PV-positive cells in the WT and the NRG1$^{tg\text{-}type\text{-}I}$ mice hippocampi

3.3.1 Results

Having established, the prominent expression of the ErbB4 receptor in the two major interneuron populations in the hippocampus, expressing either PV or CCK, I next set out to analyse the percentage of PV expressing cells in the ErbB4+ cell population across the CA1-3

area in both the WT and the NRG1$^{tg\text{-}type\text{-}I}$ mice. I performed double immunofluorescence staining for PV and ErbB4 in coronal sections of medial-ventral hippocampi. In total, 9 sections from 3 WT mice, and 12 sections from 3 NRG1$^{tg\text{-}type\text{-}I}$ mice were studied. The sections (60 μm) were obtained from both hemispheres and were scanned with epifluorescence microscopy using a 20× objective. To ensure good detection of the immunofluorescence signal for both two neuromarkers, optical sections of 1 μm were obtained at a final depth of 20 μm from the section's surface. For consistency, image scans deeper from the sections were avoided because of increasingly compromised antibody penetration by the depth. Data acquiring settings, including exposure time and image contrast were adjusted in each section for the different colour channels to enable good-standard visualization of fluorescent cells in the sections. Immunopositivity for the two neuromarkers was performed offline using a stereoinvesigator software. Cell somata were determined positive for either PV or ErbB4, only when the soma or cell nuclei came to focus with the dissector, and counted independently for each of the two colour channels. Afterwards, images of the two channels were merged, and double-labelled cells were determined and counted as PV and ErbB4 co-expressing. Distinct hippocampal areas and layers were delineated in 4 different contours that included; CA1-2-alv, s.o, s.p; CA1-2-s.r., s.l-m; CA3-alv, s.o, s.p; CA3-s.r, s.l, s.l-m. (Figure 3-3, A2).

Of note, dealing with limited amounts of the rabbit anti-ErbB4 antibody, in an equal proportion of WT and NRG1$^{tg\text{-}type\text{-}I}$ hippocampal sections a recycled preparation of the antibody from a previous round of immunoreaction was used. Analysis of the putative differences in the co-expression percentage between the WT and NRG1$^{tg\text{-}type\text{-}I}$ mice was performed by using the non-parametric Mann Whitney U test, given the non normal distribution of data in some of the contours (mainly in contours comprising s.r and and s.l-m).

First, I quantified percentages of the ErbB4 co-expression with PV in the two genotypes. Sections from both genotypes showed clear co-expression of ErbB4 with PV in neurons (~80%) (Figure 3-3, B1-2). However, slices from NRG1 over-expressing mice exhibited a trend towards a reduced co-expression. This trend reached statistical significance in the CA1-2 contour comprising the alv, s.o and s.p areas (Figure 3-3, C1). The percentages of the PV and ErbB4 co-expressing cells were normalised by the total number of PV-positive cells in the contours. The results were as follows: a) *CA1-2 alv, s.o ,sp;* WT, 85.00% (76.62 to 90.96%); $NRG1^{tg\text{-}type\text{-}I}$ 74.60% (69.97 to 76.57%), (medians, P= 0.043), b) *CA1-2 s.r & s.l-m*; WT, 100% (87.5 to 100%); $NRG1^{tg\text{-}type\text{-}I}$, 100% (66.67 to 100%), (medians, P= 0.88), c) *CA3 alv, s.o, s.p*; WT, 80.56% (75 to 84.58%); $NRG1^{tg\text{-}type\text{-}I}$, 74.84% (71.24 to 83.24%), (medians, P= 0.64), d) *CA3 s.l, s.r, s.l-m*; WT, 80.00% (65.39 to 100%); $NRG1^{tg\text{-}type\text{-}I}$, 75.00% (69.05 to 92.86%), (medians, P= 0.91) Finally, the comparison of the co-expression across all strata did not reveal any statistical difference in between the two genotypes; *Total HPC*; WT, 77.66% (75.85 to 86.85%); $NRG1^{tg\text{-}type\text{-}I}$ 75.64% (72.41 to 80.01%), (medians, P= 0.17) (Figure 3-3, D1). Overall, the data suggest that in the majority of the hippocampal areas the NRG1 over-expression may not produce significant changes in the co-expression of the ErbB4 receptor in PV cells. The observed trend for a decline in the co-expression in many hippocampal strata, reaching significance in the CA1-2 region delimited by alv and s.p could be explained by either a decreased expression of ErbB4 in PV cells or/and a reduced number of PV+ and ErbB4+ interneurons in the area.

Interestingly, further analysis of the co-expression of PV with ErbB4 showed that, apart from the s.r and s.l-m CA1-2 regions, the co- expression of PV with ErbB4 was increased in sections from the $NRG1^{tg\text{-}type\text{-}I}$ mice. The results in the specific areas were as follows: a) *CA1-2 alv, s.o, s.p;* WT, 65.52% (60.31 to 70.83%); $NRG1^{tg\text{-}type\text{-}I}$, 81.25% (77.55 to 86.78%), (medians, P< 0.001), b*) CA1-2 sr & s.l-m;* WT, 4.35% (2.42 to 12.64%); $NRG1^{tg\text{-}type\text{-}I}$ 14.58% (0 to

31.25%) (medians, P= 0.28), c) *CA3 alv,s.o,s.p*; WT, 57.14% (55.14 to 62.01%); NRG1$^{tg\text{-}type\text{-}I}$ 72.88% (62.25 to 90.84%) (medians, P= 0.021), d) *CA3 s.l, s.r, s.l-m*; WT, 13.33% (6.92 to 19.52%); NRG1$^{tg\text{-}type\text{-}I}$ 21.91% (15.64 to 31.67%), (medians, P= 0.03).

Similarly, the percentage of PV co-expression with the ErbB4 was found to be increased in NRG1 trangenic animals , when analysing the total hippocampal area; *Total HPC*; WT, 39.74% (36.74 to 41.94); NRG1$^{tg\text{-}type\text{-}I}$, 55.44 (50.48 to 74.40) (medians, P <0.001) (Figure 3-3, D2) . Of note, the observed variations in the regional amount of ErbB4 interneurons that co-express PV in the different hippocampal regions studied, could be at least partially explained by the distribution pattern of PV-positive expressing cells that show highest densities in the s.o and s.p strata and are rather sparse in the other CA1-3 strata such as s.l, s.r and s.l-m.

These differences between the two genotypes can be explained by either an increased proportion of PV+ and ErbB4+ cells in NRG1 over-expressing mice or a reduction in the total number of ErbB4 expressing cells or a reduced receptor's expression level in some neurons below the detection level in these mice. However, taken into account that the comparison of the ErbB4 co-expression with PV did not any differences between the two genotyped, these findings together suggest that the NRG1 over-expression either leads to altered number of ErbB4-positive cells, or results in a declined expression of the ErbB4 level receptor in the entire GABAergic cell population. In order to test these hypotheses, I set out to compare the density of PV+ or/and ErbB4+ interneurons in WT and NRG1$^{tg\text{-}type\text{-}I}$ mice.

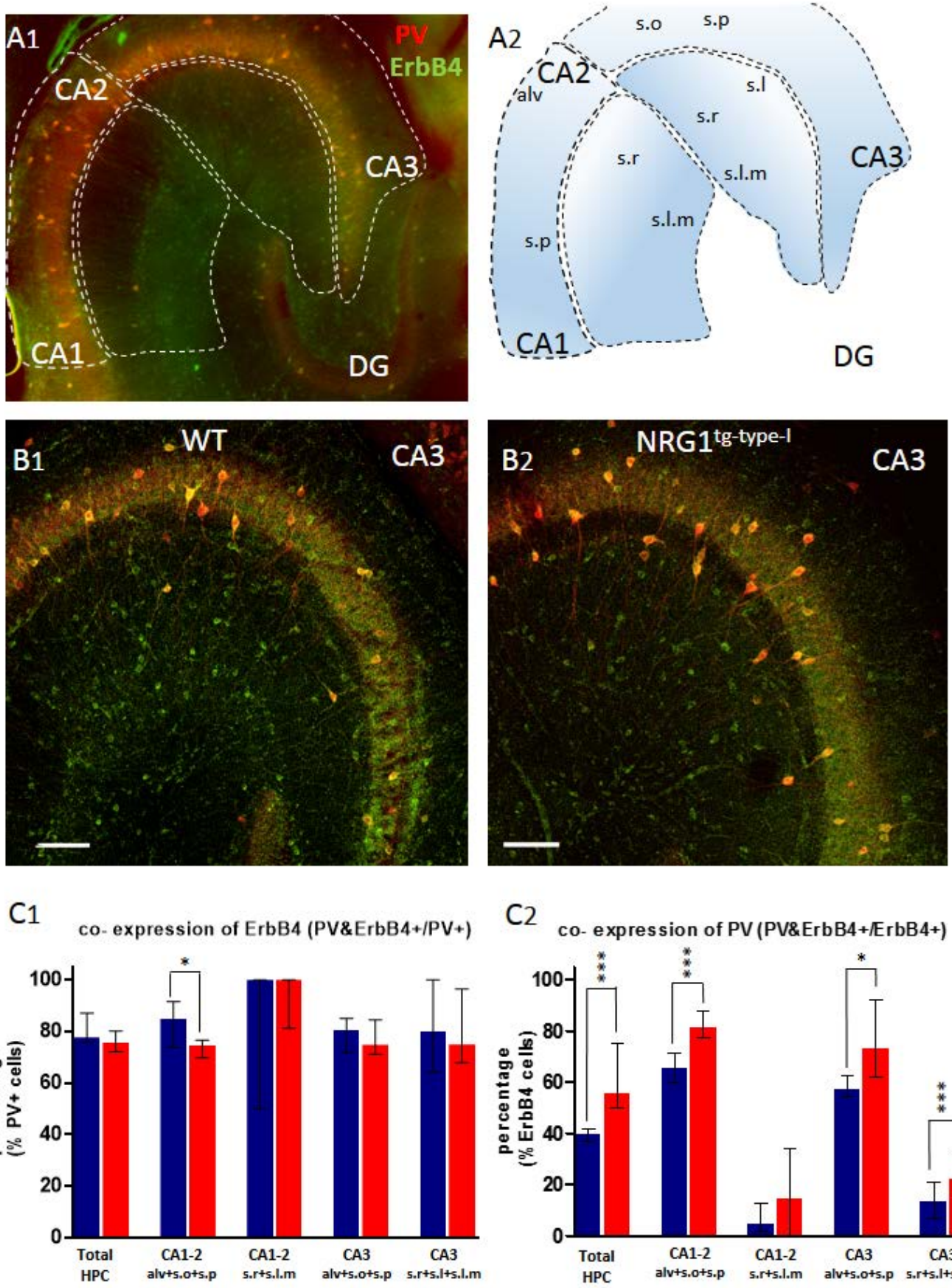
A1
PV
ErbB4
CA2
CA3
CA1
DG
A2
s.o
s.p
CA2
alv
s.l
s.r
s.r
CA3
s.l.m
s.l.m
s.p
CA1
DG
B1
WT
CA3
B2
NRG1tg-type-I
CA3
C1
co- expression of ErbB4 (PV&ErbB4+/PV+)
percentage (% PV+ cells)
100
80
60
40
20
0
Total HPC
CA1-2 alv+s.o+s.p
CA1-2 s.r+s.l.m
CA3 alv+s.o+s.p
CA3 s.r+s.l+s.l.m
C2
co- expression of PV (PV&ErbB4+/ErbB4+)
percentage (% ErbB4 cells)
100
80
60
40
20
0
Total HPC
CA1-2 alv+s.o+s.p
CA1-2 s.r+s.l.m
CA3 alv+s.o+s.p
CA3 s.r+s.l+s.l.m

Figure 3-3 Comparative analysis of the PV and ErbB4 co-expression in WT and NRG1$^{tg\text{-}type\text{-}I}$mice. (A1) Epifluorescence image of the double immunostaining for ErbB4 receptor and PV in a hippocampal slice from WT mouse (WT6 L7_1) (red, PV; green, ErbB4 immunoreaction). Note strong co-expression of the ErbB4 in s.p and s.o, enriched with PV+ cell somata. Borders of the areas of the cell counting analysis are indicated with dashed lines. (A2), graphic representation of the hippocampal areas, with the four different contours of the CA1-2 alv, s.o, s.p, CA1 s.r and s.l-m, CA3 alv, s.o, s.p, and CA3 s.l, s.r, s.l-m. Data from these areas were used for the cell counting analysis between the two genotypes. (B1-2) Merged PV and ErbB4 immunoreaction signals in an epifluorescence image, and confocal stack images from hippocampal sections of WT (WT5 L6_5) (B1), and the NRG1$^{tg\text{-}type\text{-}I}$ mice (B2) (Tg6 L8_3). Scale bars 100 µm. (C1-2) Bar plots show the presence of ErbB4-positive immunoreaction in PV+ cells (C1), and percentage of PV+ in all ErbB4+ cells (C2) in the contours (blue, WT; red, NRG1$^{tg\text{-}type\text{-}I}$ mice). Comparison of medians with interquartile range, P <0.05 *, P <0.001 *.**

3.4 Density analysis of interneurons expressing PV and ErbB4 and comparison of ErbB4 protein levels in WT vs NRG1$^{tg\text{-}type\text{-}I}$ mice

3.4.1 Results

The analysis of the PV-co expression with ErbB4 indicated alterations in the percentage of PV+ErbB4 co-expressing cells towards the total number of ErbB4-positive cells in the NRG1 over-expressing hippocampus. Therefore, I next aimed to investigate the cause of this alteration by performing density analysis for PV or/and ErbB4-positive cells in the hippocampus of WT and NRG1$^{tg\text{-}type\text{-}I}$. The cell counting approach was similar to the one described previously, whereas the volume of the different hippocampal contours was determined by the total area of the contour and the final depth of the section scan (20µm). As above, in total, 9 slices from 3 WT and 12 sections from 3 NRG1$^{tg\text{-}type\text{-}I}$ mice that underwent double immunostaining for PV and ErbB4 were included in this analysis. As in 3.2.2 section, for comparisons in between genotypes the Mann Whitney U non-parametric test was used due to non-normal data distribution in a number of hippocampal areas. The comparison of PV-positive somata density showed no differences across the four distinct contours examined nor in the total hippocampal area between the two genotypes. In further detail the statistical comparisons were as follow; a) *CA1-2 alv, s.o, s.p*; WT, 4.76 × 10^3 cells/mm^3 (4.07 to 5.53 x 10^3 cells/mm^3); NRG1$^{tg\text{-}type\text{-}I}$, 4.59 ×$10^3$ cells/mm^3 (4.08 to 5.92 × 10^3 cells/ mm^3) (medians, P= 0.86), b) *CA1-2 s.r & s.l-m*; WT,

0.14 × 10^3 cells/mm^3 (0.14 to 0.38 × 10^3 cells/ mm^3); $NRG1^{tg\text{-}type\text{-}I}$, 0.15 × 10^3 cells/mm^3 (0.00 to 0.32 × 10^3 cells/ mm^3) (medians, P= 0.59), c) *CA3 alv, s.o, s.p*; WT, 4.02 × 10^3 cells/ mm^3 (3.59 to 4.56 × 10^3 cells/mm^3); $NRG1^{tg\text{-}type\text{-}I}$, 3.20 × 10^3 cells/ mm^3 (3.06 to 3.78 × 10^3 cells/mm^3) (medians, P= 0.11), d) *CA3 s.l, s.r, s.l-m*; WT, 0.83 × 10^3 cells/ mm^3 (0.59 to 1.48 × 10^3 cells/ mm^3); $NRG1^{tg\text{-}type\text{-}I}$, 0.83 × 10^3 cells/ mm^3 (0.46 to 1.10 × 10^3 cells/ mm^3) (medians, P= 0.46) and e) Total HPC; WT, 2.44 × 10^3 cells/ mm^3 (2.03 to 2.74 × 10^3 cells/mm^3); $NRG1^{tg\text{-}type\text{-}I}$, 2.28 × 10^3 cells/ mm^3 (2.03 to 2.63 × 10^3 cells/mm^3) (medians, P= 0.70) (Figure 3-4, A1&3, B1). These findings suggest that NRG1 over-expression has no significant effects on the total population of PV-positive cells.

Nonetheless it is possible that only the subpopultion of PV cell that co-express the ErbB4 receptor are affected due to NRG1 over-expression. To answer this question, I further performed a quantitative comparison of the cell density of the PV & ErbB4 co-expressing subpopulation in WT and NRG1 over-expressing mice. Similar to the case of the general PV cell population, density analysis of the of PV& ErbB4 co-expressing cells across the two genotypes did not reveal significant changes in any of the distinct areas or of the total hippocampal region; a) *CA1-2 alv, s.o, s.p*; WT, 3.68 × 10^3 cells/mm^3 (3.18 to 5.08 × 10^3 cells/mm^3); $NRG1^{tg\text{-}type\text{-}I}$, 3.42 × 10^3 cells/mm^3 (2.44 to 4.43 × 10^3 cells/mm^3), (medians, P= 0.30), b) *CA1-2 s.r & s.l-m*; WT, 0.14 × 10^3 cells/mm^3 (0.10 to 0.16 × 10^3 cells/mm^3), (medians, P= 0.86), c) *CA3 alv, s.o, s.p*; WT, 3.16 × 10^3 cells/mm^3 (2.46 to 3.79 × 10^3 cells/mm^3); $NRG1^{tg\text{-}type\text{-}I}$, 2.69 × 10^3 cells/mm^3 (2.23 to 2.86 × 10^3 cells/mm^3), (medians, P= 0.24); d) *CA3 s.l, s.r, s.l-m*; WT, 0.64 × 10^3 cells/mm^3 (0.31 to 1.26 × 10^3 cells/mm^3); $NRG1^{tg\text{-}type\text{-}I}$, 0.72 × 10^3 cells/ mm^3 (0.39 to 0.84 × 10^3 cells/mm^3), (medians, P= 0.86) and e) *Total HPC*; WT, 1.88 × 10^3 cells/ mm3 (1.73 to 2.38 × 10^3 cells/mm3); $NRG1^{tg\text{-}type\text{-}I}$; WT 1.70 × 10^3 cells/mm3) (medians, P= 0.21) (Figure 3-4, A2&A4,B2). Altogether these comparisons of the total PV and PV and ErbB4-positive somata between $NRG1^{tg\text{-}type\text{-}I}$ and

WT mice suggest that NRG1 over-expression has no significant impact on the PV-positive cell population and cause no significant alterations in the expression of the ErbB4 receptor in these cells. However it is noteworthy to mention, these quantitative comparisons showed a subtle but not significant trend towards a reduction of both PV and PV+/ErbB4+ somata mainly in the CA1-2 and CA3 alv, s.o, sp in sections from the NRG1$^{tg\text{-}type\text{-}I}$ mice. Thus, some minor effects on the PV population cannot be completely excluded.

Subsequently, having ruled out the possibility of major alterations in the PV or the PV/ErbB4 co-expressing cells in NRG1 over-expressing mice, I set out to compare the density of PV-negative ErbB4-positive cells between the WT and NRG1 over-expressing mutants. This analysis revealed that the density of PV-negative / ErbB4-positive cells is uniformly reduced across all the hippocampal areas examined. The total reduction in the entire hippocampus was -61%; *Total HPC* WT; 3.10 × 10^3 cells/ mm^3 (2.42 to 3.30 × 10^3 cells/ mm^3); NRG1$^{tg\text{-}type\text{-}I}$, 1.20 × 10^3 cells/ mm^3 (0.57 to 1.76 × 10^3 cells/ mm^3), (medians, P< 0.001). The highest, reduction was observed in the *CA1-2 s.r, s.l-m area* (-76.99%); WT, 3.05 × 10^3 cells/ mm^3 (1.72 to 3.59 × 10^3 cells/ mm^3); NRG1$^{tg\text{-}type\text{-}I}$ 0.70 × 10^3 cells/ mm^3 (0.35 to 1.32 × 10^3 cells/ mm^3), (medians, P= 0.005), reflecting a severe reduction of ErbB4 expressing interneurons or/and ErbB4 receptor expression loss below detection levels in PV-negative GABAergic cells, enriched in this area. For the rest of the areas the cell density comparison also revealed severe reductions; a) *CA1-2 alv, s.o, s.p* (-64.67%); WT, 2.11 × 10^3 cells/ mm^3 (0.60 to 0.21 10^3 cells/ mm^3); NRG1$^{tg\text{-}type\text{-}I}$, 0.74 (0.40 to 0.12 × 10^3 cells/ mm^3) (medians, P< 0.001), b) *CA3 alv, s.o, s.p* (-53.48%) ; WT, 2.24 × 10^3 cells/ mm^3 (1.76 to 3.07 × 10^3 cells/ mm^3); NRG1$^{tg\text{-}type\text{-}I}$, 1.04 × 10^3 cells/ mm^3 (0.28 to 1.43 × 10^3 cells/ mm^3) (medians, P= 0.003) and c) *CA3 s.l, s.r, s.l-m* (-52.8%); WT, 4.75 × 10^3 cells/ mm^3 (3.88 to 5.42 × 10^3 cells/ mm^3); NRG1$^{tg\text{-}type\text{-}I}$, 2.24 × 10^3 cells/ mm^3 (1.37 to 3.03 × 10^3 cells/ mm^3), (medians, P< 0.001) (Figure 3-4, D1).

In a similar way, the comparison of the total number of ErbB4 immunoreactive somata (e.g including cells that co-express PV) showed significant differences in all four hippocampal areas examined and reached a -43.44% reduction in the *entire hippocampus* from NRG1 over-expressing mice; WT, 4.98 × 10^3 cells/mm^3 (4.65 to 5.66 × 10^3 cells/mm^3); $NRG1^{tg\text{-}type\text{-}I}$, 2.82 × 10^3 cells/mm^3 (2.37 to 3.48 × 10^3 cells/mm^3), (medians, P= 0.002) and was greatest (-72.08 %) in the *CA1-2* contour delimited by *s.r and s.l-m*; WT, 3.19 × 10^3 cells/mm^3 (1.77 to 3.76 × 10^3 cells/mm^3); $NRG1^{tg\text{-}type\text{-}I}$, 0.89 × 10^3 cells/mm^3 (0.45 to 1.74 × 10^3 cells/mm^3) (medians, P= 0.006). The percentage of the ErbB4 immunoreactive somata reduction in the rest of hippocampal areas were as follows; a) *CA1-2 alv, s.o, s.p* (-29.22%); WT, 5.67 × 10^3 cells/mm^3 (5.04 to 7.34 × 10^3 cells/mm^3); $NRG1^{tg\text{-}type\text{-}I}$, 4.02 × 10^3 cells/mm^3 (3.21 to 5.32 × 10^3 cells/mm^3), (medians, P= 0.021), b) *CA3 alv, s.o, s.p* (-38.67%); WT, 6.02 × 10^3 cells/mm^3 (4.46 to 6.22 × 10^3 cells/mm^3), $NRG1^{tg\text{-}type\text{-}I}$, 3.69 × 10^3 cells/mm^3 (2.86 to 4.24 × 10^3 cells/mm^3), (medians, P= 0.003) and c) *CA3 s.l, s.r, s.l-m* (-54.50 %); WT, 5.78 × 10^3 cells/mm^3 (4.57 to 6.12 x 10^3 cells/mm^3), $NRG1^{tg\text{-}type\text{-}I}$, 2.63 × 10^3 cells/mm^3 (2.24 to 3.61 × 10^3 cells/mm^3), (medians, P< 0.001) (Figure 3-4, C1-2, D2). The lower reduction of the density of the total ErbB4-positive cells in $NRG1^{tg\text{-}type\text{-}I}$ sections, in regards to the PV-negative ErbB4-positive cell counts in these animals, is due to the incorporation of cells that also co-express PV, whose numbers and ErbB4 expression profile is largely unaffected in $NRG1^{tg\text{-}type\text{-}I}$ mice.

Overall, these data suggest that NRG1 over-expression leads to altered numbers of ErbB4- positive cells or/and a decline in the receptors expression in GABAergic cells. These alternations are likely to occur in GABAergic cell populations other than the ones expressing parvalbumin. This, likelihood mainly derives from the finding that the density of PV and ErbB4 co-expressing cells remains largely unchanged , while PV-negative somata density is severely affected due to NRG1 over-expression. Moreover, the highest decline of ErbB4 immunoreactive

somata was observed in the CA1 s.r and s.l-m, a region that is highly enriched with ErbB4-positive interneurons expressing other neuromarkers like CCK and nNOS.

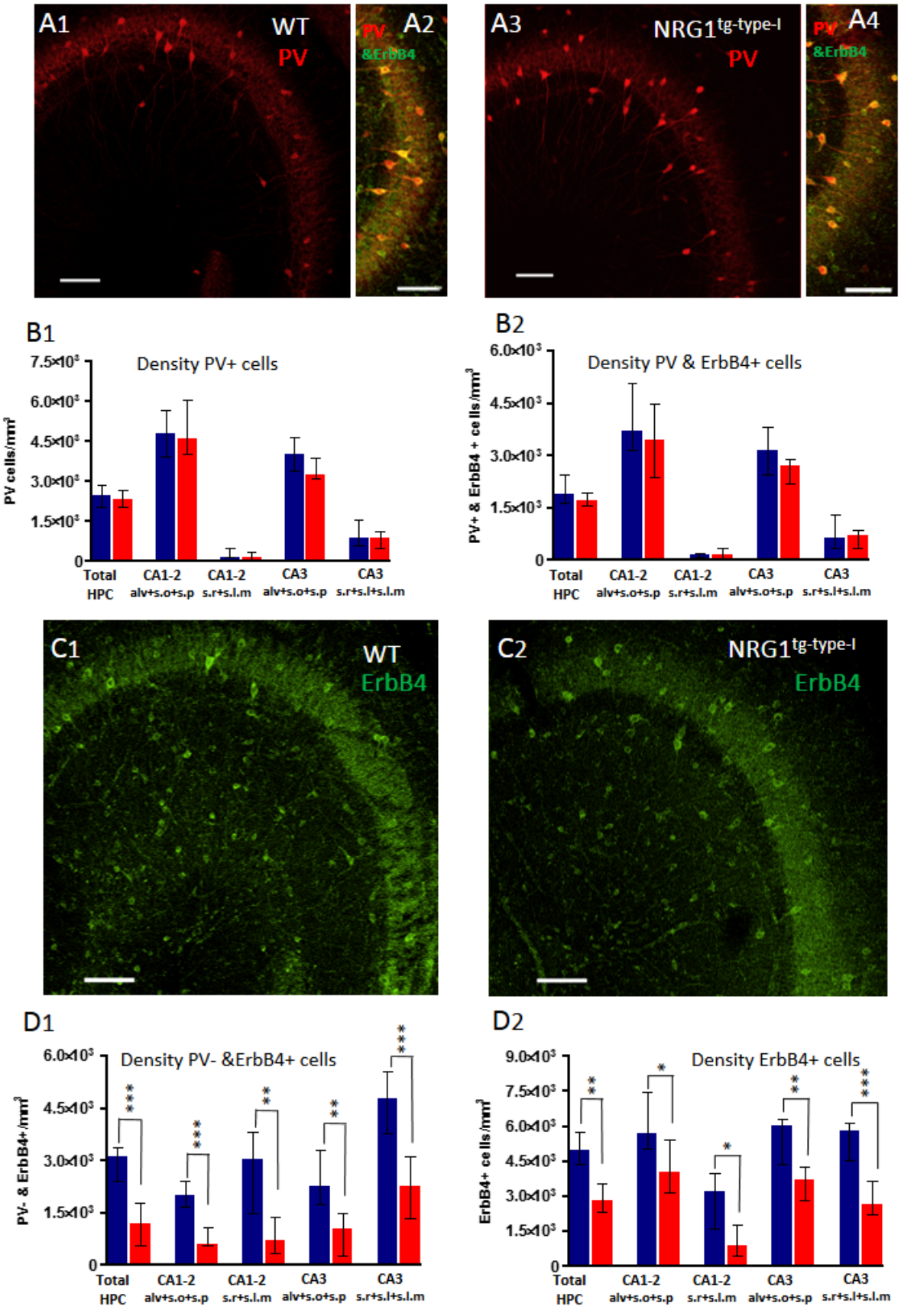
A1
WT
PV
A2
PV
&ErbB4
A3
NRG1tg-type-I
PV
A4
PV
&ErbB4
B1
Density PV+ cells
PV cells/mm3
7.5x10³
6.0x10³
4.5x10³
3.0x10³
1.5x10³
0
Total HPC
CA1-2 alv+s.o+s.p
CA1-2 s.r+s.l.m
CA3 alv+s.o+s.p
CA3 s.r+s.l+s.l.m
B2
Density PV & ErbB4+ cells
PV+ & ErbB4 + cells/mm3
6.0x10³
4.5x10³
3.0x10³
1.5x10³
0
Total HPC
CA1-2 alv+s.o+s.p
CA1-2 s.r+s.l.m
CA3 alv+s.o+s.p
CA3 s.r+s.l+s.l.m
C1
WT
ErbB4
C2
NRG1tg-type-I
ErbB4
D1
Density PV- &ErbB4+ cells
PV- & ErbB4+/mm3
6.0x10³
4.5x10³
3.0x10³
1.5x10³
0
***
***
**
**
***
Total HPC
CA1-2 alv+s.o+s.p
CA1-2 s.r+s.l.m
CA3 alv+s.o+s.p
CA3 s.r+s.l+s.l.m
D2
Density ErbB4+ cells
ErbB4+ cells/mm3
9.0x10³
7.5x10³
6.0x10³
4.5x10³
3.0x10³
1.5x10³
0
**
*
*
**
***
Total HPC
CA1-2 alv+s.o+s.p
CA1-2 s.r+s.l.m
CA3 alv+s.o+s.p
CA3 s.r+s.l+s.l.m

Figure 3-4 Quantitative density analysis of cells expressing PV or/and ErbB4 in WT and NRG1$^{tg\text{-}type\text{-}I}$ mice hippocampal sections. (A1 and A3) Confocal stack images of PV immunopositive somata in the hippocampal sections from WT (WT5 L6_5) (A1) and the NRG1$^{tg\text{-}type\text{-}I}$ (Tg6 L8_3) (A4) mice. (A2 and A4) merged immunofluorescence signals of PV and ErbB4 reactions in the CA3 s.p in the WT (A2) and the NRG1$^{tg\text{-}type\text{-}I}$ (A8) mice (red, PV; green, ErbB4). Scale bars 100 µm. (B1-2) Bar plots showing the density of the PV+ (B1) and the PV and ErbB4 immunopositve cells (B2) in distinct hippocampal contours (blue, WT; red, NRG1$^{tg\text{-}type\text{-}I}$). Comparison of medians with interquartile range. (C1-2) Confocal stack images of the ErbB4 immunpositive somatae in the hippocampal sections from the WT (WT5 L6_5) (C1) and the NRG1$^{tg\text{-}type\text{-}I}$ (Tg6 L8_3) (C2) mice (green, ErbB4). Scale bars 100 µm. (D1-2) Bar plots of the density of PV immunonegative but ErbB4+ cells, and the densities of ErbB4 expressing cells only (D2) in the studied hippocampal contours (blue, WT; red, NRG1$^{tg\text{-}type\text{-}I}$). Comparison of medians with interquartile range, P <0.05 *, P < 0.005 **, P <0.001 *.**

Finally, to validate the specificity of the ErbB4 antibody used in immunocytochemistry, (see section, 2.7) lysate preparations from WT mouse hippocampus were analysed by western blot. As shown in Figure 3-5. A1, the Rb-5941 antiserum labelled the full length of the ErbB4 receptor protein (~150 kDa) without the presence of non-specific immunoreactive bands. Furthermore, no non-specific bands were detected in the secondary antibody control blot (Figure 3-5, A1).

Moreover, given the differences I detected in the density of the ErbB4 immunoreactive somatae between WT and the NRG1 over-expressing mice, I set out to examine general ErbB4 protein levels in the hippocampi of the two genotypes. The western blot analysis was performed with hippocampal tissue lysates from 3 males and 3 females in WT, and 3 males and 3 females of NRG1$^{tg\text{-}type\text{-}I}$ mice.

This densitometry analysis of the ErbB4 protein band normalised against GADPH levels showed no significant effect of the genotype on the expression levels of ErbB4 receptor protein (2-way ANOVA, $F_{1, 11} = 1.756$, $P= 0.222$), but demonstrated higher level of expression in females compared to males ($F_{1, 11}= 6.464$, $P= 0.033$). However, *post-hoc* Bonferroni *t*-test showed no differences when the gender comparisons were made within the genotype. In detail, the analyses in WT males vs females showed displayed a $P= 0.292$, and in the NRG1$^{tg\text{-}type\text{-}I}$ males vs females a $P= 1.000$. In addition, no significant interactions between gender and genotype were

observed ($F_{1, 11} = 0.502$, $P = 0.499$) (Figure 3-5, B). These results indicate that overall levels of the ErbB4 expression are not significantly different (even though a trend towards lower expression in NRG1 mutants of both genders can be observed) between the two genotypes but there may be a gender-driven effect that merits further investigation.

Western blot analysis of ErbB4 levels suggested no significant differences between $NRG1^{tg\text{-}type\text{-}I}$ and WT mice which would fit the significantly lower number of ErbB4-positive cells seen by immunohistochemistry. This can be attributed to the fact that immunofluorescence cell counting was performed in defined hippocampal subregions, whereas the lysates for the immunoblots included entire hippocampal tissue. This could mask possible expression differences that may be specific to hippocampal subregions. Secondly, the sample size used in the western blot analysis may not be adequately powered to reveal significance between the groups.

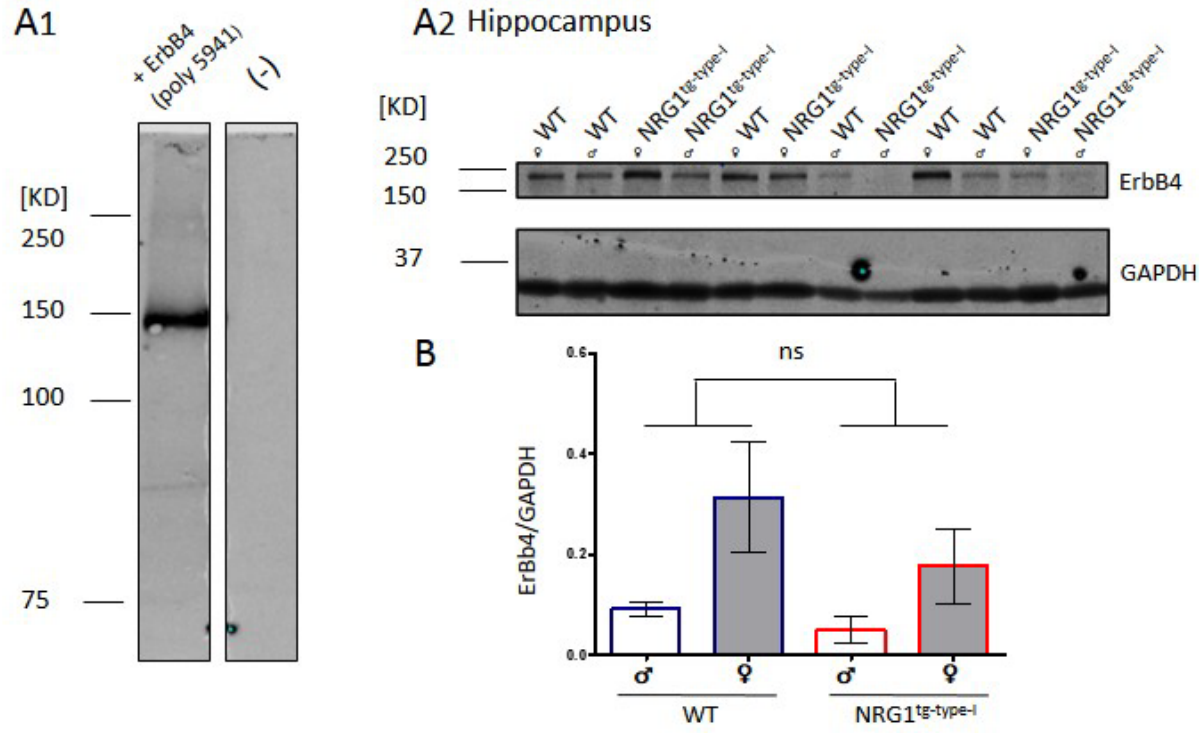

Figure 3-5 Immunoblot analysis of the ErbB4 expression in WT and the NRG1$^{tg\text{-}type\text{-}I}$ mice hippocampal lysates. (A1) Rabbit polyclonal antibody (poly 5941) against the ErbB4 detects a band of the predicted protein size (~150kDa) in hippocampal extracts from a WT mouse with no major non-specific bands. No non-specific bands were detected in the secondary-only antibody control (right lane). (A2) Hippocampal extracts from WT and NRG1$^{tg\text{-}type\text{-}I}$ mice of both genders were analysed for ErbB4 expression and GAPDH was used as a loading control. (B) Densitometry analysis comparison of ErbB4 levels normalised on GAPDH revealed a trend of higher ErB4 levels in females, but no significant difference within distinct genotypes. NB Different reducing conditions and gel percentage were used in (A) and (B) that may account for the different apparent size in the Erb4B detected band.

3.5 Discussion and conclusions

The aims of the experiments presented in this chapter were twofold. Firstly, to establish the major target neurons of the NRG1-ErbB4 signalling pathway in hippocampus, by determining the expression of the ErbB4 receptor in major populations of interneurons expressing either the neurochemical marker PV or CCK. Secondly, to explore whether the

genomic NRG1 over-expression interferes with the GABAergic neurons density that express PV and ErbB4 in the hippocampus.

Using the highly specific custom-made antibody against the ErbB4 receptor, I report that the ErbB4 receptor is strongly present in the GABAergic cells expressing either PV or CCK. In addition, the somatodendritic immunofluorescence signal of the ErbB4 protein is absent in glutamatergic pyramidal cells. My subsequent analysis showed that the great majority of hippocampal PV+ interneurons in the WTs and in the $NRG1^{tg\text{-}type\text{-}I}$ mice co-express the ErbB4 receptor. The percentage of co-expression in the total hippocampal area was equally high for the WT (~78%) for the $NRG1^{tg\text{-}type\text{-}I}$ mice (~76 %). It is worth mentioning that two earlier studies have also demonstrated the co-expression of ErbB4 receptor with PV, however with different estimates. Similar to the findings reported here, Yau and colleagues (Yau et al., 2003), reported a ~82%, co expression of ErbB4 with PV. However, in the study performed by Neddens and colleagues (Neddens and Buonanno, 2010) this estimate reached ~42%. Several reasons can account for these differences including; a) Differences in the antibodies used and in other experimental regimes. b) Differences in the sample size; 2033 PV+ cells were counted in (Neddens and Buonanno, 2010) 159 PV+ cells in (Yau et al., 2003) and 573 PV+ cells in the experiments presented here. c) Species used; the current study and the one performed by Neddens and colleagues used mice, whereas the one performed by Yau and colleagues used rats. d) Differences in the dorsoventral axis level of hippocampal sections; In the study performed by Neddens and colleagues the sections included in the analysis spanned the entire dorsoventral axis, whereas the ones included in the data presented here were obtained from mid-ventral hippocampus whereas the study performed from Yau and colleagues does not report the exact dorsoventral level of the sections analysed and e) Differences in the hippocampal regions examined; In the Neddens and colleagues study, the Dentate Gyrus (DG) and Subuculum (Sub)

areas were included in the co-expression analysis, whereas in the experiments presented here, were omitted, the study performed from Yau and colleagues do not specify the analysed areas. In the same vein, these dissimilarities in the experimental conditions can also account for the more modest variances in the percentage of PV co-expression with ErbB4 (PV+&ErbB4+ out of total number of ErbB4 cells) reported in the three studies. The study reported from Neddens and colleagues reports a ~35 % co-expression, which is similar to the estimate presented here (~40%) in WT mice, while the one from Yau and colleagues states a higher percentage (~56%).

Importantly, hippocampal sections from the NRG1 over-expressing mice displayed a higher percentage of detected PV-co-expression with the ErbB4 (~55%). This finding is attributed to the decreased density of detected ErbB4 immunopositive somata in these mice hippocampus (*total HPC*; ~43%). Notably, this reduction was mostly attributed to the lower numbers of ErbB4 immunopositive cells other than PV+. This was seen as similar densities of the PV+ and PV/ErbB4 co-expressing cells in the two genotypes, but considerably lower densities of PV- /ErbB4+ cells in the NRG1 over-expressing mice. It should be noted that, the experiments presented here, cannot discriminate whether there is a loss of ErbB4 expressing interneurons or there are alterations of the ErbB4 receptor trafficking and expression at these cells that could subsequently lead to decreased or even absence of fluorescence signals and reduced cell counts in sections from NRG1 over-expressing mutants.

Indeed, both scenarios are equally valid. The first possibility is suggested by the fact that NRG1-ErbB4 signalling pathway is crucial for the migration of interneurons from the ganglionic eminences to their final cortical destinations as well as for their survival and proliferation during neurodevelopment at the early stages of brain development (Flames et al., 2004, Li et al., 2012). Indeed, earlier studies have demonstrated that dysregulation of NRG1-ErbB4 signalling results in neuronal loss in the hippocampus and other cortical areas. For example, mice that over-express

non-soluble NRG1 (CRD-NRG1) exhibit reduced number of GABAergic cells in specific neocortical layers (Agarwal et al., 2014). Interestingly, a loss of GABAergic cells has also been reported in the hippocampus of ErbB4 knockout mice (Neddens et al., 2011). Of note, both these studies have reported a decline in the spatial distribution of PV +cells in these areas. However, the latter is not fully in line with my results which showed no alterations in the PV+ interneurons. However, given that a previous estimate of the distribution of the PV+ cells in the $NRG1^{tg\text{-}type\text{-}I}$ mice (back crossed with PV Cre $^{+/+}\times$ Ai9 $^{+/+}$ to express td-Tomato fluorescence signal specifically in PV+ cells) has also reported normal numbers of PV+ interneurons in these animals (Deakin et al., 2012), the discrepancy between my study and the ones mentioned before, probably highlights the fact that multi-directional modifications of this signalling pathway can produce dissimilar effects in the organization of cortical circuits.

Another explanation of the observed reduced density of the ErbB4 immunopositive somata in the hippocampus of the NRG1 over-expressing animals is possible alterations in the expression and trafficking of the receptor at the cell membrane. This hypothesis is strongly supported by the discovery that application of NRG1 on cultured hippocampal neurons rapidly initiates the ErbB4 receptor internalization (Longart et al., 2007). During the course of this thesis, I attempted to test this intriguing hypothesis by performing surface protein biotylination in order to measure the fraction of the ErbB4 receptors on the plasma membrane in the hippocampus of the WT and the NRG1 mutants (data not shown). However I was unable to detect the ErbB4 receptor in the cell membrane lysate fraction, likely due to unsuccessful biotylination of cell membrane proteins, and the subsequently poor levels of the protein sequestration at *in vitro* live brain tissue.

In conclusion, the experiments presented in this chapter show that the PV + as well as the CCK+ interneurons (two major populations of hippocampal interneurons), strongly express

the ErbB4 receptor. The prominent co-expression in those two interneuron subpopulations indicates that NRG1 could exert its modulatory effects on the functionality and organization of the hippocampal neuronal network through these inhibitory GABAergic interneurons. Given that both of these cell populations have clearly identified roles in network operations, it can be suggested that dysregulation in this pathway could underlie some cognitive deficits reported in NRG1 over-expressing mice and perhaps contribute to relevant traits in schizophrenic patients.

Finally, my results suggest that the density of the ErbB4-immunopositive somata in hippocampus is reduced in response to NRG1 over-expression. Even though it is not clear, whether the decline is attributed to the altered trafficking of the receptor or /and disrupted migration of the interneurons during neurodevelopment, the changes clearly show that the wiring of the hippocampal GABAergic microcircuitry is affected. At first this can be observed at macroscopic level (e.g loss of specific GABAergic cells) but can also underlie specific alterations on the synaptic communication subject to the regulatory role of NRG1-ErbB4 signalling (see section 1.1.2). In the next two chapters of this thesis, I will explore these ideas further by performing electrophysiological recordings of distinct physiologically and pharmacologically defined receptor synaptic inputs and outputs of CCK+ cells as well as, which constitute the major although yet poorly investigated target for the NRG1-ErbB4 signalling.

3.6 Perspective and future directions

In the future, further studies are warranted in order to advance our understanding on the impact of NRG1 expression changes in organization of the cortical networks. It will be important to shed light on whether this mode of dysregulation intervenes with cell migration, cell survival and cell proliferation processes in early development of the brain, and with the receptor trafficking in the cells in the adult brain. To investigate the first question, the cell counting method described here could be applied with further use of specific neuromarkers such as

Glutamic Acid Decrboxylase- 67 (GAD-67) that probes all GABAergic cells. In addition, other neuronal markers could be examined in order to uncover how spatial distribution of these interneuron subpopulations in the cortical areas are affected in response to facilitated NRG1-ErbB4 signalling. Finally, optimization of surface protein biotylination to be used with *in vitro* brain tissue samples would be a promising approach to understand possible changes in the trafficking process of the receptor in the ErbB4+ cells.

4 Glutamate receptor-mediated transmission in CCK+ interneurons of NRG1 over-expressing mice

4.1 Introduction- Effects of NRG1 on Glutamatergic transmission

The experiments reported in the previous chapter, in line with earlier studies (Vullhorst et al., 2009, Neddens and Buonanno, 2010) demonstrate that the main targets of NRG1 are specific classes of GABAergic interneurons that express the ErbB4 receptor. Given that alterations of the NRG1-ErbB4 signalling pathway recently have been linked to schizophrenia, several research efforts have focused on the role of NRG1-ErbB4 in modulating synaptic interactions and network activity.

In the past, the effects of the NRG1 peptide over-expression in glutamatergic transmission, has mainly been studied in principal neurons. For instance it has been shown that acute NRG1 application reduces NMDAR currents in principals cells in brain slices from prefrontal cortex (PFC) and in dissociated cell cultures (Gu et al., 2005), and regulates the expression of specific NMDAR receptors in granule cell synapses (Ozaki et al., 1997). Furthermore, it has been found using human *post mortem* tissue samples from prefrontal cortex that increased levels of NRG1 peptide inhibit the assembly and phosphorylation NMDAR subunits (Hahn et al., 2006). More recently, the chronic effects of NRG1 over-expression have been studied in transgenic mice lines that exhibit elevated levels of the NRG1. It was shown that elevated levels of the "cysteine –rich domain" of NRG1 (CRD-NRG1), does not affect glutamatergic transmission in CA1 pyramidal cells (Agarwal et al., 2014). However, chronic elevation of the immunoglobulin domain of the NRG1 (Ig-NRG1) and of the human NRG1-IV isoform, have been reported to impair pre-synaptic glutamate release, (Yin et al., 2013, Papaleo et al., 2016).

Discrepancies in the aforementioned studies can result both from the functional differences of distinct NRG1 peptides used in those studies (soluble vs non soluble peptides), or from differences in the degree of NRG1 levels in the brain preparations. These can have inconsistent effects on the neurodevelopment of neuronal networks. Yet, given that ErbB4 receptor is mainly expressed in GABAergic cells (Vullhorst et al., 2009, Neddens and Buonanno, 2010), the effects of NRG1 over-expression at principal neurons synapses can also highlight the possibility that ErbB4 receptors are not the sole mediators of NRG1 signalling (Yin et al., 2013).

Hippocampal neurons receive glutamatergic inputs from various afferent areas including intra- and extra-hippocampal regions, for a comprehensive review see (Somogyi, 2010). Particularly in the CA3 region of hippocampus, both principal cells and interneurons receive excitatory inputs from a) granule cell axons projecting to CA3 *stratum lucidum* (s.l), b) perforant pathway afferents targeting dendrites mainly in *stratum lacunosum moleculare* (s.l-m), c) commissural fibres from the contralateral CA3 region and d) from the associational "recurrent" fibres of the ipsilateral CA3. The latter two afferent pathways form synapses notably in *stratum radiatum* (s.r) and *stratum oriens* (s.o). Fast glutamatergic synaptic input in these pathways is mediated by AMPAR/Kainate and NMDAR receptors (McBain and Dingledine, 1992, McBain and Dingledine, 1993, Toth and McBain, 1998) whose degree of involvement depends on the post-synaptic cell type and the afferent input (Baude et al., 1995, Nusser et al., 1998, Toth and McBain, 1998, Lei and McBain, 2002, Nyiri et al., 2003, Blatow et al., 2005, Matta et al., 2013).

Here, by employing electrophysiological whole-cell recordings with *post hoc* anatomical analysis, I aim to assess whether chronic NRG1 over-expression affects the excitatory drive on to the CCK/CB_1R -expressing (CCK+/CB_1R+) cell population, a major target of the NRG1-ErbB4 signalling pathway. To address this, I studied both stimulus-evoked synaptic and spontaneous quantal mEPSCs, and analysed the post-synaptic AMPAR and NMDAR-mediated

currents in *post-hoc* immunocytochemically verified CCK/CB_1R immunopositive cells in the CA3 hippocampal area of the $NRG1^{tg\text{-}type\text{-}I}$ and the WT mice.

4.2 Analysis of the NMDAR and AMPAR-mediated current ratio in synapses onto CCK+ interneurons in $NRG1^{tg\text{-}type\text{-}I}$ and WT mice

4.2.1 Experimental paradigm

To compare properties of glutamatergic synapses on to CCK+/CB_1R+ interneurons between $NRG1^{tg\text{-}type\text{-}I}$ and WT littermate animals, I performed whole-cell voltage clamp recordings from *post hoc* confirmed immunopositive for CCK/CB_1R neurons in the ventral hippocampus CA3 area.

To allow a reliable comparison of the excitatory pathway inputs to CCK/CB_1R-positive interneurons in both genotypes, recording of excitatory currents was elicited by electrical focal (bipolar stimulation electrode) stimulation in the CA3 area *stratum oriens* (s.o) aiming to activate mainly the associative and/or commissural fibres. The EPSCs were recorded from interneurons with somata located in CA3 *stratum radiatum* (s.r) or near its border close to *stratum lucidum* (s.l) or *stratum lacunosum moleculare (s.l-m)* in whole-cell voltage clamp mode and at a variable distance from the stimulation electrode (Figure 4-1 A). In the experiments Cs-Methanesulfonate -based intracellular solution containing QX-314 (5 mM) was used. Cells were filled with neurobiotin (0.2-0.4 %) for *post-hoc* visualisation with streptavidin- conjugated fluorophores.

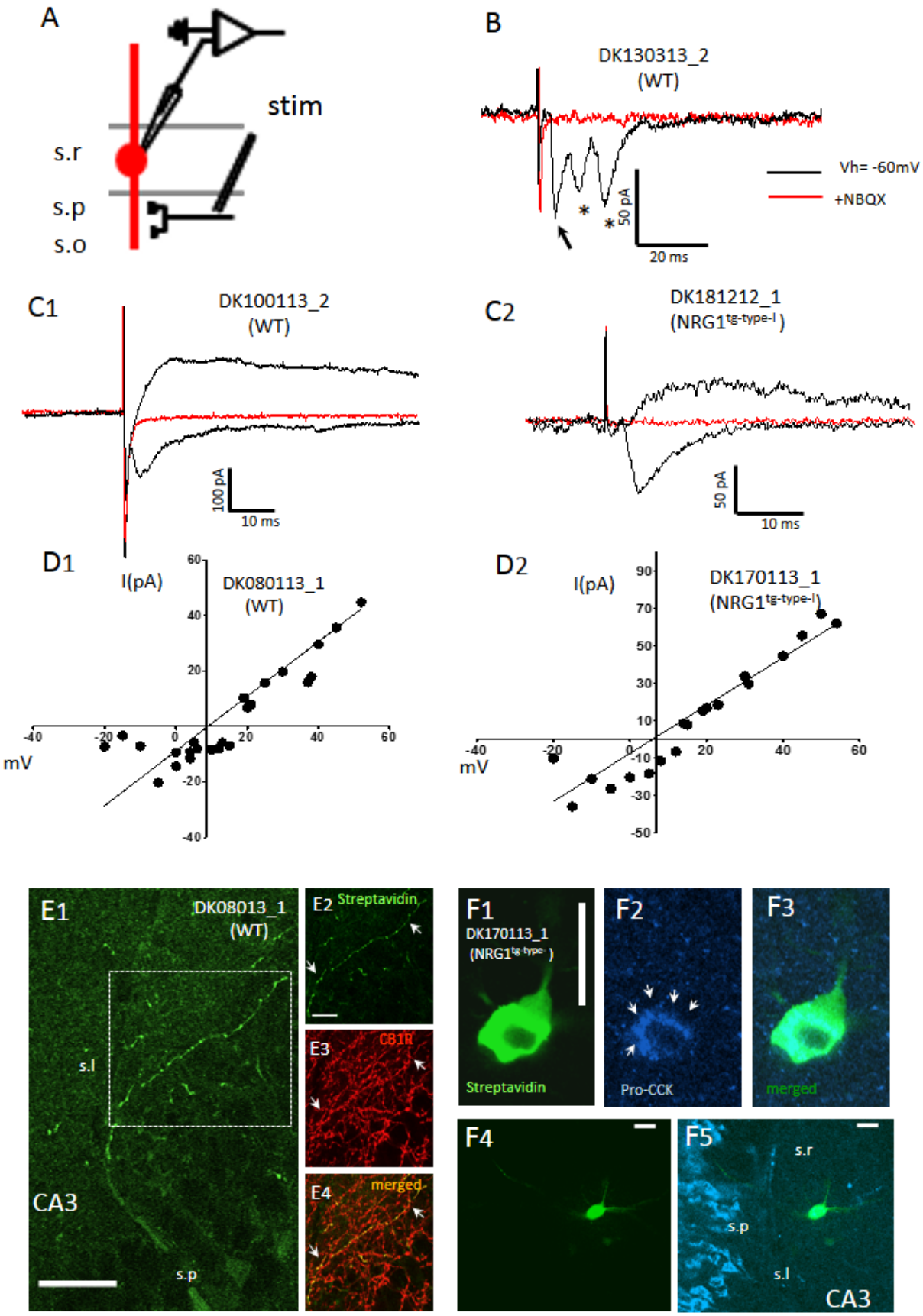
A
stim
s.r
s.p
s.o
B
DK130313_2
(WT)
Vh= -60mV
+NBQX
50 pA
20 ms
C1
DK100113_2
(WT)
100 pA
10 ms
C2
DK181212_1
(NRG1tg-type-I)
50 pA
10 ms
D1
I(pA)
DK080113_1
(WT)
mV
D2
I(pA)
DK170113_1
(NRG1tg-type-I)
mV
E1
DK08013_1
(WT)
s.l
CA3
s.p
E2 Streptavidin
E3 CB1R
E4 merged
F1
DK170113_1
(NRG1tg-type-I)
Streptavidin
F2
Pro-CCK
F3
merged
F4
F5
s.r
s.p
s.l
CA3

Figure 4-1 Assessment of NMDA/AMPA receptor-mediated currents in CCK+/CB_1R+ interneurons. (A) Experimental paradigm of electrical stimulation-elicited EPSCs in postynaptic CCK+/CB_1R+ interneurons. Focal stimulation in CA3 s.o aiming to activate associational and commissural glutamatergic fibres. The recorded cells somata were mainly located in CA3 s.r. or near its border close to s.l or s.l.m at varying distance from the stimulation electrode. (B) Activation of associational and commissural fibres to post-synaptic excitatory currents in cells located in s.r (black traces) often lead to reverberating cycles of polysynaptic excitation (asterisk noted). Stable monosynaptic responses were visually verified in whole-cell recording at -60 mV holding potential, characterised by minimal jitter and < 8ms delay (arrow noted). The post-synaptic currents (voltage clamp recordings at -60 mV) were fully blocked with the AMPAR/KAR antagonist NBQX (red trace) confirming their AMPAR origin. (C1-2) Representative AMPAR EPSC (black inward trace, at -60 mV holding potential) and the NMDAR EPSC (outward trace, at +40 mV following NBQX application from the NMDAR EPSC reversal potential) evoked by the aimed associational/commissural pathway stimulation in CCK+/CB_1R+ cells in WT and $NRG1^{tg\text{-}type\text{-}I}$ mouse hippocampus. Red trace; complete abolishment of EPSCs at -60mV holding potential after NBQX application. (D1-2) I-V relationship plot of the NMDAR-mediated currents. Lines indicate the linear fit in EPSC amplitude values recorded between -20 mV and ~ 55 mV in CCK+/CB_1R+ interneurons in the two genotypes. Data points are single current values at corresponding holding potentials or averaged when multiple measurements were performed at a given holding potential. (E1-4) Immunohistochemical characterization of CB_1R positivity. (E1-2) Streptavidin visualization of the recorded cell axon. (E3) CB_1R is expressed in the axonal compartments. (E4) Merged streptavidin and anti-CB_1R reactions reveal CB1R positivity of the axon. (F1-3) Immunhistochemical characterization of CCK positivity. (F1&4) Streptavidin visualization of a recorded cell soma in s.r/s.l. border. (F2) Characteristic somatic semi-lunar immunostaining pattern for pro-CCK. (F3) Merged streptavidin and anti-proCCK immunofluorescence signal. (F5) In s.p. of the CA3 area, there is strong immunopositivity for CCK, due to its expression in pyramidal cells. Identification of CCK interneurons is determined by aspiny cell dendrites, soma location and axon morphology. Scale bars; 20 µm

Pharmacologically isolated AMPAR-mediated EPSCs were recorded at -60 mV holding potential in the presence of GABA-A and -B receptor blockers PiTX 100 µM and CGP55845 1 µM, respectively (Figure 4-1 B, C1 & C2). Following blockade of the AMPA/kainate receptors with NBQX (25 µM), NMDAR EPSCs were measured at various membrane potentials from -20 till +55 mV and I-V relation was made in this range with linear fitting of the regression curve with the data points of NMDAR EPSC amplitude (Figure 4-1 D1 & D2). The NMDAR current value to calculate NMDA/AMPA EPSC ratio was taken from the linear curve exactly at +40 mV from the measured NMDAR EPSC reversal potential (E_{NMDAR}). AMPAR-mediated amplitude EPSCs values were measured at -60 mV. During the AMPAR EPSCs recordings, the monosynaptic component of the post-synaptic EPSCs was visually verified (Figure 4-1 B). Recordings were *post-hoc* low pass filtered at 1 kHz and the peak current amplitude was calculated with an in built function of pClamp software. For AMPAR-mediated recordings at -

60 mV, the baseline was taken ~1 ms after stimulation artifact and the current amplitude was measured as the negative current peak. For the NMDAR-mediated currents, baseline was taken 1 ms before stimulation artefact and peak amplitude was detected as the peak of the event at a ~15 ms window post-stimulus. Of note in 4 *post-hoc* identified CCK+/CB_1R+ cells the measured currents were fully blocked by DL-AP5 (100 μM) confirming their NMDAR origin (Figure 4-2 B1).

Recordings that exhibited more than 25% change in access resistance (Ra) between AMPAR and NMDAR recordings were excluded from the analysis. In cases, that Ra transiently fluctuated, only the related sweeps were removed. The slices with recorded cells, filled with neurobiotin, were fixed overnight at +4 C^o degrees in paraformaldehyde and 15% glutaraldehyde (see section2.6.1), re-sectioned and visualized with streptavidin-Alexa 488. Cells with CCK+ -like interneuron structure (Lasztoczi et al., 2011) were tested for somatic pro-CCK and/or axonal cannabinoid receptor 1 (CB_1R) immunopositivity. Immunoreactions were evaluated under a confocal microscope with appropriate filters and the reactions were concluded positive if there was a clear co-localisation of the tested marker with the streptavidin fluorophore signal (Figure 4-1 E1), and negative if no clear secondary antibody-associated fluorophore signal was detected in the cell structure when good sample cell staining were observed in other cells of the section (Figure 4-2 D2).

Altogether, I recorded from 72 neurons of which 22 with stable electrophysiological recordings were identified as CCK+ or/and CB_1R+ interneurons.

4.2.2 Results

To evaluate whether NRG1 over-expression has a role in the excitatory synaptic function on CCK+ interneurons, I analysed the ratio of the synaptic currents mediated by NMDA and AMPA glutamate ionotropic receptors (N/A ratio) in the identified CCK+/CB_1R+ interneurons. In total, 10 cells from WT and 12 cells from $NRG1^{tg\text{-}type\text{-}I}$ mice, were identified as CCK+/CB_1R+ interneurons. Table 4.1 summarizes the anatomical and neurochemical features as well as the synaptic current components of these cells, together with the coefficient of determination (R^2) of the fitted regression line for the NMDAR-mediated current data points. A comparison of the NMDAR-mediated to AMPAR-mediated peak current amplitude (N/A ratio) between the two cell groups revealed a 41.5% smaller relative NMDAR-mediated component in the $NRG1^{tg\text{-}type\text{-}I}$ mice (WT, 1.22 ± 0.56; $NRG1^{tg\text{-}type\text{-}I}$ 0.71 ± 0.14, (means, P= 0.033, t-test) (Figure 4-2A1-2).

It should be noted that in the recordings, synaptic delay after the electrical stimulation was typically < 5ms, but 3 CCK+/CB_1R+ cells (DK270713_3, DK290713_2, DK150115_1) displayed slightly longer synaptic delays (7-8 ms). This observation raised the possibility that during these recordings, focal stimulation of the excitatory fibres in s.o led to activation of the targeting pre-synaptic excitatory fibres not in a direct- monosynaptic manner, but polysynapticaly by activating firstly a number of excitatory fibres that in turn provide sufficient excitation to the pre-synaptic targeting cells. This additional cycle (s) of excitation constitutes a major limitation for N/A recordings, because application of AMPA/Kainate blockers like NBQX used to isolate NMDAR-mediated currents, attenuates the excitation of the targeting pre-synaptic fibres and can lead to inaccurate readings of NMDAR-mediated currents. Nonetheless, polysynaptic activity is mainly characterised by instable with pronounced jitter post synaptic responses (Figure 4-2 C1-2; light blue panel). On the contrary, voltage clamp recordings from these 3 cells, had an early post synaptic component that was clearly stable over time (Figure

4-2C1-2; light red panel). Moreover, isolated NMDAR-mediated currents were also prominent in one cell *(DK080113_1)* that also displayed post synaptic delay > 5ms (Figure 4-2 C2 top right inset). Thus, it was assumed that the post-synaptic events reflect activation of a direct monosynaptic input and were included in the analysis of this data set. One possible explanation for the 2-3 ms longer delay than usual, may be attributed to the morphological features of the CA3 pyramidal cells. Axons from CA3 PCs stem from near the basal dendritic region and can display a variable length before they travers s.p and reach their cellular targets in s.r, hence stimulation of glutamatergic fibres in s.o could activate axons that show increased deviation from the direct line between the stimulation electrode and the patched soma in s.r lead leading to prolonged synaptic delays. Another point of consideration is that during these experiments the stimulation electrode was not at fixed distance from the patched soma. Thus, it is possible that presynaptic glutamatergic inputs of diverse origin were activating different synaptic sites along the somatodendritic axis of the post-synaptic cell. This could have led to an inconsistent distortion of the recorded ionic currents during whole cell somatic recordings across different cell recordings. However, it is expected that the current distortion was similar across the AMPAR and NMDAR mediated ionic currents at a given cell recording, thus having minimal effects on the estimate of the N/A peak current ratio. Yet, it cannot be excluded that activation of different glutamatergic inputs as a result of the not fixed position of the stimulation electrode could result in the recording of post-synaptic currents from variable synaptic sites with a variable ionotropic receptor composition. The anatomical analysis of these CCK+/CB_1R+ interneurons indicate that the cells belong to both perisomatic (axonal arborisation in s.p) and dendritic (axonal arborisation in s.o/ s.r/s.l-m) targeting interneuron categories (Table 4-1).

Overall, these experiments, suggest that chronic elevation of NRG1, leads to a ~ 42% relative decrease of the contribution of NMDAR-mediated synaptic currents compared to AMPARs EPSCs in CCK+/CB_1R+ interneurons.

Because the change in N/A ratio is not sufficient to discriminate whether a decline of NMDAR-mediated EPSCs or an enhancement of AMPAR EPSCs occurred in these cells, and in addition it does not reveal whether it was caused by pre- or post-synaptic changes in glutamatergic transmission, I next performed whole-cell recordings of glutamatergic quantal events (miniature post synaptic currents i.e. mEPSC) from CCK+/CB_1R+ cells in the two genotypes (section 4.3).

Table 4-1 Overview of the anatomical and neurochemical features and synaptic current components of the identified CA3 CCK+/CB_1R+ cells

	Immunohistochemistry						Post-synaptic currents			
Cell record	**Genotype**	**soma**	**Axon**	**dends**	**CB_1R**	**Pro-CCK**		**NMDA/AMPA ratio**	**R^2 NMDA Regression curve**	**E_{NMDAR} (mV)**
DK101212_1	WT	n/r	s.r	n/r	+	n/t		1.25	0.76	6.99
DK080113_1	WT	n/r	s.r, s.o, hil	n/r	+	n/t		1.1	0.77	7.57
DK100113_2	WT	s.r	s.r, hiL	s.r/s.l-m	+	n/t		1.79	0.95	13.98
DK230113_1	WT	s.r	s.r/s.p	s.r/s.l-m	+	n/t		1.12	0.87	4.7
DK070213_1	WT	s.r	n/r	s.r/s.l-m	n/t	+		1.21	0.67	10.62
DK130313_2	WT	s.r/s.l	s.r/s.l	s.r/s.l-m	+	n/c		0.82	0.70	10.08
DK280313_2	WT	s.r	s.r/s.l	s.r	+ (weak)	+ (weak)		0.63	0.52	8.76
DK100513_2	WT	s.l	s.r	s.r/s.l-m	n/c	+		0.68	0.87	5.7
DK160513_2	WT	s.r	s.l/(s.r)	s.r	+	n/c		1.12	0.37*	14.73
DK270713_3	WT	s.r	s.l-m	s.r/s.p/s.o	+	n/c		2.50	0.79	11.1
DK131212_2	$NRG1^{tg\text{-}type1}$	s.r/s.l-m	s.l-m,(s.r,s.p)	s.r (s.l-m)	+	n/t		0.07	0.04*	n/a
DK181212_1	$NRG1^{tg\text{-}type1}$	n/r	s.r	n/r	+	n/t		0.57	0.74	17.9
DK110113_2	$NRG1^{tg\text{-}type1}$	s.r	s.l-	s.l-m	+	n/t		0.87	0.70	23.6
DK150113_1	$NRG1^{tg\text{-}type1}$	s.r	s.r/s.p	s.r	+	n/t		app. 0	n/a *	n/a
DK170113_1	$NRG1^{tg\text{-}type1}$	s.r	n/r	s.l-	n/t	+		0.56	0.89	10.63
DK170113_2	$NRG1^{tg\text{-}type1}$	s.r	n/r	s.o/s.r	n/t	+		1.08	0.53	9.43
DK060213_1	$NRG1^{tg\text{-}type1}$	s.r	s.r/s.l-m	s.p,s.r,s-	+ (weak)	n/t		1.21	0.78	17.8
DK210213_1	$NRG1^{tg\text{-}type1}$	n/r	s.p	s.r/s.o	+	n/t		0.54	0.59	16.7
DK080313_2	$NRG1^{tg\text{-}type1}$	n/r	s.p	s.l-m	n/c	+		0.88	0.76	12.02
DK040713_2	$NRG1^{tg\text{-}type1}$	n/r	s.r/s.l	n/r	+	n/t		0.37	0.48	5.71
DK290713_2	$NRG1^{tg\text{-}type1}$	n/r	s.r/s.p	nr	+	n/t		1.79	0.89	8.21
DK220513_1	$NRG1^{tg\text{-}type1}$	s.r	s.l-m	s.p/s.o	-	+ (weak)		0.55	0.57	5.29

hil; hilus n/r; not recovered, n/t; not tested, n/c not conclusive, n/a; not applicable. Parenthesis; axon not prominent. NB, in few cases the R^2 value indicated a high variance of the post-synaptic NMDAR currents, especially in recordings with low NMDAR component

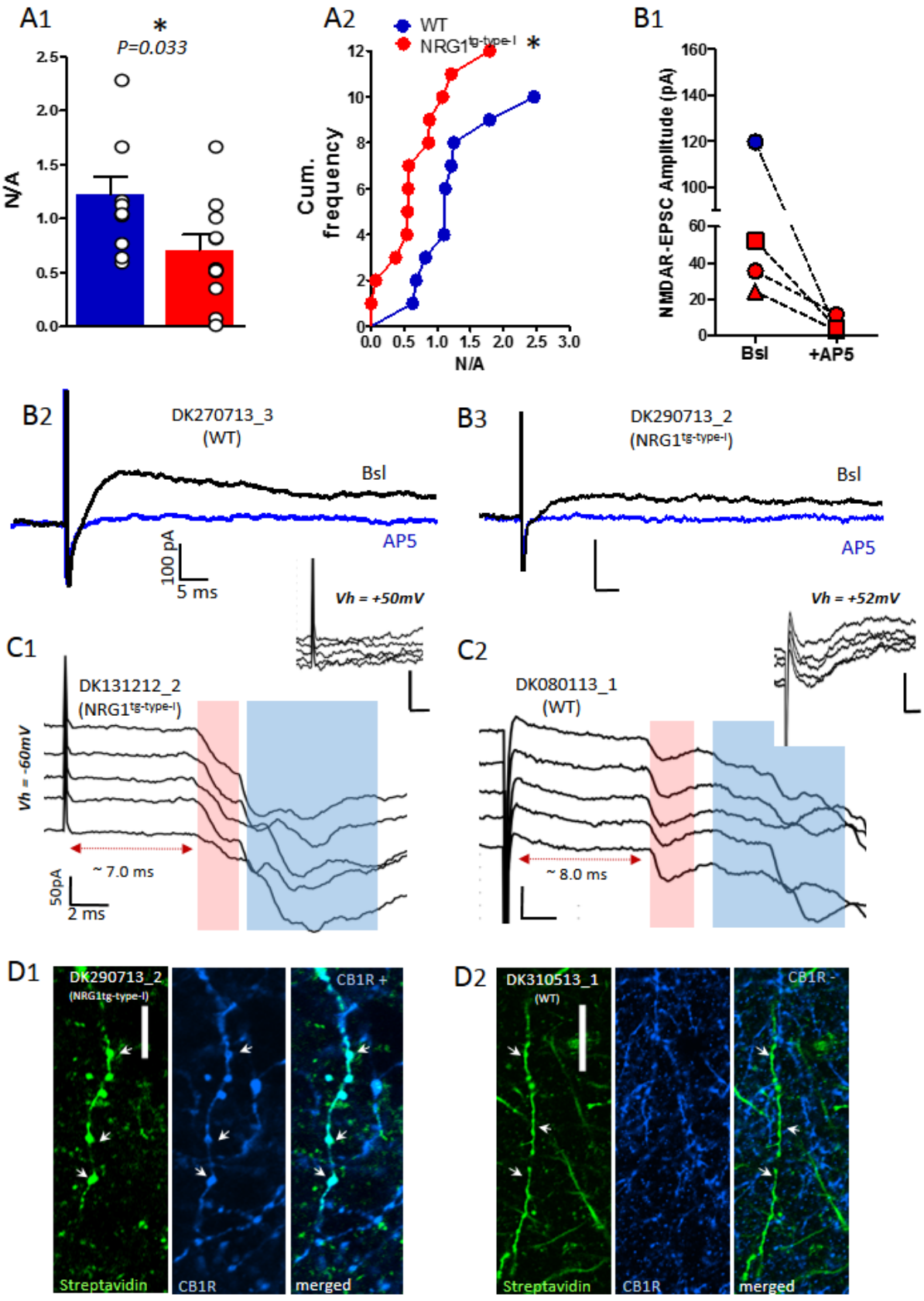
A1
*
P=0.033
N/A
A2
WT
NRG1tg-type-I
*
Cum. frequency
N/A
B1
NMDAR-EPSC Amplitude (pA)
Bsl
+AP5
B2
DK270713_3
(WT)
Bsl
AP5
100 pA
5 ms
Vh = +50mV
B3
DK290713_2
(NRG1tg-type-I)
Bsl
AP5
Vh = +52mV
C1
DK131212_2
(NRG1tg-type-I)
Vh = -60mV
~ 7.0 ms
50pA
2 ms
C2
DK080113_1
(WT)
~ 8.0 ms
D1
DK290713_2
(NRG1tg-type-I)
CB1R +
Streptavidin
CB1R
merged
D2
DK310513_1
(WT)
CB1R -
Streptavidin
CB1R
merged

Figure 4-2 NRG1 over-expression causes a decline in the NMDA/AMPA (N/A) current ratio in CCK+/ CB_1R+ interneurons. (A1) Summary graph of the N/A ratio of CCK+/ CB_1R+ cells recorded in the $NRG1^{tg\text{-}type\text{-}I}$ mice (red) and WT littermates (blue). (A2) Cumulative histograms of the N/A ratio (blue: WT, red: $NRG1^{tg\text{-}type\text{-}I}$, circles). (B1) Scatter plot, abolishment of the evoked EPSCs (in the presence of NBQX) with DL AP-5 (100 μM) confirms their NMDAR-mediated origin; tested in 3 CCK+/CB1R+ cells from $NRG1^{tg\text{-}type\text{-}I}$ and 1 from WT mice (individual cells shown with different symbols). (B2-3) Representative EPSCs traces at + 40 mV from E_{NMDAR} in baseline (Bsl) and following DL AP-5 (blue trace) application from WT and $NRG1^{tg\text{-}type\text{-}I}$ mice as indicated. (C1-2) Examples of rare cells AMPAR mediated current traces which displayed > 5 ms onset of post-synaptic responses (Vh = -60mV) in response to the electrical stimulation of associational/commissural fibres. Shaded pink background highlights current traces with stable monosynaptic-like delays; Light blue panels highlight AMPAR mediated current traces displaying characteristic polysynaptic responses originating from multiple cycles of excitation at the CA3 associational/commissural recurrent excitatory network. Insets show the evoked NMDAR-mediated EPSCs of these cells. (D1) Left; confocal image of a neurobiotin-filled axon visualized with streptavidin-Alexa 488. Middle; immunoreaction for axonal CB_1R (Cy5, arrows). Right; a merged image of the two fluorescence channels, confirming CB1R immunopositivity. (D2) As above, Left; visualized axon. Middle; CB_1R immunoreaction. Right; a merged image of the two fluorescence channels, confirming immunonegativity for CB1R. Scale bars 20 μm

4.3 AMPAR and NMDAR-mediated quantal currents in CCK+ interneurons of $NRG1^{tg\text{-}type\text{-}I}$ and WT mice

4.3.1 Experimental paradigm

To assess whether the observed alterations in the NRG1 over-expressing mice occur via a pre or post-synaptic mechanism, and whether the altered N/A ratio in CCK+/CB_1R+ interneurons stems from an increased AMPAR-current or decreased NMDAR-current, I set out to investigate spontaneous quantal miniature excitatory post-synaptic currents (mEPSCs) in hippocampal slices from WT and $NRG1^{tg\text{-}type\text{-}I}$ mice.

The mEPSCs were recorded in whole-cell mode using Cs-Methanesulfonate -based intracellular solution supplemented with 5 mM QX-314 and containing 2-4 % neurobiotin for *post hoc* cell visualization. The experiments were done in the continuous presence of GABA-A and GABA-B receptor blockers PiTX (100 μM) and CGP55845 (1 μM), respectively from interneuron somata in the CA3 stratum radiatum. In order to discriminate AMPAR- and NMDAR -mediated currents, the cells were first voltage-clamped at -65 mV (recorded for at least 2 minutes). Next the AMPA/Kainate receptors were blocked with NBQX (25μM). To exclude the posibility of missidection due to noise baseline levels as well as to confirm the

AMPAR mediated origin of neurotransmission, only recordings that the mEPSCs were efficiently blocked by NBQX were included in the analysis (76.3-100%, abolishment of detected events) (Figure 4-3 A1-2). The cells were then voltage-clamped at +40 mV in the presence of NBQX, so that post-synaptic events were solely mediated by NMDARs. In the majority of cells (except one) this was confirmed by supression of events by DL-AP5 (100μM) (suppression of detected events to 76.8-100%) (figure 4.3 C1-2).

For both AMPAR- and NMDAR-mediated mEPSCs, 2 minute-long recordings were band passed filtered at 4 Hz-5 kHz, detected and analysed with a built-in function of pClamp software. Criteria for the mEPSC detection were set as fixed threshold values for the event amplitude and duration. These criteria were first tested in preliminary recordings by visually assessing the recordings for reliable detection of mEPSCs to diminish the chance of false positive detection. Due to the higher noise level at a +40 mV holding potential than at – 65 mV, and different kinetics of the two type of currents the criteria for detection of AMPAR and NMDAR mEPSCs events differed. For the AMPAR-mediated mEPSCs, the criteria were: minimum amplitude 5 pA in 0.5-100 ms time window, with noise rejection of 0.5 ms. For the NMDAR mEPSCs the criteria were: minimum amplitude 7 pA in 0.8-200 ms time window, with noise rejection of 0.8 ms. The same criteria were applied to all recorded cells in both WT and $NRG1^{tg\text{-}type\text{-}I}$ mice. *Post-hoc* -identified CCK+/CB_1R+ cells (for anatomical identification see 4.2.1 and 4.2.2) were analysed for frequency of mEPSC occurrence, current amplitude and area under the curve from event's onset to its end. In addition, the cumulative sum of events peak amplitudes NMDAR/AMPAR ratio was calculated. However, the low signal-to-noise level (detected events mostly < 20 pA) challenged accurate analysis of the recorded currents kinetics. Access resistance was monitored throughout the recordings. In the beginning and the end of the recordings, the Ra was calculated and given as an average of the two measures (Table 4-2). Recordings with Ra >

40 MΩ were discarded., Recordings that showed more than 25% change between the AMPAR and NMDAR-mediated mEPSCs recordings were not included in the estimate of the N/A cumulative ratio either.

A total of 42 whole- cell recordings from both the genotypes were performed, out of which 13 cells from both genotypes with usefull physiology were immunocytochemically verified to be CCK+/CB_1R+ interneurons (Table 4-2).

Table 4-2 Overview of AMPAR- and NMDAR-mediated mEPSCs components in identified CA3 CCK+/CB_1R+ interneurons

	AMPAR-mediated mEPSCs (Vh= -65 mV)						NMDAR-mediated mEPSCs (Vh= +40mV)					
Cell record	**Genotype**	**Mean Frequency (Hz)**	**Mean peak Amp (pA)**	**Mean Area (pA.ms)**	**% Event Abolishment (NBQX 25µM)**	**Ra (MΩ)**	**Mean Frequency (Hz)**	**Mean peak Amp (pA)**	**Mean Area (pA.ms)**	**% Event Abolishment AP5 (100µM**	**Ra (MΩ)**	**Cum N/A**
DK021213_1	WT	5.03	17.62	38.51	100.00	*(20.52-19.94)* 20.23	1.75	16.46	79.42	100.00	*(18.0-17.76)* 17.88	0.33
DK070314_2	WT	1.34	14.74	34.13	87.31	*(24.30-17.10)* 20.7	4.50	15.38	43.53	100.00	(15.3-17.46) 16.38	3.49
DK010314_2	WT	2.08	18.86	41.24	100.00	*(26.0- n/a)* 26.00	15.79	17.66	47.89	n/a	*(18.38-17.57)* 17.98	n/a
DK130114_1	WT	1.99	11.53	20.38	100.00	*(20.79- 21.03)* 20.91	3.43	15.6	51.35	100	*(17.03-16.83)* 16.93	2.43
DK020414_1	WT	3.20	13.04	42.81	97.66	*(36.96-35.38)* 36.17	5.92	15.61	40.30	100	*(28.58-14.22)* 21.4	n/a
DK091213_1	WT	1.31	12.40	21.90	100.00	*(21.72- 20.69)* 21.21	0.74	16.72	92.75	100	*(24.57-24.5)* 24.54	0.78
DK031213_2	WT	n/a	n/a	n/a	n/a	n/a	0.30	17.36	186.93	100	*(39.6-41.03)* 40.32	n/a
DK130914_1	WT	1.34	12.85	25.15	97.51	*(23.72-25.34)* 24.53	3.90	16.62	49.48	83.84	*(16.6-14.25)* 15.43	n/a
DK030414_1	WT	n/a	n/a	n/a	n/a	n/a	9.65	16.56	59.78	99.99	*(19.78-21.72)* (20.75)	n/a
DK040214_1	$NRG1^{tg\text{-}type1}$	1.93	17.10	61.67	87.00	*(27.8-25.8)* 26.8	1.43	15.05	51.98	86.00	*(23.78-24.84)* 24.31	0.64
DK100214_2	$NRG1^{tg\text{-}type1}$	0.44	10.93	23.62	100	*(19.94.37.19)* 28.57	0.22	15.49	97.44	100.00	*(28.22-24.81)* 26.52	0.72
DK300114_1	$NRG1^{tg\text{-}type1}$	4.22	15.81	59.62	76.3	*(26.95-28.08)* 27.52	0.59	15.47	80.38	76.80	*(19.18-21.42)* 20.3	(0.13)
DK250914_3	$NRG1^{tg\text{-}type1}$	1.07	12.76	36.27	81.10	*(36.38-34.62)* 35.5	**0.73**	14.67	68.15	100	*(34.18-40.39)* 37.3	0.76

4.3.2 Results

4.3.2.1 AMPAR-mediated mEPSCs

Spontaneous miniature synaptic currents were recorded at -65 mV holding potential from the CCK+/CB_1R+ interneurons in acute slices of WT and the $NRG1^{tg\text{-}type\text{-}I}$ mice. Across 7 and 4 immunocytochemically identified CCK+/CB_1R+ interneurons from WT mice and $NRG1^{tg\text{-}type\text{-}I}$ mice, respectively, the AMPAR-mediated mEPSCs exhibited similar peak amplitudes: WT: 14.34 ± 1.06 pA; $NRG1^{tg\text{-}type\text{-}I}$ 14.15 ± 1.41 pA (means, P= 0.88) (Figure 4-3, B1). Likewise there was no significant difference in the area under the mEPSCs events curve between the two genotypes: WT: 32.02 ± 3.56 pA × ms; $NRG1^{tg\text{-}type\text{-}I}$: 45.3 ± 9.24 pA x ms. (means, P= 0.142) (fig. 4.3, B3). Furthermore, mEPSCs of both genotypes showed similar frequency of occurrence: WT, 1.99 (1.34 to 2.92) Hz; $NRG1^{tg\text{-}type\text{-}I}$, 1.5 (0.76 to 3.08) Hz (medians P= 0.412) (Figure 4-3, B2). Notably, Ra was found not to differ between the two genotypes WT, 21.1 (20.75 to 25.63) MΩ; $NRG1^{tg\text{-}type\text{-}I}$, 28.05 (27.16 to 32.04) (medians P = 0.073).

The observation that NRG1 over-expression does not cause changes in these parameters suggest that AMPAR-mediated synaptic transmission is not robustly altered either pre- or post-synaptically.

4.3.2.2 NMDAR-mediated mEPSCs

In contrast to AMPAR, recordings of NMDAR-mediated mEPSCs at +40mV in 9 and 4 immunocytochemically identified CCK+/CB_1R+ interneurons in WT and $NRG1^{tg\text{-}type\text{-}I}$ mice respectively, suggested that the NMDAR component of glutamatergic synapses is selectively compromised. In particular, the chronic NRG1 elevation in the $NRG1^{tg\text{-}type\text{-}I}$ mice seemed to cause a small (7.73%), yet statistically significant decrease in the peak amplitude of the recorded mEPSCs: WT, 16.44 ± 0.79 pA; $NRG1^{tg\text{-}type\text{-}I}$, 15.17 ± 0.39 (means, P= 0.012) (Figure 4-3, D1). Even so, the area of the mEPSCs was not found to differ between the genotypes; WT, 51.35

(46.8 to 82.75) pA × ms; NRG1tg-type-I 74.27 (60.07 to 88.91) pA x ms, (medians P= 0.247) (Figure 4-3, D3). Additionaly, it was found that frequency of the detected NMDAR mEPSCs differed between WT and the NRG1tg-type-I mice; WT, 3.9 (1.5 to 6.85) Hz; $NRG1^{tg\text{-}type\text{-}I}$, 0.66 (0.41 to 1.08) Hz (medians P= 0.037) (Figure 4-3, D2). No differeneces were found in Ra between whole-cell recordings in the two genotypes; WT, 17.98 (16.79 to 22.19) MΩ; $NRG1^{tg\text{-}type\text{-}I}$, 25.42 MΩ (22.31 to 31.91), (medians P= 0.143).

Given that amplitude and frequency of mEPSCs reflect the efficiency of the synapse, the above data indicate that chronic NRG1 elevation effects the NMDAR- mediated synaptic drive on CCK+/CB_1R+ interneurons. At first, it is generally assumed that the amplitude of mEPSCs is determined by the amount and functionality of post-synaptic receptors, as well as from the quantity the of glutamate quanta released pre-synaptically (Liu et al., 1999, Ishikawa et al., 2002). Therefore alterations in NMDAR-mediated mEPSCs magnitude, could suggest either that the number or/and functionality of post-synaptic NMDARs is changed in $NRG1^{tg\text{-}type\text{-}I}$ mutants or that neurotransmitter vesicle release probability is pre-synapticaly compromised. The latter possibility is further higlighted by the observed changes in the frequency of the detected events. However, in marked contrast to the effects on NMDAR-mediated miniature events that could suggest alterations pre- or/and post-synaptically, NRG1 over-expression had no effects on the frequency or amplitude of AMPAR-mediated events. This finding, supports that the neurotransmitter release in the synaptic cleft is principally unaltered. An explanation of the disagreement between the data obtained from AMPAR mEPSCs and NMDAR mEPSCs recordings concerning a possible pre synaptic change, might involve the chosen post-synaptic events detection and analysis approach. Due to the high noise recording conditions at +40 mV holding potential, the detection amplitude minimum was set at 7pA, thus it's possible that a higher number of NMDAR- mediated events are falling below this detection threshold in

recordings from NRG1$^{tg\text{-}type\text{-}I}$ mice. Of note, the fact that a change in the amplitude of NMDAR-mediated mEPSCs in NRG1$^{tg\text{-}type\text{-}I}$ was not accompanied by change in the area of the events, could imply alterations to NMDAR-mediated current kinetics leading to prolonged currents decay times. However, accurate analysis of the current kinetics was not feasible in the relatively small amplitude events recorded, and a possible association between NRG1 over-expression and slower NMDAR current kinetics could not be examined.

Finally a comparison of the cumulative N/A ratio from 4 and 3[1] CCK+/CB_1R+ cells in WT and NRG1$^{tg\text{-}type\text{-}I}$ mice respectively showed a non statistically significant trend towards a decline of N/A in NRG1$^{tg\text{-}type\text{-}I}$ mutants; WT, 1.61 (0.56 to 2.96); NRG1$^{tg\text{-}type\text{-}I}$, 0.72 (0.66-0.75) (medians, P = 0.4). However, the finding needs to be treated cautiously, because of the low number of cells in the analysis. (discussed further in section 4.4).

Taken together the above data on AMPAR and NMDAR-mediated mEPSCs suggest that the NMDAR component at glutamatergic synapses onto CCK+/CB_1R+ interneurons is altered in the NRG1$^{tg\text{-}type\text{-}I}$ mice, likely via a post-synaptic alteration in the composition or density of NMDA receptors without producing detectable effects in AMPA receptor-mediated transmission.

[1] The comparison of the cumulative N/A was only performed to cell recordings that displayed <25% change in the Ra between AMPAR and NMDAR mEPSCs recordings

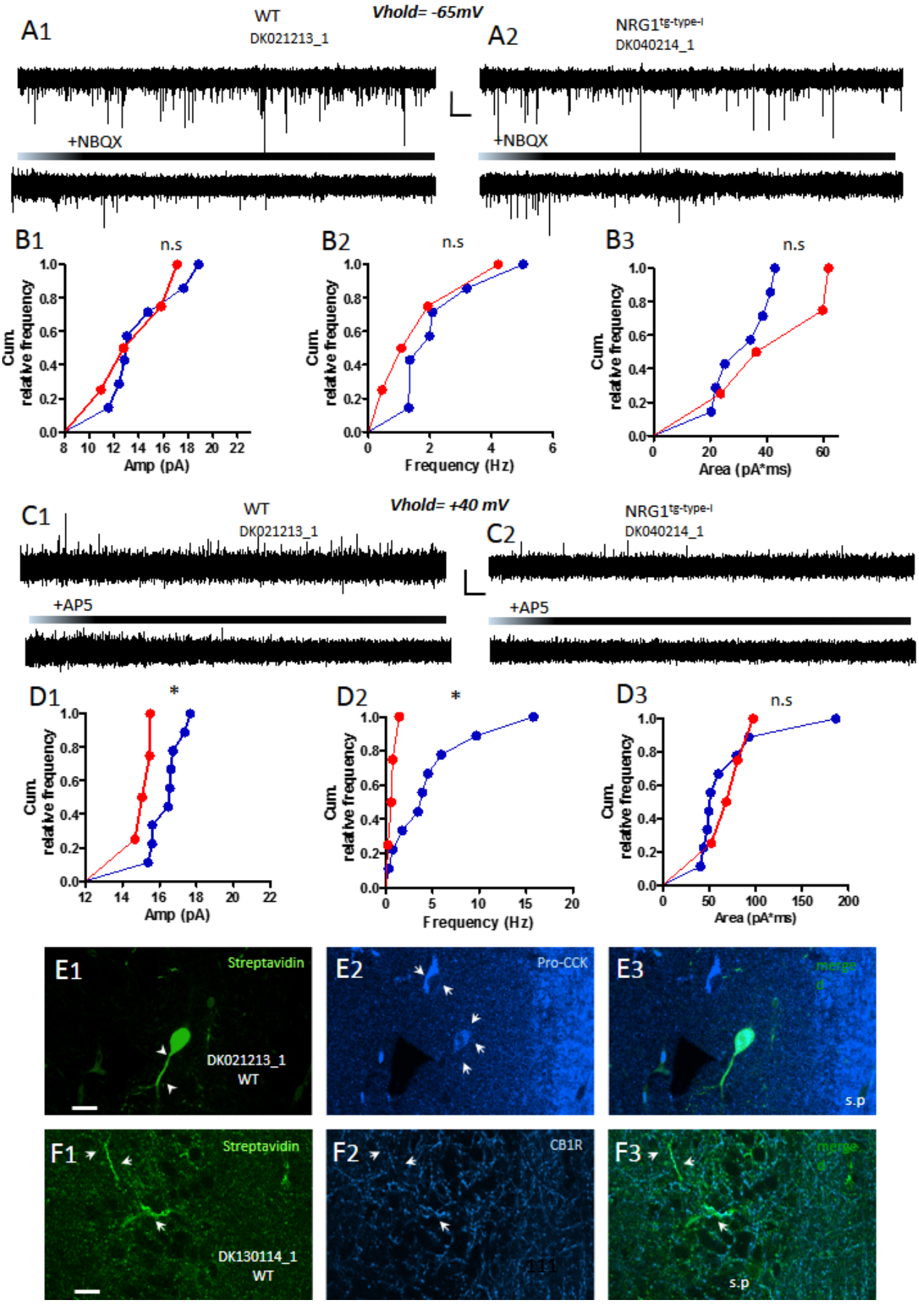
A1
WT
DK021213_1
Vhold= -65mV
+NBQX
A2
NRG1tg-type-I
DK040214_1
+NBQX
B1
n.s
Cum. relative frequency
Amp (pA)
B2
n.s
Frequency (Hz)
B3
n.s
Area (pA*ms)
C1
WT
DK021213_1
Vhold= +40 mV
+AP5
C2
NRG1tg-type-I
DK040214_1
+AP5
D1
*
Amp (pA)
D2
*
Frequency (Hz)
D3
n.s
Area (pA*ms)
E1
Streptavidin
DK021213_1
WT
E2
Pro-CCK
E3
merge
s.p
F1
Streptavidin
DK130114_1
WT
F2
CB1R
F3
merge
s.p

Figure 4-3 NRG1 over-expression selectively compromises NMDAR-mediated neurotransmission in CCK+/CB_1R+ interneurons. (A1 and A2) Upper traces: Representative AMPAR-mediated mEPSCs recordings in the CA3 area CCK+/CB_1R+ interneurons in WT (A1) and the $NRG1^{tg\text{-}type\text{-}I}$ mice (A2) in voltage-clamp at -65mV holding potential. Lower traces: abolishment of AMPAR-mediated mEPSCs by NBQX (25 µM), wash-in indicated by horizontal bar) Scale bars, vertical; 20pA, horizontal; 20ms. (B1-3) Relative cumulative probability plots of the AMPAR mEPSCs amplitude (B1), frequency B2) and the quantal current area (B3) in WT (blue) and the $NRG1^{tg\text{-}type\text{-}I}$ mice neurons (red). (C1 and C2) Upper traces: Represenative NMDAR-mediated mEPSCs recordings in the CCK+/CB_1R+ interneurons in WT (C1) and in the $NRG1^{tg\text{-}type\text{-}I}$ mice (C2) at +40 mV holding potential. Lower traces: abolishment of the mEPSCs by DL-AP5 (100 µM). (D1-3) Relative cumulative probability plots of the NMDAR mEPSCs amplitude (D1), frequency (D2) and quantal current area (D3) in WT (blue) and the $NRG1^{tg\text{-}type\text{-}I}$ mice cells (red). Scale bars, vertical; 20pA, horizontal; 20ms (E1-3) Immunostaining for pro-CCK, (E1) Streptavidin-Alexa488 visualisation of one neurobiotin-filled recorded cell. Arrows denote non-spiny dendrite of the cell. (E2) Immunoreaction for pro-CCK, arrows point at positive reaction in cytoplasm in the recorded cell and one non-recorded neuron. (E3) Merged streptavidin and pro-CCK immunofluorescence signals. (F1-3) Immunostaining for CB_1R. (F1) Streptavidin-Alexa488 visualisation of the recorded cell axon (arrows). (F2) Immunoreaction for CB_1R. (F3) Merged streptavidin and CB_1R immunofluorescence signals. Scale bars 20µm.

4.4 Discussion and conclusions

The experiments presented in this chapter were performed to elucidate the impact of NRG1 chronic over-expression in glutamatergic synapses targeting CCK/CB_1R immunopositive hippocampal interneurons. For this, two experimental approaches were employed. Firstly, the relative contribution of the two ionotropic components of glutamatergic postsynapic currents were assessed by the N/A ratio of evoked EPSCs using focal stimulation of the CA3 associational or/and commissural fibers. The N/A ratio analysis showed that NRG1 over-expression leads to reduced contribution of NMDAR-mediated transmission at glutamatergic synapses onto CCK+/CB_1R+ CA3 area interneurons.

Furthermore, to reassess the effects of NRG1 over-expression on glutamatergic synapses and to establish whether the observed N/A ratio changes were attributed to changes in the NMDAR- or/and AMPAR-mediated neurotransmission, I further studied the quantal miniature excitatory neurotransmission in WT and the $NRG1^{tg\text{-}type\text{-}I}$ mice. Consistent with the observed changes of a decline of N/A ratio in $NRG1^{tg\text{-}type\text{-}I}$ mice, the recordings of biophysicaly and pharmacalogically isolated AMPAR- and NMDAR-mediated mEPSCs showed a specific reduction of the NMDAR-mediated transmission in these mice. Both the amplitude and the

frequency of the NMDAR-mediated mEPSCs in CCK+/CB_1R+ interneurons were reduced in $NRG1^{tg\text{-}type\text{-}I}$ mice. These changes were solely observed in the NMDAR-mediated, and not in the AMPAR-mediated mEPSCs, suggesting that alterations at pre-synaptic terminals are unlikely. It follows that the parallel to the NMDAR-mediated decline in events amplitude, the observed decrease in frequency of the NMDAR-mediated detected events, could be a result of events misdetection because of the choosen amplitude threshold detection criteria, rather than an indication of alterations of neurotransmitter release at the synaptic cleft.

Further support of the hypothesis on selective post-synaptic NMDAR change in distinct hippocampal interneurons expressing the ErbB4 receptor comes from previous work in my host laboratory. It was shown that the NRG1 elevation selectively reduces NMDAR-mediated (but not AMPAR-mediated) mEPSC amplitude in CA3 PV basket cells (Nissen, 2012).

Altogether these data suggest that NRG1 exerts its effects on synaptic function in interneurons via ErbB4 receptor, and leads mainly to post-synaptic alterations of NMDAR-mediated synaptic activity.

It is important to note that the decrease of N/A ratio between the two genotypes, measured from evoked EPSCs (41.5%) was not found to reach statistical significance in mEPSCs recordings, while the decrease of NMDAR-mediated mEPSCs amplitude was found to be rather modest (~8%) in CCK+/CB_1R+ cells from $NRG1^{tg\text{-}type\text{-}I}$ mice. What could be the factors that contribute to these differences between the two sets of experiments?

One obvious explanation is the difference in the two methodological approaches. Even though mEPSCs recordings provide a good sample of the synaptic properties of glutamatergic inputs onto GABAergic cells the fact that the signal-to-noise ratio is low in +40 mV voltage clamp recordings makes these recordings prone to small amplitude event misdetection. This

raises the possibility that subtle differences could be missed. In addition, the two different experimental approaches focus on slightly different features of synaptic transmission: It is possible, as has been proposed, that the number of glutamate molecules in spontaneous single neurotransmitter vesicle release does not fully occupy either AMPAR or NMDAR receptors post-synapticaly (Liu et al., 1999, McAllister and Stevens, 2000). On the contrary, stimulus-evoked activation of glutamatergic afferents typically results in the release of multiple vesicles in many adjancent synapses (Tong and Jahr, 1994, Mainen et al., 1999), and higher degree of saturation of post-synaptic receptors. Therefore, even if the AMPAR receptor-mediated transmission and pre-synaptic neurotransmitter release were both unaffected by NRG1 over-expression, reduced number of functional of NMDARs in $NRG1^{tg\text{-}type\text{-}I}$ mice synapses might produce stronger and more clear effect on the measured post-synaptic currents evoked by multiple fiber EPSCs than by quantal release, because the released neurotransmitter molecules would more consistently occupy all post-synaptic NMDA receptors. In addition it is possible that by the electrical stimulation, extrasynaptic NMDAR receptors could in addition be activated by glutamate spillover and activate extrasynaptic NMDARs proviving larger NMDAR-mediated currents, a phenomenon that is improbable to occur by quantal release (Rusakov and Kullmann, 1998, Bidoret et al., 2015). Finally, given the reports of differences in the receptor subunit composition at different afferent synaptic inputs (Toth and McBain, 1998, Ito et al., 2000, Lei and McBain, 2002), it cannot be excluded that the excitatory synapses examined differed in their NMDAR subunit composition and conductance in a pathway-specific way. My experiments on the stimulation of glutamatergic afferents was set to activate predominantly the associational/commissural synaptic pathway. However, in the mEPSCs recordings the recorded cells receive synaptic inputs from wide range of excitatory afferents with different afferent areas (see section 4.1). In addition to the possible afferent-specific transmission properties, it is also

possible that subpopulations of CA3 area CCK+/CB_1R+ interneurons exhibit different NMDAR-mediated currents. Given that detailed anatomical analysis of the recorded CCK+/CB_1R+ interneurons types was not performed in either of those two data sets, this raises a possibility that distinct CCK+ types may differ in their AMPAR- and NMDAR-mediated currents. However, evidence that at least some distinct CCK+ interneuron types cast a rather homogenous population, in terms of their AMPAR- and NMDAR-mediated currents, comes from a recent study showing that the N/A ratio is similar in, basket cells, schaffer collateral associated cells and other dendrite-targeting CCK+ interneurons in the CA1 area of the hippocampus (Matta et al., 2013). Therefore, these results on consistent synaptic features in different CCK+ cell subgroups justify the comparison of the CCK+/CB_1R+ interneurons' synaptic parameters as a group between the $NRG1^{tg\text{-}type\text{-}I}$ and WT mice, and supports the conclusion that NMDAR hypofunction is associated with NRG1 over-expression in this interneuron population.

In conclusion, the experiments reported here aimed to address for the first time, whether glutamatergic neurotransmission onto CCK+/CB_1R+ cortical interneurons is changed by chronic NRG1 over-expression. It was shown that in $NRG1^{tg\text{-}type\text{-}I}$ mice, the glutamatergic synapses onto these interneurons, which also express the ErbB4 receptor, are hypofunctioning in the NMDAR-mediated transmission.

As I discussed in the beginning of this chapter, results here should be put in a common context on the effects of NRG1 dysregulation with caution. Different experimental approaches can often produce conflicting results. As an example, previous studies using acute application of NRG1 peptides (instead of NRG1 chronic over-expression used here) have reported elevated expression level of specific NMDA receptor channel subunits in cultured cerebellar neurons (Ozaki et al., 1997). In addition, acute NRG1 application can cause suppression of the NMDAR -mediated currents in pyramidal cells in the prefrontal cortex (Gu et al., 2005) and reduced

AMPAR-mediated neurotransmission in hippocampal pyramidal cells (Kwon et al., 2005). Conversely, a number of studies using similarly acute NRG1 exposure experimental approach in cerebellar and hippocampal slices have reported that NRG1 does not control the expression of these glutamate receptors subunits (Rieff et al., 1999, Okada and Corfas, 2004).

Of note, it has also been also proposed, that NRG1 exerts its effects mainly by modifying the phosphorylation pattern of specific NMDAR subunits. This has been demonstrated after the acute application of the NRG1 peptide both in human and rodent prefrontal cortex and hippocampal slices (Hahn et al., 2006, Pitcher et al., 2011). Studies employing chronic models of NRG1 upregulation have also produced diverging results. For instance, enhancement of AMPAR-mediated neurotransmission in PV-positive interneurons was reported in neocortical slices after the the subcutaneous injection of the NRG1 peptide in mice (Abe et al., 2011). However, no changes in glutamatergic transmission were observed onto cortical pyramidal cells in the NRG1 transgenic mice that express non-soluble peptide "CRD-NRG1" (Agarwal et al., 2014). On the contrary, impaired glutamate release onto CA1 area pyramidal cells was reported in mice over-expressing soluble peptide "Ig-NRG1" (Yin et al., 2013), and similarly the glutamatergic synapse function was compromised in medial prefrontal cortex (mPFC) pyramidal cells in mice that express a human-specific NRG1 isoform IV (NRG1-IV) (Papaleo et al., 2016). It is apparent that research efforts of the past have mainly focused on effects of NRG1 and related peptides onto pyramidal cells leaving their effects at the glutamatergic synapse onto inhibitory neurons not thoroughly examined, however during the time this study was in progress, a seminal study reporting the effects of the NRG2 isoform, (that similarly signals via the ErBb4 receptors) on the modulation of glutamatergic transmission onto inhibitory interneurons was published (Vullhorst et al., 2015). In agreement, with the experiments presented here the authors demonstrated that acute application of NRG2 to hippocampal cultures as well as to acute PFC

slices led to a robust decline of NMDAR but not of AMPAR-mediated ionic currents specifically in ErBb4-positive cells, leaving pyramidal cells unaffected.

Taken together the above research outcomes provide strong evidence that the glutamatergic synapse onto ErbB4 interneurons can be affected by NRG1 over-expression raising the possibility that this schizophrenia-associated gene can alter the function of the specific cell populations in the cortex. What is the impact of NRG1 over-expression in the GABAergic output of those cells and what is the impact of interneuronal NMDAR hypofunction on the hippocampal network remains unknown. In the following chapter (*Result chapter 5*) I aim to explore whether the NRG1 over-expression in the $NRG1^{tg\text{-}type\text{-}I}$ mouse hippocampus is associated with alterations in the GABAergic synapse formed by CCK+/CB_1R+ cells whereas in the final result chapter (*Result chapter 6*), I will examine the effects of the observed NMDAR hypofunction in hippocampal interneurons on the recurrent inhibition, which is the synaptic circuit interaction mediating the generation of co-ordinated rhythmic cell population activities in the hippocampus that previously were found to be compromised in these mice (Deakin et al., 2012).

4.5 Perspective and future Directions

In the future, further recordings assessing the glutamatergic neurotransmission in anatomically defined cell types needs to be performed in order to assess the functionality of the two components of glutamatergic neurotransmission. This could shed light on the effects of NRG1 dysregulation more specifically and reveal the cellular deficits that could underlie disrupted network operations relative to the schizophrenia-like endophenotype seen in these mice.

5 GABAergic synapses from CCK/CB_1R -expressing interneurons to pyramidal cells in NRG1 over-expressing mice

5.1 Introduction

5.1.1 Effects of NRG1 on the GABAergic transmission

Although alternations in GABAergic cortical microcircuits have been reported in association with schizophrenia pathogenesis (Lewis, 2014, Gonzalez-Burgos et al., 2015), less is known of how elevated levels of NRG1 can affect the GABAergic synapses.

Thus far, it has been reported that acute application of NRG1 facilitates the evoked release of GABA from mice slices in hippocampus without changing the basal GABA release (Chen et al., 2010) or pre-synapticaly enhancing it in the prefrontal cortex (Woo et al., 2007). On the other hand experiments with organotypic hippocampal slices that have undergone lasting treatment with the NRG1 peptide have shown post-synaptic enhancement of GABAergic transmission (Okada and Corfas, 2004). Given that NRG1 has multiple roles in neurodevelopment (see section 1.1), chronic models of enhanced NRG1-ErbB4 signalling could be more informative. Hitherto, a few transgenic mouse lines have been developed aiming to imitate this type of dysregulation. It has been reported that over-expression of the insoluble "CRD" type of NRG1 resulted in the enhancement of the synaptic input from GABAergic interneurons to CA1 pyramidal cells (Agarwal et al., 2014). In contrast, studies utilising a different transgenic mouse strain with specific over-expression of the soluble type "Ig" of NRG1 specifically in the forebrain, demonstrated post-synaptic decline of GABAergic inhibition (Yin et al., 2013). Furthermore a more recent study with a transgenic mouse model expressing the human NRG1-IV transgene (Papaleo et al., 2016), revealed no changes in the GABAergic synapses onto layer V neocortical pyramidal cells.

As it has been reported many times in this thesis the discrepancies between the results from different NRG1 upregulation models could arise from various reasons including differences in the transgenes used (soluble vs insoluble NRG1 forms), expression levels, brain areas and cell types studied (for a detailed review on the effects of NRG1 on inhibitory neurotransmission see Table 1-2). Apart from the fact that different NRG1 peptides and their isoforms can exert their effects in different ways the variability in NRG1 expression levels can also trigger different compensatory mechanisms that affect the GABAergic circuitry (Pozo and Goda, 2010). Moreover, given that interneuron types may show distinct physiological features specifically to the cortical region that are located (Ascoli et al., 2008, Klausberger and Somogyi, 2008, DeFelipe et al., 2013), studies aiming to understand the pathophysiology of GABAergic microcircuitry by elevated NRG1 levels should focus on interactions of identified neuron types. This aspect is of great importance in the case of NRG1 signalling since its main receptor, ErbB4, is, specifically localised in specific subpopulations of interneurons such as PV or CCK expressing GABAergic cells as has been shown in the chapter 3 of this thesis and in (Vullhorst et al., 2009, Neddens and Buonanno, 2010). In this chapter, I will examine the effects of chronic NRG1 upregulation on the GABAergic synapses from CCK+/CB_1R+ interneurons.

5.1.2 Physiological properties of CCK/CB_1R -expressing interneurons output

Output from CCK+/CB_1R+ interneurons has various properties characteristic of these synapses in the hippocampus. A hallmark feature is that upon their activation, they release GABA asynchronously, in sharp contrast to the PV-positive interneurons (Kraushaar and Jonas, 2000). This mode of GABA release from these interneurons was firstly reported in their synapses onto dentate gyrus granule cells (Hefft and Jonas, 2005) and was later reported in their connections to other hippocampal interneurons (Daw et al., 2009, Karson et al., 2009, Ali and Todorova, 2010).

Although the exact mechanism underlying the asynchronous GABA release in these synapses has not been fully identified, several hypothesis have been proposed. For instance, it can reflect the absence of Ca^{2+} -binding proteins such as PV, calbindin or calretinin in the CCK+ cells. This could cause a prolonged course of pre-synaptic Ca^{2+} transients, that in turn leads to a delayed and fluctuating neurotransmitter release (Atluri and Regehr, 1996, 1998). Moreover it can also be a result of the expression of distinct isoforms of Ca^{2+} sensors, like synaptotagmin in the pre-synaptic terminal that favour asynchronous rather than synchronous neurotransmitter release (Sun et al., 2007, Kerr et al., 2008) or differences in the interaction dynamics between effector proteins of the SNARE complex assembly (Rodrigues et al., 2016) . Finally, this type of neurotransmitter release can be attributed to different pre-synaptic voltage-gated calcium channels. Depolarisation-triggered Ca^{2+} influx in the CCK+/CB_1R+ interneuron pre-synaptic terminals is mediated via N-type channels, which are not as prominently clustered to the pre-synaptic zone as the P/Q- type channels which are mainly found in PV+ cells and their clustering has been suggested to control synchronous GABA release (Wu et al., 1999, Hefft and Jonas, 2005). Interestingly, it has also been suggested that N-type calcium channels are prominent at synapses that exhibit short term facilitation and are restricted to CCK+ interneurons whereas the presence of P/Q calcium channels is associated with depressing synapses (Ali, 2011). Regardless of the exact or possible combination of molecular mechanism(s) this asynchronous fashion of neurotransmitter release , has been found to result to synaptic long-lasting inhibition in post synaptic target cells over longer time windows compared to synchronous release (Glickfeld and Scanziani, 2006, Daw et al., 2009).

Concerning the synaptic excitation of CCK+/CB_1R+ interneurons, Glickfield and Scanziani (2006) showed in a series of experiments that CA1 CCK+/CB_1R+ basket cells receive weaker excitation from local pyramidal cells compared to other studied interneuron types,

including PV-positive basket cells. Thus, it was proposed that synaptic glutamatergic excitation of hippocampal CCK+/CB_1R+ interneurons requires the integration of pre-synaptic activity across large time window and summation of multiple independent inputs (Glickfeld and Scanziani, 2006).

One more distinctive feature of these cells, is the pre-synaptic expression of the CB_1 receptor (Marsicano et al., 1999, Katona et al., 2009, Glickfeld and Scanziani, 2006). This localization pattern of CB_1 receptors is critical for the emergence of post synaptic suppression of inhibitory input from CCK/CB_1R-positive cells via, the depolarization induced suppression of inhibition (DSI) after the post-synaptic release of endocannabinoids (Pitler and Alger, 1992, 1994, Wilson and Nicoll, 2001).

Together, these unique features of CCK+/CB_1R+ interneurons are important for the modulation of neuronal networks especially during the emergence of co-ordinated and synchronous rhythmic activities of cortical neurons, to which the GABAergic inhibition from these interneurons (especially the CCK+/CB_1R+ basket cells) is known to contribute. Importantly, it has been proposed that these distinct properties of the CCK/CB_1R-positive synapses may participate in the formation of "cell assemblies" during specific network activities such as gamma oscillations. This could be achieved by a more explicit segregation of pyramidal cells to "active" and "non-active" via disinhibition of cells that are actively participating to a certain oscillatory event while sustain at the same time long lasting inhibition to those not actively participating (Tukker et al., 2007, Bartos and Elgueta, 2012). Therefore, disturbances of CCK+/CB_1R+ cells mediated neurotransmission can affect significantly brain operations that give rise to higher cognitive functions and can participate in the pathogenetic mechanism exerted by the disease associated genes.

5.2 GABAergic synapses from CCK+/ CB_1R+ interneurons to pyramidal cells

5.2.1 Experimental paradigm

Given that CCK+/CB_1R+ interneurons express the NRG1 receptor, ErbB4, together with the evidence that disturbances in the NRG1-ErbB4 signalling can alter GABAergic neurotransmission, here I studied whether the chronic over-expression of NRG1 is associated with altered signalling from CCK+/CB_1R+ GABAergic cell synapses to CA3 pyramidal cells.

There are many different approaches to study GABAergic neurotransmission in neuronal networks. Most commonly, studies employ whole cell recordings of either spontaneously occurring post-synaptic currents (sIPSCs) when network effects of inhibition needs to be addressed or recordings of post- synaptic currents after the quantal release of neurotransmitter (mIPSCs). The latter condition allows the separation of pre- vs post-synaptic effects (affecting frequency vs amplitude of mIPSCs, respectively). In addition, recordings of IPSCs after “focal” stimulation of a particular afferent pathway can highlight input specific features of neurotransmission.

Despite the fact that these are regularly used methods, their limitation is that they cannot differentiate amongst the different cell specific inhibitory inputs. Hence, the most appropriate strategy to examine cell-type specific synapse characteristics, would be to record from connected single cell pairs. However, this approach has very low yield of successful experiments, without a specific reporter line that allows identification of the neuron types while experimenting.

As an alternative approach, I have employed here optogenetics to activate specifically the GABAergic synapses from CCK-expressing neurons, and combined this with whole-cell recordings of the inhibitory currents in the CA3 pyramidal cells (Figure 5-2 A).

For these experiments, slices were prepared from heterozygous BAC-CCK-Cre$^{+/-}$/NRG1$^{tg\text{-}type\text{-}I}$ (NRG1$^{tg\text{-}type\text{-}I}$) and BAC-CCK-Cre$^{+/-}$ wild-type littermates (WT) mice, transfected with (AAV2/5)-ChR2-eYFP (see methods 2.4.3) in order to achieve cre-dependent expression of ChR2-eYFP in mid-ventral hippocampus (Figure 5-1, A&B). Optimal stereotaxic injection co-ordinates were determined in 6-8 week old mice of both sexes as follows: -2.7 mm caudal; 2.75 lateral from bregma and 3.4-2.6 mm deep from the brain surface (Figure 5-1, A). In this co-ordinates 800 nl of viral particle suspension (titre ± 4 × 10^{12}/mL) was injected in hippocampi of both hemispheres. The mice were allowed to recover for 11-21 days after the surgery. For experiments, horizontal slices were prepared from the injected mice (see section 2.2.) expressing ChR2-eYFP+ in the CA3 area of hippocampus. Expression of ChR2-eYFP+ was prominent in s,p s.r and s.o, possibly due to the concomitant expression of ChR2-eYFP+ to pyramidal cells (Figure 5-1, B). However, given that the experiments were performed in the continuous presence of glutamate receptor blockers NBQX (25 μM) and DL-AP5 (100 μM), the possible release of glutamate from pyramidal cells fibres would be blocked. Moreover, the light elicited IPSCs were completely abolished by bath application of the GABAA receptor blocker picrotoxin (100 μM), confirming their GABAergic origin and verifying that there is no ChR2 photo-current contamination due to the possible ChR2-eYFP+ expression in pyramidal cells. (Figure 5-2, C2)

To confirm, cell type specific expression of ChR2-eYFP+ in CCK/CB_1R+ cells, previous immunocytochemical analysis in the lab (Rombo et al., 2015), of transfected slices with (AAV2/5)-ChR2-eYFP in CA1 confirmed the overlapping pattern of opsin expression with CCK-positive somata (Figure 5-1, C1-3)

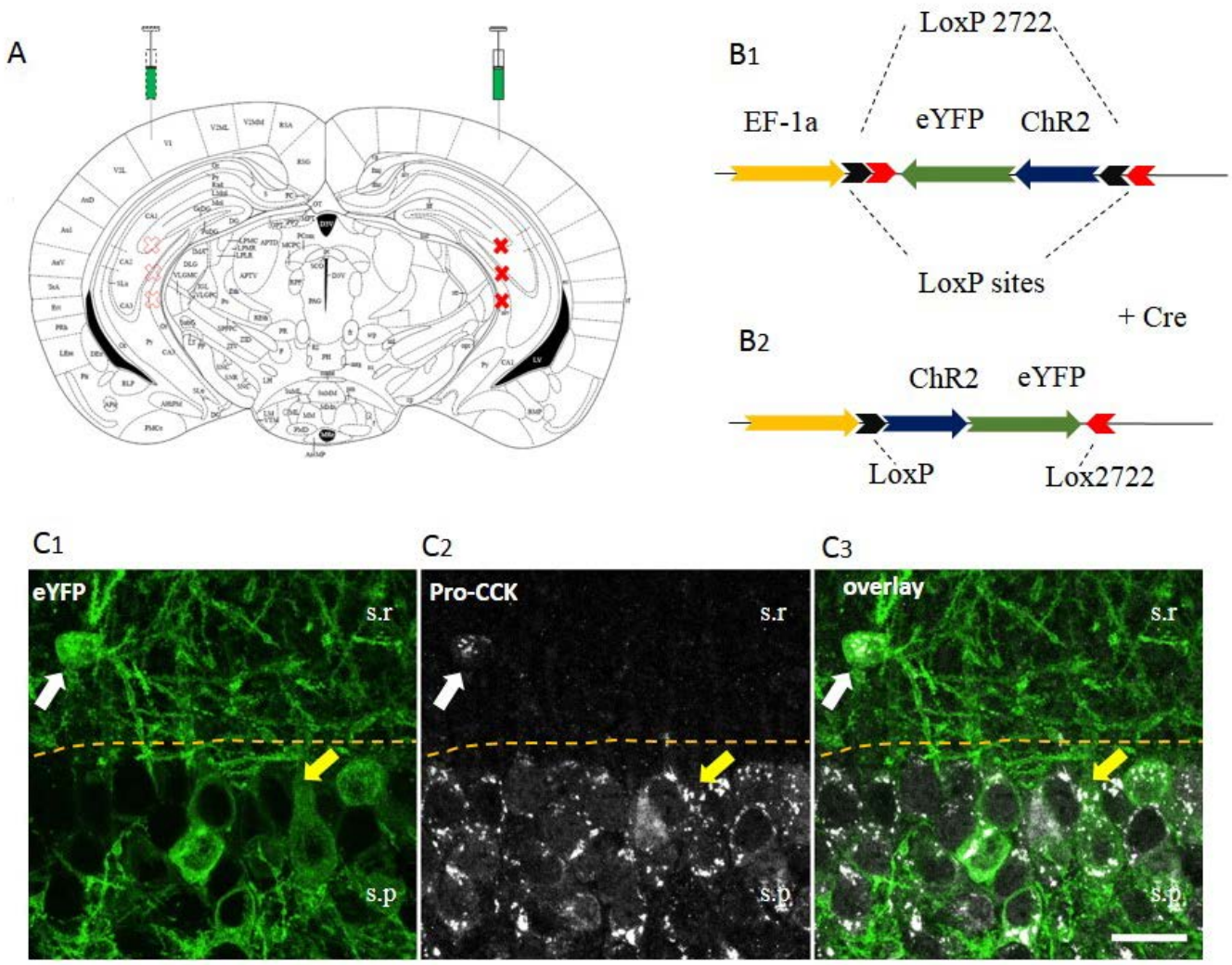

Figure 5-1 Stereotaxic injection sites of adeno-associated virus (AAV2/5)-ChR2-eYFP construct into transgenic BAC-CCK-Cre$^{+/-}$ and BAC-CCK-Cre$^{+/-}$/NRG1$^{tg\text{-}type\text{-}I}$ mice. (A) The viral injections were performed bilaterally targeting mid-ventral hippocampus as follows: 2.70 mm caudal and 2.75 mm lateral from bregma, at depths of 3.60 mm, 3.40 mm and 2.60 mm from the brain surface. The various injection depths enabled successful transfection of the viral construct along the dorso-ventral axis. (B1) Schematic shows a plasmid map of the recombination site of the (AAV2/5)-ChR2-eYFP vector. Only the cells expressing cre-recombinase do recognise the LoxP sites flanking the ChR2-eYFP construct. (B2) The cre-recombinase -mediated activation leads to transcription competent transgene. ChR2: Channelrhodopsin-2; eYFP: enhanced yellow fluorescent protein; loxP: locus of X-over P1; EF-1a: EF-1 alpha promoter. (C1) Confocal image of ChR2-eYFP -transfected cells in the CA1 hippocampal region. (C2) Immunocytochemical reaction in the same region for pro- CCK (visualised with Cy5). (C3) Merged confocal microscope micrograph of the eYFP and the pro-CCK expression in the area. White arrow shows a ChR2-eYFP -transfected cell. The cell is also immunopositive for pro-CCK. Yellow arrow points to the expression of ChR2-eYFP also in stratum pyramidale in CCK-expressing pyramidal cells. Scale bar 20µm. Strata are indicated as s.p. and s.r (Micrograph, courtesy of Dr Rombo, published in (Rombo et al., 2015)).

In slices, putative post-synaptic cell somata were patched in voltage clamp mode at + 0 mV with intracellular filling solution having 8 mM Cl^- to assure strong electrochemical driving force for the evoked $GABA_AR$-mediated currents. The recorded cells were filled with neurobiotin for *post hoc* anatomical identification of pyramidal cells. Cell type verification of the recorded cells was performed in 5 cells (2 in WT, 3 in $NRG1^{tg\text{-}type\text{-}I}$). All of them were confirmed as pyramidal cells based on their somatodendritic morphological profile and the typical mushroom-shaped spines in dendrites (Figure 5-2, B). Although identification of pyramidal cells under IR-DIC during whole cell recordings is widely used, in this study not all cells were *post-hoc* visualized thus they should be considered as putative pyramidal cells throughout the data interpretation.

To activate the GABAergic fibers, I photostimulated the ChR2 expressing CCK+/CB_1R+ cell fibers in slices with brief paired-pulse stimuli of blue light (473 nm; pulse duration 3 ms with 50 ms inter-pulse interval; max laser power 100 mW). The stimuli were focused on the vicinity of the patched soma (100- 300 μm). In addition, to allow a comparison between the CCK+ cell responses in pyramidal cells, I aimed to activate synaptic inputs in all experiments with similar criteria. For this, two experimental approaches were employed, as I explain below.

First, a minimal optical stimulation (MOS) protocol was used in order to restrict photoactivation to as few axons as possible, ideally activating a single fibre to mimic unitary IPSCs responses (uIPSCs) elicited in paired cell-to-cell connections. For this, I used a 113 μM diameter laser fibre delivering a photostimulation spot of 15-10 μm cross-sectional diameter. The laser spot was moved along s.p/s.r until a stable response was generated. Then, the laser power was reduced to an intensity, where the photostimulation was not sufficient to trigger post-synaptic current, whereupon the laser power was increased stepwise by (1-2%) until the activation reached the threshold to elicit post synaptic IPSCs again. This was determined to be the minimal optical

stimulation (MOS) intensity required to activate a single or few pre-synaptic CCK+/CB_1R+ fibers (Figure 5-2, C1). In occasions, where during the course of the recording, repetitive cycles of the light pulses failed to elicit further post-synaptic events, possibly due to ChR2 desensitization, the whole process was started again from by re-positioning the laser spot and re- adjusting the threshold of the laser power. Only recordings with laser settings (including both position and laser power) that generated lasting and stable responses were included in the analysis. This experimental paradigm is assumed to reflect activation of a single or few CCK+/CB_1R+ fibres and being, analogous to unitary IPSCs (uIPSCs) recordings of connected pairs for the following reasons: Firstly frequent IPSCs failures during MOS recordings (~30%), indicate that the activation of ChR2 was limited to a single CCK+/CB_1R+ pre-synaptic fibre. It is thus, improbable that ChR2 photoexcitation would fail to trigger action potential generation in multiple axons at the same time. Secondly, the MOS threshold from not elicited IPSCs (~ 79% failures) to lasting IPSCs recordings was achieved over 1-2% increments of the laser intensity (Figure 5-2, C1 and Table 5-1). One further, criterion to confirm that the MOS protocol triggers the activation of a single CCK+/CB_1R+ positive pre-synaptic fibre would be to compare the kinetics of the light elicited IPSCs to the ones obtained from cell paired recordings. However, this direct comparison has complications since it has been demonstrated that ChR2 expression and optical stimulation alter synaptic responses properties, probably due to slow ChR2 kinetics increasing the time window of pre-synaptic action potential generation and neurotransmitter release time precision (Zhang and Oertner, 2007, Jackman et al., 2014).

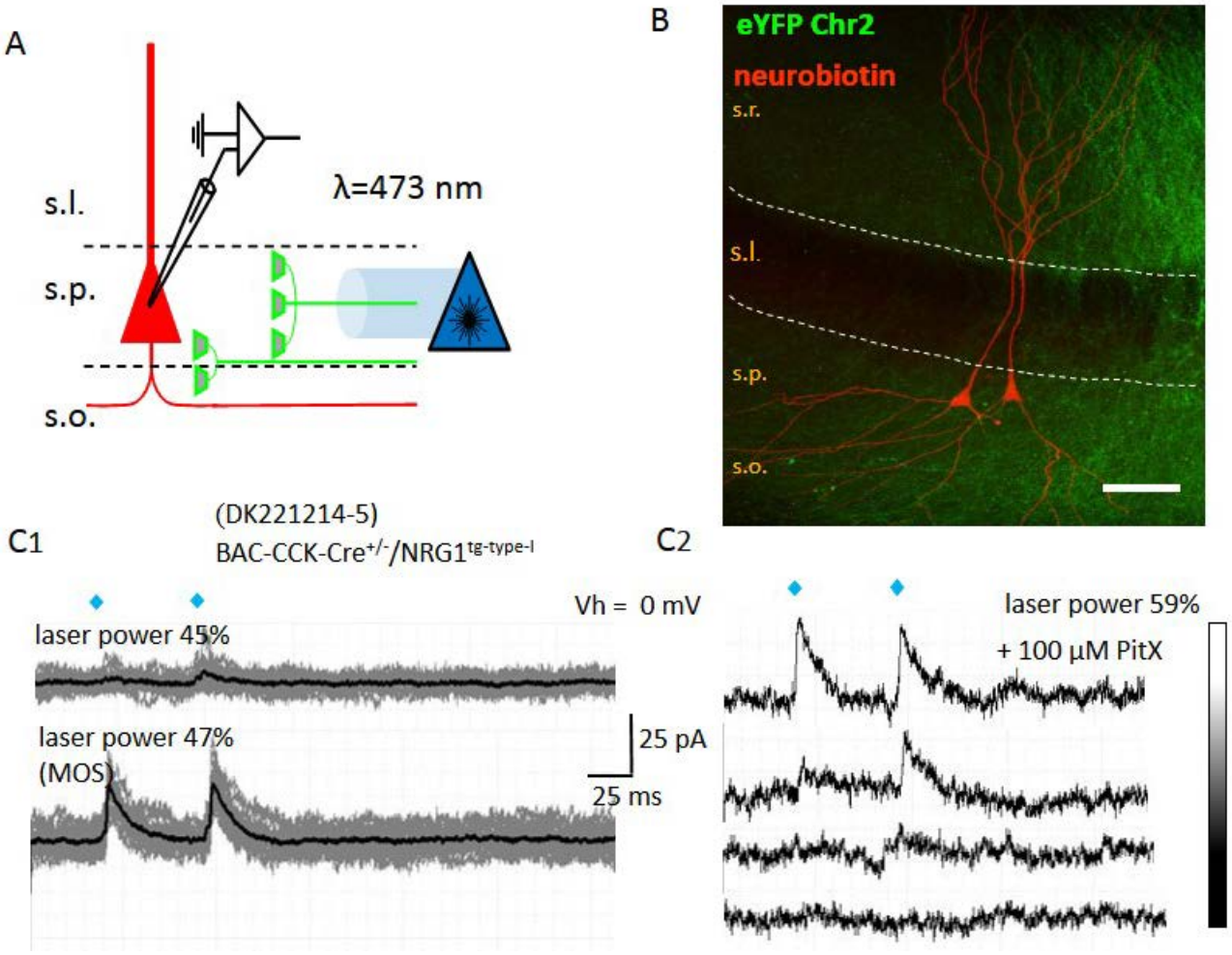

Figure 5-2 Selective photostimulation of CCK+/CB$_1$R+ axon fibers (A) Schematic shows experimental paradigm. Laser photostimulation (473 nm) of ChR2 in CCK+/CB$_1$R+ expressing neurons in the CA3 area s.p with simultaneous whole-cell recording from a CA3 pyramidal cell. Strata are indicated. (B) Neurobiotin-filled pyramidal cells (red) visualised with Streptaviding-Cy3 following sequential recording of two pyramidal cells. Note characteristic ChR2-eYFP expression (green) in the layers s.o, s.p, and sr. Scale bar 50 µm. (C1) Traces show sample IPSCs evoked in a pyramidal cell with the photostimulation of ChR2 (light pulse duration 3 ms, paired pulse with 50 ms interval, blue dots). Upper traces show responses to laser stimulation with 45% of maximum laser power, when the stimulation fails to consistently activate IPSCs. Grey; recordings for 20 consecutive individual stimulation cycles. Black; the average of the sweeps. The post-synaptic CA3 pyramidal cell was voltage-clamped at 0 mV in the presence of glutamate receptor blockers NBQX (25 µM) and DL-AP5 (100 µM). Lower traces show that a very small increment (to 47% of maximum power) in optical stimulation power evoked reliable IPSCs in the same pyramidal cell. Grey and black traces as above: 20 overlapping sweeps, and their average. (C2) The elicited IPSCs were abolished with 100 µM picrotoxin (PiTx) even if higher laser intensity (59% of maximum) was used, verifying that the post-synaptic currents were mediated by GABA$_A$ receptors. Blue dots; paired pulse laser stimulation. Vertical bar; Progressive abolishment of IPSCs, during gradual increase of PiTx in the recording aSCF (black colour gradient). All traces are from the same post-synaptic cell; DK221214-5 in a slice of a (AAV2/5)-ChR2-eYFP –injected BAC-CCK-Cre$^{+/-}$/ NRG1$^{tg\text{-}type\text{-}I}$ mouse. Scale bars equal for C1 and C2.

Because adjusting successfully the MOS protocol was not always successful, I also used a second approach. In this approach, I set the laser intensity threshold to evoke constantly successful post-synaptic IPSCs without failures. For this I used a (400 μm) diameter optical fibre generating ~ 80 μm laser light spot on the slice surface. Even though, the latter approach, is more prone to reflect post synaptic currents of more than one fibre -and likely does, the fact that the threshold was set at the exact laser intensity that constantly elicits stable and successful post synaptic currents across all recordings possibly reflects GABAergic output of similar synaptic potency along distinct cell recordings. So it was originally thought that this approach, can allow comparison of the GABAergic synapse properties between the two genotypes alongside the minimal optical stimulation paradigm where the photoexcitation of CCK+/CB_1R+ fibres was just as potent as to evoke IPSC, regardless of occasional failures in initiating them.

Of note, apart from the comparison of the paired pulse ratio (PPR) in between the two genotypes, measurements, of all other synaptic parameters are reported separately and were not pooled from the two different approaches.

5.2.2 Results

5.2.2.1 MOS elicited IPSCs (1st approach)

First, I compared the functional properties of GABA release from the ChR2-expressing CCK+/CB_1R+ cell axons in the CA3 area. By employing the MOS protocol, light evoked IPSCs mimicking unitary inhibitory post-synaptic currents (uIPSCs) were evoked by applying light pulses to the pre-synaptic CCK+/CB_1R+ fibres expressing ChR2. The first IPSCs evoked by the paired-pulse stimulation were analysed to report basic synaptic parameters. The paired pulse ratio (PPR) was performed to sweeps where the stimulation successfully elicited both 1st and 2nd IPSC. Sweeps that failed to elicit the first IPSCs were categorised as synaptic failures. Occasionally, the MOS failed to elicit a second IPSC. In these recordings, PPR was estimated at an extra session by increasing the laser power until a second IPSC was reliably evoked. Regularly, after the initial recording at a fixed laser spot position and a set MOS laser intensity, the laser spot was repositioned setting a new MOS laser intensity and a further recording round was commenced. Values of IPSCs parameters of a single recording session were averaged. Yet, when multiple recording sessions were performed the synaptic parameters quantification was carried out, as the combinatorial arithmetic mean weighted by the number of sweeps of the recordings' rounds.

Data sets were tested for parametric (normal) distribution with the Shapiro-Wilk test, and comparisons were performed either using unpaired t –test (normality test passed) or Mann-Whitney U test (normality test failed).

Comparison of the evoked IPSCs in the CA3 area pyramidal cells revealed no obvious difference between WT (n= 5 cells) and $NRG1^{tg\text{-}type\text{-}I}$ (n= 6 cells) mice (Figure 5-3). The optically-evoked IPSCs properties in the individual cells recorded in the study are listed in table 5-1. The comparison of the IPSC parameters between the two genotypes is summarized in table 5-2

The strength of the inhibitory synapses from CCK+/CB_1R+ cell axons to PCs was compared by analysing the following parameters: a) *The 1st IPSC peak amplitude*: WT, 35.83 ± 6.90 pA; $NRG1^{tg\text{-}type\text{-}I}$, 30.12 ± 6.56 pA (means, P= 0.57;Figure 5-3 B1), b) *The 1st IPSC 20-80 % rise time*: WT, 2.45 (1.37 to 3.55) ms; $NRG1^{tg\text{-}type\text{-}I}$ 3.58 (1.39 to 5.75) ms (medians, P= 0.66; Figure 5.3-B2), c) *The 1st IPSC half amplitude decay time*: WT: 9.24 ± 2.32 ms; $NRG1^{tg\text{-}type\text{-}I}$ 7.91 ± 1.93 ms (means, P= 0.67; Figure 5-3B3), d) *The 1st IPSC latency (from stimulation pulse onset to 10% rise of IPSC)*: WT, 8.44 ± 0.96 ms; $NRG1^{tg\text{-}type\text{-}I}$ 6.22 ± 0.5 ms (means, P= 0.57; Figure 5-3 B4) or from *the pulse onset to IPSC peak amplitude*: WT, 12.97± 0.71 ms; $NRG1^{tg\text{-}type\text{-}I}$, 12.85 ± 2.73 ms (means, P= 0.97), (e) The *1st IPSC failures percentage* using MOS: WT, 30.38% ± 8.90; $NRG1^{tg\text{-}type\text{-}I}$ 35.64% ± 4.60 (means, P= 0.59; Figure 5-3 B5), g) The *1st IPSC failures with stimulus intensity 1-2% decreased from the MOS* : WT, 80.64% ± 3.91; $NRG1^{tg\text{-}type\text{-}I}$, 77.75% ± 11.86 (means, P = 0.82), and i) *The PPR (2nd IPSC/1st IPSC)*: WT, 0.63 (0.43 to 0.67); $NRG1^{tg\text{-}type\text{-}I}$ 0.54 (0.33 to 0.77) (medians, P= 0.71; Figure 5.3 B6). It should be noted that the comparison of the PPR values between the two genotypes was performed by the pooled data with two optical stimulation parameters (WT, n= 10 and $NRG1^{tg\text{-}type\text{-}I}$, n= 13) and occasionally with higher than the MOS laser power (table 5.1). Application of PiTX (100μM) was studied in three cells (1 from WT and 2 from $NRG1^{tg\text{-}type\text{-}I}$ mice) and it abolished the light-elicited IPSCs by 84.76 % ± 5.37 (Figure 5.3 C1-2), confirming that the post-synaptic currents were predominantly of GABAergic origin. Access resistance in whole-cell recordings was similar across the genotypes (WT *n= 5*, 37.52 ± 3.62, $NRG1^{tg\text{-}type\text{-}I}$ *n= 6*, 27.63 ± 4.29) (means P= 0.12).

The comparable IPSCs properties in the two genotypes, the IPSC amplitude and the current kinetics together with similar PPRs, argue that NRG1 over-expression does not have a major impact either pre- or post-synaptically on CCK cell GABAergic fast transmission to CA3 area pyramidal cells. In addition, the similar failure rates and the synaptic latencies measured for the evoked IPSCs in the two genotypes further suggest that the GABAergic release properties are largely unaffected.

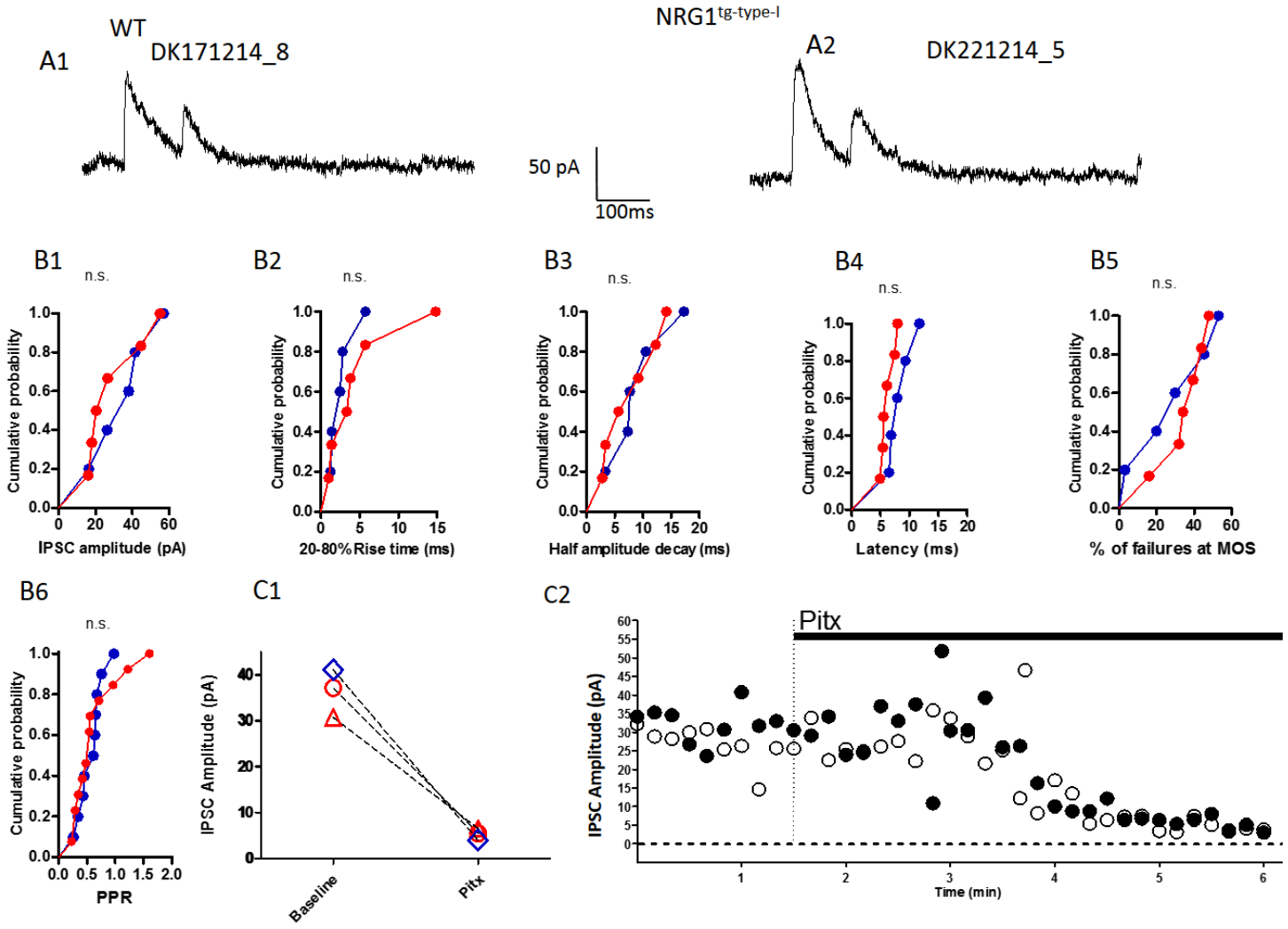

Figure 5-3 Optogenetically-elicited IPSCs in CA3 pyramidal cells evoked by CCK-expressing GABAergic fibres. A) Light elicited IPSC evoked with paired-pulse (50 ms interval) MOS in WT (BAC-CCK-Cre$^{+/-}$) mouse (A1) and NRG1$^{tg\text{-}type\text{-}I}$ (BAC-CCK-Cre$^{+/-}$/NRG1$^{tg\text{-}type\text{-}I}$) mouse (A2). (B1-6) Plots showing cumulative probability of the evoked IPSCs parameters in CA3 pyramidal cells in WT (blue) and NRG1$^{tg\text{-}type\text{-}I}$ mice (red). (B1) IPSCs amplitude; B2) IPSCs 20-80% rise time; (B3) IPSCs half amplitude decay time; (B4) Latency (light pulse onset to 10% rise of IPSC); B5) % of failures during MOS from WT (n=5) and NRG1$^{tg\text{-}type\text{-}I}$ mice (n=6); P> 0.05. (B6) Paired pulse ratio (2nd IPSC peak amplitude/1st IPSC peak amplitude), PPR, from WT (n=10) and NRG1$^{tg\text{-}type\text{-}I}$ mice (n=14); for all synaptic parameters compared p>0.05. (C1) Blockade of the evoked IPSC with GABA$_A$R antagonist picrotoxin. Plot shows averages of 1st IPSC amplitude (at high laser intensity) in control conditions and following the application of 100 µM PiTX in all experiments in WT n=1) and NRG1$^{tg\text{-}type\text{-}I}$ n=2) mice. (C2) Scatter plot illustrates one recording (1st IPSC peak amplitude, filled circles: 2nd IPSC peak amplitude, open circles) in a NRG1$^{tg\text{-}type\text{-}I}$ mouse. Wash-in of PiTX indicated by the horizontal bar.

5.2.2.2 No failures elicited IPSCs (2nd approach)

Recordings of light elicited IPSCs in WT (n= 5 cells) and NRG1$^{tg\text{-}type\text{-}I}$ (n= 8 cells) by adjusting the laser intensity to reliably and constantly elicit post-synaptic currents (~0% 1st IPSCs failures), using a 80 µm laser spot (2nd approach) showed that similarly to the 1st MOS approach both the *1st IPSC peak amplitude*; WT, 51.81 (35.00 to 105.46); NRG1$^{tg\text{-}type\text{-}I}$, 51.83 (37.33 to 74.32) (medians, P= 0.94) and *PPR* (WT, 0.65 ± 0.10; NRG1$^{tg\text{-}type\text{-}I}$, 0.47 ± 0.09) (means, P = 0.21) did not differ in between the two genotypes. Interestingly, both the *IPSC rise time* (*1st IPSC 20-80% rise time*: WT = 4.09 ± 0.95 ms; NRG1$^{tg\text{-}type\text{-}I}$ = 7.13 ± 0.88 ms) and the *IPSC decay time* (*1st IPSC half amplitude decay time*: WT = 10.18 ± 1.72 ms; NRG1$^{tg\text{-}type\text{-}I}$ = 16.11 ± 1.64 ms) were found to be statistically longer in the NRG1$^{tg\text{-}type\text{-}I}$ mice neurons (comparing means, P= 0.045 and P= 0.026, respectively). Access resistances were similar across the genotypes (WT *n=5*, 26.99 ± 2.46, *n=8*, NRG1$^{tg\text{-}type\text{-}I}$ 25.31 ± 2.92) (means P= 0.7). For comparison of PPR access resistance for the 1st and 2nd approach pooled data was: (WT *n=10*, 32.25 ± 2.708, NRG1$^{tg\text{-}type\text{-}I}$ *n=13*, 27.38 ± 2.32).

Table 5-1 Summary of optogeneticaly elicited IPSCs in cells from WT and NRG1$^{tg\text{-}type\text{-}I}$ slices

Cell code	genotype	1st IPSC amplitude (pA)	1st IPSC 20%-80% rise time (ms)	1st IPSC 100%-50% decay time (ms)	Latency (onset to 10% rise of IPSC peak amplitude) or [current peak] (ms)	PPR 2nd /1st IPSC	1st IPSC Failures at MOS intensity	1st IPSC Failures with 1-2 % reduced light from MOS	Ra MOhm
1st MOS approach (WTs)									
DK171214_2[1]	WT	**26.39** *(28)* *Int. 36%*	**2.45** *(28)* *Int. 36%*	**7.7** *(28)* *Int. 36%*	**9.30 [13.20]** *(28)* *Int. 36%*	**0.34** *(22)* *Int. 40%*	**30%** *(12/40)*	**80%** *(8/10)*	**45.3**
DK171214_8	WT	**56.9** *(28)* *Int. 36%*	**1.42** *(28)* *Int. 36%*	**17.32** *(28)* *Int. 36%*	**7.87 [11.95]** *(28)* *Int. 36%*	**0.67** *(25)* *Int. 36%*	**3.33%** *(1/30)*	**84.2%** *(16/19)*	**34.2**
DK171214_5[1]	WT	**38** *(24)* *Int. 36%*	**2.81** *(24)* *Int. 36%*	**7.33** *(24)* *Int. 36%*	**6.48 [10.91]** *(24)* *Int. 36%*	**0.61** *(15)* *Int. 39%*	**20%** *(6/30)*	**76.92%** *(10/13)*	**25.5**
DK171214_4[1]	WT	**41.56** *(18)* *Int. 28%*	**1.23** *(18)* *Int. 28%*	**10.52** *(18)* *Int. 28%*	**11.72 [14.96]** *(18)* *Int. 28%*	**0.65** *(20)* *Int. 39%*	**45.46%** *(15/33)*	**69.23%** *(9/13)*	**38.4**
DK171214_9[1]	WT	**16.3** *(15)* *Int. 45%*	**5.77** *(15)* *Int. 45%*	**3.34** *(15)* *Int. 45%*	**13.84 [6.84]** *(15)* *Int. 45%*	**0.26** *(20)* *Int. 74%*	**53.13%** *(17/32)*	**92.86%** *(1/14)*	**44.2**
2nd approach (WTs)									
DK171213_1	WT	**51.81** *(19)* *Int. 46%*	**6.04** *(19)* *Int. 46%*	**14.75** *(19)* *Int. 46%*	**n/a**	**0.45** *(19)* *Int.46%*	**0%** *(0/19)*	**n/a**	**19**
DK171213_2	WT	**260.23** *(19)* Int. 29%	**0.783** *(19)* Int. 29%	**8.11***(19)* Int. 29%	**n/a**	**0.64** *(19)* *Int. 29%*	**0%** *(0/21)*	**n/a**	**30.94**
DK171213_3	WT	**53.87** (20) Int. 32%	**3.67** (20) Int. 32%	**11.26** (20) Int. 32%	**n/a**	**0.76** *(20)* *Int 32%*	**0%** (0/24)	**n/a**	**28.97**

DK171213_4	WT	39.771 Int. 30%	2.9 Int.30%	15.71 Int. 30%	n/a	0.52 *(18)* *Int 30%*	n/a	n/a	19.98
DK120314_1[2]	WT	**17.91** a)17.7 (15) *Int. 53%* b) 18.02 (30) *Int. 52%*	**4.14** a) 4.14 (15) *Int. 53%* b) 4.14 (30) *Int. 52%*	**4.76** a) 4.12 (15) *Int. 53%* b) 5.08 (30) *int. 52%*	**n/a**	**0.97** a) 1.09 (15) *Int. 53%* b) 0.91 (30) *Int. 52%*	**0%** a)0% *0/30* b) 0% *0/15*	**n/a**	**32.24** a) 23.01 b) 36.86
DK120314_2[2]	WT	**40.70** a) 41.55 (39) *Int. 39%* b) 37.39 (10) *Int. 40%*	**5.80** a) 5.7 (39) *Int. 39%* b) 6.2 (10) *Int. 40%*	**12** a) 12.49 (39) *Int. 39%* b) 10.11 (10) *Int. 40%*	**n/a**	**0.43** a) 0.39 (39) *Int 39%* b) 0.59 (10) *int 40%*	**0%** a) 0% *0/30* b) 0% *0/10*	**n/a**	**23.79** a) 23.91 b) 23.30
1st MOS approach (NRG1tg-type-I)									
DK271114_1[2]	NRG1tg-type-I	**44.67** a) 39.96 *(20)* *Int. 30%* b) 47.53 (*33)* *Int. 32%*	**3.81** a) 3.93 *(20)* *Int. 30%* b) 3.73 *(33)* *Int. 32%*	**14.17** a) 11.23 *(20)* *Int. 30%* b) 15.95 *(33)* *Int. 32%*	**7.42 [14.71]** a) 7.96 [14.9] *(20)* *Int. 30%.* b) 7.09 [14.59] (33) *Int. 32%*	**0.55** a) 0.6 *(12)* *Int. 30%* b) 0.38 (4) *Int. 32%*	**39.53%** a) 44.44% *(16/36)* b) 36% *(18/50)*	**100%** a) 100% *(0/3)*[3] b) 100% *(0/3)*[3]	**32.8** a) 32.88 b) 32.74
DK011214_1	NRG1tg-type-I	**26.63** *(26)* *Int. 48%*	**14.84** *(26)* *Int. 48%*	**12.27** *(26)* *Int. 48%*	**7.95 [24.98]** *(26)* *Int. 48%*	n/a	**16.12%** (5/31)	**100%** *(0/4)*[3]	**12.3**
DK221214_2[1]	NRG1tg-type-I	**17.97** *(34)* *Int. 48%*	**5.75** *(34)* *Int. 48%*	**5.69** *(34)* *Int. 48%*	**5.40 [12.87]** *(34)* *Int. 48%*	**0.54** a) 0.67 *(13)* *Int. 48%* *b) 0.45 (19)* *Int 53%*	**32%** *(16/50)*	**43.75%** *(7/16)*	**40.4**

DK221214_4[1]	NRG1$^{tg\text{-}type\text{-}I}$	**16.02** *(39)* *Int. 45%*	**3.35** *(39)* *Int. 45%*	**2.81** *(39)* *Int. 45%*	**6.12 [10.32]** *(39)* *Int.45%*	**0.54** (40) *Int. 49%*	**44%** *(31/70)*	**55%** (*11/20)*	**29.6**
DK221214_5[1]	NRG1$^{tg\text{-}type\text{-}I}$	**20.36** *(52)* *Int. 47%*	**1.39** *(52)* *Int. 47%*	**3.35** *(52)* *Int. 47%*	**5.50 [7.6]** *(52)* *Int. 47%*	**1.22** 1.42 (40) *Int. 47%* 0.96 (32) *Int. 59%*	**48%** *(48/100)*	**90%** (18/20)	**32.9**
DK011214_2	NRG1$^{tg\text{-}type\text{-}I}$	**55.09** (25) *Int. 39%*	**0.98** (25) *Int. 39%*	**9.18** *(25)* *Int. 39%*	**4.90 [6.6]** (25) *Int. 39%*	**1.6** (4) *Int (39%)*	**34.21**% *(13/38)*	**n/a**	**17.76**
2nd approach (NRG1$^{tg\text{-}type\text{-}I}$)									
DK250314_1[2]	NRG1$^{tg\text{-}type\text{-}I}$	**54.73** a)59.30 *(36)* *Int. 28%* b)28.58 *(17)* *int. 28%* c)91.78 (*21)* *int. 30%* d)43.67 *(45)* *int. 27%*	**5.53** a) 6.33 *(36)* *Int. 28%* b) 6.97 *(17)* *Int.28%* c) 4.81 *(21)* *Int. 30%* d) 4.68 *(45)* *Int. 27%*	**14.22** a) 16.45 *(36)* *Int. 28%* b) 9.03 *(17)* *Int. 28%* c) 18.58 (*21)* *Int. 30%* d) 12.36 *(45)* *Int. 30%*	**n/a**	**0.96** a) 0.58 *(36)* *Int. 28%* b) 1.56 *(17)* *Int. 28%* c) 0.75 (*21)* *int. 30%* d) 1.14 *(45)* *Int. 27%*	**2.96%** a) 0% *(0/36)* b) 17.65% *(3/17)* c) 0% *(0/21)* d) 2.17% *(1/46)*	**n/a**	**17.08** b) 16.96 c) 16.86 d) 17.14 a) 17.24
DK250314_2[2]	NRG1$^{tg\text{-}type\text{-}I}$	**43.07** a) 56.07 *(11)* *Int. 31%* b) 40.15 *(49)* *Int. 32%*	**7.73** a) 6.89 *(11)* *Int. 31%* b) 7.92 *(49)* *Int. 32%*	**13.14** a) 13.62 (11) *Int. 31%* b) 13.03 (49) *Int. 32%*	**n/a**	**0.71** a) 0.55 *(11)* *Int. 31%* b) 0.75 *(49)* *Int. 32%*	**0%** a) 0% *(0/11)* b) 0% *(0/49)*	**n/a**	**17.88** a) 17.82 b) 17.89
DK140114_2	NRG1$^{tg\text{-}type\text{-}I}$	**93.90** *(11)* *Int. 40%*	**4.15** *(11)* *Int. 40%*	**19.21** *(11)* Int. 40%	**n/a**	**0.23** *(11)* *Int 40%*	**0%** *(0/11)*	**n/a**	**24.84**

DK130314_1	NRG1$^{tg\text{-}type\text{-}I}$	**123.14** *(22)* *Int. 29%*	**4.17** *(22)* *Int. 29%*	**24.63** *(11)* *Int 29%*	**n/a**	**0.29** *(22)* *Int.29%*	**0%** *(0/22)*	**n/a**	**17.96**
DK180714_2[2]	NRG1$^{tg\text{-}type\text{-}I}$	**27.09** a) 30.13 *(42)* *Int. 46%* b) 23.11 *(32)* *Int. 56%*	**6.99** a) 6.58 *(42)* *Int. 46%* b) 7.52 *(32)* *Int. 56%*	**10.50** a) 11.52 *(42)* *Int. 46%* b) 9.17 *(32)* *Int. 56%*	**n/a**	**0.42** a) 0.42 *(42)* *Int. 46%* b) 0.41 *(32)* *Int. 56%*	**0%** 0% *(0/42)* 0% *(0/32)*	**n/a**	**28.65** a) 29.52 b) 27.86
DK180714_3[2]	NRG1$^{tg\text{-}type\text{-}I}$	**52.75** a) 45.00 *(43)* *Int. 33%* b) 55.28 *(41)* *Int. 34%* *c)* 55.94 *(72)* *Int. 35%*	**11.13** a) 10.89 *(43)* *Int. 33%* b) 11.69 *(41)* *Int. 34%* *c)* 10.96 *(72)* *Int. 35%*	**17.05** a) 17.97 *(43)* *Int. 33%* b) 16.64 *(41)* *Int. 34%* *c)* 16.74 *(72)* *Int. 35%*	**n/a**	**0.34** a) 0.32 *(43)* *Int. 33%* b) 0.31 *(41)* *Int. 34%* *c)* 0.37 *(72)* *Int. 35%*	**0%** 0% *(0/43)* 0% *(0/41)* 0% *(0/72)*	**n/a**	**23.53** a) 20.89 b) 20.77 c) 26.68
DK170714_1	NRG1$^{tg\text{-}type\text{-}I}$	**31.58** *(38)* *Int. 100%*	**9.73** *(38)* *Int. 100%*	**11.83** *(38)* *Int. 100%*	**n/a**	**0.48** (38) *Int. 100%*	0% (0/100)	**n/a**	**41.1**
DK230914_1	NRG1$^{tg\text{-}type\text{-}I}$	**50.92** (37) *Int. 56%*	**7.58** (37) *Int. 56%*	**18.26** (37)	**n/a**	**0.29** (37) *Int. 56%*	**0%** (0/37)	**n/a**	**31.44**

Properties of light evoked IPSCs in NRG1$^{tg\text{-}type\text{-}I}$ and wild type mice pyramidal cells. Bold, values used for statistical comparisons; Parenthesis: number of sweeps; Int: Percentage of the maximum laser intensity applied. Letters in parenthesis indicate a paired photostimulation round at a fixed laser spot and intensity. [1)] Annotation: Recording of PPR at a higher laser intensity when MOS failed to evoke reliably an IPSC after the second light pulse. [2)] Annotation: Cell recording with multiple rounds of paired pulse photostimulation at a different laser spot and intensity. When multiple rounds of the photostimulation have been applied, parameter values are estimated as the weighted means by the number of sweeps.

Table 5-2 Comparison of optogeneticaly elicited IPSCs parameters in WT and NRG1$^{tg\text{-}type\text{-}I}$ mice

Synaptic parameter	Genotype (cells recorded)	Mean ± SEM or medians (25th; 75th quartiles)	Statistical test	Significance (p-values)
(1) 1st IPSC peak amplitude (pA)	WT *(5)* NRG1$^{tg\text{-}type\text{-}I}$ *(6)*	35.83 ± 6.90 30.12 ± 6.56	Unpaired t-test	P = 0.57
(2) 1st IPSC peak amplitude (pA)	WT*(5)* NRG1$^{tg\text{-}type\text{-}I}$ *(8)*	51.81 (35.00 to105.46) 51.83 (37.33 to 74.32)	Mann-Whitney U test	P = 0.94
(1) 1st IPSC 20-80% rise time (ms)	WT *(5)* NRG1$^{tg\text{-}type\text{-}I}$ *(6)*	2.45 (1.37 to 3.55) 3.58 (1.39 to 5.75)	Mann-Whitney U test	P = 0.66
(2) 1st IPSC 20-80% rise time (ms)	WT*(5)* NRG1$^{tg\text{-}type\text{-}I}$ *(8)*	4.09 ± 0.95 7.13 ± 0.88	Unpaired t-test	P = 0.045*
(1) 1st IPSC half amplitude decay (ms)	WT*(5)* NRG1$^{tg\text{-}type\text{-}I}$ *(6)*	9.24 ± 2.32 7.91 ± 1.93	Unpaired t-test	P = 0.67
(2) 1st IPSC half amplitude decay (ms)	WT*(5)* NRG1$^{tg\text{-}type\text{-}I}$ *(8)*	10.18 ± 1.72 16.11 ± 1.64	Unpaired t-test	P = 0.026*
(1)Latency (light pulse onset -10% rise of IPSCs	WT (5) NRG1tg-type-I (6)	8.44 ± 0.96 6.22 ± 0.5	Unpaired t-test	P = 0.057
(1) Latency (light pulse onset-peak amplitude) (ms)	WT *(5)* NRG1$^{tg\text{-}type\text{-}I}$ *(6)*	12.97 ± 0.71 12.85 ± 2.73	Unpaired t-test	P = 0.97
(1) PPR (2nd/1st IPSC peak amplitude)	WT*(5)* NRG1$^{tg\text{-}type\text{-}I}$ *(6)*	0.51 ± 0.09 0.89 ± 0.22	Unpaired t-test	P = 0.14
(2) PPR (2nd/1st IPSC peak amplitude)	WT *(5)* NRG1$^{tg\text{-}type\text{-}I}$ *(8)*	0.65 ± 0.10 0.47 ± 0.09	Unpaired t-test	P = 0.21
(1) & (2)	WT *(10)* NRG1$^{tg\text{-}type\text{-}I}$ *(14)*	0.63 (0.43 to 0.67) 0.54 (0.33 to 0.77)	Mann-Whitney U test	P = 0.71
(1) 1st IPSC failures at MOS intensity	WT *(5)* NRG1$^{tg\text{-}type\text{-}I}$ *(6)*	30.38% ± 8.90 35.64% ± 4.60	Unpaired t-test	P = 0.59
(2) 1st IPSC failures at MOS intensity	WT *(5)* NRG1$^{tg\text{-}type\text{-}I}$ *(8)*	0 (0 to 0) 0 (0 to 0)	Mann-Whitney U test	P = 0.72
(1) 1st IPSC failures at 1-2% decreased MOS intensity	WT *(5)* NRG1$^{tg\text{-}type\text{-}I}$ *(8)*	80.64% ± 3.91 77.75% ± 11.86	Unpaired t-test	P = 0.82

Summary of IPSC properties comparison between NRG1$^{tg\text{-}type\text{-}I}$ and WT mice with the statistical test used ; (1) MOS approach, (2) No failures elicited IPSC approach

5.2.3 Data interpretation between the two IPSC elicited approaches

Interestingly, results from two different optical stimulation protocols are not in complete agreement. The results with the latter approach (2^{nd}) suggest that synaptic transmission from CCK+/CB_1R+ expressing fibres to CA3 pyramidal cells is altered in the $NRG1^{tg\text{-}type\text{-}I}$ mice. In particular, solely changes in rise and decay times of post- synaptic currents can reflect changes either in the synapse morphology (i.e in the post- synaptic density (PSD) or/and synaptic cleft geometry) or changes in GABAA receptor composition (different subunit expression). However, because the former approach (MOS protocol) fails to show similar changes, the results need to be cautiously interpreted.

What could explain the different results with these two approaches? First, the second approach is likely to activate a larger number of GABAergic axons than the MOS protocol (1^{st} approach). In experiments where the MOS applied, the illuminated area (laser spot used to activate pre-synaptic CCK+/CB_1R+ positive fibres) was focused in narrow area (15-20 μm diameter) and the light stimulation was more clearly positioned in s.p or s.p/s.r. Hence, it is probable that the photoactivation used in the experiments with MOS activated mainly axons of perisoma- targeting CCK-positive interneurons (such as CCK-positive basket cells). Conversely, in the second approach the optical laser spot was wider in diameter (~80 μm). This may have led to activation of larger proportion of GABAergic fibres that form synapses along the whole somatodendritic axis (and in particular to dendrites). Because synapses targeting on different part of the PC somatodendritic axis elicits IPSCs with different recorded kinetics in somatic recordings this might explain why IPSCs showed kinetics with high variability in the second experimental approach. Therefore, it is possible that the observed differences in the IPSC kinetics between the two tested genotypes actually emerged from random differences in the types of CCK+/CB_1R+ GABAergic axons innervating the PC somatodendritic axis. Therefore, it would

be important to increase the data sample size in order to be able to conclude the second approach results on IPSC kinetics. Moreover, as it has been mentioned before, this experimental approach likely leads to the activation of more than one axon. Therefore it is possible that during ChR2 photoexcitation multiple GABAergic axons will be activated whose pre-synaptic action potential generation and neurotransmitter release may not be precisely synchronised. Thus, during ChR2 photoexcitation, multiple axons of separate origin with not precisely synchronised neurotransmitter release can produce compound IPSCs with fluctuating kinetics. It follows, that the photoexcitation protocol employed in order to induce consistently elicited CCK+/CB_1R+ fibres mediated IPSCs on pyramidal cells connection is susceptible to great technical inconsistencies in between cell recordings, and can lead to distorted assessment of the basic synaptic properties. For these reasons, I propose that emphasis in comparison of the IPSC kinetics between the two genotypes should be put in the experiments where the MOS protocol was applied.

5.3 Discussion and conclusions

The activity of CCK/CB_1R-positive cells is of great importance for the modulation of neuronal network operations given that these circuits are involved in information processing and higher brain functions. The experiments presented here aimed to assess whether the chronic elevation of NRG1 expression affects GABAergic signalling from CCK+ CA3 area interneurons to pyramidal cells.

The experimental approach employing MOS protocol revealed no significant differences between basic synaptic function in the two genotypes neither pre-synaptically (PPR- IPSCs failures) or post-synaptically (IPSC amplitude and kinetics). Yet, it is noteworthy that data obtained from the second approach, where the light activation was set to always generate post-

synaptic events, showed that the IPSCs kinetics (rise time and decay time) although not IPSC amplitude, differ between the two genotypes. Importantly, the latter methodological approach has more suboptimalities than the MOS protocol concerning the pre-synaptic origin, the activated fibre post-synaptic target domain and the number of CCK+/CB_1R+ axons activated with ChR2 excitation, and these may compromise the quantitative comparative analysis of the properties of the evoked IPSCs. Therefore, in view of the experimental limitations of the latter approach, the analysis of the CCK interneuron-to-CA3 PC synapse with MOS protocol should be emphasised in IPSCs kinetic analysis. Therefore I conclude that the NRG1 over-expression is not associated with detectable changes in the CCK+ cell GABAergic synapses to CA3 pyramidal cells.

The effects of the chronically altered NRG1-ErbB4 signalling in CCK+ GABAergic synapses have not been examined before. Instead, earlier studies have largely focused on assessing neurotransmission changes widely in GABAergic synapses and not in a cell type specific manner (Yin et al., 2013, Agarwal et al., 2004, Papaleo et al., 2016). These earlier studies have also produced conflicting results that may largely emerge from the different methodological approaches employed.

In further detail, the findings presented here are in line with a recent study examining the effects of human NRG1-IV expression in a transgenic mouse line (Papaleo et al., 2016). In that particular study the authors report no difference in mIPSCs in the mPFC pyramidal cells between transgenic mice and wild-type littermate controls. Importantly, my findings are in agreement with earlier observations from my host laboratory that reported that the GABAergic neurotransmission provided by PV+ cells is largely unaffected due to NRG1 over-expression (Nissen, 2012). On the other hand my results partially contrasts with two earlier studies utilising two other mouse strains NRG1 over-expressing mice. The first study employing a strain of animals with elevated expression of the membrane bound (CRD)-NRG1 peptide (Agarwal et al.,

2014) showed an increased frequency of post-synaptic mIPSCs in in hippocampal pyramidal cells. A finding that could indicate changes in neurotransmitter release pre-synapticaly in these mice. The second study performed in a mouse strain with (Ig)- NRG1 over-expression showed that the amplitude of mIPSCs in hippocampal pyramidal neurons were reduced whereas the frequency was found to be unaltered. (Yin et al., 2013), hence arguing for post-synaptic changes in the GABAergic synapse in these mice.

In the past the functional properties of the GABAergic synapses formed by CCK+ BSCs cells have been studied in parallel with the ones formed by the PV+ BScs ones (Hefft and Jonas, 2005, Glickfeld and Scanziani, 2006). A direct comparison of the synaptic parameters measurements resulted from the experiments presented here with the previous ones that derived from paired recordings is not well founded, mainly due to the fact that ChR2 expression and photoexcitation influence synaptic responses (Zhang and Oertner, 2007, Jackman et al., 2014). However, when the light elicited IPSCs synaptic properties as estimated from MOS experiments are compared between CCK + and PV+ outputs (Nissen, 2012) fibres (WTs) , they show proportionate variances between them that were similar to the ones estimated from synaptic pairs recordings as previously reported by Hefft and Jonas in 2005 and Glickfield and Scanziani in 2006. In further detail CCK+ vs PV+ GABAergic synapses show: Longer rise times (cell pairs recordings; 1.5 to 1.64 fold vs. 2.88 fold increase - MOS recordings), and longer synaptic latencies (cell pairs recordings; 1.95 to 2.28 fold vs 1.70 fold - MOS recordings), but similar decay times (cell pairs recordings 1.08-1.01 fold vs 0.96 fold- MOS recordings) and similar PPR (cell pairs recordings; 1.11 fold vs 0.95 fold-MOS recordings).

5.4 Perspective and future directions

My experiments here addressed the question on whether chronically elevated NRG1 levels could affect GABAergic synapses specifically from CCK+ interneurons to pyramidal cells. Even though some previous studies have reported that enhanced NRG1 signalling alters the GABAergic inhibition in general, here I showed by employing specific stimulation of CCK+ GABAergic fibres that there are no detectable differences in these synapses between the mice with chronically elevated NRG1 and wild-type controls. Yet, at this point it should be noted that in the MOS recordings in this study, even though the laser spot (15-20 μm) was restricted in s.p or at the border of s.p/s.r targeting mainly CCK+ basket cell axons, the possibility that other or multiple CCK+/CB_1R+ cell fibres running at the same focal plane cannot be excluded. Furthermore, as it has been discussed in chapter 3 the possibility of ChR2 expression in other interneuronal types and their subsequent photoactivation during MOS experiments cannot be completely ruled out. Thus, in the future, it would be useful to reproduce these experiments employing recordings from synaptically connected CCK-positive GABAergic cells and CA3 pyramidal cells. That would allow the anatomical analysis of the pre-synaptic cell type and assess with higher certainty the properties of a single fibre connections in both genotypes.

Finally it would be important to determine whether the characteristic asynchronous fashion of neurotransmitter release as well as the emergence of depolarization induced suppression of inhibition (DSI), characteristic features of CCK+/CB_1R+ GABAergic cells, are also affected by NRG1 over-expression. These features of CCK+/CB_1R+ interneurons are considered to be significant in the generation of co-ordinated rhythmic population activities in the cortex that give rise to higher brain functions, which are often impaired in schizophrenia.

6 Effects of NRG1 over-expression on the NMDA receptor-mediated recurrent inhibition in the hippocampus

6.1 Introduction - Disynaptic inhibition in hippocampal network operations

The hippocampus is involved in various co-ordinated rhythmic neuronal activities that support higher brain functions. It is able to intrinsically generate gamma-frequency range (30-80 Hz) network oscillations which play a role in hippocampal learning and memory processing in the hippocampus and neocortex (Bartos et al., 2007, Montgomery and Buzsaki, 2007, Cardin et al., 2009). The gamma frequency oscillations, observed in the hippocampal field potential are likely to reflect a diverse range of individual network phenomena with distinct functional roles. For example it has been suggested that "place cells" firing is primarily primed by high frequency gamma oscillations (Bieri et al., 2014, Lasztoczi and Klausberger, 2016), whereas, slow gamma oscillations has been found to shape the activity of "place cells" before the entrance of the animal to the centre of their corresponding place fields. (Csicsvari et al., 2003, Colgin et al., 2009, Bieri et al., 2014, Lasztoczi and Klausberger, 2014). Even though the exact synaptic mechanism for the generation of oscillations at the gamma band range is not fully understood, their generation is supposed to crucially depend on the interplay between the GABAergic inhibitory interneurons and the excitatory principal cells. In particular, recurrent feed-back inhibition in the pyramidal cells, is considered to be elemental for the gamma oscillations generation in hippocampus (Traub et al., 1997, Whittington et al., 2000). In theoretical modelling studies, this hippocampal circuit (PC-IN-PC), is often referred as "pyramidal cell - interneuron network gamma" model and abbreviated as "PING". Its rhythm-generating capacity emerges from the precisely timed synaptic inhibition of the pyramidal cells by the GABAergic interneurons and the suprathreshold phasic excitation of interneurons. In this simplistic model, the mutual

interaction of the two cell populations synchronizes the activity and the co-ordinated firing of the pyramidal cells that gives rise to the local field potential (LFP) at the gamma band frequency (Tiesinga and Sejnowski, 2009). In brain slices the rhythmic gamma oscillation activity typically occurs at lower frequency (~20 Hz) than the one reported *in vivo* (30-80 Hz). This is probably due to the compromised tissue metabolism and lower tissue temperature in the slices compared to intact brain (Mann et al., 2005, Hajos et al., 2009).

The GABAergic inhibitory interneurons in the mammalian cortex comprise different cell types, which are distinct in their functional properties, axonal arborisation and synaptic targets (Klausberger and Somogyi, 2008). Although the exact role of many interneuron types in these processes is still unknown, it is commonly accepted that fast-spiking PV-positive basket cells are crucial for the generation of the gamma band synchronous oscillations and regarded to be the "pace makers" of the gamma band oscillations. This is supported by several lines of evidence. Firstly, these cells form a reciprocally connected network of inhibitory cells (Sik et al., 1995, Gulyas et al., 1999) which is able to provide time -precise inhibition across a large number of principal neurons. Secondly, they are capable of displaying stable action potential firing at gamma frequency (Pike et al., 2000). Thirdly, experiments *in vivo* have demonstrated that the fast-spiking basket cells are strongly active during gamma frequency field potential oscillations (Tukker et al., 2007, Klausberger and Somogyi, 2008). Fourth, their network activity-driven action potential firing is phase-locked during gamma oscillations both *in vitro* (Hajos et al., 2004) and *in vivo* (Tukker et al., 2007) and follow the firing of the local pyramidal cells (Glickfeld and Scanziani, 2006). Fifth, the selective and targeted suppression of their synaptic excitation through AMPA receptor–mediated EPSPs blockade severely compromises gamma oscillations power (Fuchs et al., 2007) and sixth, their selective sustained stimulation amplifies the cortical network's gamma oscillation power (Cardin et al., 2009).

If, the PV fast-spiking basket cells are considered the “pace makers” of the gamma oscillations, the CCK+ counterparts have classically been regarded as the “fine tuners” of the oscillation spatio-temporal features (Freund and Katona, 2007, Armstrong and Soltesz, 2012).This assumption is based on the observation about the intrinsic properties of CCK+ basket cells, and their synaptic features. For instance, they have the capability to integrate multivariable synaptic inputs over wider temporal window than the PV+ ones due to their long membrane time constant (Glickfeld and Scanziani, 2006). In addition, they characteristically display asynchronous GABA release, with low fidelity and with large latency and jitter (Hefft and Jonas, 2005, Glickfeld and Scanziani, 2006) and finally are sensitive to endocannabinoids that inhibits their GABA release during the repetitive pyramidal cell firing (Foldy et al., 2007, Karson et al., 2008).

The effects of the NRG1 over-expression on hippocampal synchronous oscillations have been previously studied in slice preparations from $NRG1^{tg\text{-}type\text{-}I}$ mice (Deakin et al., 2012). In this study of carbahol-induced gamma oscillations it was found that slices from the $NRG1^{tg\text{-}type\text{-}I}$ mice, exhibited reduced mean oscillation frequency compared to slices from WTs (mean frequency; WT= 26.3 Hz vs. $NRG1^{tg\text{-}type\text{-}I}$= 22.0 Hz). Importantly, the frequency of gamma oscillations has been proposed to heavily depend on the functionality of NMDAR receptors in interneurons (Mann and Mody, 2010). However it is still unknown, which cell (s) populations is the prime suspect for this changes in the hippocampal synchronous activity.

Given the previous reports of alterations in gamma band oscillations (Deakin et al., 2012) as well as of the finding of NMDAR hypofunction in hippocampal interneurons (chapter 4 and Nissen, 2012), here I aimed to reveal the association between this synaptic dysfunction with the

disynaptic inhibition in the hippocampus which is the fundamental synaptic interaction mediating the synchronization of the PING circuit.

6.2 Contribution of NMDA receptor-mediated transmission on disynaptic inhibition during repetitive discharge of glutamatergic axons

6.2.1 Experimental paradigm

In the following experiments, I investigated the contribution of glutamate NMDA receptors on disynaptic inhibition in the hippocampus during gamma frequency discharge of pyramidal cells. For this, I employed selective optical stimulation of glutamatergic axons in the CA1 area of dorsal hippocampal slices prepared from CAMKII-Cre$^{+/-}$ mice crossed with NRG1$^{tg\text{-}type\text{-}I}$ (NRG1$^{tg\text{-}type\text{-}I}$) mice, and the CAMKII-Cre$^{+/-}$ wild-type littermates (WT). Mice were transfected using stereotaxic co-ordinates (1.70 mm caudal, 1.40 lateral from bregma and at 1.60 mm, 1.40mm and 1.20 mm depth from the brain surface) with AAV2/5 –ChR2 –eYFP construct to achieve cre-dependent expression of the gene products in pyramidal cells (for expression of AAV2/5-ChR2-eYFP, (see sections 2.4.4, 2.5 and Figure 5-1 A and B). A total volume of 800 nl of the viral particle suspension (titre ± 4 × 10^{12}/mL) was injected in hippocampus in both hemispheres, and the mice were allowed to recover for 11-21 days after the surgery. Finally, coronal brain slices from the injected mice that successfully expressed ChR2-eYFP were selected for experiments.

Local hippocampal pyramidal cell firing was optogenetically triggered at 20 Hz frequency. This activation pattern was selected, since the stimulation frequency is close to the predominant gamma oscillation frequency reported in the hippocampal slices and because previous work has shown that network oscillation at this frequency is altered in the transgenic mice (Deakin et al., 2012) The channelrhodopsin expressing pyramidal cells were

photostimulated using five consecutive laser light pulses (3 ms, 470 nm, nominal output max. 100 mW) focused in s.p/s.o and delivered at 20 Hz. The bursts were delivered every 30 s at a fixed laser spot of 15-20 µm in diameter. Simultaneously, I recorded post-synaptic responses in putative CA1 pyramidal cells in whole-cell voltage-clamp mode (Figure 6-1 A). The laser spot position and the power were adjusted so that the photoactivation elicited stable post-synaptic responses. For long term stability of post-synaptic events, slices were stored and recordings were performed in the continuous presence of CAMKII inhibitor KN-62 (3 µM) and group I metabotropic glutamate receptor antagonist RS-MCPG (200 µM) to inhibit long-term plasticity phenomena (Perez et al., 2001, Lamsa et al., 2007, Campanac et al., 2013). Recordings of excitatory and inhibitory currents were performed by sequentially clamping the pyramidal cells at the reversal potentials of synaptic inhibition and excitation respectively. The recurrent IPSCs were recorded at the measured (online) reversal potential for EPSCs (E_{EPSCs}), (WTs: 10 ±0.45 mV, n=6; $NRG1^{tg\text{-}type\text{-}I}$: 12.14 ±1.2 mV, n=7) and EPSCs were recorded at -70 mV (Figure 6-1, B)

The CA3 area was surgically isolated from the CA1 region with a cut between the areas in order to suppress polysynaptic events. Stable baseline recording of the EPSCs and the IPSCs were obtained for at least 5 minutes. The total charge of post-synaptic events was measured in 500 ms time window from the current onset. To explore the contribution of the NMDARs in disynaptic inhibition, the NMDA blocker DL-AP5 (100 µM) was applied after the recording of baseline. The disynaptic nature of the IPSCs was confirmed by their abolishment after the application of the glutamate AMPAR blocker NBQX (25 µM). Recorded post-synaptic cells were not anatomically analysed in the experiment, and hence the post-synaptic cells needs to be considered putative pyramidal cells.

It is noteworthy to mention that a substantial proportion of my recordings suffered from serious run down of evoked EPSCs during the course of the experiment, possibly due to opsin desensitization. As a matter of fact, in 20 out of 32 recorded post-synaptic cells the drift was unacceptably large (more than 10% of the evoked currents charge in five minutes), hence those recordings were excluded from the analysis.

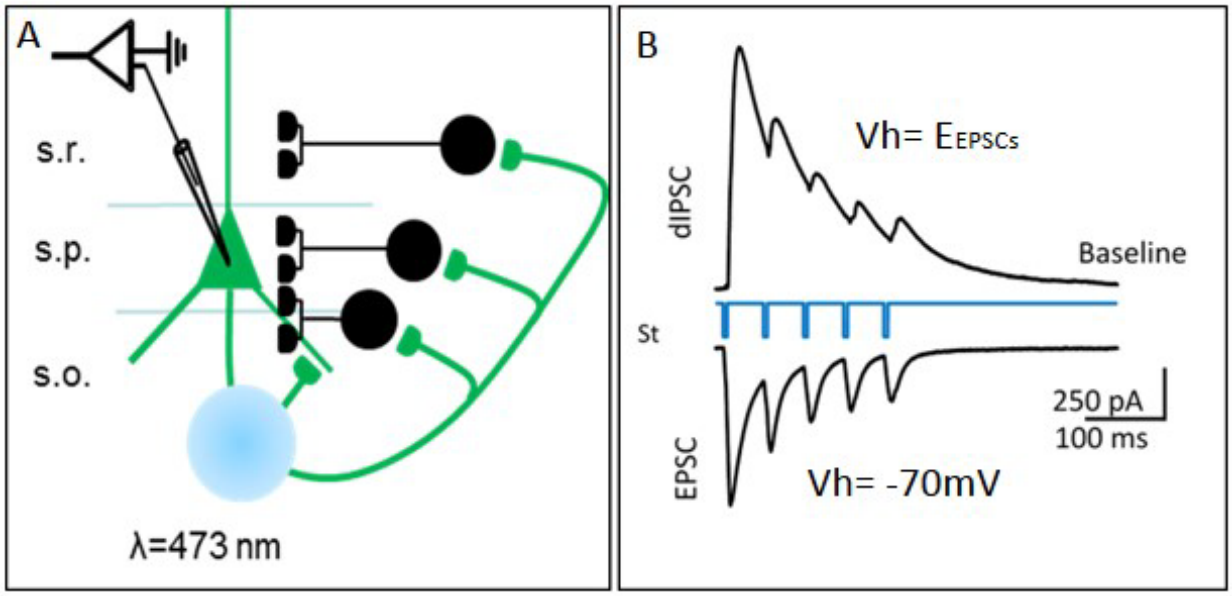

Figure 6-1 Monosynaptic EPSCs and disynaptic IPSCs after 20Hz repetitive discharging of glutamatergic fibers. (A) Schematic shows experimental design; optogenetic stimulation (fixed-spot 473 nm laser light stimulation in blue) of ChR2-expressing glutamatergic CA1 pyramidal cell fibres. Stimuli (5 pulses) were applied at 20 Hz "low gamma frequency" to activate the glutamatergic axons (green). This elicited monosynaptic EPSCs in local GABAergic interneurons (black) generating recurrent disynaptic IPSCs (dIPSCs). Hippocampal slices were from (AAV2/5)-ChR2-eYFP -transfected CAMKII-Cre $^{+/-}$ mice (WT) and CAMKII-Cre $^{+/-}$/NRG1$^{tg\text{-}type\text{-}I}$ (NRG1$^{tg\text{-}type\text{-}I}$) mice. (B) Averaged EPSCs from a sample cell recorded at -70mV in voltage-clamp configuration (black traces below). Averaged disynaptic recurrent IPSCs (black traces above) are shown (recorded at the EPSCs reversal potential) in the same putative CA1 area pyramidal cell. Timing of the optical stimuli (St) is illustrated in blue with a simple schematic between the traces.

6.2.2 Results

The contribution of NMDAR-mediated neurotransmission to recurrent inhibition during 20 Hz glutamatergic fibre activity was examined in the NRG1$^{tg\text{-}type\text{-}I}$ mice and WT littermate controls. The total charge of dIPSCs before (1.5 minutes; 3 sweeps) and after application of DL-AP5 (100 µM) (1.5 minutes; 3 sweeps after 2.5-3 minutes in DL-AP5) was recorded and then compared between 6 putative pyramidal cells from WTs (CAMKII-Cre$^{+/-}$) and 7 from NRG1

over-expressing mice (CAMKII-Cre$^{+/-}$/NRG1$^{tg\text{-}type\text{-}I}$) mice respectively. A breakdown of the dIPSC and EPSCs total charge change during the application of DL-AP5 in individual putative pyramidal cells from WT and NRG1$^{tg\text{-}type\text{-}I}$ mice is summarised in Table 6-1.

The NMDA receptor blockade significantly reduced the disynaptic IPSCs in the pyramidal cells both in the WTs and the NRG1$^{tg\text{-}type\text{-}I}$ mice. The dIPSCs charge dropped to 64.5% (means, $P<0.001$) in the WT, and to 78% from baseline in the NRG1$^{tg\text{-}type\text{-}I}$ mice (means, $P<0.003$) after DL-AP5 application (Figure 6-2 A1,2 and B 1,2). However, the effect of NMDAR blockade on recurrent IPSCs was statistically smaller in the NRG1$^{tg\text{-}type\text{-}I}$ mice compared to the WT littermates. The exact baseline-normalised dIPSCs charge following DL-AP5 application comparison between the two genotypes, was in WT; 0.65 ± 0.03 and in NRG1$^{tg\text{-}type\text{-}I}$ mice; 0.78 ± 0.045 (means, $P= 0.037$; Figure 6-2 C).

The recurrent nature of the evoked IPSCs was confirmed at the end of experiments by their total abolishment with AMPA/kainate receptor antagonist (n = 4 recordings from WT and n=4 from NRG1$^{tg\text{-}type\text{-}I}$ mice) (Figure 6-2 A1, 2, B1, 2 and C).

In addition, the EPSCs total charge showed a non-significant drop to 78 % ±11.8% in WT and 87% ±8.67% in NRG1$^{tg\text{-}type\text{-}I}$, respectively from baseline (means, $P > 0.05$) after DL-AP5 application, with no statistically difference between the two genotypes $P= 0.543$. One possibility for this drop of the EPSCs charge after the application of DL-AP5, could be the blockade of pre-synaptic NMDAR receptors leading to altered neurotransmitter release at these synapses. Moreover, space clamp problems cannot be ruled out. This could lead to a proportion of NMDARs been relieved from Mg^{2+} blockade during baseline recordings, while their contribution to the total EPSCs charge would be abolished during DL-AP5 application. Furthermore, the EPSCs charge recordings were substantially contaminated with opsin current

in the pyramidal cells. This is evident by the not total suppression of the post-synaptic events at the -70mV holding voltage after NBQX application (Figure 6-2 A1 and A2). Nonetheless this suppression was equal in between the genotypes; WT; 35.2 ± 5.2% (n = 4) and $NRG1^{tg\text{-}type\text{-}I}$; 32 ± 16.6 % (n=4) from baseline (P= 0.87). Hence, although, it would be interesting to determine whether there is a change in the global excitation/inhibition balance in the NRG1 over-expressing mice from this experimental paradigm, unfortunately for the reasons described above a direct comparison of the EPSCs to IPSCs charge ratio between individual cells in the two genotypes was not feasible.

Table 6-1 Summary of dIPSCs and EPSCs area during the 20Hz optogenetic stimulation of glutamatergic fibers (normalised to baseline conditions)

Genotype	dIPSCs charge in DL-AP5	EPSCs charge in DL-AP5	dIPSCs charge in NBQX	EPSCs charge in NBQX	E_{EPSCS} (mV)
WT	0.63	0.77	n/a	n/a	10
WT	0.71	0.70	0.00	0.28	9
WT	0.64	1.26	n/a	n/a	10
WT	0.50	0.36	0.06	0.25	9
WT	0.70	0.81	0.04	0.47	12
WT	0.69	0.78	0.03	0.41	10.
$NRG1^{tg\text{-}type1}$	0.76	0.68	0.02	0.22	12
$NRG1^{tg\text{-}type1}$	0.86	0.81	0.00	0.79	10
$NRG1^{tg\text{-}type1}$	1.01	1.03	0.02	0.01	10
$NRG1^{tg\text{-}type1}$	0.73	1.08	n/a	n/a	10
$NRG1^{tg\text{-}type1}$	0.66	1.19	n/a	n/a	12
$NRG1^{tg\text{-}type1}$	0.71	0.74	0.02	0.27	12
$NRG1^{tg\text{-}type1}$	0.73	0.59	n/a	n/a	19

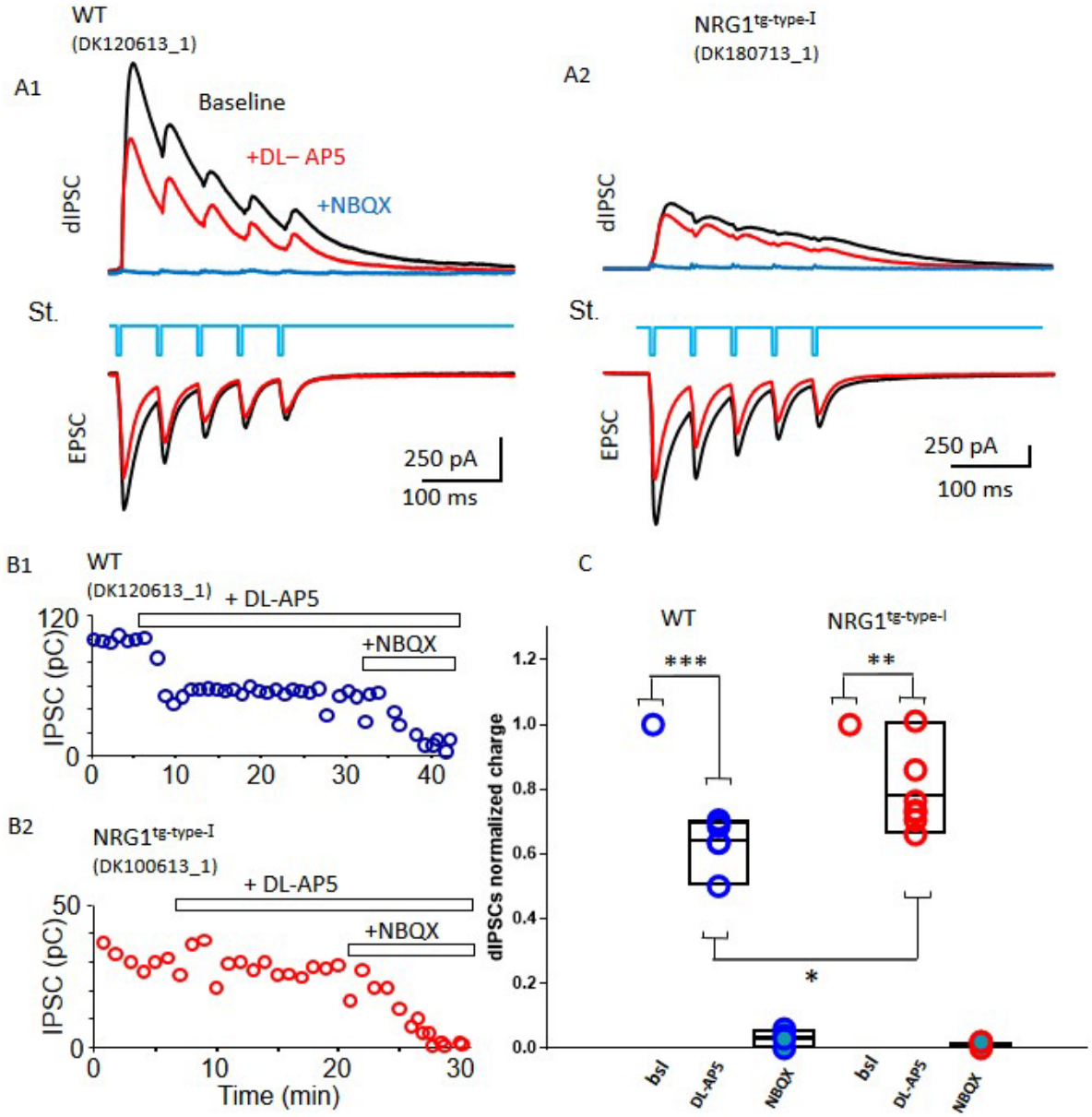

Figure 6-2 Comparison of EPSCs and IPSCs post-synaptic events in WT and NRG1$^{tg\text{-}type\text{-}I}$ mice (A) Averaged EPSCs and recurrent IPSCs in CA1 pyramidal cells evoked by the optogenetic stimulation (5 pulses at 20 Hz) (St.). (A1) Recording from WT and (A2) NRG1$^{tg\text{-}type\text{-}I}$ mouse. The NMDAR antagonist DL-AP5 (100 µM) (red) has more pronounced effect on the recurrent IPSCs in the WT mice compared to the NRG1$^{tg\text{-}type\text{-}I}$ mice. Recurrent IPSCs were fully blocked with NBQX (25 µM) (blue). (B) Recurrent IPSC charge in pyramidal cells from a WT (B1) and from a NRG1$^{tg\text{-}type\text{-}I}$ mice (B2). Application of DL-AP5 and NBQX is indicated by horizontal bars. (C) Box plot of the effect of DL-AP5 on the recurrent IPSCs charge in the WT and in the NRG1$^{tg\text{-}type\text{-}I}$ mice (IPSCs baseline-normalised). Application of DL-AP5 reveals reduced sensitivity of the IPSC charge after NMDAR blockage in the NRG1$^{tg\text{-}type\text{-}I}$ mice, open circles; dIPSCs normalized charge in individual pyramidal cells recordings. Filled blue circles dIPSCs values in the presence of NBQX, P <0.05 *, P < 0.005 **, p<0.001 *.**

6.3 Discussion and conclusions

The results presented here, on the optogenetically-driven recurrent inhibition at 20 Hz frequency, demonstrate that the feedback inhibition in the hippocampus substantially depends on activation of glutamate NMDA receptors in GABAergic interneurons. Most importantly, these experimental data showed that the recurrent inhibition during the repetitive glutamatergic fibre activity is less sensitive to NMDAR blockade in $NRG1^{tg\text{-}type\text{-}I}$ mice than in the WT control mice. This indicates that NRG1 over-expression compromises the hippocampal feedback inhibition reducing NMDAR-mediated excitation of GABAergic interneurons. The effect was observed during repetitive discharge of the glutamatergic fibres at 20 Hz frequency that corresponds to the lower range to the hippocampal gamma-frequency oscillations.

These findings together with the earlier findings of NMDAR hypofunction on PV+ and CCK+ interneurons the two major hippocampal cell populations that prominently express the ErbB4 receptor show that NRG1 over-expression leads to compromised disynaptic inhibition during the physiological relevant activation of the hippocampal network, due to interneuronal NMDAR hypofunction.

Even though, various hippocampal GABAergic interneuron types participate in the rhythmic gamma oscillations, the properties of PV-positive cells (and particularly PV+ basket cells, see above in this chapter) make them the key rhythmogenic cell population in the hippocampal gamma oscillations. On the contrary, the CCK+ GABAergic basket cells are considered to be the gamma oscillations fine tuners. In the experimental conditions here, the optogenetically-elicited disynaptic inhibition is likely to emerge from glutamatergic activation of many interneuron types. Therefore, it is challenging to differentiate which interneuron types exactly are responsible for the reduced NMDAR-driven GABAergic activity in the NRG1 over-

expressing mice. However, it is worth mentioning that distinct hippocampal interneuron types exhibit different strength of NMDAR-mediated glutamatergic transmission. Two seminal studies highlighted this diversity demonstrating large differences between the CCK+ and the PV+ GABAergic interneurons. The first, by Maccaferri and Dingledine (2002) showed that synaptically-evoked post-synaptic firing of putative CCK+ GABAergic cells strongly relies on the NMDAR activation. On the contrary, in PV+ cells the glutamatergic synaptic activation of NMDARs has turned out to be less essential for spike generation (Maccaferri and Dingledine, 2002). In addition, in a more recent study by Matta and colleagues (2013) it was demonstrated that glutamatergic synapses on the CCK+ GABAergic cells display more prominent NMDAR component than PV+ cells (Matta et al., 2013). In agreement with the later study, experiments in my host laboratory have reported that CCK+ interneurons in wild-type mice have about 3.5 - fold higher N/A (NMDAR/AMPAR EPSC amplitude ratio) in the hippocampal CA3 area compared to PV+ cells (unpublished lab observation and experiments in Chapter 4). Therefore, I suggest that NMDAR receptor hypofunction as seen in NRG1 over-expressing mice has a greater impact for the input-output function of the CCK+ cells than the PV+ cells and that the reduced NMDAR-driven disynaptic inhibition observed in the NRG1 mice here, is likely to emerge predominantly from the dysfunction of the CCK+ GABAergic cells.

Our understanding on the generation of gamma oscillations is incomplete, and investigation of the effects of cell type-specific changes on brain oscillations, and their behavioural readouts is still at the early stages. It is still poorly known how specific cellular-level changes, observed in various animal models, actually are linked with the observed symptoms and altered oscillations. An important aspect to stress again is that their possible correlation with “disease symptoms” does not indicate causal relation. In fact, some cellular-level alterations in disease animal models may actually be epiphenomena meaning that the

observed alterations are not really causing the symptoms, but they rather emerge as a more or less harmless side effect. In addition, some observed cellular-level changes may sometimes be caused by homeostatic regulation in the organism, which means the changes observed in cell function are part of a compensation mechanism developing in the organism. Thus, at this stage of research progress with the NRG1 over-expressing mice, I can only speculate how a deficit of the NMDARs in the two major inhibitory neuron populations (expressing either PV or CCK) accounts for the alterations in the cholinergically-driven hippocampal gamma oscillations.

In general, reduced gamma oscillation frequency in the cholinergic model is indicative of altered IPSCs kinetics, in particular of their decay constants in PCs. Such a change in the IPSC kinetics could emerge from reduced excitatory drive on to interneurons and compromise the temporal accuracy in the PC-IN-PC loop as reported in the present study (Fisahn et al., 1998, Oren et al., 2010). Given that, in the $NRG1^{tg\text{-}type\text{-}I}$ transgenic mice, the NMDAR hypofunction occurs both in PV+ and in CCK+ interneurons, it's important to understand how an altered input/output function of these cell populations could explain the alterations reported previously in the cholinergic gamma frequency oscillation (Deakin et al., 2012). Concerning PV+ interneurons, the effects of NMDAR hypofunction in connection to gamma rhythmogenesis have been studied in transgenic mouse lines lacking the NR1 subunit, which is the compulsory subunit for the functional NMDAR complex assembly (Moriyoshi et al., 1991, Monyer et al., 1992). Recordings of gamma oscillations in these mice showed that the PV+ cell type-specific NMDAR ablation lead to enhanced *in vivo* gamma oscillations (frequency and amplitude), despite the fact that the induction and modulation by theta band activity was impaired (Korotkova et al., 2010, Carlen et al., 2012). Although, NMDAR receptor hypofunction in PV+ cells can manifest differently in *in vivo* compared to *in vitro* conditions, these results raise the intriguing possibility that the decline in the gamma rhythm frequency observed in the $NRG1^{tg\text{-}typeI}$ mice (Deakin et al.,

2012) could stem to a great extend from NMDAR receptor hypofunction in CCK+ cells rather than PV+ cells. Two specific features of these cells could to some extent provide a connection between the NMDAR hypofunction and the altered gamma rhythomgenesis in the NRG1 over-expressing animals. As I already mentioned, compared to PV+ cells, the hippocampal CCK+ interneuron activation more heavily relies on post-synaptic NMDARs, hence NMDAR hypofunction in CCK+ cells can severely weaken their afferent excitatory input. Consequently, this can lead to less reliable GABAergic output from their synapses. Moreover, CCK cells which provide long lasting inhibition to their post-synaptic targets via the asynchronous fashion of neurotransmitter (Glickfeld and Scanziani, 2006, Daw et al., 2009) are targets of cannabinoids neuromodulation since they express CB_1R receptors in the GABAergic terminals. Hence, they are subject to depolarization induced suppression of inhibition (DSI) following the release of endocannabinoids from the local pyramidal cells (Pitler and Alger, 1992, 1994, Wilson and Nicoll, 2001) during gamma band oscillations (Fukudome et al., 2004, Neu et al., 2007). Thus, when, gamma oscillations arise, the endocannabinoid system can regulate the pyramidal cells discharge by suppressing synaptic inhibition to those cells which are prominently active "participating" whilst maintaining long lasting inhibition to the ones that are not "non-participating" at a given gamma cycle. This relief of inhibition specifically to the pyramidal cells that are active during gamma band oscillations may further increase their synchronization via the time precise excitation of the local interneurons that project back to them (Oren et al., 2006, Oren et al., 2010). Therefore, I suggest that, disrupted excitatory drive of CCK+ GABAergic cells due to NMDARs hypofunction could hamper this modulatory process of the regulation of the activity of pyramidal cells during gamma oscillation. Given that the PCs and local INs are mutually connected, this may lead to reduced temporal fidelity of the excitatory inputs from

pyramidal cells onto the interneurons, including PV+ cells, that are the main gamma rhytmogenetic cell population (PV+ basket cells) (Oren et al., 2006).

Furthermore, it has been reported that release of CCK from neurons can directly enhance the synchrony of PV+ cells firing, because CCK is depolarizing them through CCK-B receptors (Foldy et al., 2007). Hence, reduced activity of the CCK+ cell population and CCK release can further have an impact on the co-ordinated firing of PV cells during gamma oscillations.
Interestingly, it has been shown that during cholinergic gamma oscillation in $NRG1^{tg\text{-}type\text{-}I}$ mice slices, individual pyramidal cells' firing occurred over more oscillatory cycles than in their littermate controls (Nissen, 2012). In addition, their afferent synaptic excitatory input was temporally more variable and larger and in turn, the IPSCs they received, displayed longer decay times. These changes in local CA1 PCs are well correlated with reduced LFP gamma band frequency (Fisahn et al., 1998) which has also been observed NRG1 mutants (Deakin et al., 2012)

These results are in line with the scenario where CCK+ GABAergic cells are not efficiently recruited due to their high sensitivity to NMDARs hypofunction, and this in turn causes inefficient inhibition of the PCs, their confound firing and finally, temporally imprecise excitatory output from them back to the rhythmogenetic interneurons.

In conclusion my experiments in this chapter on optogenetically- driven recurrent inhibition show that NMDARs on hippocampal interneurons contribute to the GABAergic feed-back inhibition loop during 20 Hz glutamatergic fibers discharge, and their contribution is reduced in the $NRG1^{tg\text{-}type\text{-}I}$ mice. This reduction can emerge at least partially, from NMDAR hypofunction in CCK+ GABAergic cells given their high dependence on NMDARs for their excitation and can explain gamma band oscillation alterations seen in these mice.

6.4 Perspective and future directions

Glutamate NMDA receptors in interneurons contribute to GABAergic feed-back inhibition in the hippocampus. Their contribution is reduced in the $NRG1^{tg\text{-}type\text{-}I}$ mice. Importantly, the effect is prominent during discharge of glutamatergic fibres at 20 Hz frequency, which indicates that the results can have implications in the hippocampal generation of gamma frequency oscillation.

The previously reported findings that NMDAR-mediated excitation is prominent in CCK+ GABAergic cells, but relatively modest in PV+ neurons opens the possibility that the alterations in NMDAR-mediated network inhibition are for the most part mediated through the CCK+ cells. The CCK+ GABAergic cells and PV+ interneurons are the major target population for direct signalling of NRG1 since unlike most other neurons they express ErbB4 receptor. However, to gain more accurate insight into this, recordings in transgenic mouse lines replicating the NMDAR hypofunction in specific cell types are warranted. This could probably be already performed by taking advantage of the recently developed site-specific recombinase technology to ablate NMDAR complexes in specific neuron subpopulations. Such experimental approaches could also reveal any potential changes in other network oscillations than gamma, such as hippocampal theta activity or Sharp-Wave ripple complexes, in which local GABAergic inhibition is essential (Klausberger and Somogyi, 2008).

7 General Discussion

7.1 Summary of main findings

The aim of this study was to investigate effects of NRG1 over-expression on synaptic transmission of specific GABAergic inhibitory interneurons in the adult hippocampus. The results have wider importance in neuropathological processes in the brain, since various studies have reported that increased NRG1 levels and particularly of the NRG1 type I isoform in the brain, are associated with increased susceptibility for schizophrenia. To identify the specific cellular targets of the NRG1 signalling, immunocytochemical analyses were performed demonstrating that the main receptor for NRG1, ErbB4, is expressed in two major populations of hippocampal interneurons expressing either the neuromarker PV or CCK. Considering that the NRG1-ErBb4 signalling pathway has pleotropic roles in the brain, for instance by controlling neuronal migration, axonal growth and synapse formation, I first aimed to specifically examine whether NRG1 type I over-expression could affect the cytoarchitecture of interneurons in the hippocampal formation. The analysis showed that the density of immunohistochemically-detected ErbB4-expressing cells is reduced in the $NRG1^{tg\text{-}type\text{-}I}$ mutants, without a detectable effect on the density of PV+ cells. Hence, the results suggest that other ErbB4+ GABAergic interneurons than those expressing PV may be strongly altered during neurodevelopmental processes by the genomically changed NRG1 type I levels. Next, to reveal whether NRG1 type I over-expression interferes with the inhibitory and excitatory neurotransmitter systems, I performed analysis of AMPAR, NMDAR and GABAAR-mediated synaptic neurotransmission focusing on the CCK+ interneuron population that strongly expresses the ErBb4 receptor. Data from looking at the glutamatergic neurotransmission suggest that genomic NRG1 over-expression leads to NMDAR hypofunction in these cells, leaving the AMPAR-mediated neurotransmission unaffected. Furthermore, the investigation of the GABAergic synaptic

transmission provided by these cells revealed no changes between the NRG1$^{tg\text{-}type\text{-}I}$ mutant mice and the wild-type littermate controls. These observations together with previous experimental work in the lab that have demonstrated selective loss of function of the NMDAR-mediated currents in PV-positive basket cells as well as deficits in lower gamma range rhythmic network oscillations in the hippocampus (Nissen, 2012), raised the question whether this NMDAR hypofunction in hippocampal interneurons could be partly responsible for the altered rhythmic network activities observed in these mice. Notably, I found that disynaptic GABAergic inhibition, which is the key mechanism for generation of gamma-frequency oscillatory network activity, depends on the functionality of NMDAR receptors. In the current experimental conditions, the NRG1 over-expressing mice displayed reduced contribution of NMDAR-mediated excitation to the interneurons participating to the disynaptic inhibition loop. Therefore, I suggest that the altered hippocampal disynaptic inhibition microcircuit could lead to a less efficient recruitment of GABAergic interneurons during the hippocampal network activities, which in turn could contribute to the alterations previously observed in the gamma-range rhythmic oscillatory network activities in these mice. Consistent with the previously reported pleiotropic effects of NRG1 on the development of neurons, the above findings emphasize the role of the NRG1 type I in development of the synaptic architecture in brain networks.

7.2 ErbB4 receptor expression in the hippocampal interneurons and the altered ErBb4+ cell density in the NRG1tg-type-I mice

The experiments presented in chapter 3 demonstrated that two functionally diverse hippocampal interneuron populations expressing either PV or CCK, are both strongly ErbB4 immunoreactive. This finding, which is in line with some previous studies on the cellular localization of the ErBb4 receptor (Neddens and Buonanno, 2010), indicates that these

GABAergic hippocampal microcircuitries are under the modulatory effects of the NRG1 signalling pathway. However, it should be noted, that these neuromarkers are also expressed in other hippocampal interneurons than the two major subpopulations studied here. In addition, the analysis used here is not capable of identifying anatomically specialised PV+ or CCK+ interneuron types. Yet, as it is clearly shown in Figures 3-2 and 3-3, the ErbB4 immunoreactive somata and its co-expression with either PV or CCK is widespread across all hippocampal laminae, arguing that the receptor is most likely expressed in many, if not all, the different cell types in these two subpopulations. The reduction of the detected ErbB4 immunoreactive somata in the hippocampus of $NRG1^{tg\text{-}type\text{-}I}$ mice can be attributed to two different biological phenomena, which are not mutually exclusive. Consistent with the previously reported effects of the NRG1-ErBb4 signalling pathway on the migratory processes during early neurodevelopment, it is possible that the lower density of ErBb4+ somata in the NRG1 over-expressing mice could reflect a disturbance in the migratory stream or survival of these interneurons. Indeed, it has been previously shown that the number of GABAergic interneurons, including PV expressing cells, in $ErbB4^{-/-}$ mice is significantly declined (Neddens and Buonanno, 2010). In the same vein, reduced numbers of PV expressing cells in the neocortex have been reported in a mouse line that exhibits increased levels of the non- soluble form of NRG1 (CRD-NRG1) (Agarwal et al., 2014). However, the density of PV + hippocampal interneurons is basically unaltered in the NRG1 mutant mice of this study. This discrepancy is likely to reflect the fact that diverse NRG1-ErBb4 truncations could lead to slightly different effects on their target cell types. Interestingly, the observation of the lower number of ErBb4+ cells in the hippocampus of $NRG1^{tg\text{-}type\text{-}I}$ animals is consistent with the reports of impaired neurogenesis and cell proliferation of hippocampal neurons in the brain of patients diagnosed with schizophrenia (Barbeau et al., 1995, Reif et al., 2006, Allen et al., 2016). Another possibility to explain the reduced number of ErbB4 immunopositive cells is that the NRG1 type I over-

expression could lead to decreased levels of the ErbB4 receptor in ErbB4+ cells, through the increased endocytosis of the receptor in response to NRG1 upregulation (Longart et al., 2007). This latter finding raises the possibility that the ErbB4 receptor could be indeed internalised in the hippocampus of NRG1$^{tg\text{-}type\text{-}I}$ leading to reduced immunofluorescence signal bellow the detection level, resulting to the lower ErbB4+ cell number counts in the slices from the NRG1$^{tg\text{-}type\text{-}I}$ animals. Given that the percentage of PV+ cells that co-express the ErBb4 receptor is very similar in the two genotypes, this suggests that speculated endocytocis of the ErBb4 receptor should be far less prominent in PV+ cells than in PV- interneurons such as the CCK + and for instance nNOS-positive cells. Whatever is the reason for this reduction of detected ErbB4 cell somata, it is conceivable that this change could also lead to NRG1-ErBb4 signalling-dependent alterations in the network functionality. In the case that this lower density of ErBb4-positive cells reflects a decreased number of the GABAergic interneurons, particularly those expressing nNOS or CCK with prominent ErBb4 immunoreactivity (Neddens and Buonanno, 2010), this could cause deficits in the cortical excitation-inhibition balance and result consequently in alterations in the information processing and network operations depending on these circuits. Both the CCK+ and the nNOS+ GABAergic cells display phase locked action potential discharge with common hippocampal network oscillations such as theta, SWRs and gamma associated with information processing (Tukker et al., 2007, Fuentealba et al., 2008, Lasztoczi et al., 2011). Thus, it follows that their reduced cell density would inevitably affect information processing in the hippocampus and give rise to alterations in the oscillatory activities in the NRG1$^{tg\text{-}type\text{-}I}$ mice. Alternatively, the possible increased levels of ErBb4 internalization could interfere with the NRG1-ErbB4 signalling as it has been discussed in detail in the introductory chapter (see section 1.1) This would very likely also affect the function of hippocampal synaptic circuits and the generation of the network oscillations. Given the pleotropic roles of the NRG1 signalling in the brain, the two above scenarios can be two different manifestations of a common pathogenetic

mechanism, affecting the neurodevelopment of several GABAergic interneuron populations including their synaptic function within the brain networks. However, further work needs to be performed in order to investigate these hypotheses. A future immunocytochemical study could shed light on whether the numbers of several interneuron populations expressing specific neuromarkers, are compromised in the NRG1 over-expressing mice. In addition, a biochemical analyses such as the biotylination of cell surface proteins assay could reveal the rates of ErbB4 internalization. Given that both the hyper- and the hypo-signalling of NRG1 produce changes in the behavioural and the neurophysiological level, it has been proposed that the effects of NRG1 signalling follow an inverted U shape mode of action. This means that the two opposite directions of altering levels of NRG1 could affect functionality of the brain networks in a similar way (Agarwal et al., 2014). The exact molecular mechanisms of the inverted U shape mode of action are currently unknown. Therefore, exploring the rates of ErbB4 internalization in regards to NRG1 expression could reveal whether the NRG1-ErBb4 hypo- and hypersignalling are two distinct pathogenetic mechanisms that could produce similar neurophysiological effects or these bidirectional truncations could converge to a common pathogenetic pathway due to ErBb4 loss of function instead.

7.3 Excitatory input and inhibitory output of CCK+ in the hippocampus of NRG1$^{tg\text{-}type\text{-}I}$ mice and alterations in the disynaptic inhibition loop

In chapter 4 the glutamatergic synaptic input to CCK cells in the NRG1$^{tg\text{-}type\text{-}I}$ mice was explored. I found that both the NMDAR/AMPAR-mediated synaptic current ratio and the NMDAR-mediated quantal currents were reduced in the NRG1 over-expressing mice. In line with these findings, similar NMDAR hypofunction has also been reported in PV expressing

basket cells in the same area of the NRG1 mutant mice (Nissen, 2012). Interestingly, a recent study has reported hypofunction of NMDAR receptors specifically in ErBb4 immunopositive hippocampal interneurons following an exposure of the tissue to NRG2 peptide, which similar to the NRG1, signals via the ErbB4 receptor (Vullhorst et al., 2015). Synaptic excitation of CCK+ cells depends to a greater extent on the NMDAR activation, than the excitation of the PV+ ones (Maccaferri and Dingledine, 2002, Matta et al., 2013). Hence, the observed changes in slices from $NRG1^{tg\text{-}type\text{-}I}$ mice concerning the dependence of disynaptic inhibition on NMDAR-mediated synaptic excitation, could primarily stem from the impaired NMDAR-mediated signalling in CCK+ GABAergic interneurons (chapter 6). Importantly, this sequence of synaptic events is essential for the generation of gamma frequency oscillations (see PING model in sections 1.3.1.5 and 6.1) (Traub et al., 1997, Whittington et al., 2000). Therefore, it is tempting to speculate that during gamma band activity, the synaptic recruitment of CCK+ GABAergic cells could be less efficient and reliable due to NMDAR hypofunction in the NRG1 mutant mice. Since, it has been suggested that during gamma frequency network activity, CCK+ GABAergic cells could set a threshold for the spiking of pyramidal cells (Tukker et al., 2007) hence contributing to the formation of cell assemblies during the oscillatory activity, it is possible that the weakened recruitment of the CCK+ GABAergic cells during repeated cycles of disynaptic inhibition would ultimately lead to confound firing of the pyramidal cells and less temporally precise timing of the synaptic excitatory inputs to the GABAergic cells, including PV+ basket cells which are the key moderators for the generation and maintenance of the hippocampal network gamma activity (Cardin et al., 2009).

Results from the analysis of *in vitro* -generated gamma oscillation in slices from the $NRG1^{tg\text{-}type\text{-}I}$ mice have shown that the oscillation frequency is significantly compromised in these mice, whereas the firing of the pyramidal cells tends to be less accurate, and the decay

times of IPSC were found to be prolonged. (Deakin et al., 2012). These observations together with the finding that the GABAergic synaptic outputs from both the PV+ (Nissen, 2012) and the CCK+ (chapter 5) cells, remain unaffected in the NRG1 mutant mice, support the hypothesis on the compromised firing precision presented above. It follows that the NMDAR hypofunction in the CCK+ GABAergic cells could be a pathogenic mechanism giving rise to aberrant network activities, such as the altered gamma oscillations described earlier in these mice, and underlie some of the deficits of higher brain functions that have also been reported. As discussed in detail in the introductory chapter (section 1.1.2.1), the effects of NRG1 signalling on glutamatergic transmission are diverse and partially contradictory. Those discrepancies could be attributed to distinct experimental paradigms employed, such as differences in the NRG1 peptide used, genomic *versus* acute modulation of NRG1 levels, and differences in brain areas and cell types investigated in these studies. From a mechanistic point of view, the NRG1-ErBb4 signalling can modulate the trafficking and the expression of NMDARs subunits (Ozaki et al., 2004, Gu et al., 2005) as well as regulate their phosphorylation status (Hahn et al., 2006, Bjarnadottir et al., 2007, Pitcher et al., 2011). Given that both the ErBb4 receptor and the NMDARs physically interact with post-synaptic density protein 95 (PSD-95) at the post-synaptic density (PSD) (Garcia et al., 2000, Huang et al., 2000, Kim and Sheng, 2004), it is possible that disturbances in this signalling pathway could destabilize the receptor assembly in the PSD. Interestingly, it has been shown that changes of the phosphorylation status of NMDAR subunits control the expression and the endocytocis of specific NMDAR subunits, especially of GluN2A and B (Prybylowski et al., 2005, Nakazawa et al., 2006). In addition, it was recently demonstrated that the treatment of hippocampal neuron cultures with NRG2 peptide facilitates physical interaction of the ErBb4 receptor with the GluN2B subunit, and that this interaction leads to the subunit internalization causing NMDAR-mediated current downregulation in ErBb4+ interneurons (Vullhorst et al., 2015). Yet, it is unknown whether the observed NMDAR hypofunction in CCK+ GABAergic

cells in the NRG1$^{tg\text{-}type\text{-}I}$ mice is mediated through changes in the expression level of specific NMDAR subunits like GluN2B or for instance via changes in their phosphorylation states in the PSD.

7.4 NRG1 signalling and its putative relevance for the pathophysiology of schizophrenia

The findings described above, as well as the previous results on aberrant gamma oscillations and cognitive deficits described in the NRG1$^{tg\text{-}type\text{-}I}$ mutant mice (Deakin et al., 2009, Deakin et al., 2012) argue that NRG1 over-expression produces alterations in the basic synaptic function, which might partly explain the reported changes in the co-ordinated activity at neuronal networks level. It is tempting to speculate that these high-order changes have their roots in the disturbed neurodevelopment observed also as down-regulation of the NMDAR-mediated transmission in ErBb4+ GABAergic neurons. Over a decade ago, the first report of an association of NRG1 signalling with schizophrenia (risk haplotype HapICE) (Stefansson et al., 2002) was published. Now this finding has been chiefly supported by a report showing increased levels of the NRG1 peptide in the brain of schizophrenia patients (Weickert et al., 2012). Up to now, a number of animal studies have tried to phenocopy dysregulations of NRG1-ErBb4 signalling pathway, and many of these have shown that altered NRG1 signalling produces specific endophenotypes (this topic is reviewed in detail in section 1.2.2) akin to those implicated in cognitive symptoms associated with schizophrenia; deficits in brain networks synchronicity, altered paired-pulse inhibition (PPI) response to sensory stimuli, and changes in glutamatergic and GABAergic neurotransmission. The results argue for relevance of these animals models as a tool to understand neuropathophysiology of this neuropsychiatric disorder.

The exact cause or causes of the emergence of schizophrenia are still largely unclear, but there is growing evidence that its pathogenesis is a multifactorial process with multiple genetic and environmental risk factors acting synergistically (Desbonnet et al., 2009). Apart from the complex genetic background of the disorder, and the multiple environmental interactions considered relevant for the development of the disease, there are specific factors in the animal models that need to be taken into consideration for interpretation of the results. Specifically for the $NRG1^{tg\text{-}type\text{-}I}$ mutant mouse line, the magnitude of the NRG1 type I level is clearly higher than what has been reported in human schizophrenia patients' brain post mortem studies. It is also unknown, whether its over-expression starts at similar or corresponding neurodevelopmental stages of the human and the mice ontogeny. Thus for many transgenic lines, including the one used in this study, it is unclear what is the extent to which the phenotypic manifestations originate from the pathophysiological traits observed in the animals. Moreover, although this study focus on cognitive symptoms associated with the disease, a large part of schizophrenia symptomatology such as positive symptoms cannot be assessed with current animal models. These general considerations highlight that genetic mouse models, currently used in order to conceptualise psychiatric disorders even when, as in this thesis, approximate genetic alternations identified in diseased humans, fail to recapitulate the full entity of a complex and multifactorial disease phenotype. Therefore, the research outcomes like the ones described here should be interpreted with caution, keeping in mind that the specific endophenotype is only dependent on the effects of a single gene (Walters and Owen, 2007). Even so, the single gene mutation studies can still be highly useful when they affect relevant developmentally regulated biochemical and molecular signalling pathways, and produce endophenotypes akin to those observed in the complex full disease phenotype. The relevance of the specific synaptic dysfunctions reported here for schizophrenia pathogenesis, remains to be further determined. Nonetheless the present results, could help to refine the hypothesized interaction between

specific components of the hippocampal neuronal networks and NRG1 signalling that originally framed the major aims of this thesis (Figure 1-3).

A pathogenetic mechanism that gives rise to schizophrenia traits could include disturbances in the density of ErbB4+ immunoreactive interneurons, or alterations in the receptor expression in these cells, both of which are likely to have severe consequences in the cortical information processing mediated by these GABAergic neuron subpopulations. An additional putative pathogenic mechanism is the downregulation of the synaptic NMDAR-mediated neurotransmission in ErbB4 expressing GABAergic cells, including the CCK+ cells. In turn, alterations of the disynaptic inhibition loop function can explain changes in the neuronal network co-ordinated activities including gamma oscillations previously reported in these mice. Importantly, aberrant cortical gamma oscillations are often associated with cognitive disorders in the disease. If similar NMDAR hypofunction in GABAergic cells further occurs beyond the cortex in subcortical areas, this could affect the regulation of the dopaminergic system which is the predominant cause underlying the positive and the negative symptoms of the disease (Figure 7-1).

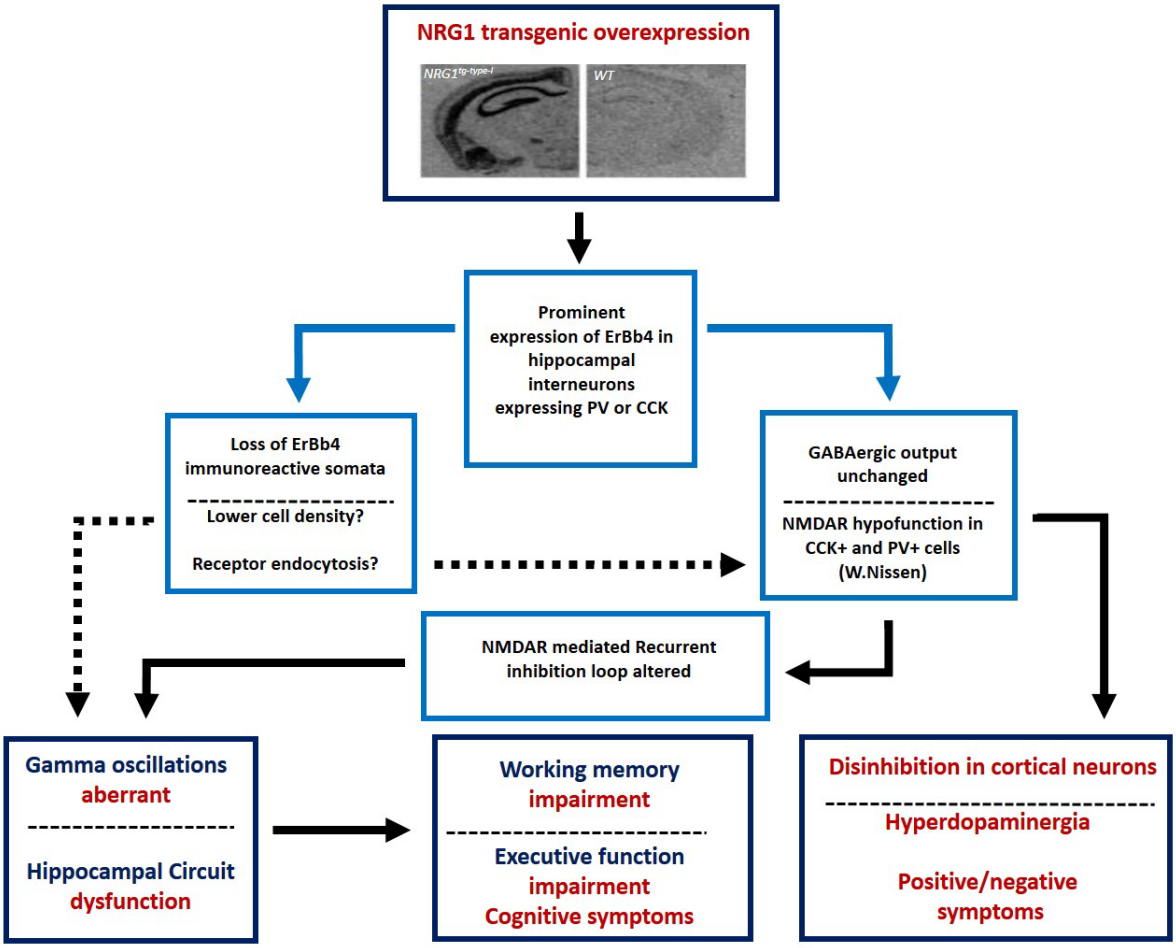

Figure 7-1 A simplified schematic showing the main discoveries in this thesis. A hypothesised interaction between the effects of NRG1 and the function of cortical neuronal networks can provide a schizophrenia pathogenic mechanism. In the mutant mouse model mimicking the increased NRG1 levels of human schizophrenia patients, the NRG1 over-expression is widely observed in various brain regions including the hippocampus. Upper panel: *In situ* hybridization for NRG1 type 1 mRNA in the NRG1$^{tg\text{-}type\text{-}1}$ mice (left) and the WT littermate mice brain (right) (Deakin et al., 2009). Immunocytochemical analysis reveals strong expression of the ErbB4 receptor in interneurons expressing ether PV+ or CCK+. The NRG1 over-expression leads to NMDAR hypofunction in interneurons expressing CCK or PV, but no detected changes in their GABAergic output. In addition, there is significant loss of ErbB4 immunoreactive somata in the NRG1$^{tg\text{-}type\text{-}1}$ mice hippocampus, either suggesting lower ErbB4+ cell density in these animals or an increased rate of the receptor endocytocis. The reduced number of hippocampal ErbB4+ neurons can directly interfere with the cortical network function including hippocampal gamma oscillations (vertical dotted arrow). On the other hand, the ErbB4 receptor endocytosis can interfere with synaptic NMDAR receptors and explain the reported NMDAR hypofunction in the GABAergic cells (horizontal dotted arrow). The NMDAR hypofunction in the hippocampal GABAergic interneurons leads to alterations in disynaptic inhibition microcircuit, offering an explanation to the observed alterations in the hippocampal gamma oscillation in these mice. Altered gamma oscillogenesis is commonly associated with observed decline in higher brain functions such as working memory and executive function, both of which are features of the cognitive symptomatology in schizophrenia. NMDAR hypofunction could also be involved in subcortical disinhibition and hypodopaminergia underlying the schizophrenia negative and the positive symptoms.
Dark blue: Multilevel neurophysiological interactions that participate in the neural network operations and the cognitive processes. Red: A possible, pathogenetic cascade resulting in a range of schizophrenia-associated features. Light blue: Rational flow and research outcomes of this thesis.

7.5 Future and translational perspective

The microcircuit level effects of genomic NRG1 type I over-expression in the brain are still not well described and further work will be needed to get a better understanding of them. In particular, future research on this topic needs to address the following specific points:

1) To clarify whether the differences observed here in the density of ErbB4+ immunoreactive somata in the hippocampus are due to the receptors' endocytosis in response to the NRG1 hypersignalling, or if they reflect genuinely reduced interneuron numbers caused by alterations in the migratory route and the proliferation of hippocampal GABAergic neurons. The study could be performed by immunocytochemical tests for specific neurochemical markers characterising various distinct GABAergic cells. In addition, a cell surface protein biotylination biochemical approach could reveal whether the rates of the ErbB4 endocytosis differ between WT and the $NRG1^{tg\text{-}type\text{-}I}$ mice.

2) Using anatomical analyses to characterise the neurons types that display altered glutamatergic input at the level of NMDAR receptor. Even though it has been previously shown that several CCK+ hippocampal cells in general exhibit similar NMDAR-mediated component of glutamatergic transmission, it is possible that differences between structurally specialised cell types exist. The analysis will shed light on maladaptive alterations in specific type of inhibitory connections caused by NRG1 signalling disturbances.

3) To explore whether the NMDAR hypofunction emerges from changes in the expression and trafficking of the receptors subunits, or are caused by alterations of their phosphorylation status. This can be performed by whole-cell recordings of the NMDAR currents in brain slices using specific subunit blockers whereas western blot analysis could reveal the subunit phosphorylation status.

4) To determine the activity of hippocampal neurons in the NRG1 over-expressing animals, during distinct rhythmic activities in the hippocampus. Ideally this could be done using juxtacellular recordings of the spiking of single cells and their subsequent labelling and anatomical identification. This could reveal if and how the co-ordinated activity of specific neuron types in the hippocampal network is altered in the mutant mice.

Answers to these questions would expand our understanding of the specific behavioural and neurobiological changes associated with chronic NRG1 signalling enhancement and point out the potential clinical benefit of the use of agents that could normalize the awry consequences of the dysfunction of this pathway.

Towards that direction, initial studies have shown promising results by the administration of agents that interfere with the NRG1 downstream signal transduction by reversing several neurobehavorial traits in transgenic mice expressing NRG1 (Yin et al., 2014, Papaleo et al., 2016). Furthermore this work may help pave the way in designing methodologies of pharmacological intervention targeting schizophrenia. One direction would be the development and the subsequent clinical testing of agents that could enhance NMDA receptor mediated neurotransmission in CCK+ or/and other hippocampal interneurons reported with compromised receptor function in Schizophrenia. The main objective of such drug discovery programs would be the design of compounds restoring or ameliorating the functionality of NMDARs in a cell type specific manner. Both electrophysiological and in situ hybridization experiments have suggested that in the hippocampus pyramidal cells express NMDA receptors with higher participation of GluN2A and GluN2B subunits compared to interneurons that more prominently express GluN2C and GluN2D subunits instead (Monyer et al., 1994, Martina et al., 2003). Importantly similar overrepresentation of GluN2 subunits has recently been demonstrated specifically in hippocampal CCK+ interneurons (Martina et al., 2013). This distinctive nature of

the receptors' subunit arrangement could serve as a starting point in the chemical design of therapeutic compounds able to target and potentiate NMDARs in a cell type specific way. A promising category of agents that are likely to fulfil this objective are the positive modulators of the allosteric site of NMDA receptors (PAMs). Firstly, this type of modulators' action on ionotropic receptors is characterized by high receptor sub-type specificity, due to the less conserved homology across the allosteric binding sites of distinct receptors subunits. Secondly, their mode of action depends on the presence of the endogenous neurotransmitter at the synapse, therefore ensuring the receptors activation during the physiological relevant spatio-temporal synapse activation (Christopoulos, 2002). So far amongst several allosteric NMDA receptor modulators; the substituted tetrahydroisoquinoline CIQ (3-chlorophenyl) (6,7-dimethoxy-1-((4-methoxyphenoxy)methyl)-3,4-dihydroisoquinolin-2(1 H)-yl)methanone, has been shown to have good selectivity for GluN2C/2D containing receptors (Mullasseril et al., 2010) and is the only compound that its putative therapeutic effects have been so far studied in a schizophrenia like phenotype. Interestingly, it was shown that CIQ can reverse some key schizophrenia- like phenotypic traits such as prepulse inhibition of the startle reflex (PPI) deficit and working memory impairment in mice treated with the NMDAR antagonist MK-801 (Suryavanshi et al., 2014). Thus, these initial findings together with the data presented in this work, highlight the potential benefit of developing novel therapeutic strategies focusing on specific subclasses of NMDAR receptors, that are compromised in distinct classes of neurons such as CCK+ interneurons.

Up to now treatment of mental disorders heavily relies in the advancement of chemical compounds, however the recent molecular tools advents provide an unprecedented opportunity towards a more "personalized" approach that tackles the pathopsysiological heterogeneity of the disease. In that respect, the findings of this study highlight the potential therapeutic benefits of

the successful generation of human induced pluripotent stem cells (IPSCs) derived from patients to CCK+ interneurons. Given the possibility that neurotransmission systems are dysfunctional in CCK+ cells, it would be possible to monitor the disease physiology in particular patient cells, design and screen new drug therapies tailored to the genetic makeover of an individual. Furthermore, generation of specific interneurons population derived from schizophrenia patients, should also advance our understanding of how disease pathology progresses and the possible common disease pathways of this multifactorial disorder.

In addition, progress to cell based therapies, such as transplantation of stem cells derived specific interneuron types open new possibilities for the disease treatment (Watanabe et al., 2005, Alvarez-Dolado et al., 2006). The data presented here also suggest that NRG1 over-expression in mice induce loss of ErbB4 immunopositive interneurons that could be attributed to perturbation in proliferation and or survival of distinct GABAergic cell subtypes. Based on this, a cell-based therapy whereby stem cell-derived interneurons are transplanted in patients is a plausible therapeutic approach.

7.6 Final conclusion

In conclusion, the results of this thesis together with previously published findings (Deakin et al., 2012, Nissen, 2012) suggest that chronic increase of the NRG1 type I levels in the brain has specific effects on ErbB4+ GABAergic inhibitory interneurons in the hippocampus. Given that enhanced NRG1 type I expression has been observed in human schizophrenia patients, it is possible that the biological events seen in these mouse mutants can in part mirror what happens in human disease.

Taking into consideration that the approximation of the NRG1 genomic over-expression to a clinical phenotype remains to be validated, these preclinical findings could assist in the future design of therapeutic schemes. Targeting the NMDARs on specific GABAergic cell populations could be further explored with a potential therapeutic value especially regarding cognitive symptoms of the disease, against which most current clinical treatments are ineffective.

References

Abe Y, Namba H, Kato T, Iwakura Y, Nawa H (2011) Neuregulin-1 signals from the periphery regulate AMPA receptor sensitivity and expression in GABAergic interneurons in developing neocortex. *J Neurosci,* 31:5699-5709.

Acsady L, Arabadzisz D, Freund TF (1996) Correlated morphological and neurochemical features identify different subsets of vasoactive intestinal polypeptide-immunoreactive interneurons in rat hippocampus. *Neuroscience* 73:299-315.

Agarwal A, Zhang M, Trembak-Duff I, Unterbarnscheidt T, Radyushkin K, Dibaj P, Martins de Souza D, Boretius S, Brzozka MM, Steffens H, Berning S, Teng Z, Gummert MN, Tantra M, Guest PC, Willig KI, Frahm J, Hell SW, Bahn S, Rossner MJ, Nave KA, Ehrenreich H, Zhang W, Schwab MH (2014) Dysregulated expression of neuregulin-1 by cortical pyramidal neurons disrupts synaptic plasticity. *Cell Rep,* 8:1130-1145.

Ali AB (2011) CB1 modulation of temporally distinct synaptic facilitation among local circuit interneurons mediated by N-type calcium channels in CA1. *J Neurophysiol,* 105:1051-1062.

Ali AB, Todorova M (2010) Asynchronous release of GABA via tonic cannabinoid receptor activation at identified interneuron synapses in rat CA1. *Eur J Neurosci*, 31:1196-1207.

Allen KM, Fung SJ, Weickert CS (2016) Cell proliferation is reduced in the hippocampus in schizophrenia. *Aust N Z J Psychiatry,* 50:473-480.

Alvarez-Dolado M, Calcagnotto ME, Karkar KM, Southwell DG, Jones-Davis DM,Estrada RC, Rubenstein JL, Alvarez-Buylla A, Baraban SC (2006) Cortical inhibition modified by embryonic neural precursors grafted into the postnatal brain. *J Neurosci*, 26: 7380-7389.

Amaral DG (1993) Emerging principles of intrinsic hippocampal organization. *Curr Opin Neurobiol,* 3:225-229.

Amaral DG, Witter MP (1989) The three-dimensional organization of the hippocampal formation: a review of anatomical data. *Neuroscience,* 31:571-591.

Armstrong C, Krook-Magnuson E, Soltesz I (2012) Neurogliaform and Ivy Cells: A Major Family of nNOS Expressing GABAergic Neurons. *Front Neural Circuits,* 6:23.

Armstrong C, Soltesz I (2012) Basket cell dichotomy in microcircuit function. *J Physiol,* 590:683-694.

Armstrong N, Gouaux E (2000) Mechanisms for activation and antagonism of an AMPA-sensitive glutamate receptor: crystal structures of the GluR2 ligand binding core. *Neuron,* 28:165-181.

Armstrong N, Mayer M, Gouaux E (2003) Tuning activation of the AMPA-sensitive GluR2 ion channel by genetic adjustment of agonist-induced conformational changes. *Proc Natl Acad Sci U S A,* 100:5736-5741.

Ascoli GA, Alonso-Nanclares L, Anderson SA, Barrionuevo G, Benavides-Piccione R, Burkhalter A, Buzsaki G, Cauli B, Defelipe J, Fairen A, Feldmeyer D, Fishell G, Fregnac Y, Freund TF, Gardner D, Gardner EP, Goldberg JH, Helmstaedter M, Hestrin S, Karube F, Kisvarday ZF, Lambolez B, Lewis DA, Marin O, Markram H, Munoz A, Packer A, Petersen CC, Rockland KS, Rossier J, Rudy B, Somogyi P, Staiger JF, Tamas G, Thomson AM, Toledo-Rodriguez M, Wang Y, West DC, Yuste R (2008) Petilla terminology: nomenclature of features of GABAergic interneurons of the cerebral cortex. *Nat Rev Neurosci,* 9:557-568.

Atluri PP, Regehr WG (1996) Determinants of the time course of facilitation at the granule cell to Purkinje cell synapse. *J Neurosci,* 16:5661-5671.

Atluri PP, Regehr WG (1998) Delayed release of neurotransmitter from cerebellar granule cells. *J Neurosci,* 18:8214-8227.

Ayalon G, Segev E, Elgavish S, Stern-Bach Y (2005) Two regions in the N-terminal domain of ionotropic glutamate receptor 3 form the subunit oligomerization interfaces that control subtype-specific receptor assembly. *J Biol Chem,* 280:15053-15060.

Ayalon G, Stern-Bach Y (2001) Functional assembly of AMPA and kainate receptors is mediated by several discrete protein-protein interactions. *Neuron,* 31:103-113.

Bao J, Lin H, Ouyang Y, Lei D, Osman A, Kim TW, Mei L, Dai P, Ohlemiller KK, Ambron RT (2004) Activity-dependent transcription regulation of PSD-95 by neuregulin-1 and Eos. *Nat Neurosci,* 7:1250-1258.

Bao J, Wolpowitz D, Role LW, Talmage DA (2003) Back signaling by the Nrg-1 intracellular domain. *J Cell Biol,* 161:1133-1141.

Barbeau D, Liang JJ, Robitalille Y, Quirion R, Srivastava LK (1995) Decreased expression of the embryonic form of the neural cell adhesion molecule in schizophrenic brains. *Proc Natl Acad Sci U S A,* 92:2785-2789.

Bartos M, Elgueta C (2012) Functional characteristics of parvalbumin- and cholecystokinin-expressing basket cells. *J Physiol,* 590:669-681.

Bartos M, Vida I, Jonas P (2007) Synaptic mechanisms of synchronized gamma oscillations in inhibitory interneuron networks. *Nat Rev Neurosci,* 8:45-56.

Baude A, Nusser Z, Molnar E, McIlhinney RA, Somogyi P (1995) High-resolution immunogold localization of AMPA type glutamate receptor subunits at synaptic and non-synaptic sites in rat hippocampus. *Neuroscience,* 69:1031-1055.

Belforte JE, Zsiros V, Sklar ER, Jiang Z, Yu G, Li Y, Quinlan EM, Nakazawa K (2010) Postnatal NMDA receptor ablation in corticolimbic interneurons confers schizophrenia-like phenotypes. *Nat Neurosci,* 13:76-83.

Berger B, Minarik T, Griesmayr B, Stelzig-Schoeler R, Aichhorn W, Sauseng P (2016) Brain Oscillatory Correlates of Altered Executive Functioning in Positive and Negative Symptomatic Schizophrenia Patients and Healthy Controls. *Front Psychol,* 7:705.

Bi LL, Sun XD, Zhang J, Lu YS, Chen YH, Wang J, Geng F, Liu F, Zhang M, Liu JH, Li XW, Mei L, Gao TM (2015) Amygdala NRG1-ErbB4 is critical for the modulation of anxiety-like behaviors. *Neuropsychopharmacology,* 40:974-986.

Bidoret C, Bouvier G, Ayon A, Szapiro G, Casado M (2015) Properties and molecular identity of NMDA receptors at synaptic and non-synaptic inputs in cerebellar molecular layer interneurons. *Front Synaptic Neurosci,* 7:1.

Bieri KW, Bobbitt KN, Colgin LL (2014) Slow and fast gamma rhythms coordinate different spatial coding modes in hippocampal place cells. *Neuron,* 82:670-681.

Bjarnadottir M, Misner DL, Haverfield-Gross S, Bruun S, Helgason VG, Stefansson H, Sigmundsson A, Firth DR, Nielsen B, Stefansdottir R, Novak TJ, Stefansson K, Gurney ME, Andresson T (2007)

Neuregulin1 (NRG1) signaling through Fyn modulates NMDA receptor phosphorylation: differential synaptic function in NRG1+/- knock-outs compared with wild-type mice. *J Neurosci*, 27:4519-4529.

Blatow M, Caputi A, Monyer H (2005) Molecular diversity of neocortical GABAergic interneurones. *J Physiol*, 562:99-105.

Boehm J, Kang MG, Johnson RC, Esteban J, Huganir RL, Malinow R (2006) Synaptic incorporation of AMPA receptors during LTP is controlled by a PKC phosphorylation site on GluR1. *Neuron*, 51:213-225.

Boer S, Berk M, Dean B (2009) Levels of neuregulin 1 and 3 proteins in Brodmann's area 46 from subjects with schizophrenia and bipolar disorder. *Neurosci Lett*, 466:27-29.

Braff D, Stone C, Callaway E, Geyer M, Glick I, Bali L (1978) Prestimulus effects on human startle reflex in normals and schizophrenics. *Psychophysiology*, 15:339-343.

Bragin A, Jando G, Nadasdy Z, Hetke J, Wise K, Buzsaki G (1995) Gamma (40-100 Hz) oscillation in the hippocampus of the behaving rat. *J Neurosci*, 15:47-60.

Brinkmann BG, Agarwal A, Sereda MW, Garratt AN, Muller T, Wende H, Stassart RM, Nawaz S, Humml C, Velanac V, Radyushkin K, Goebbels S, Fischer TM, Franklin RJ, Lai C, Ehrenreich H, Birchmeier C, Schwab MH, Nave KA (2008) Neuregulin-1/ErbB signaling serves distinct functions in myelination of the peripheral and central nervous system. *Neuron*, 59:581-595.

Brun VH, Otnass MK, Molden S, Steffenach HA, Witter MP, Moser MB, Moser EI (2002) Place cells and place recognition maintained by direct entorhinal-hippocampal circuitry. *Science*, 296:2243-2246.

Buhl EH, Halasy K, Somogyi P (1994) Diverse sources of hippocampal unitary inhibitory postsynaptic potentials and the number of synaptic release sites. *Nature*, 368:823-828.

Buhl EH, Szilagyi T, Halasy K, Somogyi P (1996) Physiological properties of anatomically identified basket and bistratified cells in the CA1 area of the rat hippocampus in vitro. *Hippocampus*, 6:294-305.

Buzsaki G (2015) Hippocampal sharp wave-ripple: A cognitive biomarker for episodic memory and planning. *Hippocampus*, 25:1073-1188.

Buzsaki G, Leung LW, Vanderwolf CH (1983) Cellular bases of hippocampal EEG in the behaving rat. *Brain Res*, 287:139-171.

Buzsaki G, Wang XJ (2012) Mechanisms of gamma oscillations. *Annu Rev Neurosci*, 35:203-225.

Bygrave AM, Masiulis S, Nicholson E, Berkemann M, Barkus C, Sprengel R (2016) Knockout of NMDA-receptors from parvalbumin interneurons sensitizes to schizophrenia-related deficits induced by MK-801. *Transl Psychiatry*, 6:e778.

Cajal S Ramón y (1922) Studien über die Sehrinde der Katze. *Journal of Psychology and Neurology*, 29:161-181.

Calvigioni D, Mate Z, Fuzik J, Girach F, Zhang MD, Varro A, Beiersdorf J, Schwindling C, Yanagawa Y, Dockray GJ, McBain CJ, Hokfelt T, Szabo G, Keimpema E, Harkany T (2016) Functional Differentiation of Cholecystokinin-Containing Interneurons Destined for the Cerebral Cortex. *Cereb Cortex*, 27:2453-2468

Campanac E, Gasselin C, Baude A, Rama S, Ankri N, Debanne D (2013) Enhanced intrinsic excitability in basket cells maintains excitatory-inhibitory balance in hippocampal circuits. *Neuron*, 77:712-722.

Cardin JA, Carlen M, Meletis K, Knoblich U, Zhang F, Deisseroth K, Tsai LH, Moore CI (2009) Driving fast-spiking cells induces gamma rhythm and controls sensory responses. *Nature*, 459:663-667.

Carlsson A (1977) Does dopamine play a role in schizophrenia? *Psychol Med,* 7:583-597.

Caroni P (1997) Overexpression of growth-associated proteins in the neurons of adult transgenic mice. *J Neurosci Methods,* 71:3-9.

Chen MS, Bermingham-McDonogh O, Danehy FT, Jr., Nolan C, Scherer SS, Lucas J, Gwynne D, Marchionni MA (1994) Expression of multiple neuregulin transcripts in postnatal rat brains. *J Comp Neurol,* 349:389-400.

Chen YJ, Johnson MA, Lieberman MD, Goodchild RE, Schobel S, Lewandowski N, Rosoklija G, Liu RC, Gingrich JA, Small S, Moore H, Dwork AJ, Talmage DA, Role LW (2008) Type III neuregulin-1 is required for normal sensorimotor gating, memory-related behaviors, and corticostriatal circuit components. *J Neurosci*, 28:6872-6883.

Chen YJ, Zhang M, Yin DM, Wen L, Ting A, Wang P, Lu YS, Zhu XH, Li SJ, Wu CY, Wang XM, Lai C, Xiong WC, Mei L, Gao TM (2010) ErbB4 in parvalbumin-positive interneurons is critical for neuregulin 1 regulation of long-term potentiation. *Proc Natl Acad Sci U S A,* 107:21818-21823.

Chong VZ, Thompson M, Beltaifa S, Webster MJ, Law AJ, Weickert CS (2008) Elevated neuregulin-1 and ErbB4 protein in the prefrontal cortex of schizophrenic patients. *Schizophrenia Res*, 100:270-280.

Christopoulos A (2002). Allosteric binding sites on cell-surface receptors: novel targets for drug discovery. *Nat Rev Drug Discov,* 1: 198-210

Chung HJ, Huang YH, Lau LF, Huganir RL (2004) Regulation of the NMDA receptor complex and trafficking by activity-dependent phosphorylation of the NR2B subunit PDZ ligand. *J Neurosci*, 24:10248-10259.

Claiborne BJ, Amaral DG, Cowan WM (1986) A light and electron microscopic analysis of the mossy fibers of the rat dentate gyrus. *J Comp Neurol,* 246:435-458.

Cobb SR, Halasy K, Vida I, Nyiri G, Tamas G, Buhl EH, Somogyi P (1997) Synaptic effects of identified interneurons innervating both interneurons and pyramidal cells in the rat hippocampus. *Neuroscience*, 79:629-648.

Colgin LL (2013) Mechanisms and functions of theta rhythms. *Annu Rev Neurosci,* 36:295-312.

Colgin LL (2016) Rhythms of the hippocampal network. *Nat Rev Neurosci*, 17:239-249.

Colgin LL, Denninger T, Fyhn M, Hafting T, Bonnevie T, Jensen O, Moser MB, Moser EI (2009) Frequency of gamma oscillations routes flow of information in the hippocampus. *Nature*, 462:353-357.

Corfas G, Falls DL, Fischbach GD (1993) ARIA, a protein that stimulates acetylcholine receptor synthesis, also induces tyrosine phosphorylation of a 185-kDa muscle transmembrane protein. *Proc Natl Acad Sci U S A*, 90:1624-1628.

Corfas G, Rosen KM, Aratake H, Krauss R, Fischbach GD (1995) Differential expression of ARIA isoforms in the rat brain. *Neuron,* 14:103-115.

Csicsvari J, Jamieson B, Wise KD, Buzsaki G (2003) Mechanisms of gamma oscillations in the hippocampus of the behaving rat. *Neuron,* 37:311-322.

Davis KL, Kahn RS, Ko G, Davidson M (1991) Dopamine in schizophrenia: a review and reconceptualization. *Am J Psychiatry,* 148:1474-1486.

Daw MI, Tricoire L, Erdelyi F, Szabo G, McBain CJ (2009) Asynchronous transmitter release from cholecystokinin-containing inhibitory interneurons is widespread and target-cell independent. *J Neurosci,* 29:11112-11122.

Deakin IH, Law AJ, Oliver PL, Schwab MH, Nave KA, Harrison PJ, Bannerman DM (2009) Behavioural characterization of neuregulin 1 type I overexpressing transgenic mice. *Neuroreport,* 20:1523-1528.

Deakin IH, Nissen W, Law AJ, Lane T, Kanso R, Schwab MH, Nave KA, Lamsa KP, Paulsen O, Bannerman DM, Harrison PJ (2012) Transgenic overexpression of the type I isoform of neuregulin 1 affects working memory and hippocampal oscillations but not long-term potentiation. *Cereb cortex* 22:1520-1529.

Dean B, Karl T, Pavey G, Boer S, Duffy L, Scarr E (2008) Increased levels of serotonin 2A receptors and serotonin transporter in the CNS of neuregulin 1 hypomorphic/mutant mice. *Schizophr Res* 99:341-349.

DeFelipe J, Lopez-Cruz PL, Benavides-Piccione R, Bielza C, Larranaga P, Anderson S, Burkhalter A, Cauli B, Fairen A, Feldmeyer D, Fishell G, Fitzpatrick D, Freund TF, Gonzalez-Burgos G, Hestrin S, Hill S, Hof PR, Huang J, Jones EG, Kawaguchi Y, Kisvarday Z, Kubota Y, Lewis DA, Marin O, Markram H, McBain CJ, Meyer HS, Monyer H, Nelson SB, Rockland K, Rossier J, Rubenstein JL, Rudy B, Scanziani M, Shepherd GM, Sherwood CC, Staiger JF, Tamas G, Thomson A, Wang Y, Yuste R, Ascoli GA (2013) New insights into the classification and nomenclature of cortical GABAergic interneurons. *Nat Rev Neurosci,* 14:202-216.

Delay J, Deniker P, Harl JM (1952) [Therapeutic use in psychiatry of phenothiazine of central elective action (4560 RP)]. *Ann Med Psychol (Paris),* 110:112-117.

Desbonnet L, Waddington JL, Tuathaigh CM (2009) Mice mutant for genes associated with schizophrenia: common phenotype or distinct endophenotypes? *Behav Brain Res,* 204:258-273.

Devane WA, Hanus L, Breuer A, Pertwee RG, Stevenson LA, Griffin G, Gibson D, Mandelbaum A, Etinger A, Mechoulam R (1992) Isolation and structure of a brain constituent that binds to the cannabinoid receptor. *Science, 258*: 1946-1949.

Dupret D, O'Neill J, Pleydell-Bouverie B, Csicsvari J (2010) The reorganization and reactivation of hippocampal maps predict spatial memory performance. *Nat. Neurosci,* 13:995-1002.

English DF, Peyrache A, Stark E, Roux L, Vallentin D (2014) Excitation and inhibition compete to control spiking during hippocampal ripples: intracellular study in behaving mice. *J Neurosci,* 34:16509-16517.

Falls DL, Rosen KM, Corfas G, Lane WS, Fischbach GD (1993) ARIA, a protein that stimulates acetylcholine receptor synthesis, is a member of the neu ligand family. *Cell* 72:801-815.

Fazzari P, Paternain AV, Valiente M, Pla R, Lujan R, Lloyd K, Lerma J, Marin O, Rico B (2010) Control of cortical GABA circuitry development by Nrg1 and ErbB4 signalling. *Nature,* 464:1376-1380.

Fisahn A, Pike FG, Buhl EH, Paulsen O (1998) Cholinergic induction of network oscillations at 40 Hz in the hippocampus in vitro. *Nature,* 394:186-189.

Flames N, Long JE, Garratt AN, Fischer TM, Gassmann M, Birchmeier C, Lai C, Rubenstein JL, Marin O (2004) Short- and long-range attraction of cortical GABAergic interneurons by neuregulin-1. *Neuron* 44:251-261.

Foldy C, Lee SY, Szabadics J, Neu A, Soltesz I (2007) Cell type-specific gating of perisomatic inhibition by cholecystokinin. *Nat. Neurosci,* 10:1128-1130.

Freund TF, Antal M (1988) GABA-containing neurons in the septum control inhibitory interneurons in the hippocampus. *Nature,* 336:170-173.

Freund TF, Buzsaki G (1996) Interneurons of the hippocampus. *Hippocampus*, 6:347-470.

Freund TF, Katona I (2007) Perisomatic inhibition. *Neuron*, 56:33-42.

Fuchs EC, Zivkovic AR, Cunningham MO, Middleton S, Lebeau FE, Bannerman DM, Rozov A, Whittington MA, Traub RD, Rawlins JN, Monyer H (2007) Recruitment of parvalbumin-positive interneurons determines hippocampal function and associated behavior. *Neuron*, 53:591-604.

Fuentealba P, Begum R, Capogna M, Jinno S, Marton LF, Csicsvari J, Thomson A, Somogyi P, Klausberger T (2008) Ivy cells: a population of nitric-oxide-producing, slow-spiking GABAergic neurons and their involvement in hippocampal network activity. *Neuron*, 57:917-929.

Fukudome Y, Ohno-Shosaku T, Matsui M, Omori Y, Fukaya M, Tsubokawa H, Taketo MM, Watanabe M, Manabe T, Kano M (2004) Two distinct classes of muscarinic action on hippocampal inhibitory synapses: M2-mediated direct suppression and M1/M3-mediated indirect suppression through endocannabinoid signalling. *Eur J Neurosci*, 19:2682-2692.

Furukawa H, Gouaux E (2003) Mechanisms of activation, inhibition and specificity: crystal structures of the NMDA receptor NR1 ligand-binding core. *EMBO J*, 22:2873-2885.

Fyhn M, Molden S, Witter MP, Moser EI, Moser MB (2004) Spatial representation in the entorhinal cortex. *Science*, 305:1258-1264.

Garcia RA, Vasudevan K, Buonanno A (2000) The neuregulin receptor ErbB-4 interacts with PDZ-containing proteins at neuronal synapses. *Proc Natl Acad Sci U S A,* 97:3596-3601.

Geibel M, Badurek S, Horn JM, Vatanashevanopakorn C, Koudelka J, Wunderlich CM, Bronneke HS, Wunderlich FT, Minichiello L (2014) Ablation of TrkB signalling in CCK neurons results in hypercortisolism and obesity. *Nat Commun,* 5:3427.

Gerecke KM, Wyss JM, Karavanova I, Buonanno A, Carroll SL (2001) ErbB transmembrane tyrosine kinase receptors are differentially expressed throughout the adult rat central nervous system. *J Comp Neurol,* 433:86-100.

Girardeau G, Benchenane K, Wiener SI, Buzsaki G, Zugaro MB (2009) Selective suppression of hippocampal ripples impairs spatial memory. *Nat Neurosci*, 12:1222-1223.

Glickfeld LL, Scanziani M (2006) Distinct timing in the activity of cannabinoid-sensitive and cannabinoid-insensitive basket cells. *Nat Neurosci,* 9:807-815.

Gonzalez-Burgos G, Cho RY, Lewis DA (2015) Alterations in cortical network oscillations and parvalbumin neurons in schizophrenia. *Biol Psychiatry,* 77:1031-1040.

Gu Z, Jiang Q, Fu AK, Ip NY, Yan Z (2005) Regulation of NMDA receptors by neuregulin signaling in prefrontal cortex. *J Neurosci*, 25:4974-4984.

Gulyas AI, Hajos N, Freund TF (1996) Interneurons containing calretinin are specialized to control other interneurons in the rat hippocampus. *J Neurosci*, 16:3397-3411.

Gulyas AI, Hajos N, Katona I, Freund TF (2003) Interneurons are the local targets of hippocampal inhibitory cells which project to the medial septum. *Eur J Neurosci*, 17:1861-1872.

Guy PM, Platko JV, Cantley LC, Cerione RA, Carraway KL, 3rd (1994) Insect cell-expressed p180erbB3 possesses an impaired tyrosine kinase activity. *Proc Natl Acad Sci U S A* 91:8132-8136.

Hahn CG, Wang HY, Cho DS, Talbot K, Gur RE, Berrettini WH, Bakshi K, Kamins J, Borgmann-Winter KE, Siegel SJ, Gallop RJ, Arnold SE (2006) Altered neuregulin 1-erbB4 signaling contributes to NMDA receptor hypofunction in schizophrenia. *Nat Med*, 12:824-828.

Haig AR, Gordon E, De Pascalis V, Meares RA, Bahramali H, Harris A (2000) Gamma activity in schizophrenia: evidence of impaired network binding? *Clin Neurophysiol*, 111:1461-1468.

Hajos N, Ellender TJ, Zemankovics R, Mann EO, Exley R, Cragg SJ, Freund TF, Paulsen O (2009) Maintaining network activity in submerged hippocampal slices: importance of oxygen supply *Eur J Neurosci*,29:319-327.

Hajos N, Mody I (1997) Synaptic communication among hippocampal interneurons: properties of spontaneous IPSCs in morphologically identified cells. *J Neurosci*, 17:8427-8442.

Hajos N, Palhalmi J, Mann EO, Nemeth B, Paulsen O, Freund TF (2004) Spike timing of distinct types of GABAergic interneuron during hippocampal gamma oscillations in vitro. *J Neurosci*, 24:9127-9137.

Hancock ML, Canetta SE, Role LW, Talmage DA (2008) Presynaptic type III neuregulin1-ErbB signaling targets {alpha}7 nicotinic acetylcholine receptors to axons. *J Cell Biol*, 181:511-521.

Hashimoto R, Straub RE, Weickert CS, Hyde TM, Kleinman JE, Weinberger DR (2004) Expression analysis of neuregulin-1 in the dorsolateral prefrontal cortex in schizophrenia. *Mol Psychiatry*, 9:299-307.

Hashimoto T, Volk DW, Eggan SM, Mirnics K, Pierri JN, Sun Z, Sampson AR, Lewis DA (2003) Gene expression deficits in a subclass of GABA neurons in the prefrontal cortex of subjects with schizophrenia. *J Neurosci*, 23:6315-6326.

Hefft S, Jonas P (2005) Asynchronous GABA release generates long-lasting inhibition at a hippocampal interneuron-principal neuron synapse. *Nat Neurosci* 8:1319-1328.

Howes OD, Kapur S (2009) The dopamine hypothesis of schizophrenia: version III--the final common pathway. *Schizophr Bull*, 35:549-562.

Hu H, Gan J, Jonas P (2014) Interneurons. Fast-spiking, parvalbumin(+) GABAergic interneurons: from cellular design to microcircuit function. *Science*, 345:1255263.

Hu X, Hicks CW, He W, Wong P, Macklin WB, Trapp BD, Yan R (2006) Bace1 modulates myelination in the central and peripheral nervous system. *Nat Neurosci*, 9:1520-1525.

Huang YZ, Won S, Ali DW, Wang Q, Tanowitz M, Du QS, Pelkey KA, Yang DJ, Xiong WC, Salter MW, Mei L (2000) Regulation of neuregulin signaling by PSD-95 interacting with ErbB4 at CNS synapses. *Neuron*, 26:443-455.

Ishikawa T, Sahara Y, Takahashi T (2002) A single packet of transmitter does not saturate postsynaptic glutamate receptors. *Neuron*, 34:613-621.

Ishizuka N, Weber J, Amaral DG (1990) Organization of intrahippocampal projections originating from CA3 pyramidal cells in the rat. *J Comp Neurol*, 295:580-623.

Ito I, Kawakami R, Sakimura K, Mishina M, Sugiyama H (2000) Input-specific targeting of NMDA receptor subtypes at mouse hippocampal CA3 pyramidal neuron synapses. *Neuropharmacology*, 39:943-951.

Jackman SL, Beneduce BM, Drew IR, Regehr WG (2014) Achieving high-frequency optical control of synaptic transmission. *J Neurosci*, 34:7704-7714.

Jackson MB, Scharfman HE (1996) Positive feedback from hilar mossy cells to granule cells in the dentate gyrus revealed by voltage-sensitive dye and microelectrode recording. *J Neurophysiol*, 76:601-616.

Javitt DC, Zukin SR (1991) Recent advances in the phencyclidine model of schizophrenia. *Am J Psychiatry*, 148:1301-1308.

Karlsson MP, Frank LM (2009) Awake replay of remote experiences in the hippocampus. *Nat Neurosci*, 12:913-918.

Karson MA, Tang AH, Milner TA, Alger BE (2009) Synaptic cross talk between perisomatic-targeting interneuron classes expressing cholecystokinin and parvalbumin in hippocampus. *J Neurosci*, :29:4140-4154.

Karson MA, Whittington KC, Alger BE (2008) Cholecystokinin inhibits endocannabinoid-sensitive hippocampal IPSPs and stimulates others. *Neuropharmacology*, 54:117-128.

Kato T, Kasai A, Mizuno M, Fengyi L, Shintani N, Maeda S, Yokoyama M, Ozaki M, Nawa H (2010) Phenotypic characterization of transgenic mice overexpressing neuregulin-1. *PloS One* 5:e14185.

Katona I, Sperlagh B, Sik A, Kafalvi A, Vizi ES, Mackie K, Freund TF (1999) Presynaptically located CB1 cannabinoid receptors regulate GABA release from axon terminals of specific hippocampal interneurons. *J Neurosci*, 19:4544-4558.

Katona L, Lapray D, Viney TJ, Oulhaj A, Borhegyi Z, Micklem BR, Klausberger T, Somogyi P (2014) Sleep and movement differentiates actions of two types of somatostatin-expressing GABAergic interneuron in rat hippocampus. *Neuron*, 82:872-886.

Kawaguchi Y, Katsumaru H, Kosaka T, Heizmann CW, Hama K (1987) Fast spiking cells in rat hippocampus (CA1 region) contain the calcium-binding protein parvalbumin. *Brain Res*, 416:369-374.

Kerber G, Streif R, Schwaiger FW, Kreutzberg GW, Hager G (2003) Neuregulin-1 isoforms are differentially expressed in the intact and regenerating adult rat nervous system. *J Mol Neurosci*, 21:149-165.

Kerr AM, Reisinger E, Jonas P (2008) Differential dependence of phasic transmitter release on synaptotagmin 1 at GABAergic and glutamatergic hippocampal synapses. *Proc Natl Acad Sci U S A*, 105:15581-15586.

Kim E, Sheng M (2004) PDZ domain proteins of synapses. *Nat Rev Neurosci*, 5:771-781.

Klausberger T, Marton LF, O'Neill J, Huck JH, Dalezios Y, Fuentealba P, Suen WY, Papp E, Kaneko T, Watanabe M, Csicsvari J, Somogyi P (2005) Complementary roles of cholecystokinin- and parvalbumin-expressing GABAergic neurons in hippocampal network oscillations. *J Neurosci*, 25:9782-9793.

Klausberger T, Roberts JD, Somogyi P (2002) Cell type- and input-specific differences in the number and subtypes of synaptic GABA(A) receptors in the hippocampus. *J Neurosci*, 22:2513-2521.

Klausberger T, Somogyi P (2008) Neuronal diversity and temporal dynamics: the unity of hippocampal circuit operations. *Science*, 321:53-57.

Kohus Z, Kali S, Rovira L, Schlingloff D, Papp O, Freund TF, Hajos N, Gulyas AI (2016) Properties and dynamics of inhibitory synaptic communication within the CA3 microcircuits of pyramidal cells and interneurons expressing parvalbumin or cholecystokinin. *J Physiol*, 594:3745-74

Korotkova T, Fuchs EC, Ponomarenko A, von Engelhardt J, Monyer H (2010) NMDA receptor ablation on parvalbumin-positive interneurons impairs hippocampal synchrony, spatial representations, and working memory. *Neuron*, 68:557-569.

Kraushaar U, Jonas P (2000) Efficacy and stability of quantal GABA release at a hippocampal interneuron-principal neuron synapse. *J Neurosci*, 20:5594-5607.

Krivosheya D, Tapia L, Levinson JN, Huang K, Kang Y, Hines R, Ting AK, Craig AM, Mei L, Bamji SX, El-Husseini A (2008) ErbB4-neuregulin signaling modulates synapse development and dendritic arborization through distinct mechanisms. *J Biol Chem*, 283:32944-32956.

Krystal JH, Karper LP, Seibyl JP, Freeman GK, Delaney R, Bremner JD, Heninger GR, Bowers MB, Jr., Charney DS (1994) Subanesthetic effects of the noncompetitive NMDA antagonist, ketamine, in humans. Psychotomimetic, perceptual, cognitive, and neuroendocrine responses. *Arch Gen Psychiatry*, 51:199-214.

Ksir C, Hart CL (2016) Cannabis and Psychosis: a Critical Overview of the Relationship. *Curr Psychiatry Rep*, 18: 12.

Kubota D, Colgin LL, Casale M, Brucher FA, Lynch G (2003) Endogenous waves in hippocampal slices. *J Neurophysiol*, 89:81-89.

Kudrimoti HS, Barnes CA, McNaughton BL (1999) Reactivation of hippocampal cell assemblies: effects of behavioral state, experience, and EEG dynamics. *J Neurosci*, 19:4090-4101.

Kuusinen A, Abele R, Madden DR, Keinanen K (1999) Oligomerization and ligand-binding properties of the ectodomain of the alpha-amino-3-hydroxy-5-methyl-4-isoxazole propionic acid receptor subunit GluRD. *J Biol Chem*, 274:28937-28943.

Kwon JS, O'Donnell BF, Wallenstein GV, Greene RW, Hirayasu Y, Nestor PG, Hasselmo ME, Potts GF, Shenton ME, McCarley RW (1999) Gamma frequency-range abnormalities to auditory stimulation in schizophrenia. *Arch Gen Psychiatry*, 56:1001-1005.

Kwon OB, Longart M, Vullhorst D, Hoffman DA, Buonanno A (2005) Neuregulin-1 reverses long-term potentiation at CA1 hippocampal synapses. *J Neurosci*, 25:9378-9383.

Kwon OB, Paredes D, Gonzalez CM, Neddens J, Hernandez L, Vullhorst D, Buonanno A (2008) Neuregulin-1 regulates LTP at CA1 hippocampal synapses through activation of dopamine D4 receptors. *Proc Natl Acad Sci U S A*, 105:15587-15592.

Lacaille JC, Mueller AL, Kunkel DD, Schwartzkroin PA (1987) Local circuit interactions between oriens/alveus interneurons and CA1 pyramidal cells in hippocampal slices: electrophysiology and morphology. *J Neurosci*, 7:1979-1993.

Lampinen M, Settimo L, Pentikainen OT, Jouppila A, Mottershead DG, Johnson MS, Keinanen K (2002) Discrimination between agonists and antagonists by the alpha-amino-3-hydroxy-5-methyl-4-isoxazole propionic acid-selective glutamate receptor. A mutation analysis of the ligand-binding domain of GluR-D subunit. *J Biol Chem*, 277:41940-41947.

Lamsa KP, Heeroma JH, Somogyi P, Rusakov DA, Kullmann DM (2007) Anti-Hebbian long-term potentiation in the hippocampal feedback inhibitory circuit. *Science*, 315:1262-1266.

Lapray D, Lasztoczi B, Lagler M, Viney TJ, Katona L, Valenti O, Hartwich K, Borhegyi Z, Somogyi P, Klausberger T (2012) Behavior-dependent specialization of identified hippocampal interneurons. *Nat Neurosci*, 15:1265-1271.

Lasztoczi B, Klausberger T (2014) Layer-specific GABAergic control of distinct gamma oscillations in the CA1 hippocampus. *Neuron*, 81:1126-1139.

Lasztoczi B, Klausberger T (2016) Hippocampal Place Cells Couple to Three Different Gamma Oscillations during Place Field Traversal. *Neuron*, 91:34-40.

Lasztoczi B, Tukker JJ, Somogyi P, Klausberger T (2011) Terminal field and firing selectivity of cholecystokinin-expressing interneurons in the hippocampal CA3 area. *J Neurosci*, 31:18073-18093.

Lavoie AM, Tingey JJ, Harrison NL, Pritchett DB, Twyman RE (1997) Activation and deactivation rates of recombinant GABA(A) receptor channels are dependent on alpha-subunit isoform. *Biophys J*, 73:2518-2526.

Law AJ, Kleinman JE, Weinberger DR, Weickert CS (2007) Disease-associated intronic variants in the ErbB4 gene are related to altered ErbB4 splice-variant expression in the brain in schizophrenia. *Hum Mol Genet*, 16:129-141.

Law AJ, Lipska BK, Weickert CS, Hyde TM, Straub RE, Hashimoto R, Harrison PJ, Kleinman JE, Weinberger DR (2006) Neuregulin 1 transcripts are differentially expressed in schizophrenia and regulated by 5' SNPs associated with the disease. *Proc Natl Acad Sci U S A*, 103:6747-6752.

Law AJ, Shannon Weickert C, Hyde TM, Kleinman JE, Harrison PJ (2004) Neuregulin-1 (NRG-1) mRNA and protein in the adult human brain. *Neuroscience*, 127:125-136.

Lee AK, Wilson MA (2002) Memory of sequential experience in the hippocampus during slow wave sleep. *Neuron*, 36:1183-1194.

Lei S, McBain CJ (2002) Distinct NMDA receptors provide differential modes of transmission at mossy fiber-interneuron synapses. *Neuron*, 33:921-933.

Leuschner WD, Hoch W (1999) Subtype-specific assembly of alpha-amino-3-hydroxy-5-methyl-4-isoxazole propionic acid receptor subunits is mediated by their n-terminal domains. *J Biol Chem*, 274:16907-16916.

Lewis DA (2014) Inhibitory neurons in human cortical circuits: substrate for cognitive dysfunction in schizophrenia. *Curr Opin Neurobiol*, 26:22-26.

Li B, Woo RS, Mei L, Malinow R (2007) The neuregulin-1 receptor erbB4 controls glutamatergic synapse maturation and plasticity. *Neuron*, 54:583-597.

Li H, Chou SJ, Hamasaki T, Perez-Garcia CG, O'Leary DD (2012) Neuregulin repellent signaling via ErbB4 restricts GABAergic interneurons to migratory paths from ganglionic eminence to cortical destinations. *Neural Dev*, 7:10.

Lichtenstein P, Yip BH, Bjork C, Pawitan Y, Cannon TD, Sullivan PF, Hultman CM (2009) Common genetic determinants of schizophrenia and bipolar disorder in Swedish families: a population-based study. *Lancet*, 373:234-239.

Lin DT, Huganir RL (2007) PICK1 and phosphorylation of the glutamate receptor 2 (GluR2) AMPA receptor subunit regulates GluR2 recycling after NMDA receptor-induced internalization. *J Neurosci*, 27:13903-13908.

Lin DT, Makino Y, Sharma K, Hayashi T, Neve R, Takamiya K, Huganir RL (2009) Regulation of AMPA receptor extrasynaptic insertion by 4.1N, phosphorylation and palmitoylation. *Nat Neurosci*, 12:879-887.

Lisman J, Buzsaki G (2008) A neural coding scheme formed by the combined function of gamma and theta oscillations. *Schizophr Bull*, 34:974-980.

Lisman JE, Coyle JT, Green RW, Javitt DC, Benes FM, Heckers S, Grace AA (2008) Circuit-based framework for understanding neurotransmitter and risk gene interactions in schizophrenia. *Trends Neurosci* 31:234-242

Liu G, Choi S, Tsien RW (1999) Variability of neurotransmitter concentration and nonsaturation of postsynaptic AMPA receptors at synapses in hippocampal cultures and slices. *Neuron*, 22:395-409.

Liu X, Bates R, Yin DM, Shen C, Wang F, Su N, Kirov SA, Luo Y, Wang JZ, Xiong WC, Mei L (2011) Specific regulation of NRG1 isoform expression by neuronal activity. *J Neurosci*, 31:8491-8501.

Liu Y, Ford B, Mann MA, Fischbach GD (2001) Neuregulins increase alpha7 nicotinic acetylcholine receptors and enhance excitatory synaptic transmission in GABAergic interneurons of the hippocampus. *J Neurosci*, 21:5660-5669.

Liu Y, Ford BD, Mann MA, Fischbach GD (2005) Neuregulin-1 increases the proliferation of neuronal progenitors from embryonic neural stem cells. *Dev Biol*, 283:437-445.

Loeb JA, Susanto ET, Fischbach GD (1998) The neuregulin precursor proARIA is processed to ARIA after expression on the cell surface by a protein kinase C-enhanced mechanism. *Mol and Cell Neurosci*, 11:77-91.

Long LE, Anderson P, Frank E, Shaw A, Liu S, Huang XF, Pinault D, Karl T, O'Brien TJ, Shannon Weickert C, Jones NC (2015) Neuregulin 1 expression and electrophysiological abnormalities in the Neuregulin 1 transmembrane domain heterozygous mutant mouse. *PloS One*, 10:e0124114.

Long LE, Chesworth R, Huang XF, Wong A, Spiro A, McGregor IS, Arnold JC, Karl T (2012) Distinct neurobehavioural effects of cannabidiol in transmembrane domain neuregulin 1 mutant mice. *PloS One*, 7:e34129.

Longart M, Chatani-Hinze M, Gonzalez CM, Vullhorst D, Buonanno A (2007) Regulation of ErbB-4 endocytosis by neuregulin in GABAergic hippocampal interneurons. *Brain Res Bull* 73:210-219.

Lopez-Bendito G, Cautinat A, Sanchez JA, Bielle F, Flames N, Garratt AN, Talmage DA, Role LW, Charnay P, Marin O, Garel S (2006) Tangential neuronal migration controls axon guidance: a role for neuregulin-1 in thalamocortical axon navigation. *Cell*, 125:127-142.

Louie K, Wilson MA (2001) Temporally structured replay of awake hippocampal ensemble activity during rapid eye movement sleep. *Neuron*, 29:145-156.

Luo X, He W, Hu X, Yan R (2014) Reversible overexpression of bace1-cleaved neuregulin-1 N-terminal fragment induces schizophrenia-like phenotypes in mice. *Biol Psychiatry*, 76:120-127.

Maccaferri G, Dingledine R (2002) Control of feedforward dendritic inhibition by NMDA receptor-dependent spike timing in hippocampal interneurons. *J Neurosci*, 22:5462-5472.

Mainen ZF, Malinow R, Svoboda K (1999) Synaptic calcium transients in single spines indicate that NMDA receptors are not saturated. *Nature*, 399:151-155.

Mann EO, Mody I (2010) Control of hippocampal gamma oscillation frequency by tonic inhibition and excitation of interneurons. *Nat Neurosci*, 13:205-212.

Mann EO, Suckling JM, Hajos N, Greenfield SA, Paulsen O (2005) Perisomatic feedback inhibition underlies cholinergically induced fast network oscillations in the rat hippocampus in vitro. *Neuron* 45:105-117.

Manns JR, Zilli EA, Ong KC, Hasselmo ME, Eichenbaum H (2007) Hippocampal CA1 spiking during encoding and retrieval: relation to theta phase. *Neurobiol Learn Mem*, 87:9-20.

Manseau MW, Goff DC (2015) Cannabinoids and Schizophrenia: Risks and Therapeutic Potential. *Neurotherapeutics*, 12: 816-824.

Markram H, Toledo-Rodriguez M, Wang Y, Gupta A, Silberberg G, Wu C (2004) Interneurons of the neocortical inhibitory system. *Nat Rev Neurosci*, 5:793-807.

Marsicano G, Lutz B (1999) Expression of the cannabinoid receptor CB1 in distinct neuronal subpopulations in the adult mouse forebrain. *Eur J Neurosci*, 11:4213-25

Martina M, Comas T, Mealing GA (2013) Selective Pharmacological Modulation of Pyramidal Neurons and Interneurons in the CA1 Region of the Rat Hippocampus. *Front Pharmacol*, 4, 24.

Martina M, Krasteniakov NV, Bergeron R (2003) D-Serine differently modulates NMDA receptor function in rat CA1 hippocampal pyramidal cells and interneurons. *J Physiol*, 548 (Pt 2).

Matsuda LA, Lolait SJ, Brownstein MJ, Young AC, Bonner, TI (1990) Structure of a cannabinoid receptor and functional expression of the cloned cDNA. *Nature*, *346*(6284), 561-564.

Matta JA, Pelkey KA, Craig MT, Chittajallu R, Jeffries BW, McBain CJ (2013) Developmental origin dictates interneuron AMPA and NMDA receptor subunit composition and plasticity. *Nat Neurosci*, 16:1032-1041.

McAllister AK, Stevens CF (2000) Nonsaturation of AMPA and NMDA receptors at hippocampal synapses. *Proc Natl Acad Sci U S A*, 97:6173-6178.

McBain C, Dingledine R (1992) Dual-component miniature excitatory synaptic currents in rat hippocampal CA3 pyramidal neurons. *J Neurophysiol*, 68:16-27.

McBain CJ, Dingledine R (1993) Heterogeneity of synaptic glutamate receptors on CA3 stratum radiatum interneurones of rat hippocampus. *J Physiol*, 462:373-392.

McGrath J, Saha S, Chant D, Welham J (2008) Schizophrenia: a concise overview of incidence, prevalence, and mortality. *Epidemiol Rev*, 30:67-76.

Mechawar N, Lacoste B, Yu WF, Srivastava LK, Quirion R (2007) Developmental profile of neuregulin receptor ErbB4 in postnatal rat cerebral cortex and hippocampus. *Neuroscience* 148:126-139.

Mechoulam, R., Ben-Shabat, S., Hanus, L., Ligumsky, M., Kaminski, N. E., Schatz, A. R., . . . et al (1995) Identification of an endogenous 2-monoglyceride, present in canine gut, that binds to cannabinoid receptors. *Biochem Pharmacol*, 50: 83-90.

Meddows E, Le Bourdelles B, Grimwood S, Wafford K, Sandhu S, Whiting P, McIlhinney RA (2001) Identification of molecular determinants that are important in the assembly of N-methyl-D-aspartate receptors. *J Biol Chem*, 276:18795-18803.

Mei L, Nave KA (2014) Neuregulin-ERBB signaling in the nervous system and neuropsychiatric diseases. *Neuron*, 83:27-49.

Mei L, Xiong WC (2008) Neuregulin 1 in neural development, synaptic plasticity and schizophrenia. *Nat Rev Neurosci*, 9:437-452.

Michailov GV, Sereda MW, Brinkmann BG, Fischer TM, Haug B, Birchmeier C, Role L, Lai C, Schwab MH, Nave KA (2004) Axonal neuregulin-1 regulates myelin sheath thickness. *Science*, 304:700-703.

Minier F, Sigel E (2004) Positioning of the alpha-subunit isoforms confers a functional signature to gamma-aminobutyric acid type A receptors. *Proc Natl Acad Sci U S A*, 101:7769-7774.

Montgomery SM, Buzsaki G (2007) Gamma oscillations dynamically couple hippocampal CA3 and CA1 regions during memory task performance. *Proc Natl Acad Sci U S A*, 104:14495-14500.

Monyer H, Sprengel R, Schoepfer R, Herb A, Higuchi M, Lomeli H, Burnashev N, Sakmann B, Seeburg PH (1992) Heteromeric NMDA receptors: molecular and functional distinction of subtypes. *Science*, 256:1217-1221.

Monyer, H., Burnashev, N., Laurie, D. J., Sakmann, B., & Seeburg, P. H. (1994). Developmental and regional expression in the rat brain and functional properties of four NMDA receptors. *Neuron, 12*, 529-540.

Moriyoshi K, Masu M, Ishii T, Shigemoto R, Mizuno N, Nakanishi S (1991) Molecular cloning and characterization of the rat NMDA receptor. *Nature*, 354:31-37.

Morino P, Herrera-Marschitz M, Castel MN, Ungerstedt U, Varro A, Dockray G,Hökfelt T (1994) Cholecystokinin in cortico-striatal neurons in the rat:immunohistochemical studies at the light and electron microscopical level. *Eur J Neurosci*, 1994 May 1;6:681-92

Mostaid MS, Lloyd D, Liberg B, Sundram S, Pereira A, Pantelis C, Karl T, Weickert CS, Everall IP, Bousman CA (2016) Neuregulin-1 and schizophrenia in the genome-wide association study era. *Neurosci Biobehav Rev*, 68:387-409.

Mullasseril P, Hansen KB, Vance KM, Ogden KK, Yuan H, Kurtkaya NL, Santangelo R, Orr AG, Le P, Vellano KM, Liotta DC, Traynelis SF (2010) A subunit-selective potentiator of NR2C- and NR2D-containing NMDA receptors. *Nat Commun*, 1, 90.

Nakashiba T, Buhl DL, McHugh TJ, Tonegawa S (2009) Hippocampal CA3 output is crucial for ripple-associated reactivation and consolidation of memory. *Neuron*, 62:781-787.

Nakazawa T, Komai S, Watabe AM, Kiyama Y, Fukaya M, Arima-Yoshida F, Horai R, Sudo K, Ebine K, Delawary M, Goto J, Umemori H, Tezuka T, Iwakura Y, Watanabe M, Yamamoto T, Manabe T (2006) NR2B tyrosine phosphorylation modulates fear learning as well as amygdaloid synaptic plasticity. Embo J, 25:2867-2877.

Neddens J, Buonanno A (2010) Selective populations of hippocampal interneurons express ErbB4 and their number and distribution is altered in ErbB4 knockout mice. *Hippocampus*, 20:724-744.

Neddens J, Buonanno A (2011) Expression of the neuregulin receptor ErbB4 in the brain of the rhesus monkey (Macaca mulatta). *PloS One*, 6:e27337.

Neddens J, Fish KN, Tricoire L, Vullhorst D, Shamir A, Chung W, Lewis DA, McBain CJ, Buonanno A (2011) Conserved interneuron-specific ErbB4 expression in frontal cortex of rodents, monkeys, and humans: implications for schizophrenia. *Biol Psychiatry*, 70:636-645.

Neu A, Foldy C, Soltesz I (2007) Postsynaptic origin of CB1-dependent tonic inhibition of GABA release at cholecystokinin-positive basket cell to pyramidal cell synapses in the CA1 region of the rat hippocampus. *J Physiol*, 578:233-247.

Newell KA, Karl T, Huang XF (2013) A neuregulin 1 transmembrane domain mutation causes imbalanced glutamatergic and dopaminergic receptor expression in mice. *Neuroscience*, 248:670-680.

Nissen W (2012) *Altered hippocampal fast oscillations and GABAergic circuits in neuregulin 1 over-expressing mice*, DPhil thesis. Lincoln College, University of Oxford, Oxford.

Nusser Z, Lujan R, Laube G, Roberts JD, Molnar E, Somogyi P (1998) Cell type and pathway dependence of synaptic AMPA receptor number and variability in the hippocampus. *Neuron*, 21:545-559.

Nyiri G, Freund TF, Somogyi P (2001) Input-dependent synaptic targeting of alpha(2)-subunit-containing GABA(A) receptors in synapses of hippocampal pyramidal cells of the rat. *Eur J Neurosci*, 13:428-442.

Nyiri G, Stephenson FA, Freund TF, Somogyi P (2003) Large variability in synaptic N-methyl-D-aspartate receptor density on interneurons and a comparison with pyramidal-cell spines in the rat hippocampus. *Neuroscience*, 119:347-363.

Oh MC, Derkach VA (2005) Dominant role of the GluR2 subunit in regulation of AMPA receptors by CaMKII. *Nat Neurosci*, 8:853-854.

Okada M, Corfas G (2004) Neuregulin1 downregulates postsynaptic GABAA receptors at the hippocampal inhibitory synapse. *Hippocampus*, 14:337-344.

O'Keefe J, Recce ML (1993) Phase relationship between hippocampal place units and the EEG theta rhythm. *Hippocampus*, 3:317-330.

Oren I, Hajos N, Paulsen O (2010) Identification of the current generator underlying cholinergically induced gamma frequency field potential oscillations in the hippocampal CA3 region. *J Physiol*, 588:785-797.

Oren I, Mann EO, Paulsen O, Hajos N (2006) Synaptic currents in anatomically identified CA3 neurons during hippocampal gamma oscillations in vitro. *J Neurosci*, 26:9923-9934.

Ozaki M, Itoh K, Miyakawa Y, Kishida H, Hashikawa T (2004) Protein processing and releases of neuregulin-1 are regulated in an activity-dependent manner. *J Neurochem*, 91:176-188.

Ozaki M, Sasner M, Yano R, Lu HS, Buonanno A (1997) Neuregulin-beta induces expression of an NMDA-receptor subunit. *Nature*, 390:691-694.

Papaleo F, Yang F, Paterson C, Palumbo S, Carr GV, Wang Y, Floyd K, Huang W, Thomas CJ, Chen J, Weinberger DR, Law AJ (2016) Behavioral, Neurophysiological, and Synaptic Impairment in a Transgenic Neuregulin1 (NRG1-IV) Murine Schizophrenia Model. *J Neurosci*, 36:4859-4875.

Parlapani E, Schmitt A, Wirths O, Bauer M, Sommer C, Rueb U, Skowronek MH, Treutlein J, Petroianu GA, Rietschel M, Falkai P (2010) Gene expression of neuregulin-1 isoforms in different brain regions of elderly schizophrenia patients. *World J Biol Psychiatry*, 11:243-250.

Pawelzik H, Hughes DI, Thomson AM (2002) Physiological and morphological diversity of immunocytochemically defined parvalbumin- and cholecystokinin-positive interneurones in CA1 of the adult rat hippocampus. *J Comp Neurol*, 443:346-367.

Perez Y, Morin F, Lacaille JC (2001) A hebbian form of long-term potentiation dependent on mGluR1a in hippocampal inhibitory interneurons. *Proc Natl Acad Sci U S A*, 98:9401-9406.

Pike FG, Goddard RS, Suckling JM, Ganter P, Kasthuri N, Paulsen O (2000) Distinct frequency preferences of different types of rat hippocampal neurones in response to oscillatory input currents. *J Physiol*, 529 Pt 1:205-213.

Pitcher GM, Beggs S, Woo RS, Mei L, Salter MW (2008) ErbB4 is a suppressor of long-term potentiation in the adult hippocampus. *Neuroreport*, 19:139-143.

Pitcher GM, Kalia LV, Ng D, Goodfellow NM, Yee KT, Lambe EK, Salter MW (2011) Schizophrenia susceptibility pathway neuregulin 1-ErbB4 suppresses Src upregulation of NMDA receptors. *Nat Med*, 17:470-478.

Pitler TA, Alger BE (1992) Postsynaptic spike firing reduces synaptic GABAA responses in hippocampal pyramidal cells. *J Neurosci*, 12:4122-4132.

Pitler TA, Alger BE (1994) Depolarization-induced suppression of GABAergic inhibition in rat hippocampal pyramidal cells: G protein involvement in a presynaptic mechanism. *Neuron*, 13:1447-1455.

Pozo K, Goda Y (2010) Unraveling mechanisms of homeostatic synaptic plasticity. *Neuron*, 66:337-351.

Prybylowski K, Chang K, Sans N, Kan L, Vicini S, Wenthold RJ (2005) The synaptic localization of NR2B-containing NMDA receptors is controlled by interactions with PDZ proteins and AP-2. *Neuron*, 47:845-857.

Rapoport JL, Giedd JN, Gogtay N (2012) Neurodevelopmental model of schizophrenia: update 2012. *Mol Psychiatry*, 17:1228-1238.

Reif A, Fritzen S, Finger M, Strobel A, Lauer M, Schmitt A, Lesch KP (2006) Neural stem cell proliferation is decreased in schizophrenia, but not in depression. *Mol Psychiatry*, 11:514-522.

Rieff HI, Raetzman LT, Sapp DW, Yeh HH, Siegel RE, Corfas G (1999) Neuregulin induces GABA(A) receptor subunit expression and neurite outgrowth in cerebellar granule cells. *J Neurosci*, 19:10757-10766.

Roche KW, O'Brien RJ, Mammen AL, Bernhardt J, Huganir RL (1996) Characterization of multiple phosphorylation sites on the AMPA receptor GluR1 subunit. *Neuron*, 16:1179-1188.

Rodrigues S, Desroches M, Krupa M, Cortes JM, Sejnowski TJ, Ali AB (2016) Time-coded neurotransmitter release at excitatory and inhibitory synapses. *Proc Natl Acad Sci U S A*,113:E1108-1115.

Rombo DM, Newton K, Nissen W, Badurek S, Horn JM, Minichiello L, Jefferys JG, Sebastiao AM, Lamsa KP (2015) Synaptic mechanisms of adenosine A2A receptor-mediated hyperexcitability in the hippocampus. *Hippocampus* 25:566-580.

Rusakov DA, Kullmann DM (1998) Extrasynaptic glutamate diffusion in the hippocampus: ultrastructural constraints, uptake, and receptor activation. *J Neurosci*, 18:3158-3170.

Sanchez-Perez AM, Felipo V (2005) Serines 890 and 896 of the NMDA receptor subunit NR1 are differentially phosphorylated by protein kinase C isoforms. *Neurochem Int*, 47:84-91.

Schaffer K (1892) Beitrag zur Histologie der Ammonshornformation. *Archiv für mikroskopische Anatomie*, 39:611-632.

Schizophrenia Working Group of the Psychiatric Genomics C (2014) Biological insights from 108 schizophrenia-associated genetic loci. *Nature*, 511:421-427.

Schmiedt C, Brand A, Hildebrandt H, Basar-Eroglu C (2005) Event-related theta oscillations during working memory tasks in patients with schizophrenia and healthy controls. *Brain Res Cogn Brain Res*, 25:936-947.

Schofield PR, Darlison MG, Fujita N, Burt DR, Stephenson FA, Rodriguez H, Rhee LM, Ramachandran J, Reale V, Glencorse TA, et al. (1987) Sequence and functional expression of the GABA A receptor shows a ligand-gated receptor super-family. *Nature*, 328:221-227.

Scott DB, Blanpied TA, Ehlers MD (2003) Coordinated PKA and PKC phosphorylation suppresses RXR-mediated ER retention and regulates the surface delivery of NMDA receptors. *Neuropharmacology*, 45:755-767.

Scott DB, Blanpied TA, Swanson GT, Zhang C, Ehlers MD (2001) An NMDA receptor ER retention signal regulated by phosphorylation and alternative splicing. *J Neurosci*, 21:3063-3072.

Siapas AG, Wilson MA (1998) Coordinated interactions between hippocampal ripples and cortical spindles during slow-wave sleep. *Neuron*, 21:1123-1128.

Sigel E, Baur R, Trube G, Mohler H, Malherbe P (1990) The effect of subunit composition of rat brain GABAA receptors on channel function. *Neuron*, 5:703-711.

Sigel E, Steinmann ME (2012) Structure, function, and modulation of GABA(A) receptors. *J Biol Chem*, 287:40224-40231.

Sik A, Penttonen M, Ylinen A, Buzsaki G (1995) Hippocampal CA1 interneurons: an in vivo intracellular labeling study. *J Neurosci,* 15:6651-6665.

Silberberg G, Darvasi A, Pinkas-Kramarski R, Navon R (2006) The involvement of ErbB4 with schizophrenia: association and expression studies. *Am J Med Genet B Neuropsychiatr Genet,* 141b:142-148.

Skosnik PD, Cortes-Briones JA, Hajos M (2016) It's All in the Rhythm: The Role of Cannabinoids in Neural Oscillations and Psychosis. *Biol Psychiatry,* 79: 568-577.

Somogyi J, Szabo A, Somogyi P, Lamsa K (2012) Molecular analysis of ivy cells of the hippocampal CA1 stratum radiatum using spectral identification of immunofluorophores. *Front Neural Circuits,* 6:35.

Somogyi P (2010) Hippocampus: intrinsic organization. *Handbook of brain microcircuits,* 148-164.

Somogyi P, Klausberger T (2005) Defined types of cortical interneurone structure space and spike timing in the hippocampus. *J Physiol,* 562:9-26.

Somogyi P, Nunzi MG, Gorio A, Smith AD (1983) A new type of specific interneuron in the monkey hippocampus forming synapses exclusively with the axon initial segments of pyramidal cells. *Brain Res,* 259:137-142.

Spencer KM, Nestor PG, Niznikiewicz MA, Salisbury DF, Shenton ME, McCarley RW (2003) Abnormal neural synchrony in schizophrenia. *J Neurosci,* 23:7407-7411.

Stefansson H, Sigurdsson E, Steinthorsdottir V, Bjornsdottir S, Sigmundsson T, Ghosh S, Brynjolfsson J, Gunnarsdottir S, Ivarsson O, Chou TT, Hjaltason O, Birgisdottir B, Jonsson H, Gudnadottir VG, Gudmundsdottir E, Bjornsson A, Ingvarsson B, Ingason A, Sigfusson S, Hardardottir H, Harvey RP, Lai D, Zhou M, Brunner D, Mutel V, Gonzalo A, Lemke G, Sainz J, Johannesson G, Andresson T, Gudbjartsson D, Manolescu A, Frigge ML, Gurney ME, Kong A, Gulcher JR, Petursson H, Stefansson K (2002) Neuregulin 1 and susceptibility to schizophrenia. *Am J Hum Genet,* 71:877-892.

Steffenach HA, Sloviter RS, Moser EI, Moser MB (2002) Impaired retention of spatial memory after transection of longitudinally oriented axons of hippocampal CA3 pyramidal cells. *Proc Natl Acad Sci U S A,* 99:3194-3198.

Steinthorsdottir V, Stefansson H, Ghosh S, Birgisdottir B, Bjornsdottir S, Fasquel AC, Olafsson O, Stefansson K, Gulcher JR (2004) Multiple novel transcription initiation sites for NRG1. *Gene,* 342:97-105.

Steward O (1976) Topographic organization of the projections from the entorhinal area to the hippocampal formation of the rat. *J Comp Neurol,* 167:285-314.

Sugiura T, Waku K (2000) 2-Arachidonoylglycerol and the cannabinoid receptors. *Chem Phys Lipids, 108*: 89-106.

Sullivan PF, Kendler KS, Neale MC (2003) Schizophrenia as a complex trait: evidence from a meta-analysis of twin studies. *Arch Gen Psychiatry,* 60:1187-1192.

Sun J, Pang ZP, Qin D, Fahim AT, Adachi R, Sudhof TC (2007) A dual-Ca2+-sensor model for neurotransmitter release in a central synapse. *Nature,* 450:676-682.

Sun L, Castellanos N, Grutzner C, Koethe D, Rivolta D, Wibral M, Kranaster L, Singer W, Leweke MF, Uhlhaas PJ (2013) Evidence for dysregulated high-frequency oscillations during sensory processing in medication-naive, first episode schizophrenia. *Schizophr Res,* 150:519-525.

Suryavanshi PS, Ugale R R, Yilmazer-Hanke D, Stairs DJ, Dravid, SM (2014) GluN2C/GluN2D subunit-selective NMDA receptor potentiator CIQ reverses MK-801-induced impairment in prepulse inhibition and working memory in Y-maze test in mice. *Br J Pharmacol, 171*:799-809

Swanson LW, Wyss JM, Cowan WM (1978) An autoradiographic study of the organization of intrahippocampal association pathways in the rat. *J Comp Neurol,* 181:681-715.

Swerdlow NR, Weber M, Qu Y, Light GA, Braff DL (2008) Realistic expectations of prepulse inhibition in translational models for schizophrenia research. *Psychopharmacology,* 199:331-388.

Szabadics J, Varga C, Molnar G, Olah S, Barzo P, Tamas G (2006) Excitatory effect of GABAergic axo-axonic cells in cortical microcircuits. *Science,* 311:233-235.

Szabo GG, Holderith N, Gulyas AI, Freund TF, Hajos N (2010) Distinct synaptic properties of perisomatic inhibitory cell types and their different modulation by cholinergic receptor activation in the CA3 region of the mouse hippocampus. *Eur J Neurosci,* 31:2234-2246.

Thompson M, Lauderdale S, Webster MJ, Chong VZ, McClintock B, Saunders R, Weickert CS (2007) Widespread expression of ErbB2, ErbB3 and ErbB4 in non-human primate brain. *Brain Res,* 1139:95-109.

Tiesinga P, Sejnowski TJ (2009) Cortical enlightenment: are attentional gamma oscillations driven by ING or PING? *Neuron,* 63:727-732.

Ting AK, Chen Y, Wen L, Yin DM, Shen C, Tao Y, Liu X, Xiong WC, Mei L (2011) Neuregulin 1 promotes excitatory synapse development and function in GABAergic interneurons. *J Neurosci,* 31:15-25.

Tingley WG, Ehlers MD, Kameyama K, Doherty C, Ptak JB, Riley CT, Huganir RL (1997) Characterization of protein kinase A and protein kinase C phosphorylation of the N-methyl-D-aspartate receptor NR1 subunit using phosphorylation site-specific antibodies. *J Biol Chem,* 272:5157-5166.

Tong G, Jahr CE (1994) Multivesicular release from excitatory synapses of cultured hippocampal neurons. *Neuron,* 12:51-59.

Toth K, McBain CJ (1998) Afferent-specific innervation of two distinct AMPA receptor subtypes on single hippocampal interneurons. *Nat Neurosci,* 1:572-578.

Traub RD, Jefferys JG, Whittington MA (1997) Simulation of gamma rhythms in networks of interneurons and pyramidal cells. *J Computat Neurosci,* 4:141-150.

Traynelis SF, Wollmuth LP, McBain CJ, Menniti FS, Vance KM, Ogden KK, Hansen KB, Yuan H, Myers SJ, Dingledine R (2010) Glutamate receptor ion channels: structure, regulation, and function. *Pharmacol Rev,* 62:405-496.

Tricoire L, Pelkey KA, Erkkila BE, Jeffries BW, Yuan X, McBain CJ (2011) A blueprint for the spatiotemporal origins of mouse hippocampal interneuron diversity. *J Neurosci,* 31:10948-10970.

Tukker JJ, Fuentealba P, Hartwich K, Somogyi P, Klausberger T (2007) Cell type-specific tuning of hippocampal interneuron firing during gamma oscillations in vivo. *J Neurosci,* 27:8184-8189.

Tzahar E, Waterman H, Chen X, Levkowitz G, Karunagaran D, Lavi S, Ratzkin BJ, Yarden Y (1996) A hierarchical network of interreceptor interactions determines signal transduction by Neu differentiation factor/neuregulin and epidermal growth factor. *Mol Cell Biol,* 16:5276-5287.

Ujike H, Takaki M, Nakata K, Tanaka Y, Takeda T, Kodama M, Fujiwara Y, Sakai A, Kuroda S (2002) CNR1, central cannabinoid receptor gene, associated with susceptibility to hebephrenic schizophrenia. *Mol Psychiatry,* 7: 515-518

Varga V, Hangya B, Kranitz K, Ludanyi A, Zemankovics R, Katona I, Shigemoto R, Freund TF, Borhegyi Z (2008) The presence of pacemaker HCN channels identifies theta rhythmic GABAergic neurons in the medial septum. *J Physiol,* 586:3893-3915.

Vida I, Halasy K, Szinyei C, Somogyi P, Buhl EH (1998) Unitary IPSPs evoked by interneurons at the stratum radiatum-stratum lacunosum-moleculare border in the CA1 area of the rat hippocampus in vitro. *J physiol,* 506 (Pt 3):755-773.

Volk D, Austin M, Pierri J, Sampson A, Lewis D (2001) GABA transporter-1 mRNA in the prefrontal cortex in schizophrenia: decreased expression in a subset of neurons. *Am J Psychiatry,* 158:256-265.

Volk DW, Austin MC, Pierri JN, Sampson AR, Lewis DA (2000) Decreased glutamic acid decarboxylase67 messenger RNA expression in a subset of prefrontal cortical gamma-aminobutyric acid neurons in subjects with schizophrenia. *Arch Gen Psychiatry,* 57:237-245.

Volk, DW, Lewis, DA (2016). The Role of Endocannabinoid Signaling in Cortical Inhibitory Neuron Dysfunction in Schizophrenia. *Biol Psychiatry,* 79, 595-603.

Vullhorst D, Mitchell RM, Keating C, Roychowdhury S, Karavanova I, Tao-Cheng JH, Buonanno A (2015) A negative feedback loop controls NMDA receptor function in cortical interneurons via neuregulin 2/ErbB4 signalling. *Nat commun,* 6:7222.

Vullhorst D, Neddens J, Karavanova I, Tricoire L, Petralia RS, McBain CJ, Buonanno A (2009) Selective expression of ErbB4 in interneurons, but not pyramidal cells, of the rodent hippocampus. *J Neurosci,* 29:12255-12264.

Walsh T, McClellan JM, McCarthy SE, Addington AM, Pierce SB, Cooper GM, Nord AS, Kusenda M, Malhotra D, Bhandari A, Stray SM, Rippey CF, Roccanova P, Makarov V, Lakshmi B, Findling RL, Sikich L, Stromberg T, Merriman B, Gogtay N, Butler P, Eckstrand K, Noory L, Gochman P, Long R, Chen Z, Davis S, Baker C, Eichler EE, Meltzer PS, Nelson SF, Singleton AB, Lee MK, Rapoport JL, King MC, Sebat J (2008) Rare structural variants disrupt multiple genes in neurodevelopmental pathways in schizophrenia. *Science,* 320:539-543.

Walters JT, Owen MJ (2007) Endophenotypes in psychiatric genetics. *Mol Psychiatry,* 12:886-890.

Watanabe K, Kamiya D, Nishiyama A, Katayama T, Nozaki S, Kawasaki H, Watanabe Y, Mizuseki K, Sasai Y (2005) Directed differentiation of telencephalic precursors from embryonic stem cells. *Nat Neurosci,* 8: 288-296

Weickert CS, Tiwari Y, Schofield PR, Mowry BJ, Fullerton JM (2012) Schizophrenia-associated HapICE haplotype is associated with increased NRG1 type III expression and high nucleotide diversity. *Transl Psychiatry,* 2:e104.

Weinberger DR (1987) Implications of normal brain development for the pathogenesis of schizophrenia. *Arch Gen Psychiatry,* 44:660-669.

Wen L, Lu YS, Zhu XH, Li XM, Woo RS, Chen YJ, Yin DM, Lai C, Terry AV, Jr., Vazdarjanova A, Xiong WC, Mei L (2010) Neuregulin 1 regulates pyramidal neuron activity via ErbB4 in parvalbumin-positive interneurons. *Proc Natl Acad Sci U S A*, 107:1211-1216.

Whittington MA, Traub RD, Kopell N, Ermentrout B, Buhl EH (2000) Inhibition-based rhythms: experimental and mathematical observations on network dynamics. *Int J Psychophysiol*, 38:315-336.

Wilson MA, McNaughton BL (1994) Reactivation of hippocampal ensemble memories during sleep. *Science*, 265:676-679.

Wilson RI, Nicoll RA (2001) Endogenous cannabinoids mediate retrograde signalling at hippocampal synapses. *Nature*, 410:588-592.

Wo ZG, Oswald RE (1995) Unraveling the modular design of glutamate-gated ion channels. *Trends Neurosci*, 18:161-168.

Woo RS, Li XM, Tao Y, Carpenter-Hyland E, Huang YZ, Weber J, Neiswender H, Dong XP, Wu J, Gassmann M, Lai C, Xiong WC, Gao TM, Mei L (2007) Neuregulin-1 enhances depolarization-induced GABA release. *Neuron*, 54:599-610.

Woodruff AR, Anderson SA, Yuste R (2010) The enigmatic function of chandelier cells. *Front Neurosci* 4:201.

Wu LG, Westenbroek RE, Borst JG, Catterall WA, Sakmann B (1999) Calcium channel types with distinct presynaptic localization couple differentially to transmitter release in single calyx-type synapses. *J Neurosci*, 19:726-736.

Yau HJ, Wang HF, Lai C, Liu FC (2003) Neural development of the neuregulin receptor ErbB4 in the cerebral cortex and the hippocampus: preferential expression by interneurons tangentially migrating from the ganglionic eminences. *Cereb Cortex*, 13:252-264.

Yin DM, Chen YJ, Lu YS, Bean JC, Sathyamurthy A, Shen C, Liu X, Lin TW, Smith CA, Xiong WC, Mei L (2013) Reversal of behavioral deficits and synaptic dysfunction in mice overexpressing neuregulin 1. *Neuron*, 78:644-657.

Yokozeki T, Wakatsuki S, Hatsuzawa K, Black RA, Wada I, Sehara-Fujisawa A (2007) Meltrin beta (ADAM19) mediates ectodomain shedding of Neuregulin beta1 in the Golgi apparatus: fluorescence correlation spectroscopic observation of the dynamics of ectodomain shedding in living cells. *Genes Cells*, 12:329-343.

Yuan H, Hansen KB, Vance KM, Ogden KK, Traynelis SF (2009) Control of NMDA receptor function by the NR2 subunit amino-terminal domain. *J Neurosci*, 29:12045-12058.

Zhang YP, Oertner TG (2007) Optical induction of synaptic plasticity using a light-sensitive channel. *Nat. Methods*, 4:139-141.

Zhong C, Du C, Hancock M, Mertz M, Talmage DA, Role LW (2008) Presynaptic type III neuregulin 1 is required for sustained enhancement of hippocampal transmission by nicotine and for axonal targeting of alpha7 nicotinic acetylcholine receptors. *J Neurosci*, 28:9111-9116.